FINAL PROJECT REPORT

SEISMIC BEHAVIOR OF PRECAST CURTAIN WALLS

IN HIGH-RISE BUILDINGS

NSF Award Number
PFR-7720884

Submitted To

PROBLEM FOCUSED RESEARCH APPLICATIONS

NATIONAL SCIENCE FOUNDATION

by

Ronald L. Sack, Professor

Graduate Students:
Richard J. Beers, Jr.
Dennis J. Rains
Vincent A. Sessa
David L. Thomas
Edward A. Wicher

Department of Civil Engineering
University of Idaho
Moscow, Idaho 83843

January, 1981

FINAL PROJECT REPORT


SEISMIC BEHAVIOR OF PRECAST CURTAIN WALLS

IN HIGH-RISE BUILDINGS

Submitted To

PROBLEM FOCUSED RESEARCH APPLICATIONS
NATIONAL SCIENCE FOUNDATION


by

Ronald L. Sack, Professor

Graduate Students:
  Richard J. Beers, Jr.
  Dennis J. Rains
  Vincent A. Sessa
  David L. Thomas
  Edward A. Wicher


Department of Civil Engineering

University of Idaho

Moscow, Idaho 83843


January, 1981

50272-101

| REPORT DOCUMENTATION PAGE | 1. REPORT NO. NSF/CEE-81003 | 2. | 3. Recipient's Accession No. PB81-193039 |
|---|---|---|---|

**4. Title and Subtitle**
Seismic Behavior of Precast Curtain Walls in High-Rise Buildings, Final Project Report

**5. Report Date** January 1981

**6.**

**7. Author(s)**
R. L. Sack, R. J. Beers, Jr., D. J. Rains, V. A. Sessa,*

**8. Performing Organization Rept. No.**

**9. Performing Organization Name and Address**
University of Idaho
Department of Civil Engineering
Moscow, ID 83843

**10. Project/Task/Work Unit No.**

**11. Contract(C) or Grant(G) No.**
(C)
(G) PFR7720884

**12. Sponsoring Organization Name and Address**
Office of Planning and Resources Management (OPRM)
National Science Foundation
1800 G Street, N.W.
Washington, D.C. 20550

**13. Type of Report & Period Covered**
Final

**14.**

**15. Supplementary Notes**
*D. L. Thomas, E. A. Wicher

**16. Abstract (Limit: 200 words)**
Investigations to explore the nature of curtain wall participation in the structural response characteristics of high rise buildings subjected to seismic excitation are reported. Structural plans from a number of typical buildings were studied to establish current practice. Four basic insert types, plus various combinations of types of connector bodies, were tested to obtain static stiffness properties and low cycle fatigue data. Full scale tests were run on a one-story, single bay structure. The assemblage (consisting of a steel rigid frame with AISC Type 1 connections and two precast concrete panels attached with dissociated connections at the top and integrative connections at the bottom) was subjected to several earthquakes using a closed loop servo-controlled hydraulic loading system. Exceedence levels, power spectra density, and time response plots were obtained for approximately twelve transducers. These studies were augmented with a finite element representation of the assemblage to study the static and dynamic response. Experimental data were utilized in a feedback loop to the analytical model studies to allow crosschecking and improvement of the structural idealization.

**17. Document Analysis   a. Descriptors**

Earthquakes
Dynamic structural analysis
Buildings
Curtain walls

Seismic arrays
Composite structures
Static structural analysis

**b. Identifiers/Open-Ended Terms**

Earthquake Hazards Mitigation

**c. COSATI Field/Group**

| 18. Availability Statement | 19. Security Class (This Report) | 21. No. of Pages |
|---|---|---|
| NTIS | 20. Security Class (This Page) | 22. Price |

(See ANSI-Z39.18) | See Instructions on Reverse | OPTIONAL FORM 272 (4-77)
(Formerly NTIS-35)
Department of Commerce

## NOTICE

THIS DOCUMENT HAS BEEN REPRODUCED
FROM THE BEST COPY FURNISHED US BY
THE SPONSORING AGENCY. ALTHOUGH IT
IS RECOGNIZED THAT CERTAIN PORTIONS
ARE ILLEGIBLE, IT IS BEING RELEASED
IN THE INTEREST OF MAKING AVAILABLE
AS MUCH INFORMATION AS POSSIBLE.

# ACKNOWLEDGEMENT

TABLE OF CONTENTS

LIST OF CHARTS AND FIGURES

## LIST OF PHOTOS

## LIST OF TABLES

## 1.0  INTRODUCTION AND LITERATURE REVIEW

The use of precast concrete panels for exterior cladding is becoming
very common in the construction of many high-rise buildings.  In general,
these precast panels are used because they are architecturally attractive
and relatively maintenance free.  In most instances, precast concrete panels
are regarded as non-structural elements; that is, they do not contribute
significantly to the stiffness of the structural system.  Presently, the
Applied Technology Council (page 367, 1978) recommends that stiffnesses other
than those of the seismic resisting system should not be included in seismic
analysis as they may not be reliable at higher, inelastic strain levels.
Neglecting the additional stiffness provided by panel elements may in fact
be a conservative assumption with regard to static loads but may not be con-
servative for dynamic loading.  A stiffer structure could sustain high damage
because the building cannot absorb as much energy.  Undesirable loads may
also be transmitted into the precast panels causing damage to individual
panel elements.

### 1.1.  Previous Investigations

A number of papers have been written on the interaction between struc-
tural framing and precast concrete panels due to seismic events and wind,
particularly with the increasing use of exterior precast curtain walls in
high-rise construction (Goodno *et al.* 1979; Mak 1977; Briggs 1976; Eaton
1976; Freeman 1975; McCue *et al.* 1975; Gjelsvik 1974; Tanner 1974; Weidlinger
1973; Oppenheim 1972; Raggett 1972; Rousseau 1972; Sharpe 1972).  Related to
this subject is the interaction of structural framing and shear walls subject

to dynamic loading (Basu *et al.* 1979; Tso and Ruttenburg 1977; Mahin and Bestro 1977; Becker and Llorente 1977; Irwin *et al.* 1971) as well as structural frames with filler walls (Kost *et al.* 1974; Fiorato *et al.* 1970).

Tanner (1974) showed that for the 100 Colony Square Building in Atlanta, the precast concrete panels contributed a considerable amount of lateral stiffness to the structure. This conclusion is based on the comparison of natural frequencies of analytical models with full-scale experimental results from measurements on the building. The analytical model was based on a lumped mass idealization with 21-degrees-of freedom, one degree of freedom for each floor that is not laterally restrained. Full-scale building response measurements were based on low levels of building excitation from the wind. These experiments provided insight into the behavior of structures with panels when the structure is loaded in the linear elastic range. The actual amount of additional lateral stiffness provided by precast concrete cladding will vary from building to building depending on the type of structural system, the building geometry, the panel thickness and design, and the connection detail between the panel and the framework.

The connection between the panel and the structural frame can have a significant effect on the lateral stiffness contribution of the precast panels. There are two primary areas of concern when this stiffness is to be estimated: (1) the type of panel-structural frame connection, and (2) the mechanical properties of these connections when loaded in both the linear and nonlinear range and the ultimate strength of these connections when loaded to failure. McCue *et al.* (1975) categorized the types of panel-frame connections into two areas which suggest the extremes for a wide spectrum of alternatives for design.

1. "The isolation of structure and architectural systems to make the two behave relatively independently. This strategy seeks to minimize the effect of connections between the primary structure and the architectural systems in such a way that the relative displacements and inertia interaction effects are minimal."

2. "The integration of structural and architectural systems to allow them to move together during a seismic event. This strategy calls for a primary structure designed for deformations that are acceptable to commonly used architectural systems, or alternatively, for architectural systems engineered to sustain larger deformations. Thus the architectural and structural systems must be analyzed as a unit."

Prior to recent work done by Sessa (1980), only limited experimental studies had been performed on panel-frame connections. Gjelsvik (1974) investigated bolt or rod connections for different length-to-diameter ratios including testing in the post yield or inelastic range. Sessa performed extensive experimental testing of these panel-frame connections based on a survey of the connections currently used in practice. Sessa investigated both load support (bearing) and lateral (flexible and slotted) connections and considered the different types of fasteners imbedded in the concrete (ferrule loops, etc.). Testing was performed in both the linear elastic and post yield ranges and was based on static loading conditions. Results of these tests and recommendations for determining the mechanical properties of these connections can be found in his thesis.

Gjelsvik (1974) developed an elastic perfectly plastic analysis model to be used to predict the interaction between steel frames and precast curtain wall panels at collapse under static loading. Three groups of assumptions were made when the method was developed.

1. The structural frame and the panel-frame connections behave in an elastic perfectly plastic manner.

2. The panels are rigid, weightless, and have enough strength to transmit the forces applied to them. Each panel is connected to the frame at four points and provides stiffness only in the plane of the panel.

3. The frames and panels interact only through the connecting bolts and there is no interaction between the individual panels.

Although this analysis method predicts the interaction between the structure and the panels at collapse, it fails to describe the behavior of the structure when it is loaded less than the collapse load and provides little insight into the dynamic characteristics of the system.

Briggs (1976) and Mak (1977) worked together to develop an analytical method to predict the interaction between structural framing and precast curtain walls under static loading. Briggs developed both two and three dimensional element stiffness matrices for an exterior precast curtain wall. Mak then incorporated the two dimensional panel elemental stiffness matrix into a static linear and nonlinear computer program for the analysis of the interaction between precast panels and structural framing.

The panel element derived by Briggs consists of a precast curtain wall with four discrete attachments between the panel and the supporting beam. The panel is assumed to be rigid while all the deformation is attributed to the four panel-frame connections. Again, it is assumed that the frames and panels interact only through the connections and there is no interactions between individual panels. However, Briggs did perform a kinematic analysis of the panel movement to determine at what point panel interference occurs. Briggs, with the aid of the computer program developed by Mak, performed a parameter study of the interstory shear stiffness for each combination of frame (with both AISC Type I and II) and panel connections (isolation or integration). The value representative of the panel interstory shear stiffness of the 100 Colony Square Office Building was compared to the experimental study done by Tanner (1974) with good correlation of results.

Mak developed his computer program assuming that the structural framing behaves linearly elastic while the panel-frame connections behave in either an elastic or a nonlinear fashion. Mak used an incremental procedure to approximate the nonlinear behavior and investigates the effect of panel stiffness on structural behavior under static loading conditions. Both isolation and integration connections are addressed including a discussion of the nonlinear behavior of these connections. Also included in Mak's thesis is a discussion of the interference of the panels based on kinematics and computer work. It should be noted that the computer program developed by Mak in its present form is limited to two dimensional frameworks with a maximum height of three stories with exactly two panels per story, and the program only considers static loading.

Goodno *et al.* (1979) developed finite element models and analysis procedures for predicting the dynamic response of structural framing with precast curtain walls, and analytically and experimentally studied the cladding interaction with primary structure. A finite element model was developed for a prototype structure (a building in downtown Atlanta) with a precast concrete curtain wall system. The building was modeled as a system of masses lumped at the floor level and supported by an elastic frame; thus, each floor level was represented by three degrees of freedom (two translational, one rotational). The cladding system was initially idealized as having a uniform interstory shear stiffness. The interstory shear stiffnesses required to match experimental frequencies of the actual structure with the analytical frequencies obtained from the finite element model were determined by performing parameter studies. Finally, a detailed finite element model of a precast concrete panel with connections was formulated to verify the interstory shear stiffness developed in the previous parameter study.

Goodno *et al.* (1979) idealized the precast panel and panel-frame connections as a combination of two dimensional, bending, eight node brick, and one dimensional space frame elements. Figure 1.1 shows the precast panel and the corresponding finite element model. The interstory shear stiffness per panel was determined from the inverse of the displacement resulting from a unit load applied at the top of the cladding panel. With this model, the influence of common panel-frame connection details on the interstory shear stiffness was performed and summarized. Results showed that the interstory shear stiffness can be estimated using this method and that the contribution
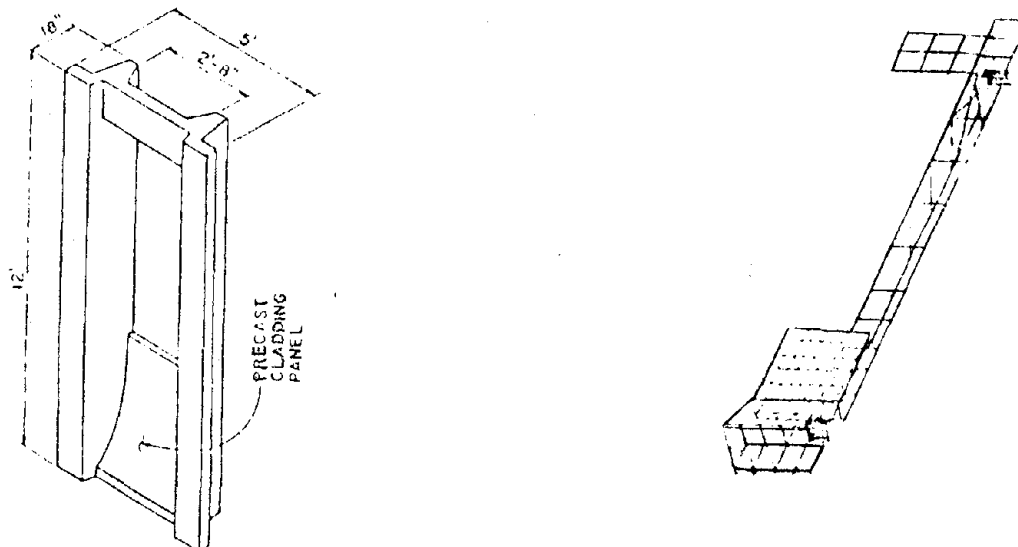
a) Typical Cladding Panel

b) Finite Element Model of One-Half of Cladding Panel

Figure 1.1. Idealization of Precast Concrete Panel (from Goodno *et al.* 1979)

of interstory shear stiffness to the structure from the precast panels is greatly affected by the connection details used. Presently, the analysis and experimental procedures developed here are limited to the linear elastic range. Note that a more detailed analysis considering the effect of many

panels interacting with the structure is probably not practical using the detailed finite element model because of the complexity of the individual panel elements.

## 1.2 Current Research at the University of Idaho

Full-scale laboratory tests and analytical studies were conducted at the University of Idaho to explore the nature of curtain wall participation in the gross structural response characteristics of high-rise buildings subject to seismic excitation. This research was performed by the Civil Engineering Department and was sponsored by the National Science Foundation through Awards #77-02805 and #77-20884. To accomplish the objectives of the project, the research was divided up into three specific tasks as follows:

Task I:     Full-scale laboratory tests of precast curtain wall connec-
            tions.

Task II:    Analytical investigation of curtain assemblages.

Task III:   Full-scale experimental studies of curtain wall assemblages.

Figure 1.2, taken from the original National Science Foundation proposal, shows the interrelationship of the four tasks as originally envisaged by the principal investigators. The contract as it was finally agreed upon between NSF and the principal investigators included only Tasks I, II, and III. This report is organized such that the work on each of the major tasks is discussed individually in the following three sections.

The contract began on May 1, 1978 with an 18 month budget, with a completion date, as indicated by NSF, of April 30, 1980. A six month no-cost extension was granted; therefore, the contract expired on October 31, 1980.
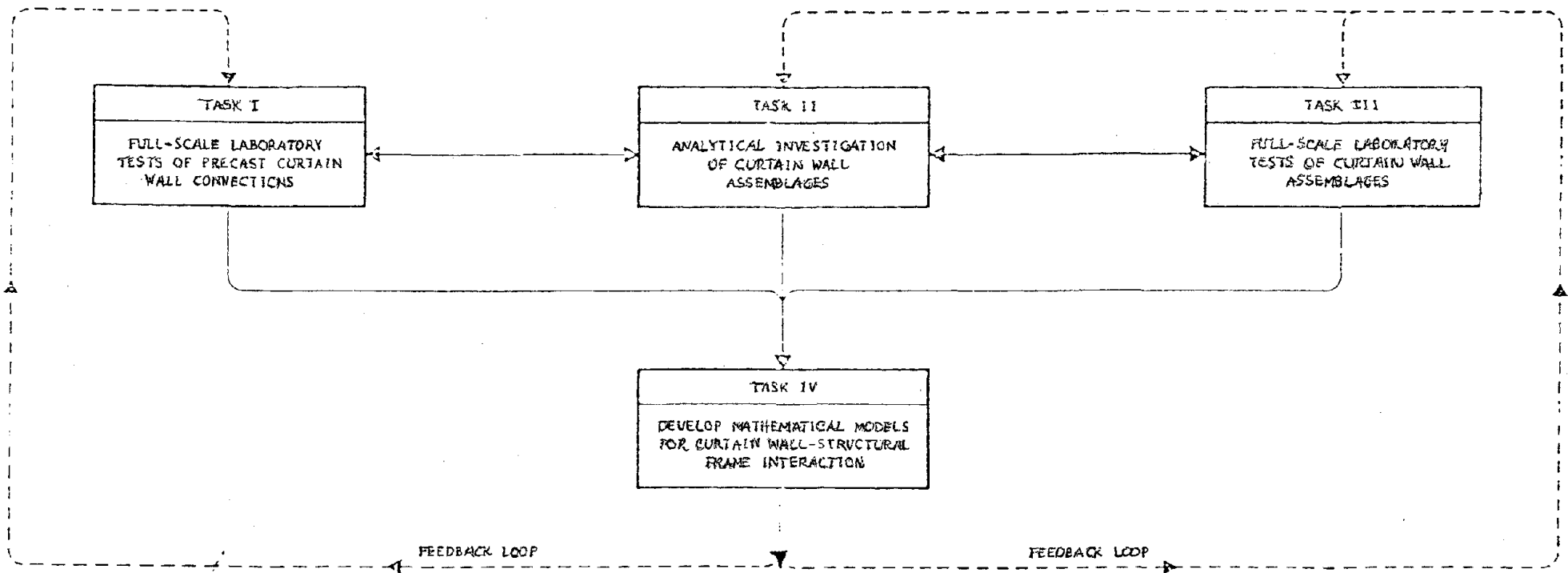
Figure 1.2.   Research Plan

∞

## 2.0 TASK I: FULL-SCALE LABORATORY TEST OF PRECAST CURTAIN WALL CONNECTIONS

### 2.1 Connection Utilization Survey

#### 2.1.1 The General Philosophy of Connection Design

A survey of the structural engineering offices in the San Francisco Bay Area was conducted in October, 1978, to obtain industry input on what connection designs are currently being used. A few of the leading precast companies, as well as the local building code agencies, were interviewed in order to obtain their input on current "state of the art" designs. It quickly became apparent that there is a large variety of connections in use and that these connection designs are very specifically detailed in order to accommodate such constraints as complex geometry of the panels, structural integrity of the system, erection tolerances and procedures, economic considerations, and serviceability requirements. It also became apparent, however, that there are basic components for the most commonly used connections and that there were some valid concerns about the safety and durability (ductility and strength) of these types of connections.

#### 2.1.2 Design Approach

Concerning the behavior of curtain wall panels during a seismic event, it is generally accepted that damage to curtain wall panels is going to occur from a maximum earthquake. Current codes (ACI, 1978; ATC, 1978; UBC, 1979; SEAOC, 1973) place specific requirements on the design of panels and connection hardware such that the induced loads are limited by the use of "isolation" connections or that the connections have sufficient ductility and

strength so as to accommodate movements due to lateral forces and thermal changes.

There are then two ways of ensuring this behavior. Either panels are held on using "slotted" connections or "flexible" connections. Specific design procedures for both types are discussed in Section 3. It was also found during the examination of several structural drawings (as listed in Table 2.1-1) of recently constructed high-rises in the San Francisco area that there are several commonly used components for either type of connection. Table 2.1-2 identifies these connection components and Figures 2.1.1 throug 2.1.4 illustrate several representative connection designs. It was, therefore, decided that these basic components would be tested full scale. (Discussion of the full scale connections experimental study is found in Section 2.3).

## 2.1.3 Safety Concerns

During interviews with several structural engineers within the industry and Government agencies, it was stated that there are aspects of the connection behavior which are not sufficiently understood. There were concerns common to both industry and government, however, there were some very obvious differences in what each group felt were the major issues for concern.

Those responsible for design (structural engineers) and fabrication (the precasting industry) believe in the use of flexible as well as slotted freedom of movement type connections, depending on the firms queried. Their concerns are associated with the possible brittle fracture of the flexible connections at the panel interface after a limited number of load reversals at high acceleration, and also with the fact

Table 2.1.-1  List of Building Drawings Surveyed

| Building | Story Height | Cladding Type | Connectors Used |
|---|---|---|---|
| 100 Colony Square Atlanta, Georgia | 22 | Window box | Cast in bolts Welded angles Wedge inserts |
| Pacific Gas and Electric San Francisco, California | 34 | Column casing Spandral casing | Cast in bolts Bolted angles |
| 575 Market Street San Francisco, California | 40 | Window box | Slotted angles Bolted angles |
| Fantasy Records and Films Berkeley, California | 7 | Column to column | Ferrule inserts and rods Bolted angles to inserts |
| 601 Montgomery Street San Francisco, California | 30 | Window box | No connection details |
| 333 Market Building San Francisco, California | 33 | Column casing | Loop inserts Threaded rods Angles bolted and welded |
| 595 Market Street San Francisco, California | 31 | Spandral to spandral | Loop inserts Bolted angles Threaded rods |
| General Foods Boiler House San Leandro, California | 3 | Multistory | Cast in bolt Face plate Bent plate Steel with slotted holes |
| Transamerica Building San Francisco, California | 60 | Window box | Inserts and threaded rods Bolted angles |

Table 2.1-2 Connection Components

| Panel Fasteners | Connection Body | Structure Fastener |
|---|---|---|
| Wing Nut | Threaded bars | Bolts |
| Four Strut | Partially threaded bars | Angles and bolts |
| Loop | Slotted angles | Cast in bearing |
| Thin Slab | Non-slotted angles | plates |
| Plate Steel with | Gusset plated angles | Direct welding |
| Nelson Studs | Tee sections with welded rebar | |

Precast Panel

Structure Spandral Beam

Ferrule Inserts or
embedded bolts are
used as fasteners

Welded or bolted
to the spandral

Rod may be continuous thread or
partial thread.
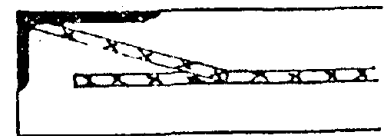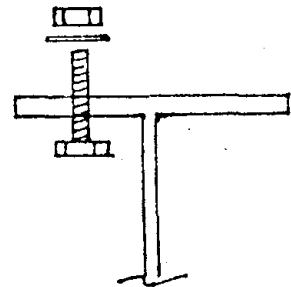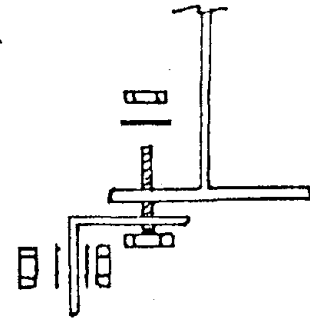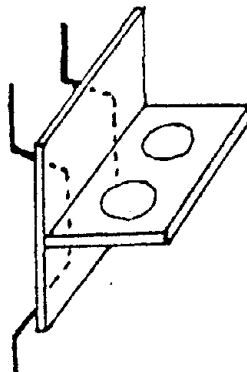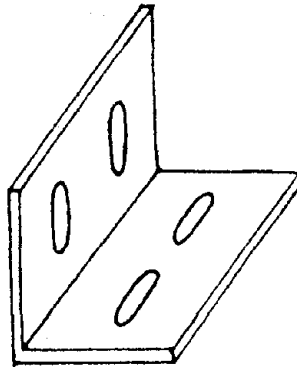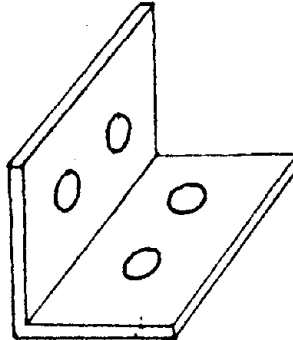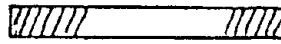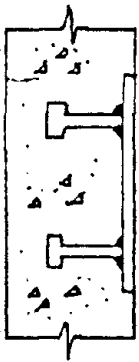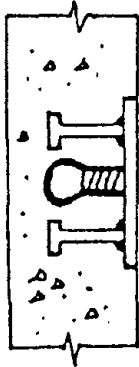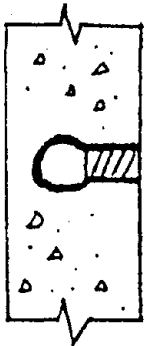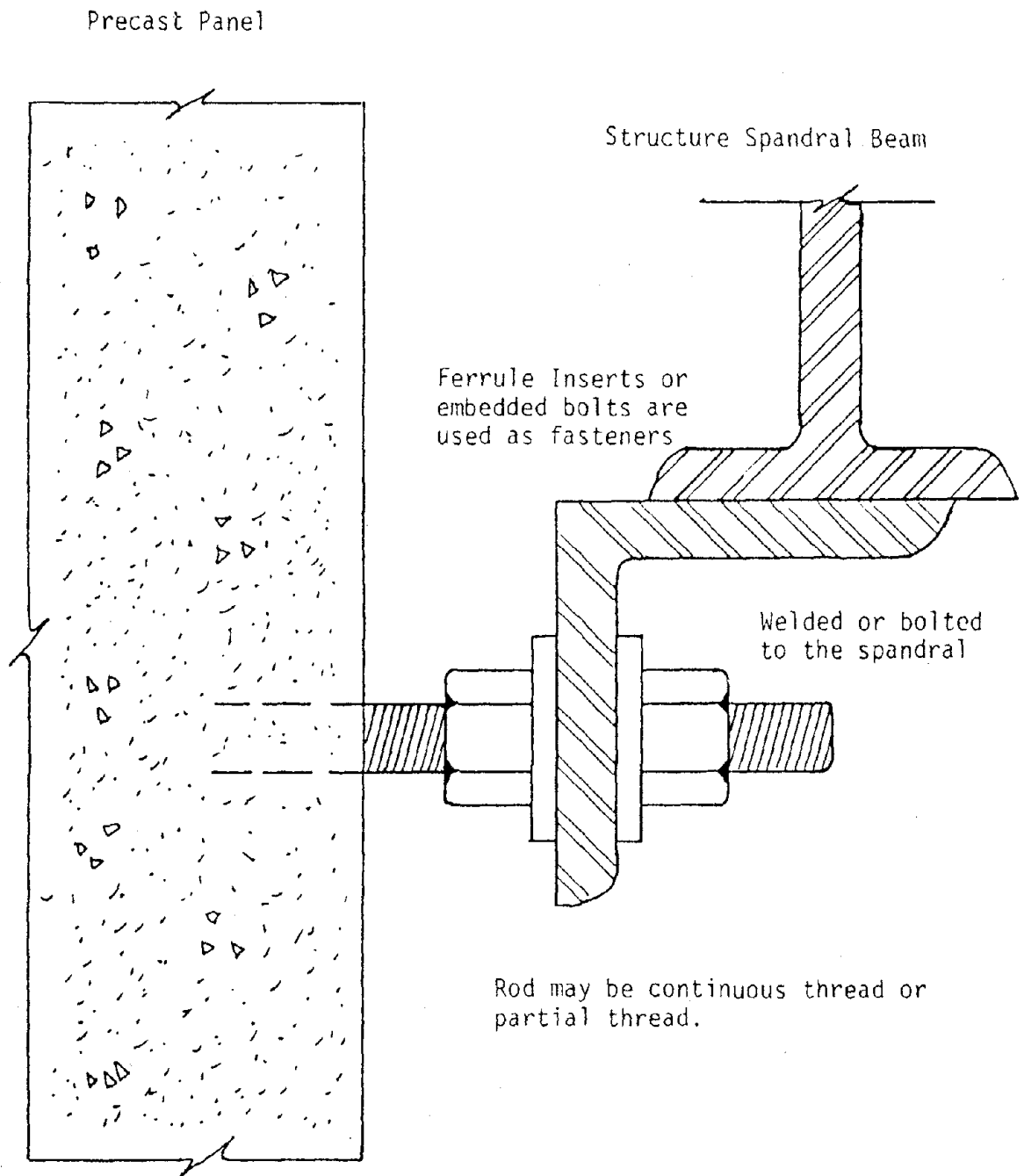
Figure 2.1.1  Flexible Rod Connection ( Dissociative )

Precast Panel                    Structure  Floor Slab



Tack welded nut after being
finger tightened.

Frictionless washers.
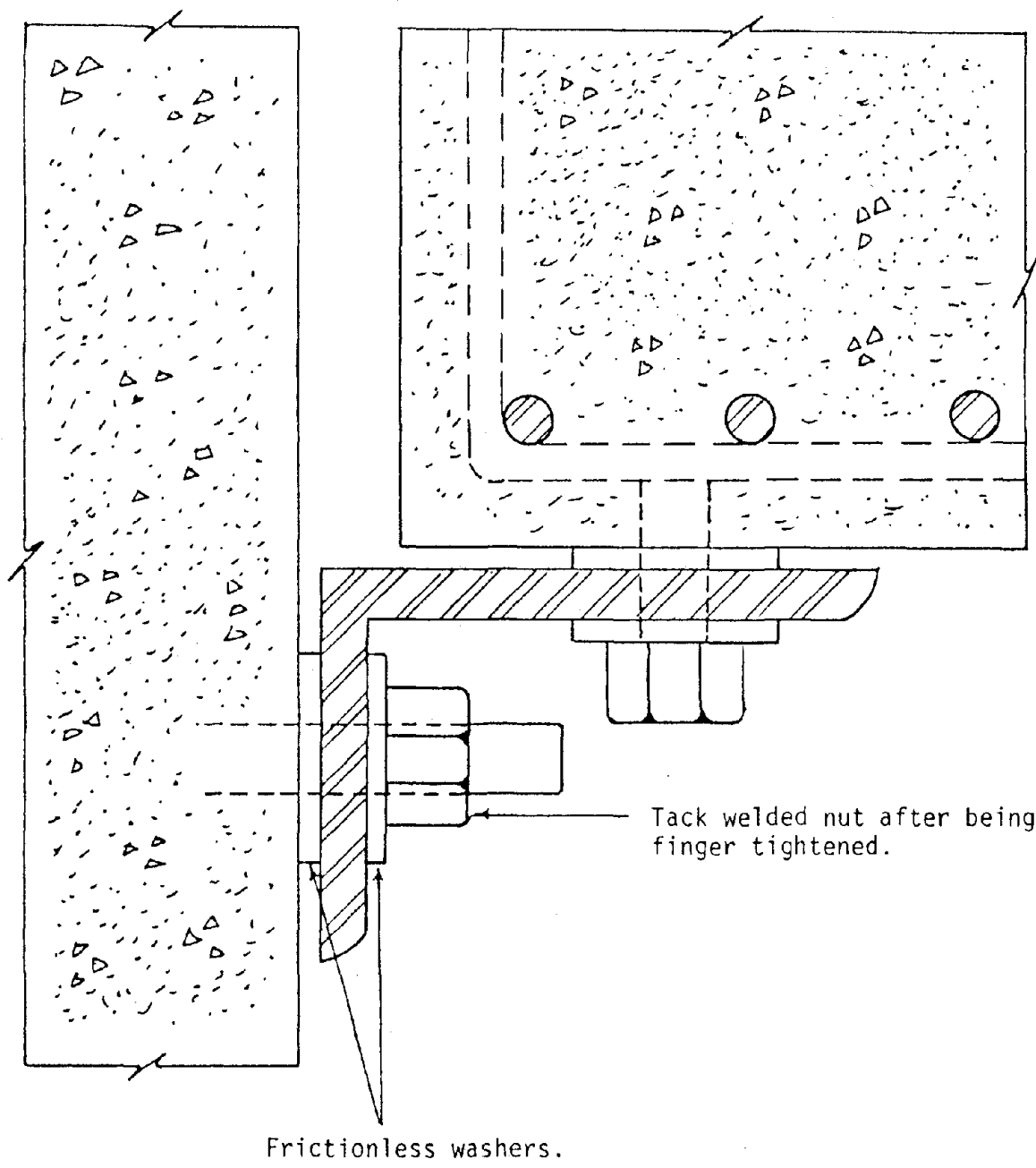
Figure 2.1.2  Slotted Angle Connection  ( Dissociative )

Fillet welds

Floor slab

Fillet welds

Floor slab
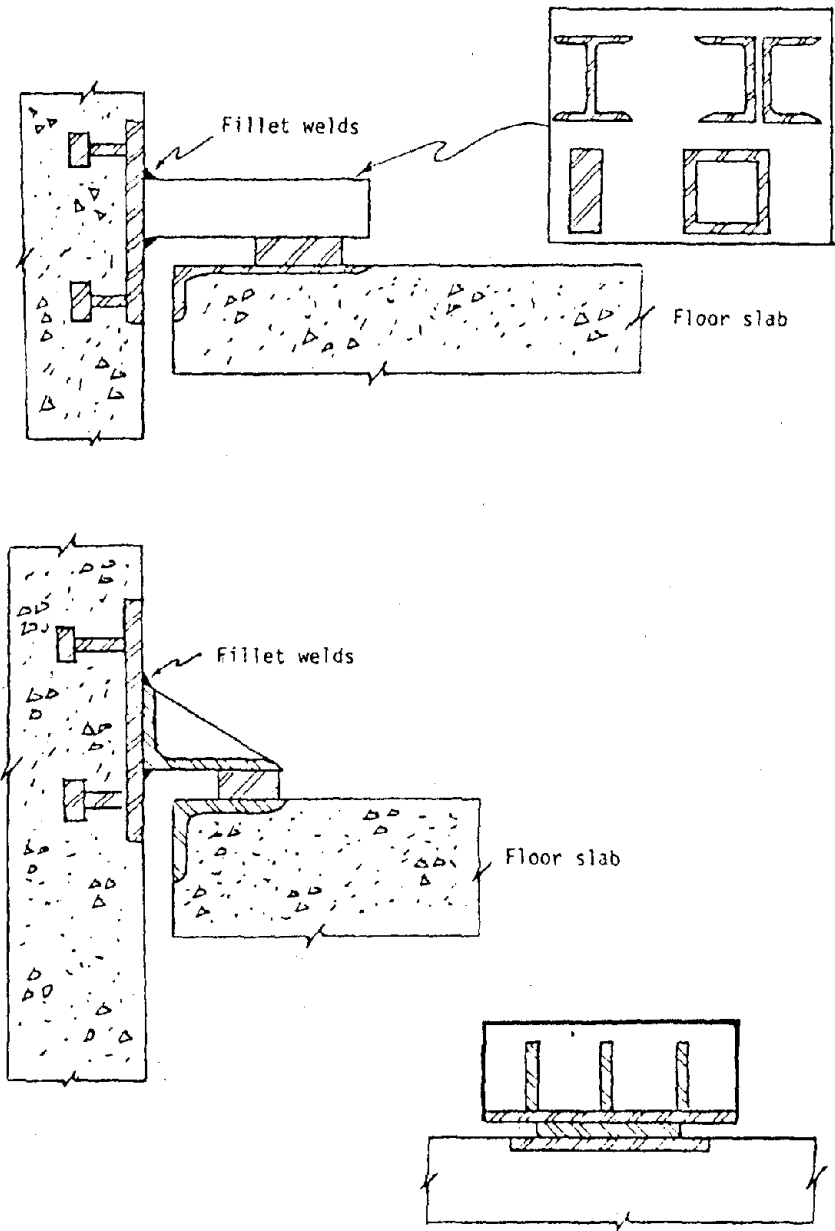
Figure 2.1.3 Fixed Support Welded Connection ( Integrative )

Precast Panel

Standard angle

Structure floor slab

a)

Precast Panel

Elastomeric Shims

Structure
Spandral beam
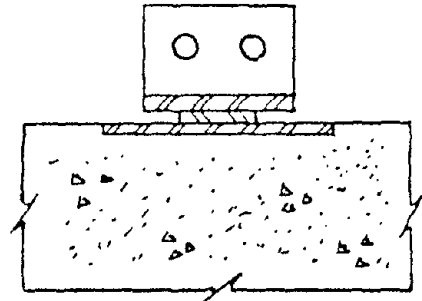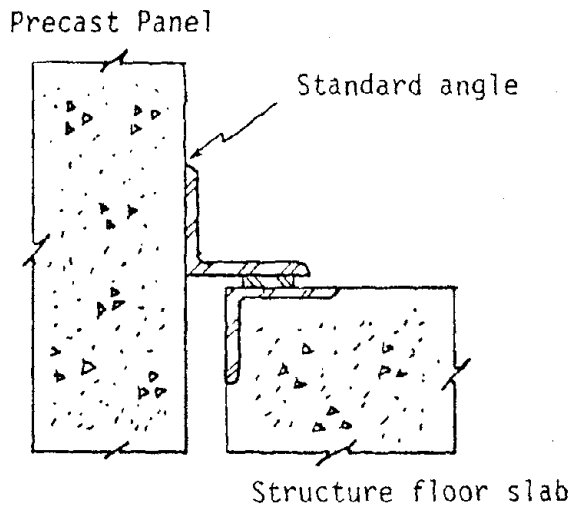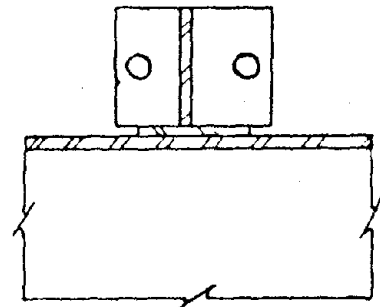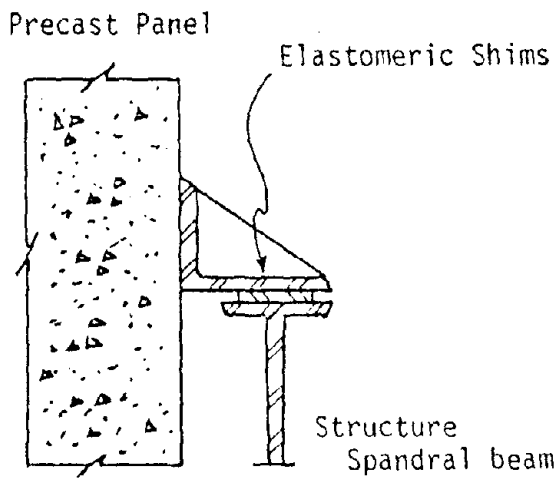
b)

Figure 2.1.4 Fixed Support Bolted Angle Connection ( Integrative )

that the UBC requirements are forcing the over-design of panels and con-
nections. On the other hand, those agencies responsible for administer-
ing the code requirements are concerned with the overall performance of
the "isolation" connections. The concerns of these agencies include:

1) brittle fracture of flexible connections;

2) slotted types rendered ineffective by movements that do not
   return the connection to the center position of the slot;

3) slotted connections not being properly aligned during construc-
   tion;

4) welded connections lacking ductility.

The experimental study of the various connection configurations was
implemented so that information on these aspects of connection behavior
could be obtained. Section 2.5 discusses the finding of the study with
regards to these concerns.

## 2.2 CURRENT DESIGN PROCEDURES

### 2.2.1 Code Requirements and Guidelines

The three principal design considerations for the fabrication and utilization of architectural precast panels are:

1) strength and deformability;

2) function and expected performance (serviceability, geometry, etc.);

3) fabrication and erection procedures.

Connections which hold the panels on the structural framework should be designed such that the proper transfer of laods is made considering:

1) safe performance under gravity, wind, and earthquake loads;

2) fabrication and erection process and tolerances, to include economic constraints;

3) protection from fire and corrosion and building water tightness;

4) architectural geometry.

With these facts in mind, the general design approach involves the solution of several basic structrual mechanics problems in order to achieve the desired performance of the individual connections. A complete discussion of the seismic load requirements and how the governing codes are affected is the primary objective of this paper; whereas the other design conditions will not be investigated.

Loads transmitted to the individual connections by seismic activity are a function of the ground accelerations experienced by the building foundation, the position of the panel on the building, the mass of

the panel, and the relative stiffness of the supporting structure.

According to Section 2312 of the latest revision of the UBC (1979), precast non-load bearing wall panel connections should be designed to resist a lateral force Fp to be applied at the center of gravity and in any horizontal direction, and is calculated using the equation;

$$Fp = Z \ I \ Cp \ Wp \ . \ . \ . \ . \ . \ . \ . \ \text{Eqn 12-8 Ref. 8}$$

where Z = numerical seismicity of the site as specified by

the seismic contour maps of UBC.

| Zone Number | 1 | 2 | 3 | 4 |
|---|---|---|---|---|
| Z Value | 3/16 | 3/8 | 3/4 | 1 |

I = occupancy importance factor, which shall be taken as 1.0 for

an entire connector assembly.

Wp = the weight of the panel.

The latest established provisions for Cp, the horizontal force factor:

Cp = .30 for the wall panel;

Cp = .40 for the body of the connector; 1-1/3 times the force

determined for the wall panel;

Cp = 1.20 for the connector fasteners; 4 times the load determined

for the wall panel.

Also from UBC (1979) and SEAOC (1973) require that for seismic loads, connections and the joints between panels accomodate the following movements not less than

1) 2.0 times the story drift caused by wind loads; or

2) 3.0/K times the seismic story drift;

3) or 1/2 inch, whichever is greater,

where K = horizontal force factor, as given by Table 23-I of

the 1979 UBC.

The current code provisions for the Cp factor are based on the assumption that "the additional design capacity of the fastener (e.g., inserts, welds, dowels, or bolts) will force any potential excess distortion to occur in the more ductile connector body (e.g., structural

Table 23.-I of the 1979 UBC

| Type or Arrangement of Resisting Elements | Value of K |
|---|---|
| 1. All building framing systems except as hereinafter classified | 1.00 |
| 2. Buildings with a box system | 1.33 |
| 3. Buildings with a dual bracing system consisting of a ductile moment resisting space frame and shear walls or braced frames using the following design criteria:<br><br>a. The frames and shear walls shall resist the total lateral force in accordance with their relative rigidities considering the interaction of the shear walls and frames<br><br>b. The shear walls acting independently of the ductile moment resisting portions of the space frame shall resist the total required lateral forces<br><br>c. The ductile moment resisting space frame shall have the capacity to resist not less than 25 percent of the required lateral force | 0.80 |
| 4. Buildings with a ductile moment resisting space frame designed in accordance with the following criteria: The ductile moment resisting space frame shall have the capacity to resist the total required lateral forces | 0.67 |

steel angle rods, or plates) rather than the more brittle fastening." (Murphy, 1971). This emphasis on the performance of the body connector has influenced the current designs toward either the use of slotted connections or flexible members having the necessary ductility to accomodate the design movement.

## 2.2.2 Flexible Connections

Flexible connections are used as a lateral support normal to the plane of the panel for the curtain wall panel. These connection bodies are often comprised of completely threaded rods, partially threaded rods, thin angle structural steel, or thin plate steel welded to anchor plates which in turn are anchored with welded Nelson studs. The panel fasteners are either ferrule inserts only, ferrule inserts with plate and Nelson studs, or just the plate and studs. Attachment to the panels, therefore, is made by bolting to inserts or welding to the plates.

The basic approach most generally used to design this type of connection is outlined in Sessa (1980). The flexible lateral connection, as seen in Figure 2.2.1, is designed to withstand gravity and seismic loads which are applied normal to the panel surface.
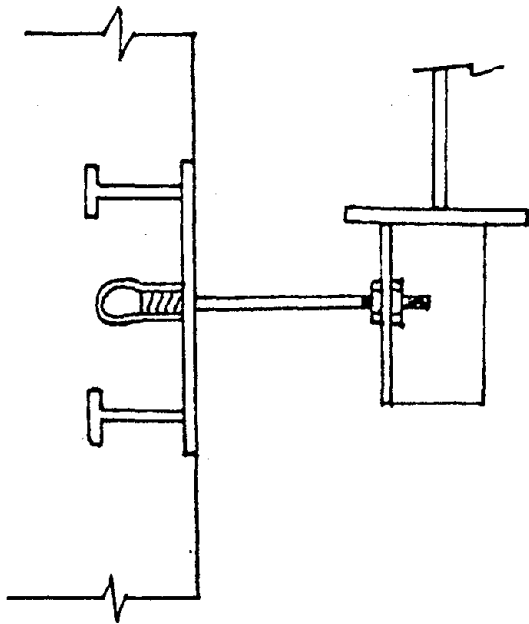


Figure 2.2.1.  Flexible lateral connection.

The approach then is to define the critical combination of loads and design the panel fastener, connection body, and structural fasteners accordingly.

### 2.2.3 Slotted Connections

Slotted connections are used as a lateral support for the curtain wall panel as are flexible connections. The only real difference between the two types is that the slotted connection (which is a very popular type among structural engineers today) eliminates the need for designing flexibility and ductility into the connector body. All movement of the structural frame is accommodated by the free travel in the plane of the panel as provided by the slotted holes. Slotted holes are used with various types of structural angles, tees, and plate steel, with angles being the most widely used.

The design of the angle with the slotted holes provided for freedom of movement, is straight forward in that only loads normal to the panel need careful attention. There is no load in the connection in the horizontal or vertical direction in the plane of the panel. Therefore, the approach in designing this type of connection is to, first, define the panel displacement that the connections must accommodate and second, to identify the normal design load and third, to solve for the appropriate panel fasteners, connection body, and structural fasteners.

### 2.2.4 Bearing Connections

The support connection is that connection (usually two per panel) which is used to support the gravity loads of the panel and consequently

it must serve to transfer forces from the panel to the structural framework. This is the most complex of connections to design in that the loads applied are the most severe and translation and rotation of the panel must be restricted in all directions at this point.

The procedure, therefore, is similar to designing a flexible connection in that critical design loads must first be identified in the normal direction as well as vertically and horizontally in the plane of the panel. Additionally, these loads must be accommodated while movement is constrained for the most part. (Some designs allow some displacement through elastomeric pads, etc. to accommodate minor movements.) Again, once the critical loads are identified, each part of the connection from panel reinforcement to structural steel framework attachment must be analyzed for proper transfer of forces.

## 2.3 EXPERIMENTAL STUDY

### 2.3.1 Connection Description

An extensive array of connection configurations was tested during
the program. The four basic inserts used as fasteners on the precast
panel were tested in three sizes. These inserts were tested with and
without face plate steel to identify any possible advantages for either
configuration. Threaded bars were used as the connection body during
the loading of the block-insert test specimens. Photos 2.3.1 and 2.3.2 depict
a typical insert-threaded bar connection configuration. Table 2.3-1
lists the insert types, sizes, and indicates those also tested with face
plates. Ferrule inserts with threaded bars spanning from panel to
structural framework is a standard flexible connection of the industry
which are used as the lateral support for the tops of panels.

Table 2.3-1   List of Bar Insert Connections Studied

| Insert Type | Size (without plate) | | | Size (with 1 in. thick plate) | |
| --- | --- | --- | --- | --- | --- |
| Ferrule loop | 1/2" | 3/4" | 1" | 3/4" | 1" |
| Wing nut | 1/2" | 3/4" | 1" | 3/4" | 1" |
| Thin slab | 1/2" | 3/4" | 1" | 3/4" | 1" |
| Four strut | 1/2" | 3/4" | 1" | 3/4" | 1" |

Structural steel angles are utilized as "dissociative" connections
when slotted holes are employed and as "integrative" connections when

either they are bolted tightly in place an/or they are welded directly

to the face plate poured in the panel and to the structural framework.

A dissociative connection is one which allows the structural and archi-

tectural systems to behave independently.   An integrative connection is

one which allows the structural and architectural systems to jointly

participate in resisting movement during the seismic event.   Table 2.3-2

indicates the sizes and  and thicknesses of the structural angles tested,

and the type of panel configurations used.

Table 2.3-2   List of Angle Connections Studied

| Angle Size<br><br>$L_1$ x $L_2$ x t | Two 3/4 in.<br>Inserts Only | Two 3/4 in.<br>Inserts<br>and Plate | 3/8 in. Fillet<br>Welded to<br>Plate |
|---|---|---|---|
| 4 x 6 x 3/8 | X | X | X |
| 4 x 6 x 1/2 | X | X | X |
| 4 x 6 x 5/8 | X | X | X |
| 6 x 8 x 1/2 | X | X | X |
| 6 x 8 x 3/4 | X | X | X |

Each angle size was tested as an "integrative" type by torquing down the

bolts and by welding to the plates.   Also, each angle size was tested as

an associative type by using slotted holes.   Photos 2.3.3 and 2.3.4 show the

three mounting blocks and slotted type angles, respectively.

Photos 2.3.5 through 2.3.12 clearly show the pre-casting configurations of

each insert type and the structural steel angle fastening systems.   The

industry standard for anchoring face plates is by welding Nelson studs

to the plates or by welding rebar bent to meet the plate.   The use of

rebar was chosen over Nelson studs because the purpose of the study did

not dictate a need to test either system specifically and the rebar was
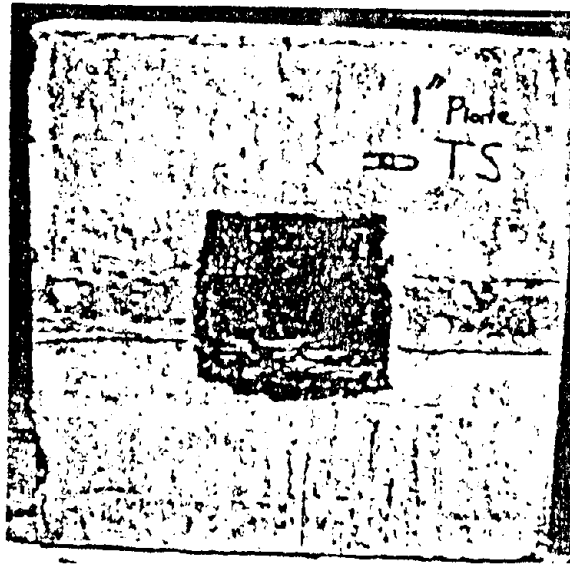
Photo 2.3.1 Insert Test Block with Plate
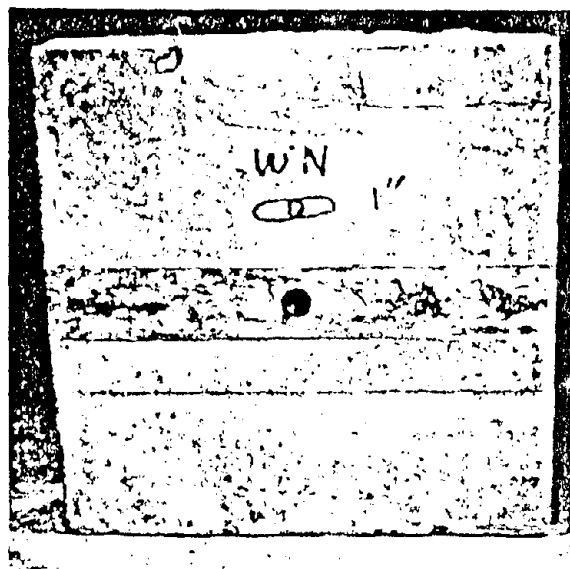


Photo 2.3.2 Insert Test Block without Plate
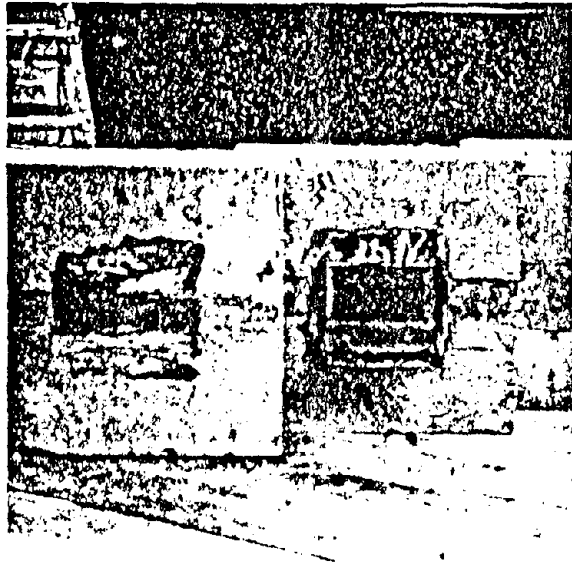
Photo 2.3.3   The Three Mounting Blocks for Testing Angles
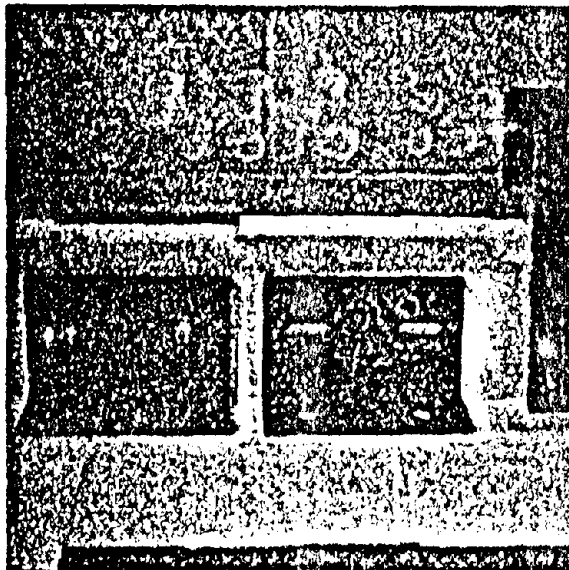


Photo 2.3.4   Typical Angles Tested
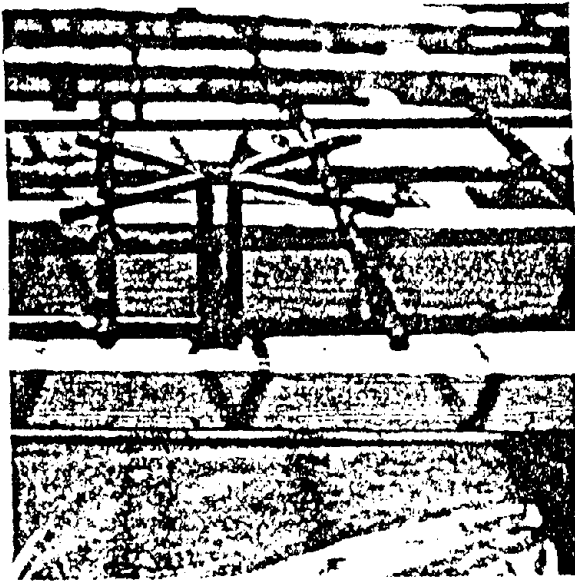
Photo 2.3.5  Four Strut Insert
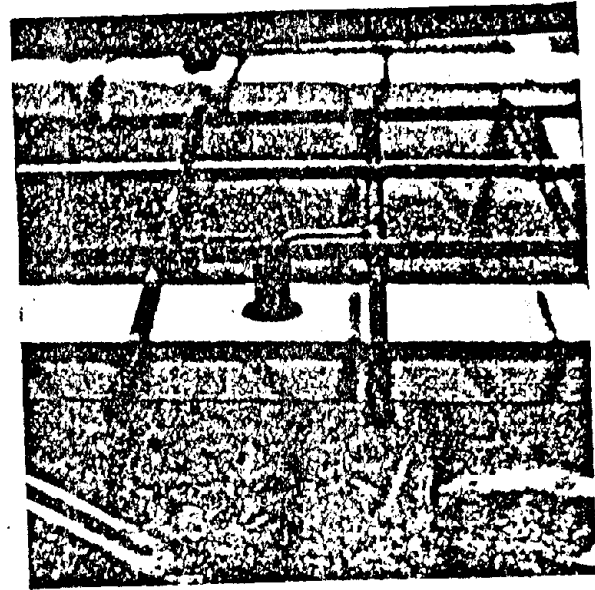


Photo 2.3.6     Wing Nut Insert



Photo 2.3.7  Loop Insert
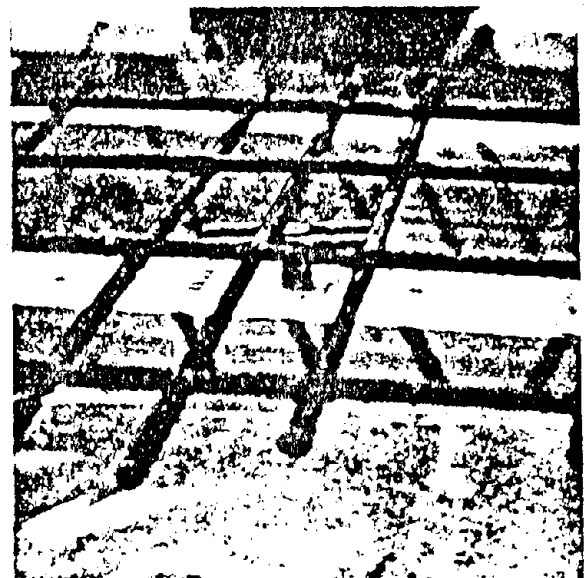


Photo 2.3.8  Thin Slab Insert
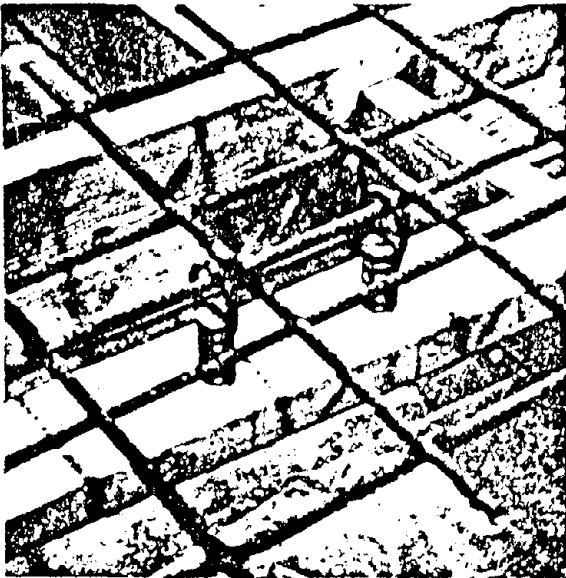
Photo 2.3.9   Inserts for Structural
Angle Mounting
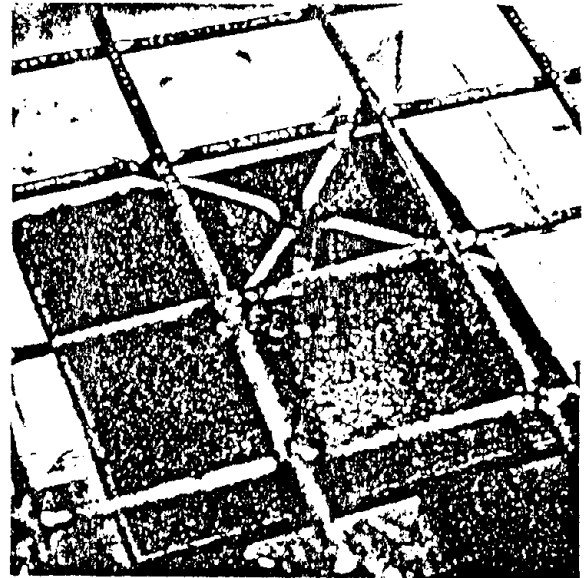


Photo 2.3.10   Four Strut Insert with
Steel Plate
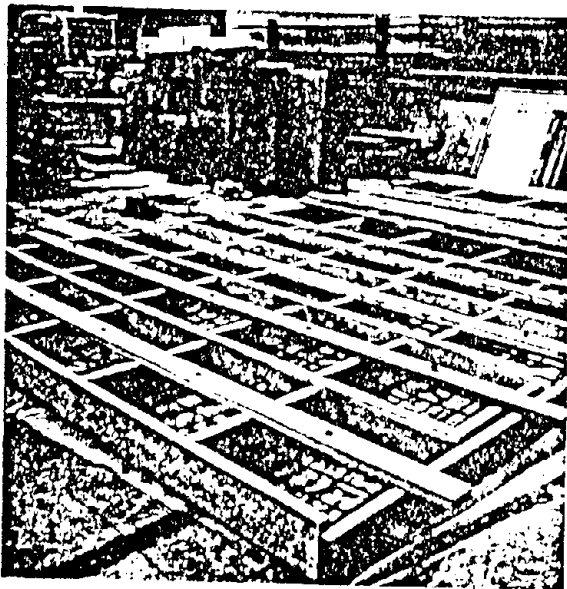


Photo 2.3.11   Precasting Forms
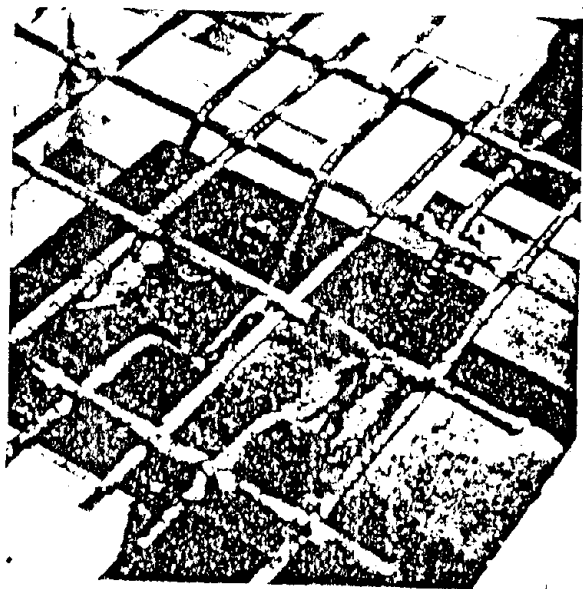


Photo 2.3.12   Anchored Plate

easier to work and was readily available.

Photo Series 2.3.5 through 2.3.12 also contains details of the pre-cast rebar, insert, and plate setups for those blocks used to test the various angles shown in Table 2.3-2. All angles tested were 9 inches long and the holes were centered 5 inches on center as shown in Figure 2.3.1
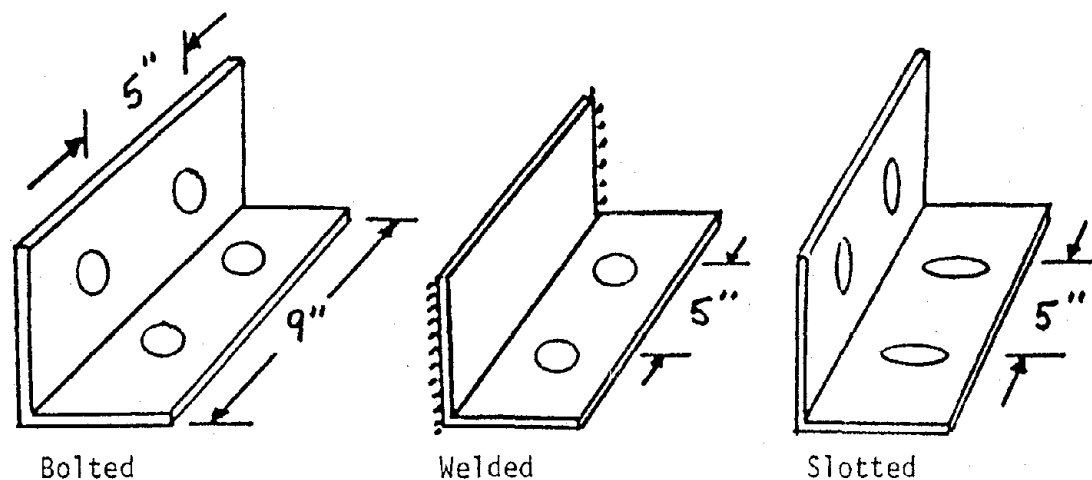


Figure 2.3.1    Typical Angles Tested

## 2.3.2 Testing Equipment

The objectives of this study dictated a need for equipment for material handling, load application, and data recording. The procedures established for obtaining the load displacement and energy dissipation data set the equipment requirements. The investigator also used the University's existing MTS equipment (manufactured by the MTS Systems Corporation) for load application and the Vishay digital strain indicators, dial gauges, voltmeter, and the X-Y plotter incorporated into the

MTS system for data acquisition.

The material handling equipment which was used to move the 300 pound concrete test specimens into position on the connector reaction frame was built by project help. The connector reaction frame was also designed and built by the project. The civil engineering lab contains 18 in. x 16 in. x 1 in. built up box section rigid frames built into the wall and floor system. The connector reaction frame was bolted to the south wall box member.

The reaction frame which was designed and built before the concrete test specimens were fabricated was given the necessary adjustability and strength to accept and hold various size connection test blocks. Figure 2.3.2 shows the frame dimensions and material specifications. Photo 13 shows the entire frame assembly. The frame was made capable of accepting blocks ranging in size from 20 in. x 20 in. x 1 in. to 26 in. x 26 in. x 16 in. The vertical load capabilities of the MTS actuator system was 6.5 kips and the frame therefore was built to withstand this amount of load with negligible deflection. The mechanism used to hold the blocks in place is shown in Photo 2.3.14. This hold down plate was brought to bear on the concrete by tightening down the four 1/2 in. x 4 in. bolts threaded through the clamped angle.

The procedure for installing a test block in the reaction frame is as follows:

1. Loosen the 3/4 in. bolts of the base on the reaction frame and lower the base with the 1-1/2 ton hydraulic jack as shown in Photo 15.
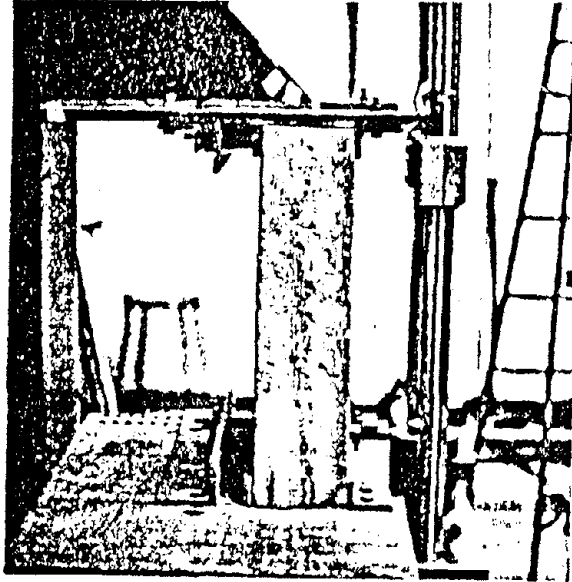
Photo 2.3.13 Connector Reaction Frame
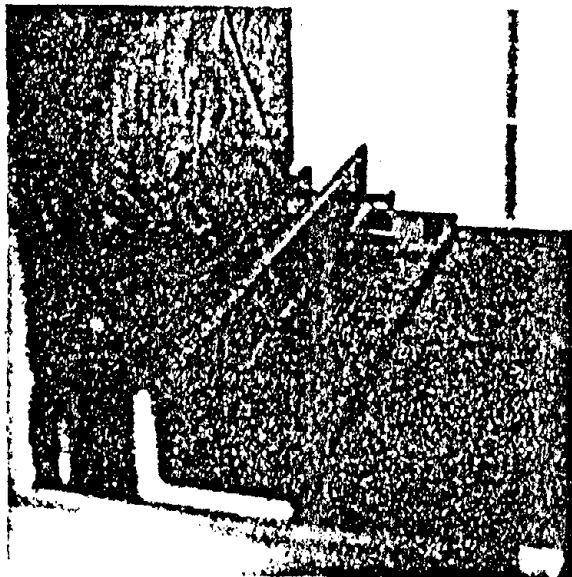


Photo 2.3.14 Adjustable Clamp Mechanism of the Reaction Frame

1/2" Gusset Plates

3/4" Plate

1/2" SAE Bolts

1/2"x2"x24"

3" x 2" x 1/2" L

Holes are drilled and

tapped for the 1/2"x 13

course threaded bolts.

Building
Reaction
Frame

3/4" Plate

3" X 3" X 1/2" L (spans from one

side to other)

Side View
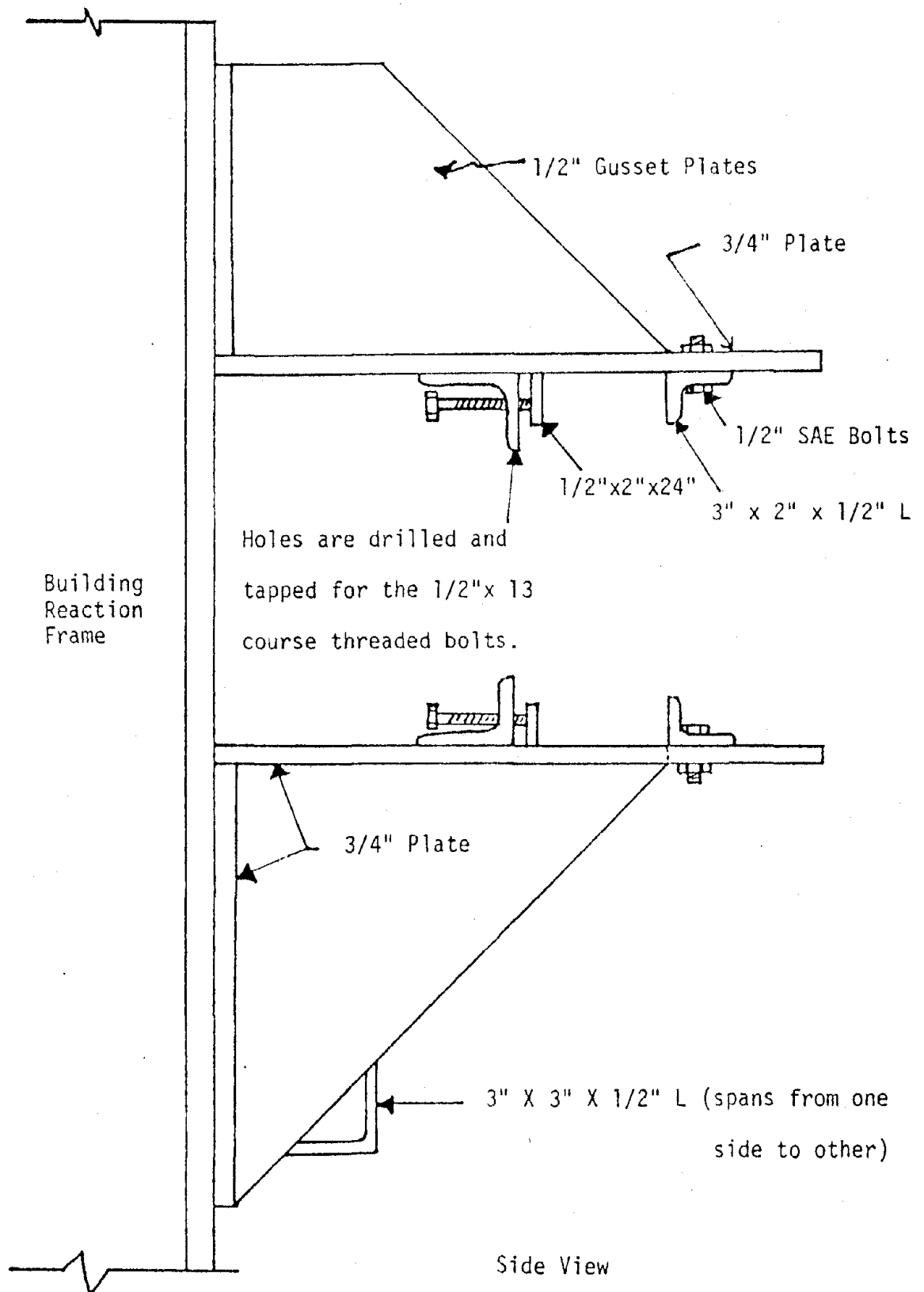
Figure 2.3.2   Connection Reaction Frame

16"

11.5"

3/4" Bolts

14.5"

18.5"

3/4" Bolts

3 in. X 2 in. X 1/2 in.
Structural Angle

Building
Reaction
Frame

Note: The bottom half
of the frame is not
shown here.

24"

Front View
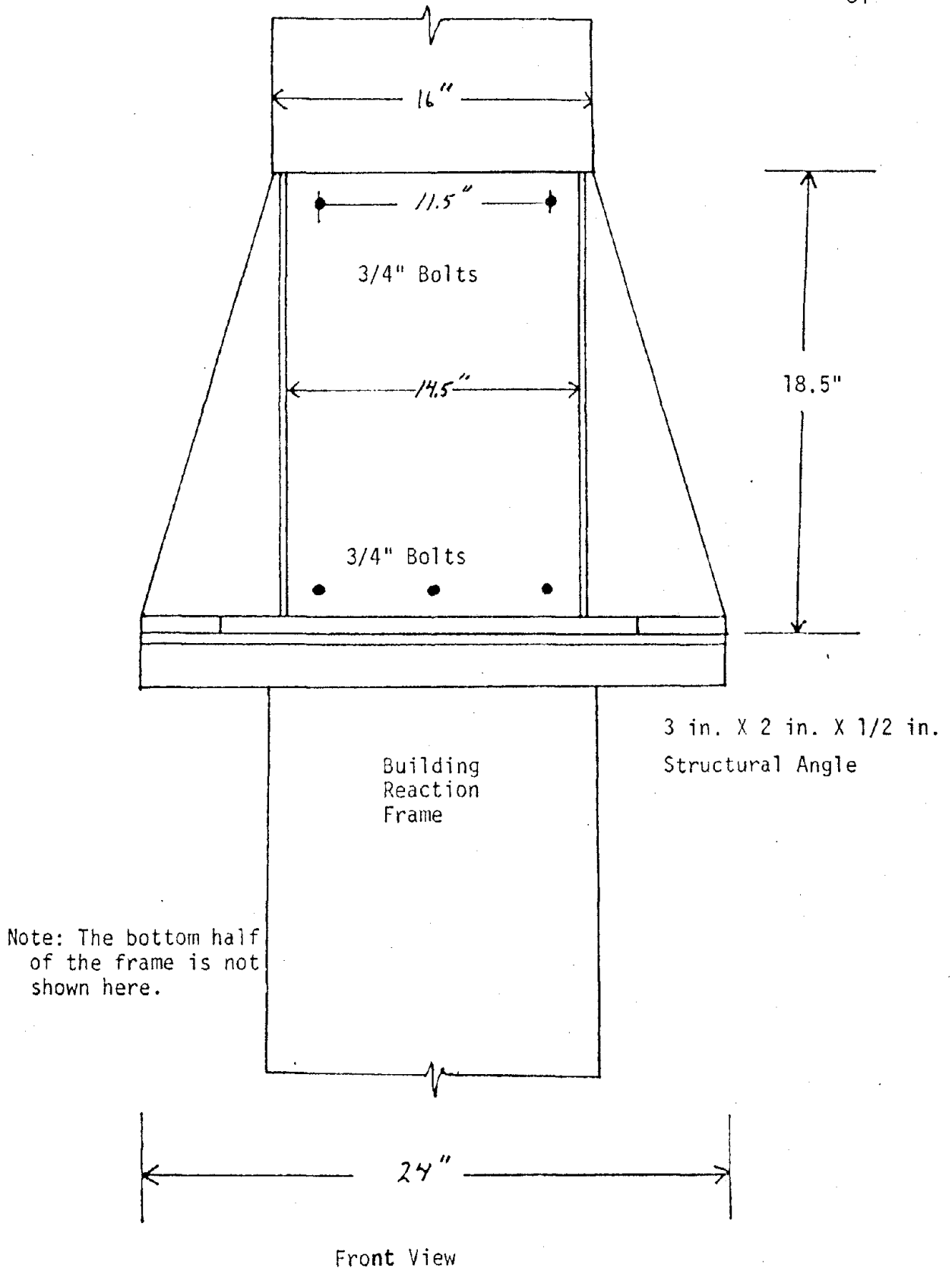
Figure 2.3.2 Continued
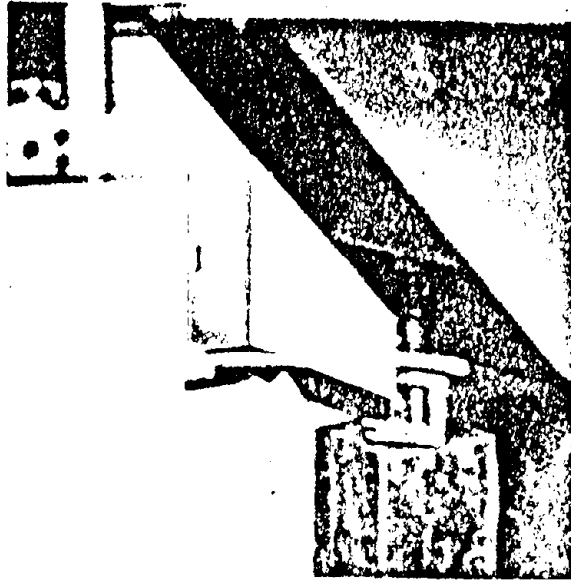
Photo 2.3.15  Lower Base of Reaction Frame
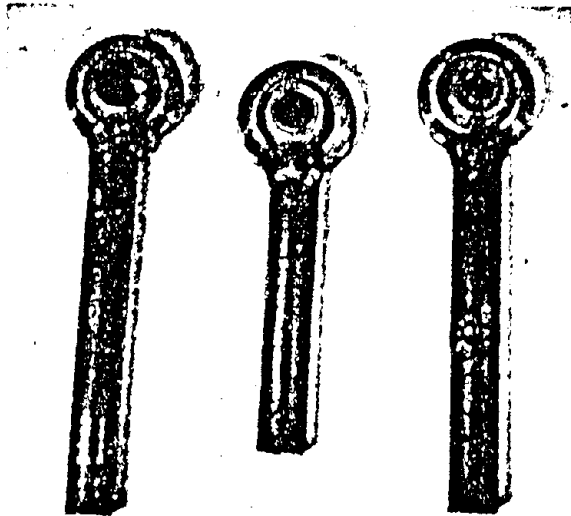


Photo 2.3.16   Pinned End Load Applicators

2.  Raise the block up to the base level via chain hoist, and slide into the frame.

3.  Center the block and tighten the bottom clamp against the block.

4.  Jack up the block and base to meet the top half of the frame as tightly as possible without cracking the block.

5.  Tighten the top clamps securely.
With this procedure completed, the block is ready to receive the connector body and begin the testing procedure.


In order to obtain the desired load-displacement information for connections which are pinned at the structural framework and also for those that are fixed at the supporting structure, special adaptors had to be designed and fabricated for the MTS actuator. The pinned effect was obtained by using ball swivel joints in three sizes (1/2 in., 3/4 in., and 1 in.) for the three sized bars used as connector bodies. A "Weld-on" ball socket was welded to a short length of threaded rod for attachment to the MTS load cell. Press fit bushings were used to obtain the three sizes of adaptors. Photo 2.3.16 shows each of the three swivel joint assemblies with bushings in place. See Figure 2.3.3 for detailed drawings of each adaptor.

To obtain the fixed end effect at the load point on the bar-insert connector test, two different assemblies were designed and fabricated. The first assembly was used to load the 1/2 in. and 3/4 in. bars and the second assembly was used to test the 1 in. bars and then used to check data which was collected using assemly one on the 1/2 in. and 3/4 in.

LOAD ADAPTOR MECHANISMS FOR THE MTS



BUSHING

1/2" Bar Adaptor          3/4" Bar Adaptor          1" Bar Adaptor
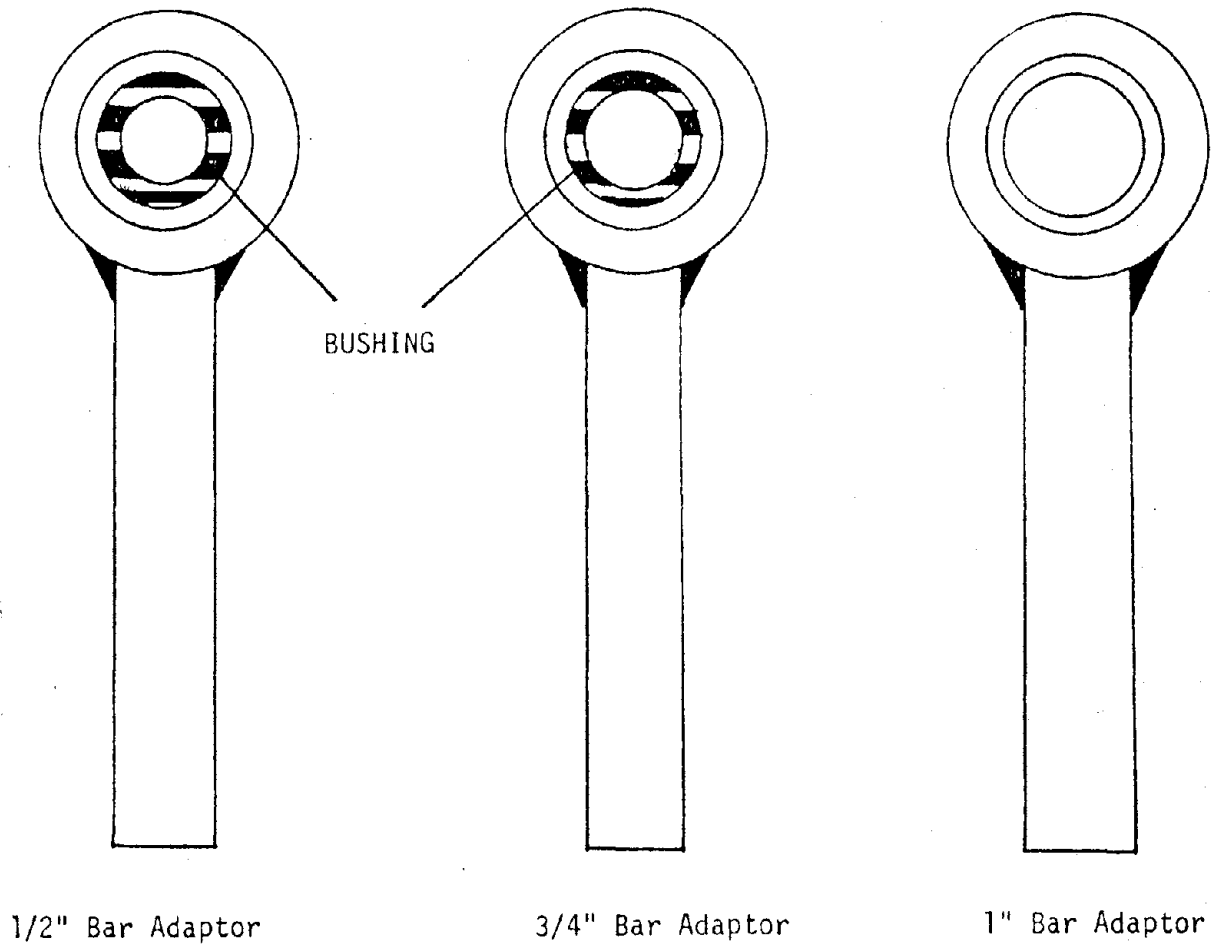
Figure 2.3.3a   Pinned End Load Adaptors
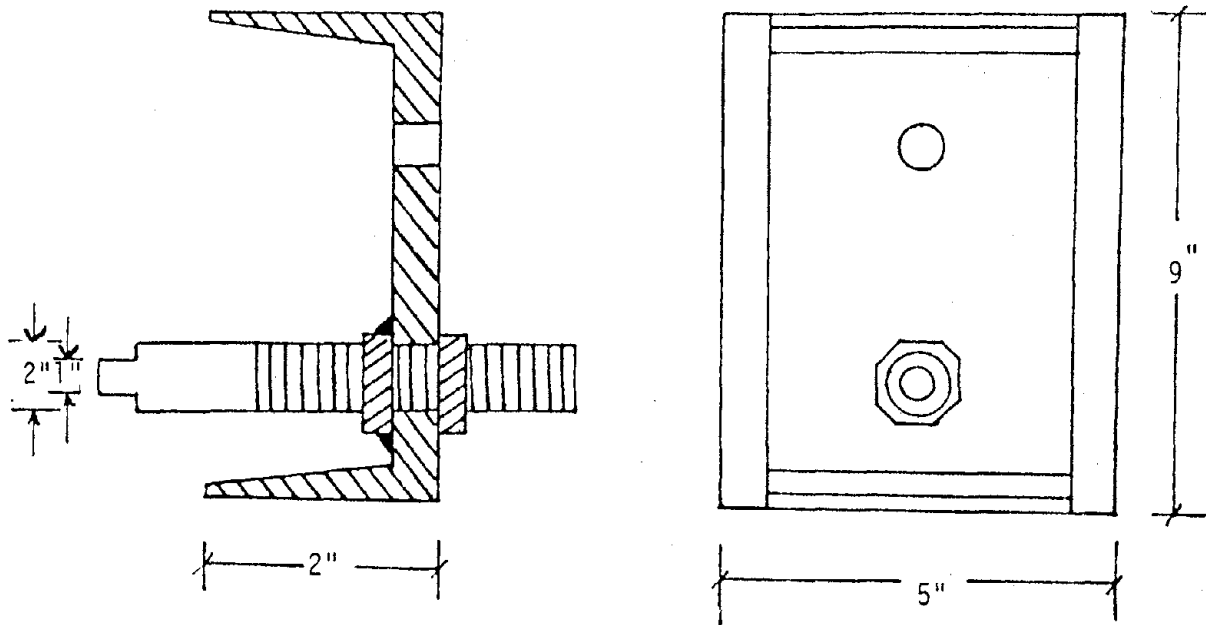
2.3.3b   Fixed End Load Adaptor #1
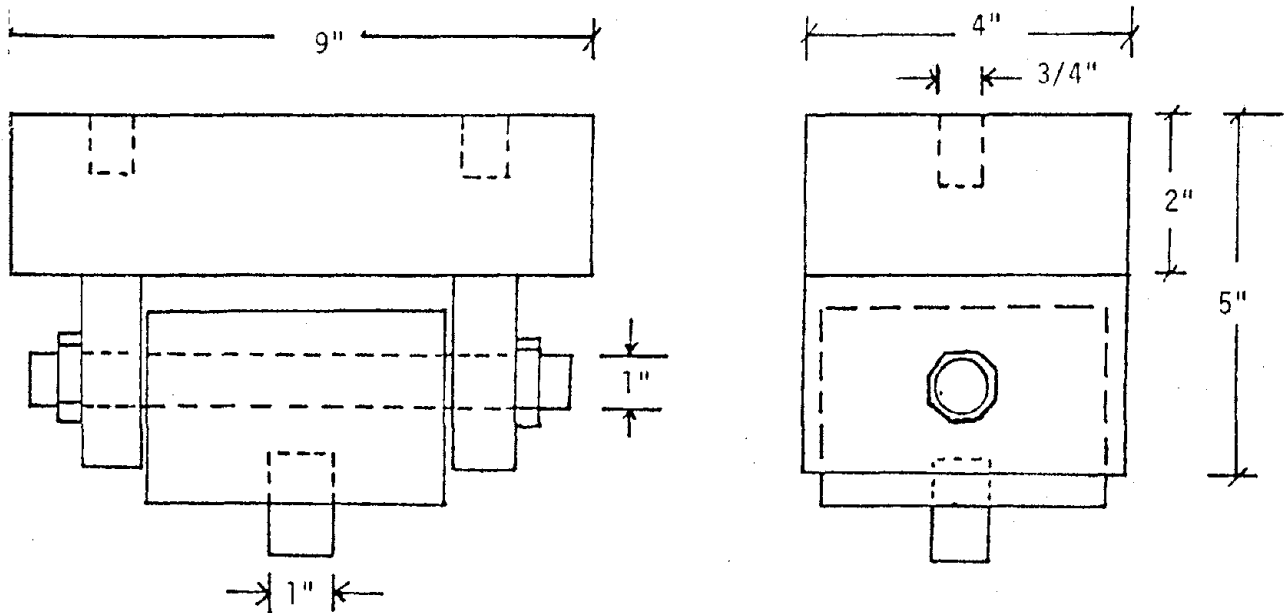
Figure 2.3.3c

bars. Photo 2.3.17 shows the two assemblies. Figure 2.3.3 contains detailed drawings of each. The need for a simple easily mounted adaptor dictated the use of the lever arm system to induce a moment on the threaded bar at the point of loading equal in magnitude and opposite in sign to accomplish fixity.

Adjusting the length of the lever arm, as shown in Figure 2.3.4, the researcher was able to match the fixed end moments within the bar. Exact end moment parity was not necessary for obtaining the load-displacement data, however, care was taken to get them as close as possible to simulate maximum possible fixity.



If $\bar{x} = \ell/2$, then

$$m_1 = P\ell - \bar{x}P = P(\ell - \bar{x})$$
$$= P\frac{\ell}{2}$$
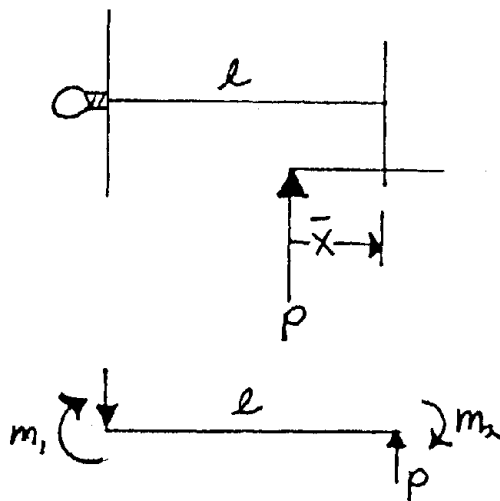
$$m_2 = \bar{x}P = P\frac{\ell}{2}$$

Figure 2.3.4   Fixed End Load Application System

For the tests involving the various structural angles, a load application adaptor was fabricated as shown in Photo 18. This mechanism was designed to produce only normal vertical loads with negligible moment induced to the MTS actuator. (MTS actuators are designed to withstand only axial loads.) Although this mounting system was fabricated in order
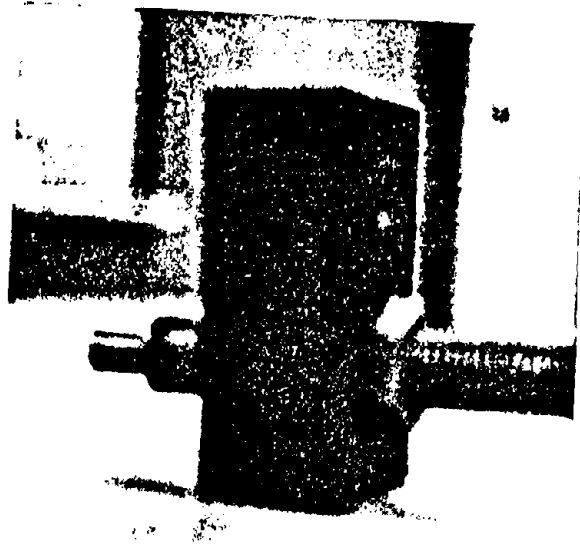
Photo 2.3.17 Fixed End Load Applicator #1



Photo 2.3.18   Structural Angle Load Applicator

to test the angles, it proved useful in testing the bar connections.
(It was the base for assembly 2 used to test the 1 in. bar-insert panels.)
It was a more stable and repeatable testing mechanism and was chosen over
the original fixed end adaptor to complete the bar test for those reasons.
See Photo 2.3.19.   Figure 2.3.3b provides a detailed drawing of the setup.
When the experimental study reached a point where the angles were too
large for the MTS actuator to load to their yield point, an extension
was installed on the angle to gain the necessary mechanical advantage.

The MTS actuator had to be held down in order to be able to
reverse loads in any of the tests.  A piece of channel (4 in. x 2 in.)
was welded to the floor box section.  The channel had two sets of slotted
holes in which 3/4 in. x 6 in. bolts were slipped through before the
welding occurred.  Two S shaped sections (3 in. x 4 in.) with 1/2 in.
plates welded on one side (see Photo 2.3.20) were used to span between the
actuator base legs, and were bolted down with the two 3/4 in. bolts from
the channel.  This system showed no upward movement of the actuator
during the tests (as indicated by a dial gauge indicator graduated in
thousands of an inch).  These hold downs were used primarily during the
cyclic tests, the static tests were all conducted in a positive vertical
force method.

## 2.3.3 The Test Procedure

The test procedure used for this study was determined by the type
of connection that was being tested and what type of test that was being
conducted.  The various experimental procedures used are difficult to
comprehend without listing each of them in a step-by-step manner.  The
discussion here will therefore be general in nature with Sessa (1980).
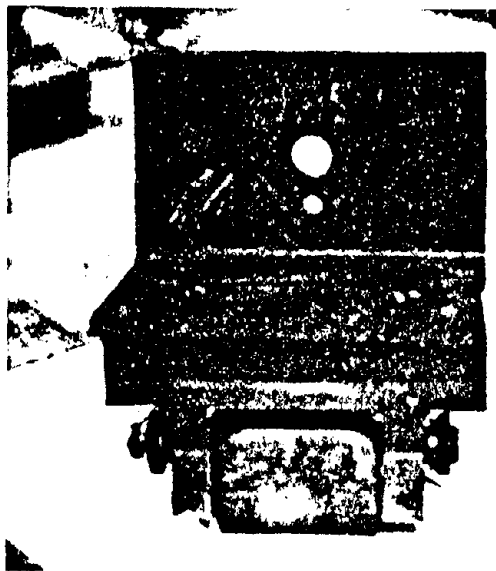
Photo 2.3.19 Fixed End Load Applicator #2
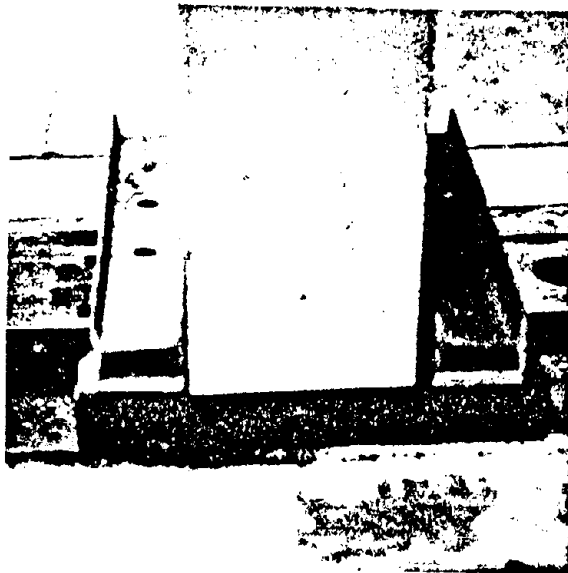


Photo 2.3.20 Hold Down Assembly for MTS Actuator

providing detailed notes on the step-by-step methods used throughout

the data collection phase of the program. Also, Sessa (1980)is provided

in such detail so that repeating the test procedure exactly would be

feasible.

In the beginning of the testing program it was decided that each

bar connection would be loaded vertically in a pinned end static mode

at points 3 in., 5 in., 7 in., and 9 in. from the concrete panel surface.

A typical x-y plot from the MTS system is shown on Figure 2.3.5. Note

that only one load application is done at each point. It was originally

thought that this would provide the accurate characteristic load dis-

placement curves needed. This procedure was used for all of the 1/2 in.

bars and a few of the 3/4 in. bars. Subsequently, tests were repeated

three times at each length to ensure an accurate repeatable performance.
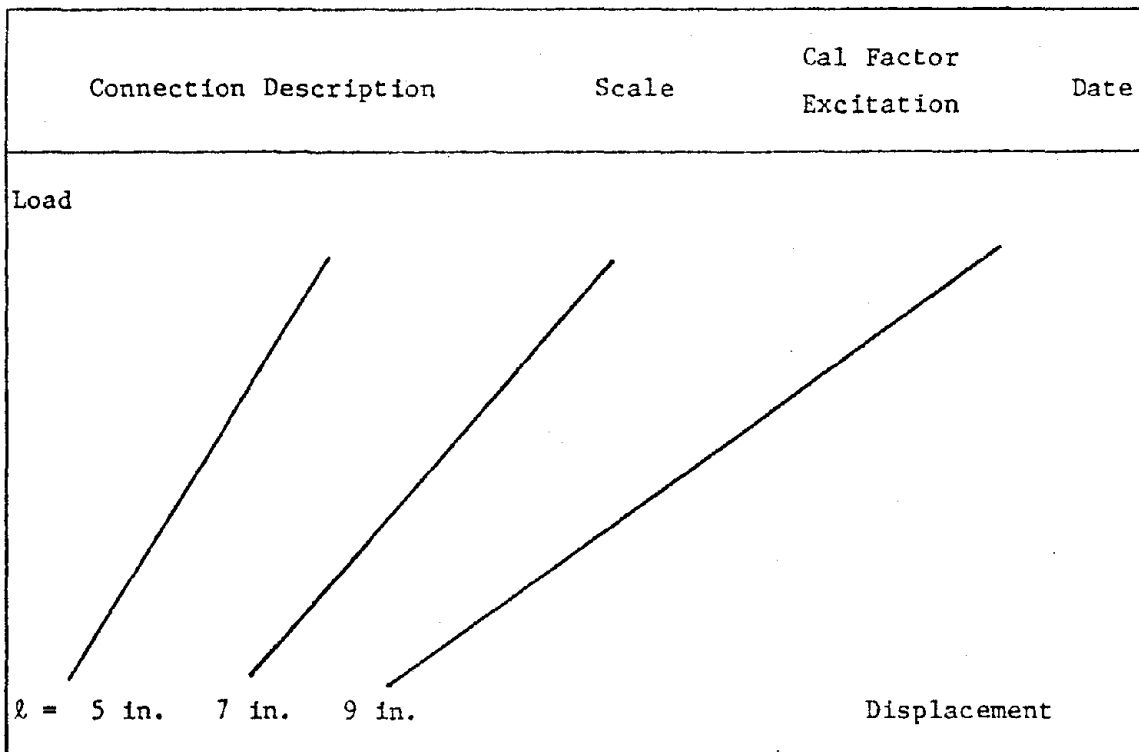


Figure 2.3.5. Facsimile of the MTS X-Y Plot of Load-Displacement

Calibration of the MTS was accomplished with a voltmeter, a known value load ring, and the x-y plotter of the MTS. Appendix C includes the calibration procedure used and the results for later reference.

The loading sequence for each insert-bar test block was as follows:

1. Static load to a predetermined set point (% of theoretical yield) for each pinned end loading at lengths 3 in., 5 in., 7 in., and 9 in. on one chart.

2. Static load past the yield point for lengths 7 in. and 9 in. pinned end. (Also on the same chart as 1.)

3. Static load to a predetermined set point (% of theoretical yield) for fixed end loading at lengths of 7 in. and 9 in. on the second chart.

4. Static load past yield point for lengths 7 in. and 9 in. Also on the second chart.

5. Clamp down the MTS actuator and run cyclic tests at 2 cps with the loads 10% past the yield point and with fixed displacements.

(Note: This was done only for selected test specimens when it became apparent that this was a very time consuming procedure and that the MTS had very marginal cyclic load capability for the frequency and the large displacements necessary for the flexible connections.) A detailed description of the cyclic loading procedure may be found in Sessa (1980).

The procedural loading sequence then became steps 1 through 4 only, with step 5 postponed until all static tests were completed. The only changes made on this sequence as the program progressed was that each test was done three times to ensure a repeatable load application.

During the load application for each bar strain measurements were recorded in order to insure repeatable performance of the test specimen and to compare with the theoretically predicted stresses. During the 1/2 in. bar tests, electrical strain gauges were installed on each bar and the yielding of the bar during the second test required the installation of new gauges on new bars for each set of tests. In order to save time and money, as well as to improve the data gathered, it was decided to use the same bars with gauges installed for all elastic range tests. This meant that only six bars of each size would need to be instrumented with gauges. Those test specimens that were loaded past their yield point were not instrumented. The data received from such tests (the yield point and post-yield stiffness) did not require strain readings for further comparisons. The six bars used for each size of insert tested were:

1. Number one, for testing specimens without steel face plate and pinned end load application.

2. Number two, for testing specimens having steel face plates of various thicknesses and pinned end load application.

3. Number three, for testing specimens without steel face plates and fixed end load application. (9 in. bar length)

4. Number four, for testing specimens having steel face plates and fixed end load application. (9 in. bar length)

5. Number five, for testing specimens without face plate steel and fixed end load application. (7 in. bar length)

6. Number six, for testing specimens having face plate steel and fixed end load application (7 in. bar length)

The object of using these same six bars for each sized insert was to be able to attribute any significant variations in load-displacement curves to the insert itself and not the bars. The reason for loading each bar length at leat three times was to make certain that the load application adaptor was performing the same function each time.

During the calibration runs using the load cell and LVDT Of the MTS system, it was found that for various settings of the calibration factor and excitation controls the chart print out (x-y plot) was different for the same loads and displacements. The excitation and calibration factor settings were recorded on each chart and the appropriate correction factors were employed to generate the accurate load and displacement values necessary to obtain the stiffness coefficients. A voltmeter was used to read the output electrical signal from the MTS load cell directly. These values were recorded for each load sequence in order to check the x-y plots for accurate load representation. Dial gauges were placed on the MTS at the point of loading in order to check the corresponding deflections produced by the applied loads. The voltmeter readings and the dial gauge recordings served as a check for the MTS print out obtained on the x-y plotter.

The tests run on the structural angles were conducted in the same manner as those for the bars. The only significant difference being the actual loading sequence and the adaptors used to apply the load. The dial gauges and voltmeter were used to check MTS print outs as in the case of the bar tests.

Figure 2.3.6 is provided to illustrate the layout of the test equipment, in a simplistic form, as it was used for the duration of the

Connection Load Assembly                MTS Console

Strain Indicator and Switching Box
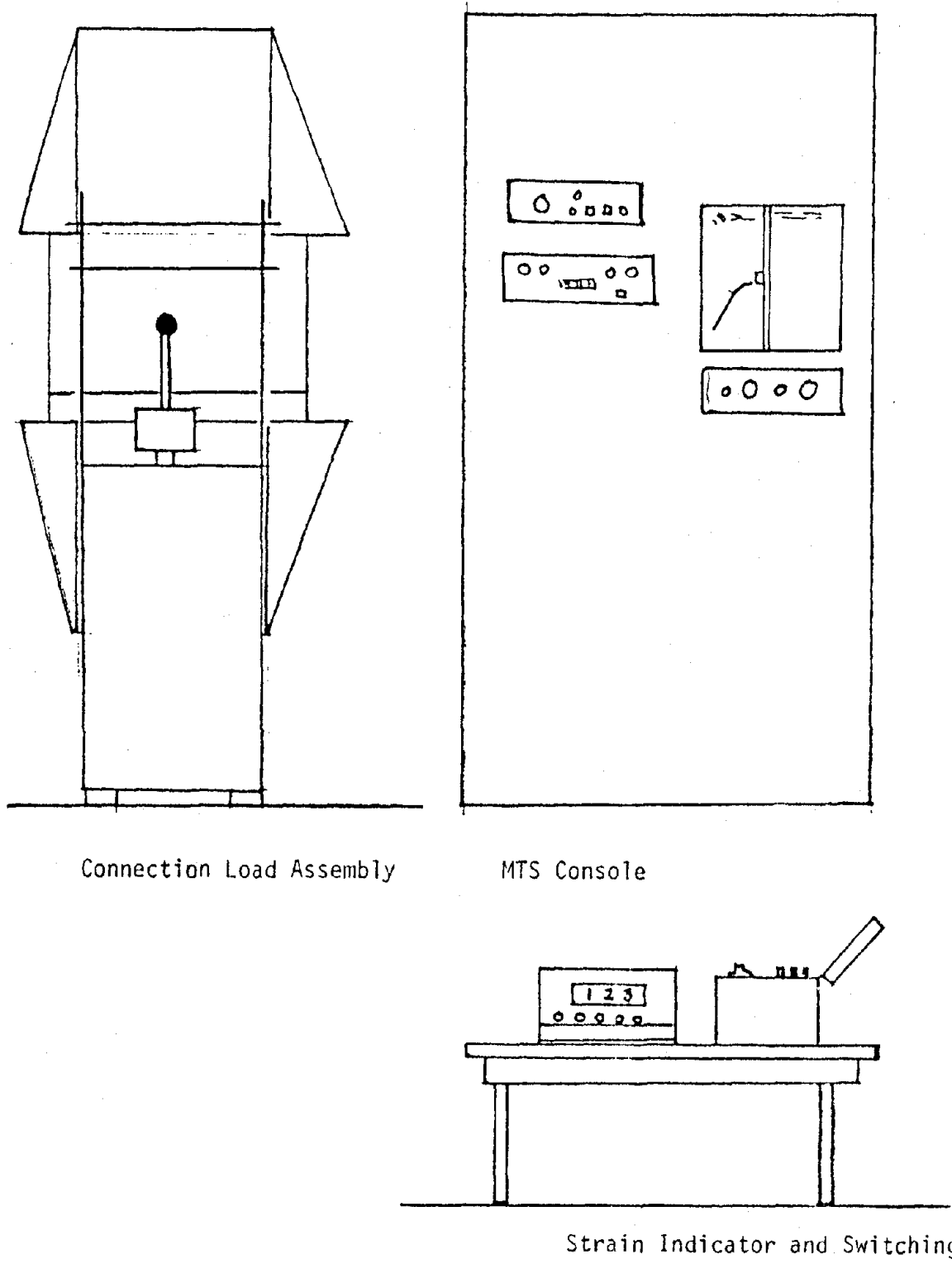
Figure 2.3.6  Layout of the Test Equipment

experimental study.

## 2.3.4 Results of the Experimental Study

The results of the study are presented for the three basic types
of connections tested; the bar-insert connection, the slotted structural
angles, and the welded and bolted structural angles. Sessa (1980) lists
the following information in tabulated format:

1) ferrule insert specifications; and connection hardware
   specifications;

2) the concrete compressive strength cylincer test results;

3) recorded strain readings, for those tests in which gauges
   were used;

4) loads and displacements for each connection tested statically;

5) yield points of each connection loaded past the yield point;

6) the pre-yield and post-yield load-displacement coefficients.

## 2.3.4.1 Bar Insert Connections

The bar-insert static tests showed that the stiffness coefficients
for a particular connection depends on the following:

1) the unbraced length of the connection body, as measured from
   the concrete panel fastener (at the surface of the panel) to
   the fastened point on the structural frame;

2) the moment of inertia of the connector body;

3) the degree of fixity at the point of attachment to the struc-
   tural frame.

Figure 2.3.7 is a normalized plot of the elastic stiffness coefficients
versus the $\ell/d$ ratios for each of the inserts tested with pinned end load

application. Figure 2.3.8 is the plot of the elastic stiffness coefficients versus $\ell/d$ ratios for each of the inserts tested with fixed end load applications. The shape of these plots can be seen when it is realized that

$$\delta \propto \frac{PL^3}{EI}$$

and for a circular section

$$I \propto d^4$$

hence

$$K = \frac{P}{\delta} \propto \frac{Ed^4}{L^3}$$

and

$$K/d \propto \left(\frac{d}{L}\right)^3 .$$

The effect of the $\ell/d$ ratio on the stiffness coefficient is most obvious in the range of $\ell/d$ between 5 and 10 for the pinned end configuration, and between 10 and 15 for the fixed end configuration. The effect of the panel insert type on the stiffness for given size connection is minor when comparing various types of ferrule inserts. This effect is minimum due to the similarity of dimensions for a given type and size of fastener. In Figure 2.3.9 the shaded area between the pinned end curve and the fixed end curve is where the elastic stiffness coefficients for most conventional bar-insert connections will be located. Those inserts which obtain greater fixity at the panel and structure attachments may have stiffness coefficients greater than those found in this experimental study. The post-yield or inelastic stiffness coefficients are plotted for various $\ell/d$ ratios in Figure 2.3.10 for the fixed and pinned end load application. This data indicates that the post-yield
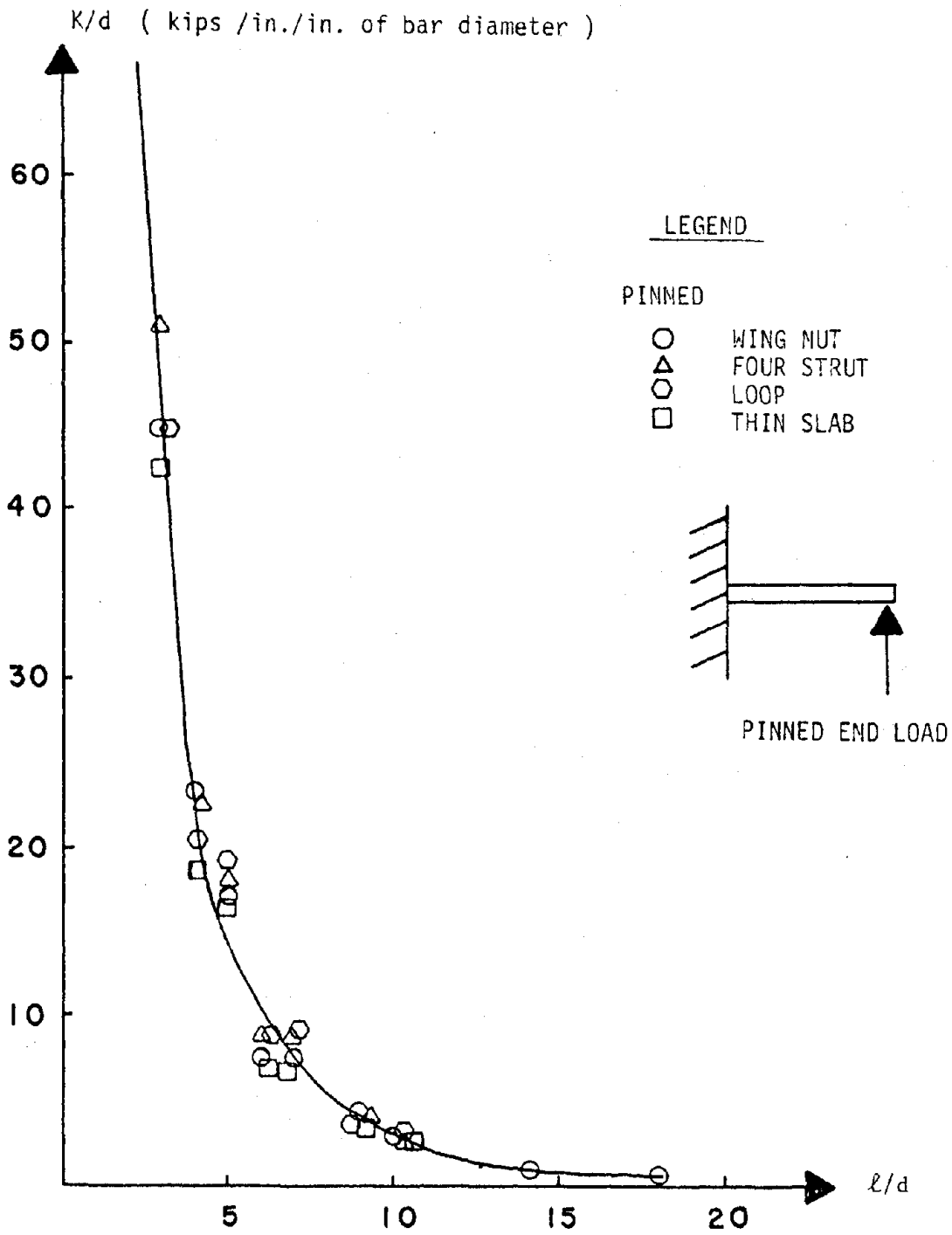
Figure 2.3.7 Elastic Stiffness Coefficients for (Pinned End) Bar-Insert
Connections, Experimental Results
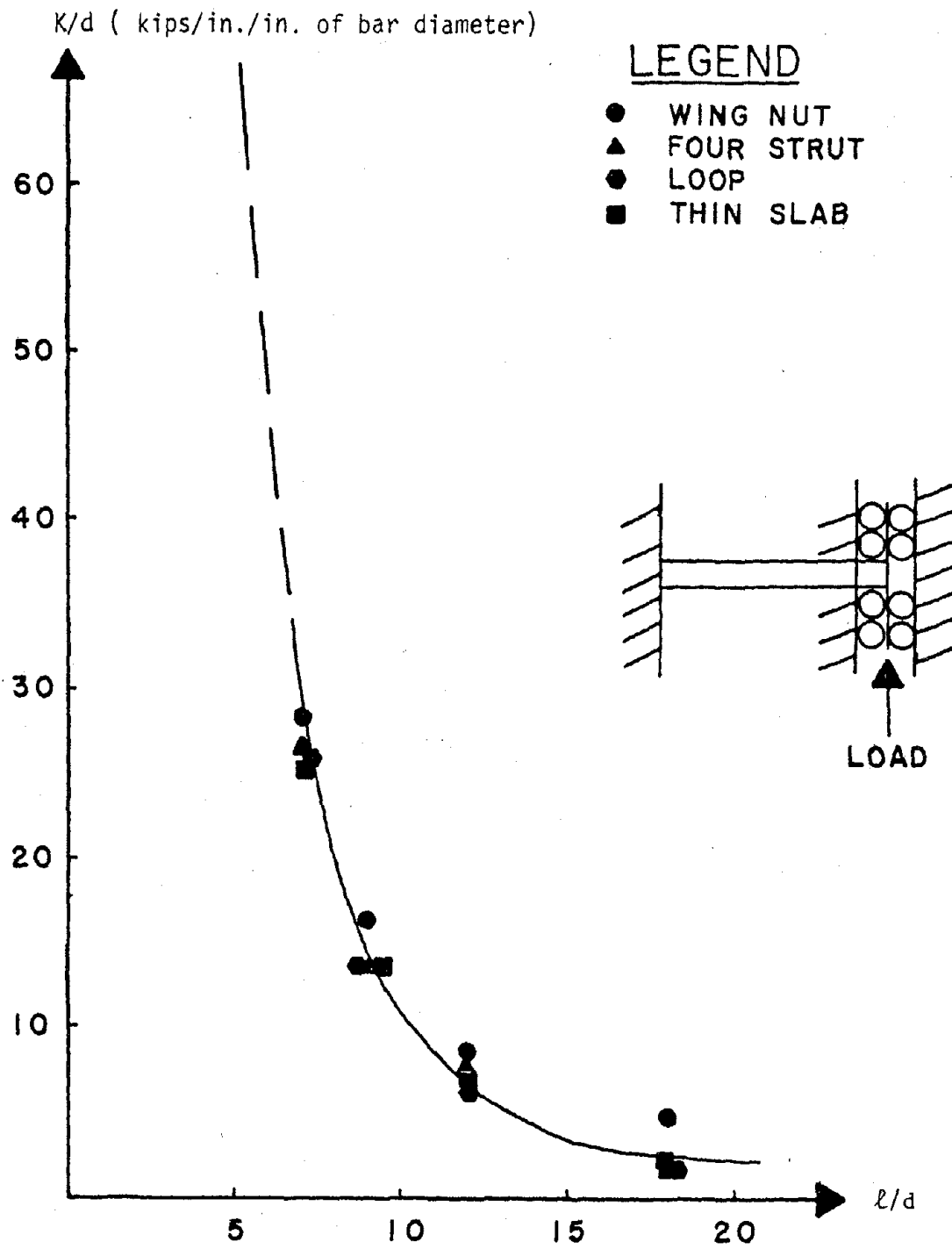
Figure 2.3.8 Elastic Stiffness Coefficients for Bar-Insert
        Connections without a plate, experimental results.
        (Fixed end)
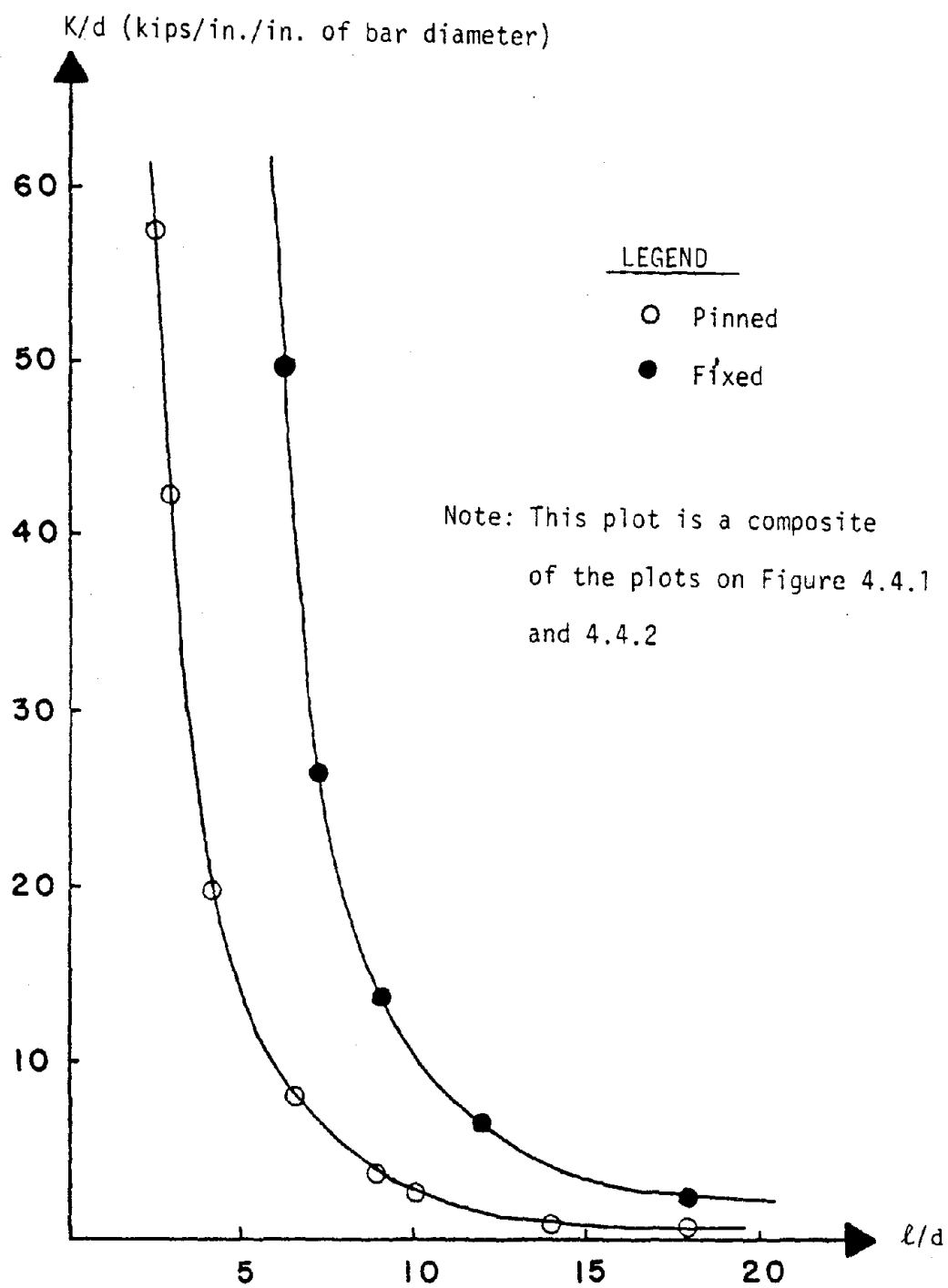
Figure 2.3.9 Comparison Plot of Fixed and Pinned End Elastic
Stiffness Coefficients, Experimental Results
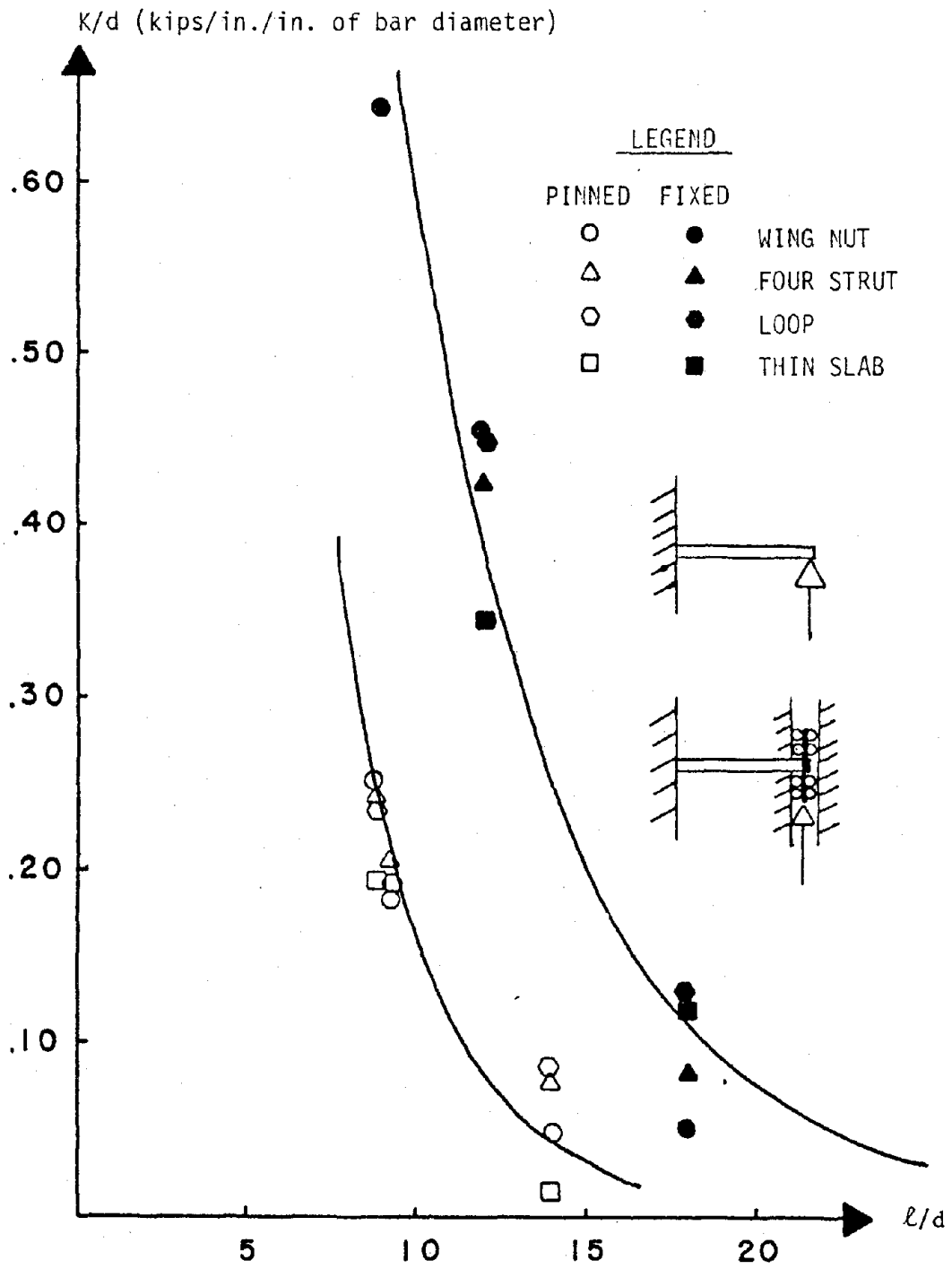
Figure 2.3.10 Post Yield Stiffness Coefficients for Bar-Insert Connections without Plate, Experimental Results

stiffness factors are negligible when compared to the elastic range values, i.e. elastic-perfectly plastic behavior is probably an adequate idealization.

Similar tests were conducted on the bar-insert connection with a steel face plate added. The insert was tack welded to the face plate and cast in concrete with the plate surface flush with the panel surface as shown in figure 2.3.11.



12" x 12" x (1/2, 3/4, 1") plate

Tack welded insert

Rebar attached to insert
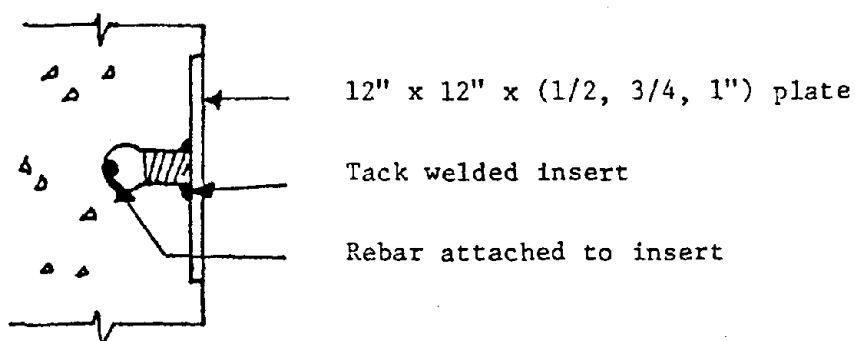
Figure 2.3.11  Cut away view of insert with plate panel.

Hole size in the plate is the critical parameter when determining the effect of the face plate on the stiffness coefficient.  If the bar which is threaded into the insert contacts the hole surface, then the distance $\ell$ is measured from the plate surface.  However, if the hole is large enough that the bar does not contact the hole surface, then the distance $\ell$ is measured from the insert itself.  The obvious effect of hole size is to change the effective length of the bar and thereby alter the stiffness of the connection, depending on the fit of the bar and thickness of the plate.  Throughout the connection tests, the concrete surrounding the individual inserts remained intact and showed no signs of failure. Some local cracking did occur occasionally but the integrity of the system was not affected.  The value of face plating inserts does not lie

with protecting the concrete. The lack of significant cracking around the insert during repeated yielding of the bar and the fact that the stiffness coefficients remain the same indicates that steel face plates are not necessary. Figure 2.3.12 is a plot of the elastic stiffness coefficients for various $\ell/d$ ratios for fixed and pinned end load application on bar-insert connections with face plate steel. Figure 2.3.13 is a plot of the stiffness coefficients vs. $\ell/d$ ratios for the various connections loaded into the inelastic range. The post-yield stiffness values are again found to be negligible when compared with the elastic range values. Although there is quite a range of post-yield values the overall ratio of values is always very low. Other results of the experimental tests on bar-insert connections cannot easily be listed in a table or shown on a graph and should be discussed here. The stiffness of the bar-insert connection is affected by several factors that may be described as construction dependent. These effects are:

1. It was observed that the amount of exposed threads on the bar after being threaded into the insert affects the stiffness coefficient by reducing the nominal cross sectional area which resists the bending of the bar. The amount of threads appears to reduce the number of plastic load cycles the system can tolerate before developing a crack. Note that the only bar to develop a crack was the 1/2 in. size insert connection after approximately two hundred cycles into the plastic range (at 2 hz) which had 1/4 in. of thread exposed at the panel side.

2. The stiffness of a bar insert connection can also be reduced by not matching the thread gauge of the bar to that of the insert. This phenomenon exists when the bar has a loose fit into the insert.
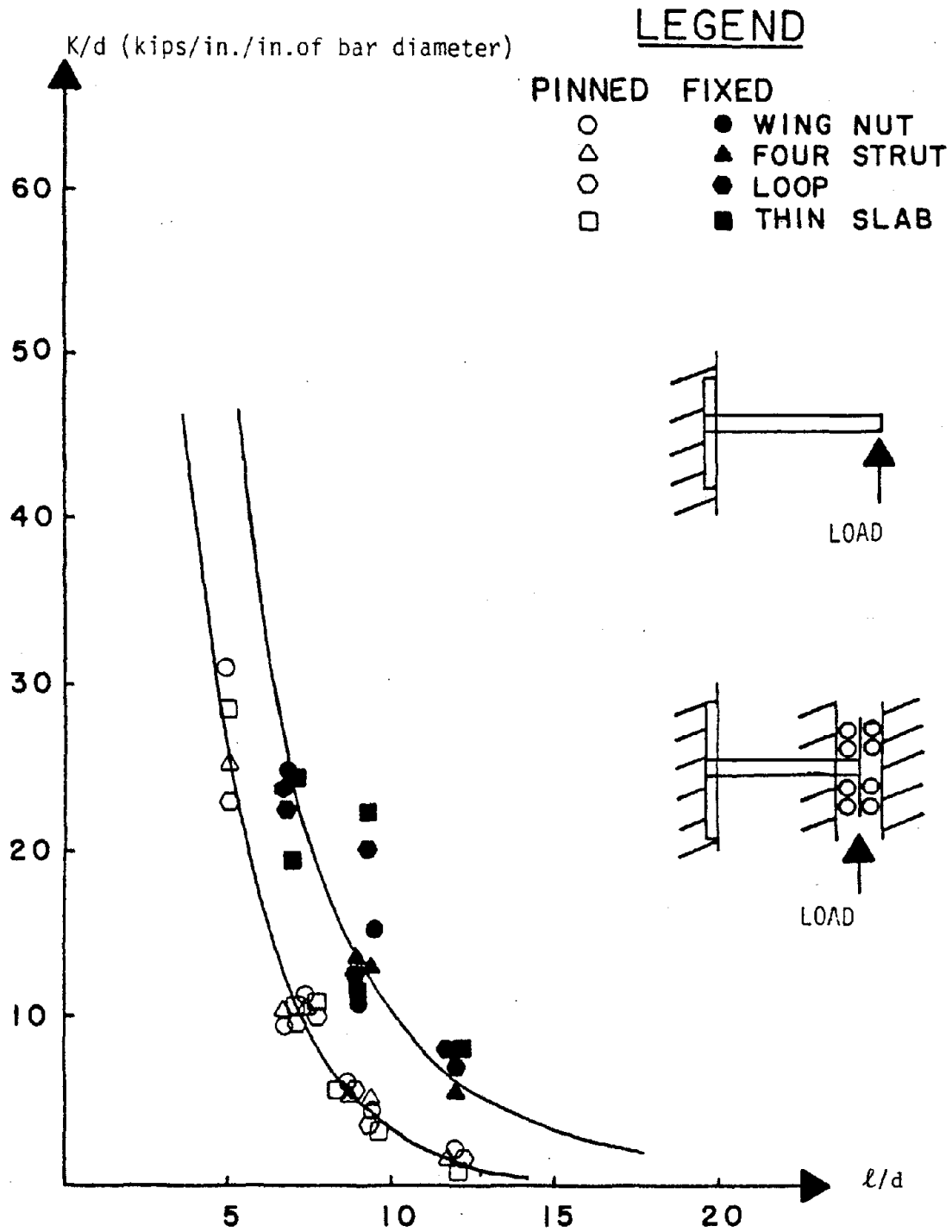
Figure 2.3.12    Elastic Stiffness Coefficients for Bar-Insert Connections with Plates, Experimental Results
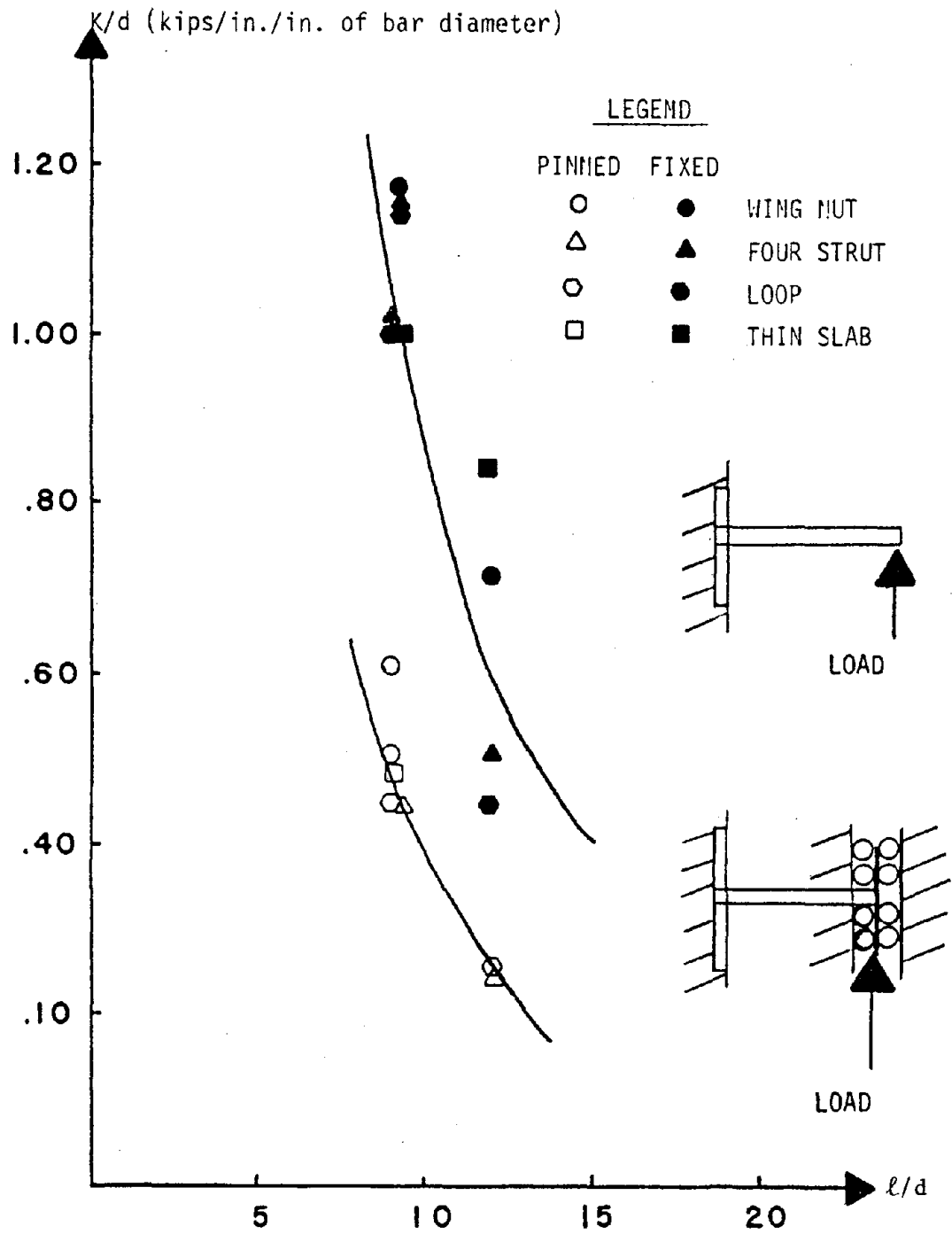
Figure 2.3.13 Post Yield Stiffness Coefficients for Bar-Insert Connections with Plates, Experimental Results.

3. As specified by the manufactor of inserts, the full strength of an insert in pullout is obtained when the bar is threaded into the insert within 1/2 in. of the base. Not adhering to this requirement will also reduce the in-plane stiffness of the bar insert connection system, although not as much as the first two items will.

4. The yield point of a bar insert connection will increase when cyclically loaded past the elastic load limit. A yield point of 160 pounds was experienced before any cycles and 244 pounds after 500 cycles for a 1/2 in. bar-insert connection. This increase in elastic load limit is due to strain hardening of the low carbon steel bars.

## 2.3.4.2 Structural Angle Connections

The stiffness coefficients obtained from testing the various angles in the welded, slotted, and the bolted configurations of fastening are listed in Table 2.3-3 and shown in Figure 2.3.1 for vertically applied loads and Table 2.3-4 for horizontally applied loads. The stiffness coefficients for angles are dependent upon the following:

1) the distance from the applied load to the panel surface, $\ell$;

2) the thickness of the structural angle, t; and

3) the stiffness of the panel at the attachment point of the connection.

The welded angles are particularly sensitive to point 3) above in that thin flexible anchor plates allowed rotation where thick rigid anchor plates resisted rotation significantly.

It was observed that for the slotted angle connections tested, the overall performance of the connection system was dependent on the method of attachment. Tables 2.3-3 and 2.3-4 list the stiffness coefficients

Table 2.3-3  Stiffness coefficients for structural angles, vertically applied load (lbs/in)

| | Non-Slotted Angles | | | †Slotted Structural Angles | | | | | |
| --- | --- | --- | --- | --- | --- | --- | --- | --- | --- |
| | | | *Insert with Plate Bolted | Insert Only | | | Insert with Plate | | |
| Size (in.) $L_1$ x $L_2$ x t | Welded | Insert Bolted | | Vertical Loose | Vertical Horizontal Loose | Both Tight | Vertical Loose | Horizontal and Vertical Loose | Both Tight |
| 4 × 6 × 3/8 | 70,195 | 28,586 | 37,214 | 15,151 | -- | 22,763 | 27,964 | 26,562 | 31,250 |
| 4 × 6 × 1/2 | 75,721 | 64,794 | 74,124 | 28,782 | -- | 30,625 | 32,258 | 29,904 | 52,083 |
| 4 × 6 × 5/8 | 223,671 | 102,986 | 146,970 | 45,776 | -- | 47,169 | 105,042 | 93,552 | 129,533 |
| 6 × 8 × 1/2 | 71,526 | 49,586 | 51,409 | 40,952 | 37,513 | 54,347 | 40,322 | 37,878 | 52,083 |
| 6 × 8 × 3/4 | 131,497 | 84,667 | 79,316 | 62,662 | 54,704 | 111,940 | 88,967 | 80,906 | 125,000 |

*Inserts used with the angle tests were 3/4 in. ferrule loop type.

†Slotted angles were used 3/4 in. A-325 bolts for attachment
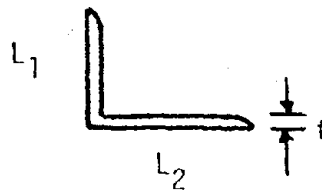
$L_1$  $L_2$  t

Table 2.3-4   Stiffness coefficients for structural angles, horizontally applied load (lbs/in)

| Non-Slotted Angles | | | | †Slotted Structural Angles | | | | | |
| | | | *Insert with Plate Bolted | Insert Only | | | Insert with Plate | | |
| Size (in.) L₁ x L₂ x t | Welded | *Insert Bolted | | Vertical Loose | Horizontal and Vertical Loose | Both | Vertical Loose | Horizontal and Vertical | Both Tight |
|---|---|---|---|---|---|---|---|---|---|
| 4 × 6 × 3/8 | 182,052 | 214,071 | 208,083 | 137,751 | -- | 208,333 | 227,272 | 62,500 | 312,500 |
| 4 × 6 × 1/2 | 203,125 | 249,416 | 312,250 | 260,416 | 58,823 | 416,666 | 240,384 | 67,204 | 416,666 |
| 4 × 6 × 5/8 | 272,161 | 374,500 | 356,852 | 277,777 | 107,142 | 833,333 | 373,134 | 142,914 | 500,000 |
| 6 × 8 × 1/2 | 260,260 | 313,000 | 169,152 | 94,696 | 57,471 | 277,777 | 390,625 | 91,028 | 625,000 |
| 6 × 8 × 3/4 | 301,590 | 357,785 | 215,086 | 294,117 | 93,632 | 357,142 | 104,602* | 42,515* | 178,571* |

*Inserts used with the angle
tests were 3/4 in. ferrule
loop type.

†Slotted angles used 3/4 in.
A-325 bolts for attachment.

$L_1$ $L_2$ t
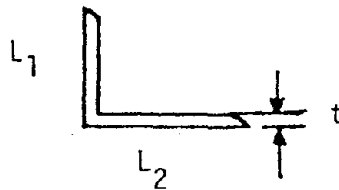
for the various methods of attachments used during the tests.

Slotted angles attached to panels with face plates showed no per-
formance advantage over slotted angles attached to panels without face
plates. The panel slid over both surfaces with equal efficiency provided
the bolts were sufficiently loose (backed off approximately one half turn
from finger tight). If, however, the bolts were left finger tight, the
angle tended to bind up and not slide freely from one end of the slot to
the other. The stiffness coefficients listed for slotted angles are
those obtained by loading the angle after the bolts had been brought to
bear on the end of the slotted holes. During the sliding part of the
motion, the angle provides zero stiffness. Figure 2.3.14 illustrates
schematically how the angles moved during this test sequence.



Before load is applied                    After load is applied
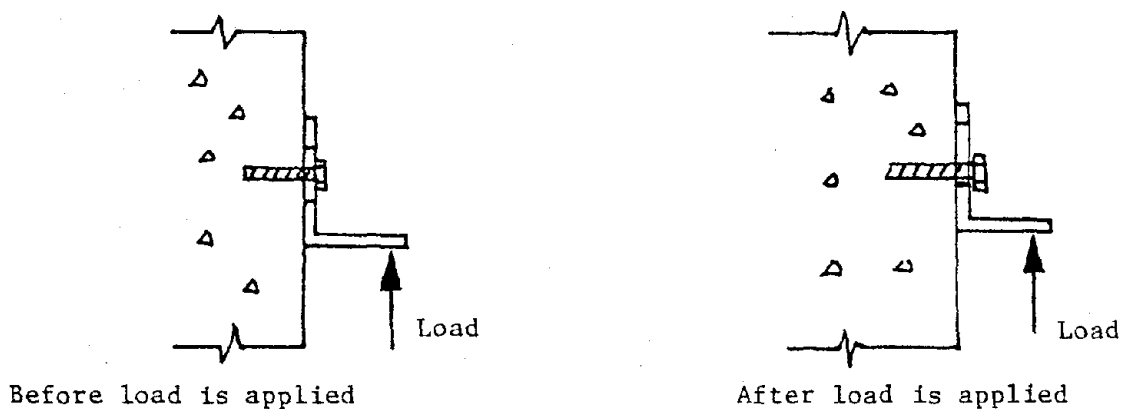
Figure 2.3.14 Loading diagram for slotted structural angles

Having pointed out the calculated results through the two Tables 2.3-3
and 4 and the basic parameters to which the stiffness coefficient of
structural angles are dependent, a brief discussion of some other find-
ings is in order. The following observations which were made during the
test sequence for the various structural angles indicate the aspects of
the connection details which affected the experimentally obtained stiff-

ness coefficients.

1. "Welded" (nonslotted) angles were secured to various sized steel plates embedded in the concrete specimens. Fillet welds (3/8 in.) were run only on the vertical edges of the angles as shown in Figure 2.3.1 to secure the angle to the plate. It was observed during the vertical loading of these angles that the base of the angle would pull away from the plate remaining attached only at the welded edges. This accounts for some of the differences between columns 2, 3, and 4 in Tables 2.3-3 and 2.3-4. The thickness of the embedded plate as previously stated also contributes to the variance in stiffness coefficients as compared to those obtained for the angles attached with bolts and inserts.

2. The stiffness of an angle connection is also dependent upon the direction of load application. For example, a vertically upward applied load will give a lower stiffness coefficient than for a vertically downward applied load. The reason for this difference is simply the geometry of the deflected shape.

3. The stiffness coefficients of the various slotted angles is affected by the amount of clearance between the head of the bolts and the angle because any additional space allows more rotation by the angle and therefore reduces the stiffness.

4. Cyclic load tests were run on the 4 in. x 6 in. x 3/8 in. welded angles only, because the MTS system used in this project does not have the necessary load capability to yield 4 in x 6 in. angles larger than 3/8 in. thick. During these tests there were no signs of concrete cracking or welds cracking. In one specimen, it was found that

some very minor cracks in the concrete occurred due to the flexing of the anchor plate; however the integrity of the system was maintained throughout the sequence of loading (2000 cycles) and the original stiffness of the connection was also maintained.

5. Yield tests were run on the larger angles (greater in size than the 4 in. x 6 in. x 3/8 in.) using an extender on the horizontal leg which measured 12 in. x 9 in. x 2 in. thick and increased the nominal lever arm from 2.5 in. to 10.5 in. This loading sequence showed that again the post yield stiffness may be assumed neglibible, i.e. elastic perfectly plastic behavior of the connection is a realistic idealization.

2.4    ANALYTICAL STUDY OF THE CONNECTIONS

2.4.1 Structural Analysis of Bar Insert Connections

The bar insert connection design is often based on the pullout strength of the insert and the axial loads expected for the connection body. The emphasis here, however, will be the panel in-plane loading effects and to determine the stiffness and yield point expected using theoretical strength of materials methods and finite element analysis methods.

The solution presented for the theoretical elastic stiffness, and the yield point for the bending of a bar insert connection, is based on the following assumptions:

1.    Complete moment fixity at the panel-bar interface.

2.    The bar is initially straight.

3.    The bar has a constant cross section through the entire length.

4.    The cross section is symmetrical about the center line lying in the plane of bending.

5.    The load applied is defined as a point load for the pinned end configuration and completely fixed (point load and point moment) for the fixed end configuration.

6.    Plane sections before bending remain plane after bending.

The bar insert connection loading configuration is expressed in the idealized form in Figure 2.4.1a and b for the pinned end fixed end cases, respectively.

The stiffness K is defined as the ratio of load to displacement

and has the units of force/length. The theoretical stiffness for a bar-insert connection that is loaded as shown in figure 2.4.1a is found using elementary strength of materials to be,

$$K = \frac{P}{\delta} = \frac{3EI}{L^3} \qquad 2.4.1$$

where P = point load,

   $\delta$ = deflection at the point of loading due to the point load P.



CASE I
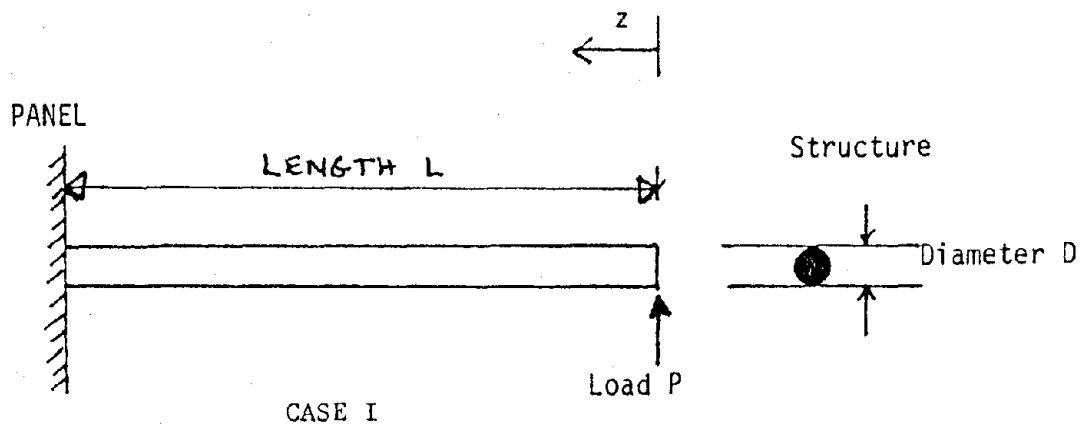
Figure 2.4.1a.   Pinned end load application



CASE II
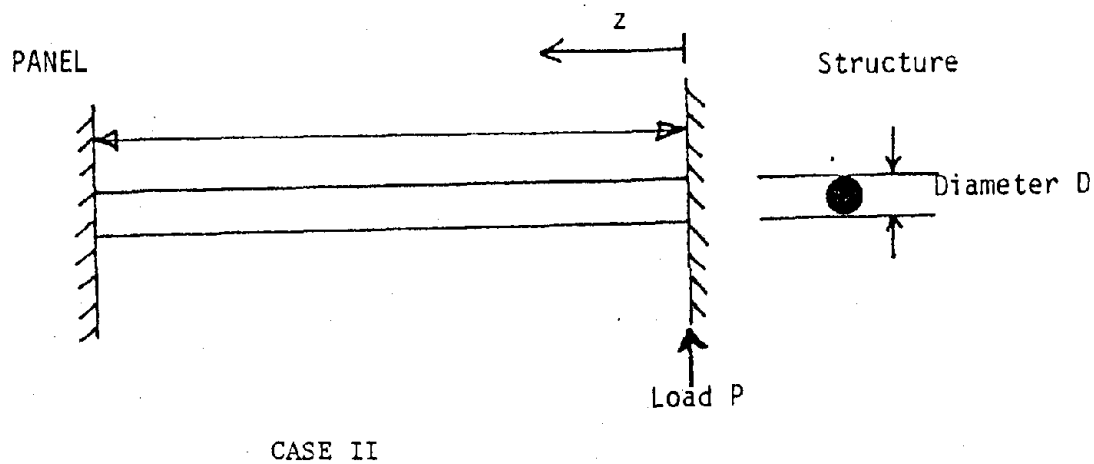
Figure 2.4.1b.   Fixed end load application.

The theoretical stiffness for the double fixed configuration shown in Figure 2.4.1b is found using a similar strength of materials approach, to be,

$$K = \frac{P}{\delta} = \frac{12EI}{L^3}$$ 
2.4.2

The moment acting on a beam may be written as

$$m = \sigma \frac{I}{C} = \sigma w_E$$

where $w_E$ is defined as the elastic section modulus. Figure 2.4.2 depicts a typical stress strain relationship for the bending of beams made from mild steel. Below the yield point the stress distribution is linear and the relationship is defined as E, modulus of elasticity. At the point in loading when $\sigma y$, the yield point value, is reached, the linear distribution is no longer valid. The yield point moment value is defined as

$$m_{yp} = \sigma_y \, w_E$$ 
2.4.3

For the two loading situations being discussed here, the yield point load is then

Case I $\quad P_{yp} = \frac{m_{yp}}{L} = \frac{\sigma_y w_E}{L}$ 
2.4.4

Case II $\quad P_{yp} = \frac{2m_{yp}}{2} = \frac{2\sigma_y w_E}{L}$ 
2.4.5
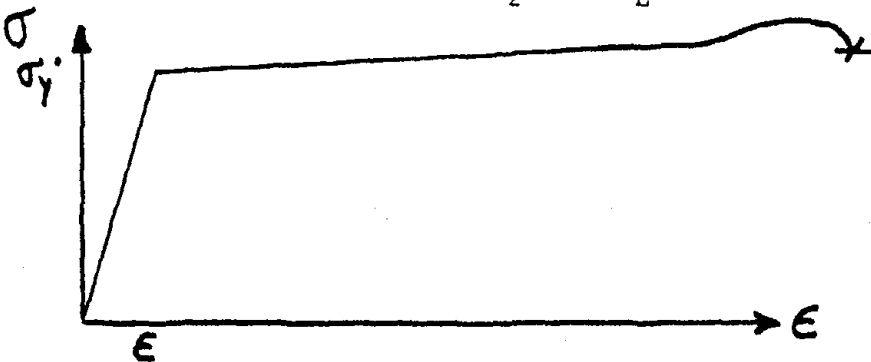


Figure 2.4.2 Stress strain relationship during the elastic plastic bending of beams.

For the loading Cases I and II, the load which produces a fully

plastic stress strain relationship in the bending of the bar is for

Case I

$$P_p = \frac{m_p}{L} = \frac{\sigma_y w_p}{L} \qquad\qquad 2.4.6$$

and Case II

$$P_p = \frac{2m_p}{L} = \frac{2\sigma_y w_p}{L} \qquad\qquad 2.4.7$$

where $w_p$ is the plastic section modulus. The equations given for the

plastic load limits $P_p$ may also be written as a function of the elastic

load limit $P_y$ and the shape factor $\omega$. The shape factor is defined as the

$$\omega = \frac{W_p}{W_E} \qquad\qquad 2.4.8$$

and turns out to be equal to 1.7 for beams of circular cross section.

## 2.4.2 Structural Analysis of Structural Angle Connections

The analysis of bending for the structural angles tested during

the experimental study is based on the following assumptions:

1.  The load application may be idealized as a line load at a
    distance L from the base of the angle.

2.  Complete fixity is obtained by whatever attachment method is
    used between the panel and the angle.

3.  Neglect the Poisson effect in the plane normal to the bending
    plane.

The three methods of attachments to the concrete specimens for the angle

tests were:

1.  Weld each vertical edge of the longest leg to an anchored base
    plate. See Photo 2.3.4.

2.  Fully tightened 3/4 in. A325 bolts into ferrule loop inserts

    with the angle bearing on either concrete or steel.

3.  Slotted holes with 3/4 in. A325 bolts and ferrule loop inserts

    with the angle bearing on either concrete or steel.

Figures 2.4.3 a, b, and c illustrate the idealized configuration of each

attachment method and are the basis for the following analysis.

Equation 2.4.1 for a fully fixed cantilever bar insert

$$K = \frac{3EI}{L^3}$$
2.4.9

also applies to the fully fixed cantilever idealization shown in Figures

2.4.3a and c. The moment of inertia I for the horizontal leg $L_1$ of the

angle may be calculated as

$$I = \frac{1}{12}bt^3,$$
2.4.10

where b is the width of the angle and t is the thickness. The moment

arm $L_1$ is defined as the distance from the point of load application to

the point of maximum stress. It is assumed here that the point of mini-

mum cross section where the maximum bending stress occurs, i.e., a dis-

tance k (tabulated in the AISC Steel Construction Manual) from the base

of the angle. The stiffness coefficient for either a welded angle or a

bolted angle loaded in the downward direction can be written as,

$$K = \frac{P}{\delta} = \frac{Ebt}{4L^3}$$
2.4.11

where P is defined as a line load and K is the stiffness angle.

The stiffness for a bolted angle loaded vertically up is not

described by equation 2.4.2  The moment induced by the load P shown in

Figure 2.4.3b causes rotation at the base of the angle and also at the

location of the hold down bolts. Therefore, the load displacement rela-
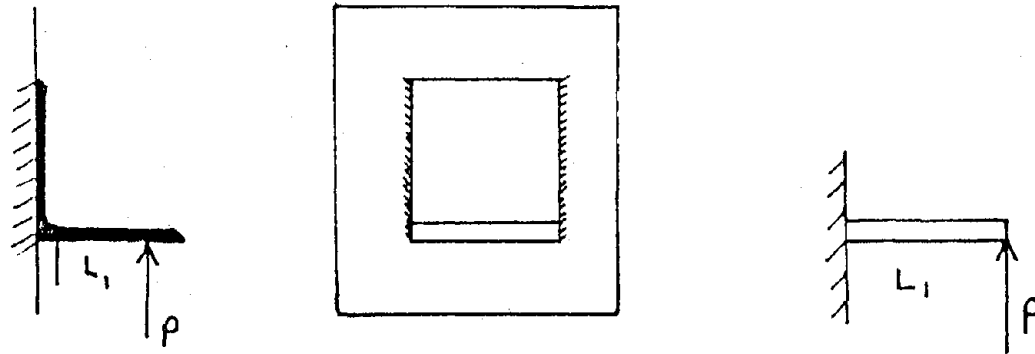
Figure 2.4.3a.  Idealized angle load application (welded).
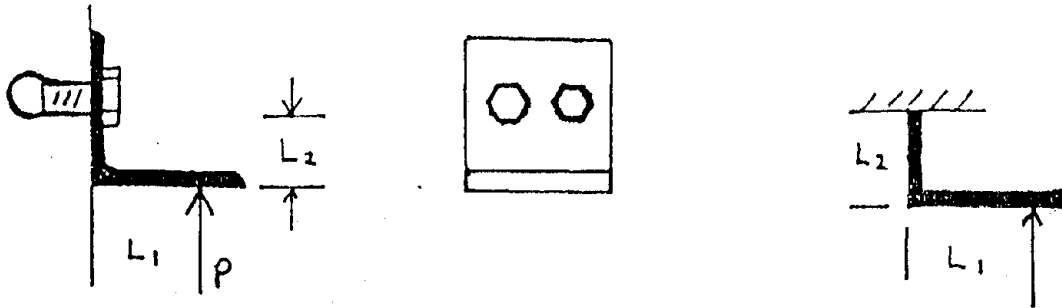


Figure 2.4.3b.  Idealized angle load application (bolted).
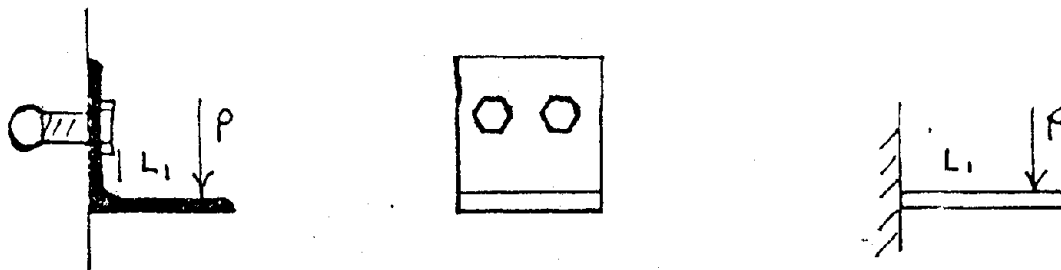


Figure 2.4.3c.  Idealized angle load application (bolted with load down).

tionship will be dependent on the total movement of the angle. Figure 2.4.4 illustrates the kinematics used to obtain the stiffness equation characteristic for this type of loading. The deflection induced in leg $L_1$ induced by load P can be described mathematically for the configuration shown in Figure 2.4.3a as

$$\delta_1 = \frac{PL_1^3}{3EI} \qquad\qquad 2.4.12$$

The deflection at point C can be calculated to be

$$\delta_2 = \left(\frac{PL_1L_2}{EI}\right)\left(\frac{L_2}{2}\right) = \frac{PL_1L_2^2}{2EI} \qquad 2.4.13$$

and the rotation at point C to be

$$\theta_C = \frac{PL_1L_2}{EI} \qquad\qquad 2.4.14$$

For small displacements

$$\delta_3 = \theta_C L_1 \qquad\qquad 2.4.15$$

Therefore, the total deflection of point B due to a load P is

$$\delta_{total} = \delta_1 + \delta_3 = \frac{PL_1^3}{3EI} + \frac{PL_1^2L_2}{EI} \qquad 2.4.16$$

and the stiffness coefficient is

$$k = \frac{P}{\delta} = \frac{EI}{\frac{L_1^3 + L_1^2L_2}{3}} \qquad\qquad 2.4.17$$

where $I = \frac{bt^3}{12}$

The analysis of the load displacement relationship for slotted angles is complicated by the fact that the angles are not held fast to the panel and movement is not resisted until the full travel of the slot is used. The values for $L_1$ and $L_2$ depend on the length and position of
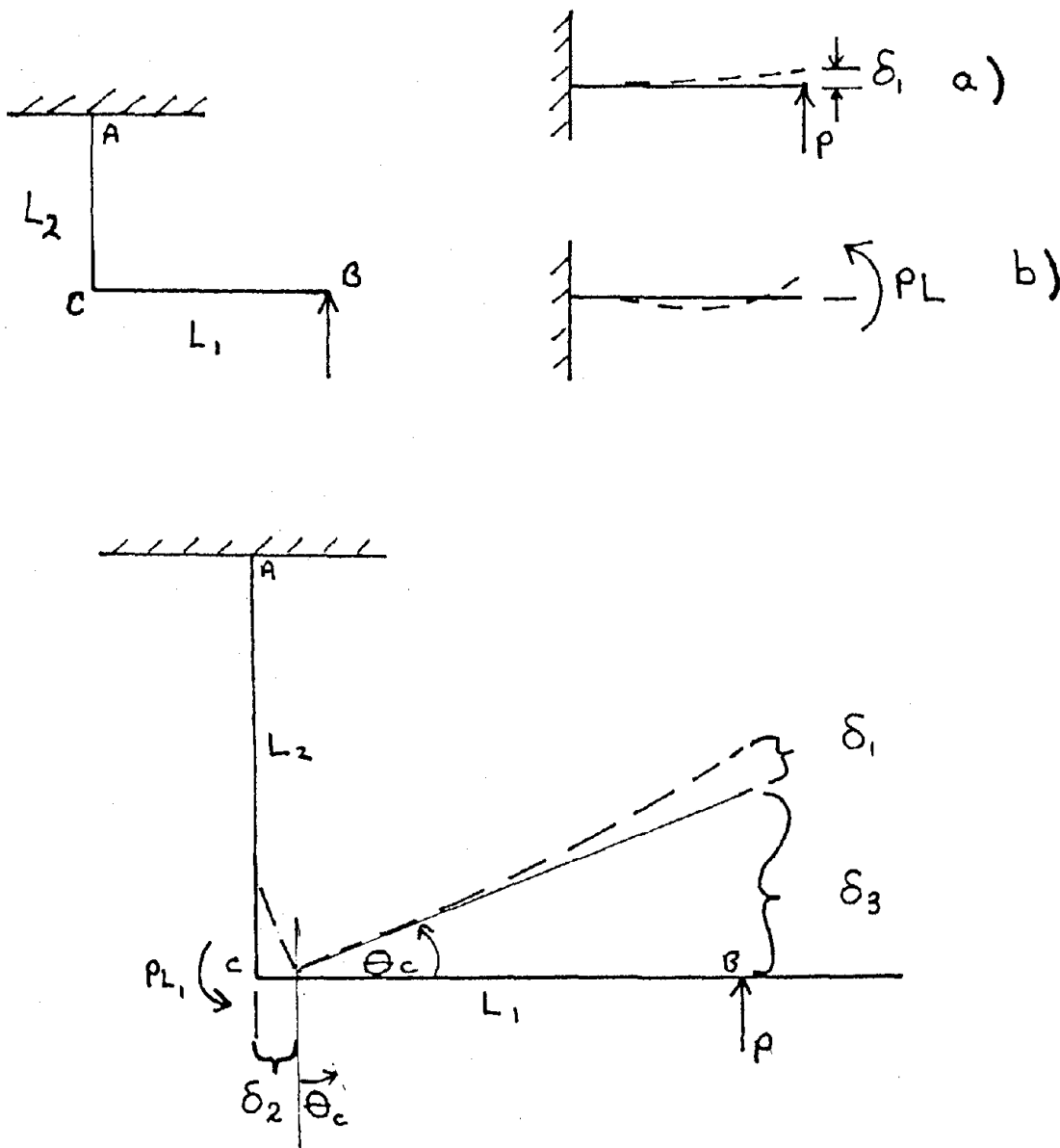
Figure 2.4.4   Idealized angle load-displacement

the slots.  It must be stated here that the elementary strength of mater-

ials and structural analysis approach used to predict the behavior of

structural angles under the prescribed loading situations does have limi-

tations.  These limitations are due to the assumptions made in order to

keep the analysis on a simplistic level. There are several aspects of the actual connection construction that are not included in the model for analysis which also affect the predicted theoretical stiffness. They are,

1. The face plate steel used to anchor the welded angles is not rigid as was assumed for analysis purposes.

2. The moment arm $L_1$ does not act exactly like a fully fixed cantilever beam, therefore it is not as stiff as is predicted theoretically.

3. The central portion of the angle has two holes drilled in it which tends to increase the flexibility of the system.

4. The bolts used to secure the angle to both the panel and the structure have a certain flexibility which will contribute to the overall flexibility of the connection system. The elongation of the bolts changes the geometry of deformation of the connection system, and reduces the system stiffness. This effect is not considered during the theoretical solution due to the assumed fixity at the bolt attachments.

5. Those angles welded to the face plate of the panel are done so only at the vertical edges of the angle. This form of attachment allows the base of the angle to move away from the plate during upward loading. This also increases the flexibility of the connection system, and is not accounted for in the simplistic structural analysis models described earlier.

Table 2.4-1 is presented here as a summary of the equations used to theoretically obtain the stiffness coefficients and the yield point values for the connections tested experimentally. Note that for slotted

angles the equations used for bolted angles loaded up; apply with an

appropriate $L_2$ value substituted.

Table 2.4-1  Elastic Stiffness Coefficient and Elastic Load Limit
Equation Summary

| Connection Type | Stiffness K | Elastic Load Limit, Yield Point, |
|---|---|---|
| Bar Insert Pinned | $\dfrac{3EI}{L^3}$ | $\dfrac{\sigma_y{}^W E}{L}$ |
| Bar Insert Fixed | $\dfrac{12EI}{L^3}$ | $\dfrac{2\sigma_y{}^W E}{L}$ |
| Welded Angle Loaded Vertical Up | $\dfrac{Ebt^3}{4L_1^3}$ | $\dfrac{\sigma_y{}^W E}{L_1}$ |
| Welded Angle Loaded Vertically Down | $\dfrac{Ebt^3}{4L_1^3}$ | $\dfrac{\sigma_y{}^W E}{L_1}$ |
| Slotted or Bolted Angle Loaded Vertically Up | $\dfrac{EI}{\dfrac{L_1^3}{3} + L_1^2 L_2}$ | $\dfrac{\sigma_y{}^W E}{L_1}$ |
| Slotted of Bolted Angle Loaded Vertically Down | $\dfrac{Ebt^3}{4L_1^3}$ | $\dfrac{\sigma_y{}^W E}{L_1}$ |

## 2.4.3 Finite Element Analysis for Structural Angle Connections

In order to efficiently analyze a structural angle connection while

incorporating as many actual boundary conditions as possible and obtaining

the most realistic solution it is necessary to use a computer solution.

A brief discussion will follow on the SAP IV, computer analysis runs which

were made for each of the welded angles loaded vertically upward, and

each of the bolted angles loaded in a similar manner.  Using the SAP IV

program, it is possible to achieve solutions for the stiffnesses which more closely approximate what was obtained during the experimental study of the connections.

Figure 2.4.5 and 6 are the finite element models of the welded angle connection and the bolted angle connection respectively. The assumption used to model the experimental loading situations are:

1. When a node is located at a weld it is considered fixed in all directions.

2. When a node is located at a bolt position it is considered fixed in all directions.

3. Those nodes which are located at the bearing surface of the angle to panel contact are not fixed during the first computer run. Those are nodes 1, 2, 3, 4, 5, 6, and 10. During the second run those nodes were fixed in the x direction to simulate the bearing surface of the panel and angle.

4. All loads are assumed to be line loads and applied as concentrated loads at the five nodes across the base leg of the angle.

5. A plate-thin shell element was used in order to effectively model the thickness of the angles.

The results of the finite element analysis are discussed in section 2.4.4.2

## 2.4.4 Results of the Analytical Study

The theoretical results of this study are presented in three sections. The first contains the calculated stiffness coefficients and yield points for the bar insert connections, the second deals with the
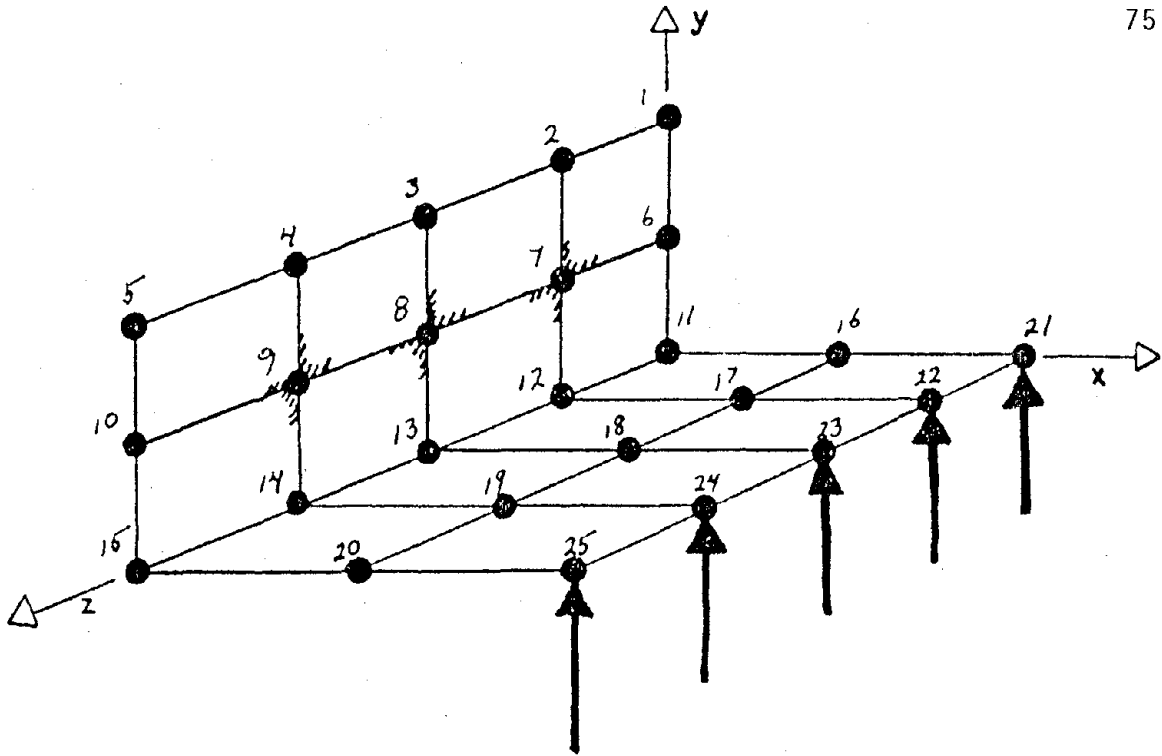
Figure 2.4.6 Finite Element Model for Bolted
Structural Angle Connection

Fixed Node-
all directions
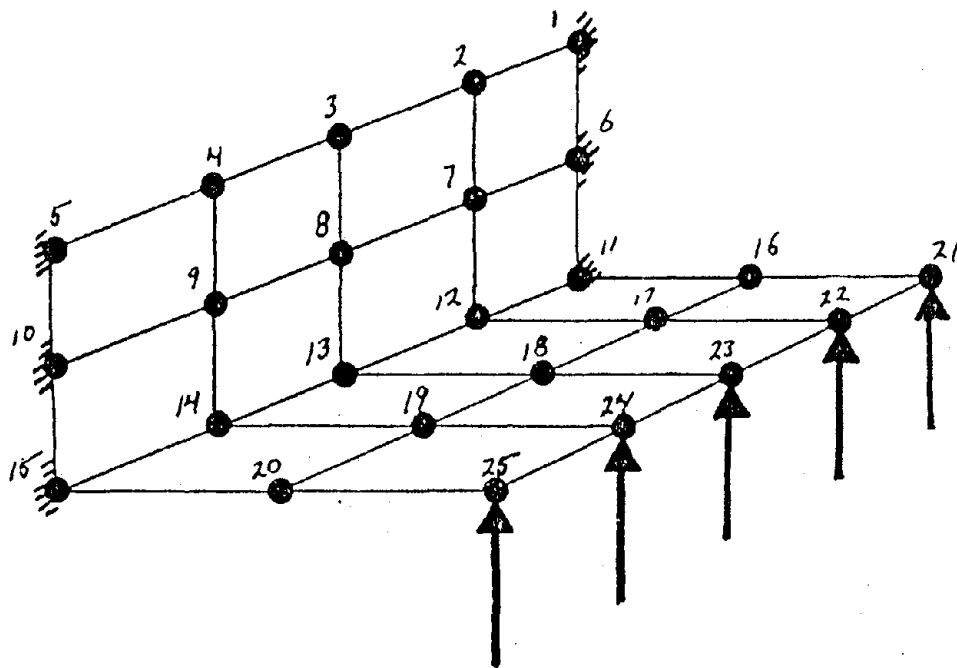


Figure 2.4.5 Finite Element Model for Edge Welded Structural
Angle Connection

calculated stiffness coefficients and yield points for the structural

angle connections, and the third section contains a brief discussion on

the energy dissipation values obtainable for the bar insert connections.

## 2.4.4.1 Bar Insert Connections

The stiffness coefficients for the various sizes and lengths of

the bar-insert connections tested are assembled in Table 2.4-2. These

values are calculated using the equations developed in Section 2.4.1 and are

valid only in the elastic range of the stress strain curve for the par-

ticular connection considered. The linear relationship between load and

displacement is interrupted between the elastic load limit $P_{yp}$ and the

plastic load limit $P_p$. Between these two limits there is a short transi-

tion curve and the relationship is again linear after the plastic load

limit is obtained. Figure 2.4.7 depicts the typical load displacement

relationship described here.

The value of the elastic load limit is dependent on the yield

strength of the steel used in the connection and the elastic section

modulus which is determined by the shape of the connection. The shape

of the curve between the elastic and plastic load limits is found empiri-

cally by direct lab testing. Table 2.4-3 lists the calculated values of

the elastic load limit and plastic load limits for the pinned end and

fixed end load applications. The yield strength for the 1 018 steel bars

used in the experimental study is taken to be 40,000 psi for hot rolled

and 70,000 psi for cold rolled.

Figure 2.4.8 is provided here to show the general theoretical

relationship for ℓ/d of the bar insert connection and the normalized

stiffness value K/D. This plot will be used in Section 2.5.1 in comparison
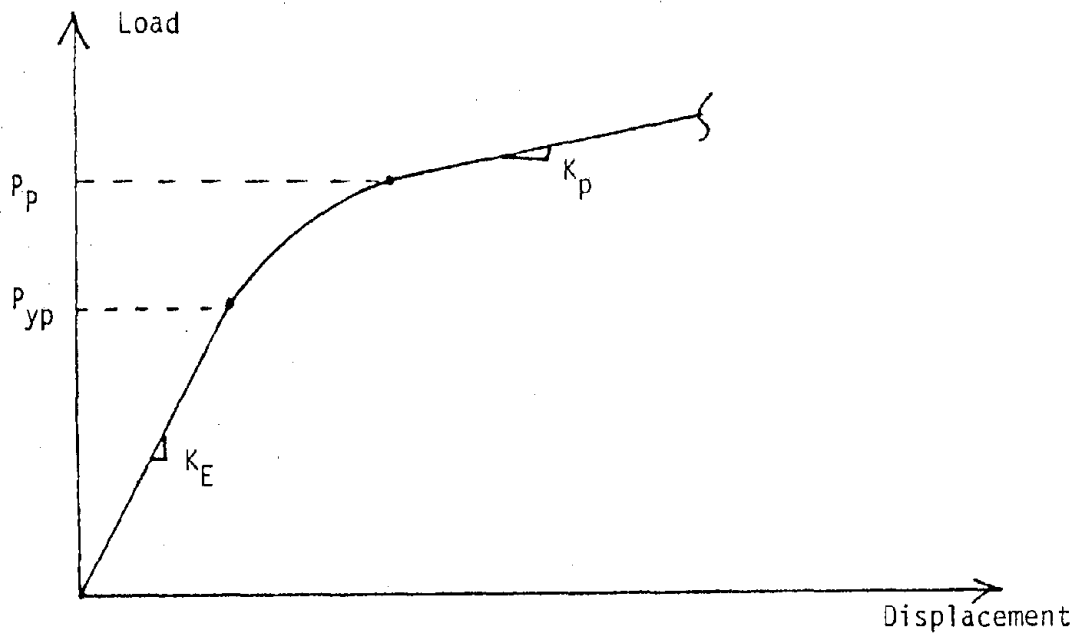
Figure 2.4.7. Typical load displacement relationship.

Table 2.4-2    Elastic stiffness coefficients, calculated theoretically for
               bar insert connections using Table 5.2-1.

| Bar | $\ell$ | 3" | 5" | 7" | 9" |
|-----|--------|-----|-----|-----|-----|
| | | Pinned End Configuration | | | |
| 1/2" | | 9,988 | 2,157 | 786 | 369 |
| 3/4" | | 49,944 | 10,788 | 3,931 | 1,849 |
| 1" | | 158,211 | 34,173 | 12,453 | 5,859 |
| | | Fixed End Configuration | | | |
| 1/2" | | 39,955 | 8,630 | 3,145 | 1,479 |
| 3/4" | | 199,777 | 43,152 | 15,725 | 7,399 |
| 1" | | 632,844 | 136,694 | 49,815 | 23,438 |

with the experimental results.

K/d  (kips/in./in. of diameter)
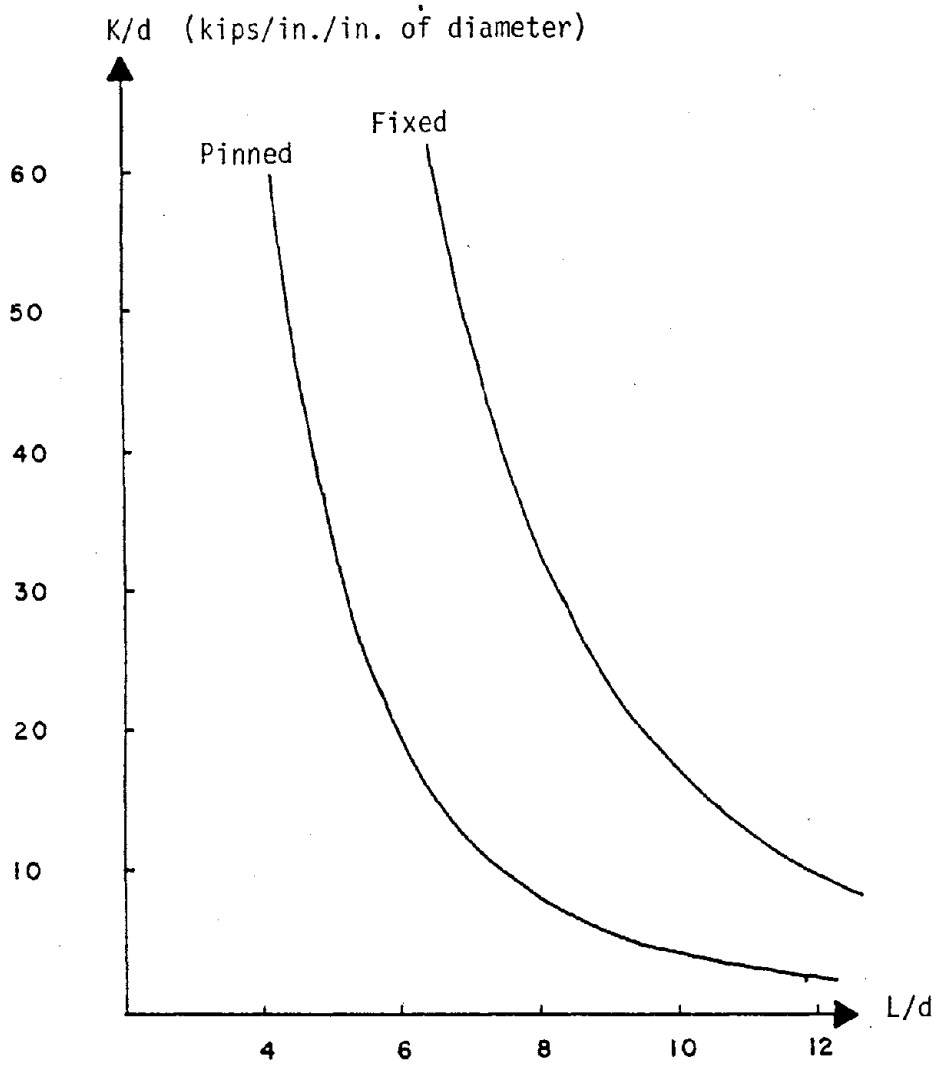


Figure 2.4.8. Elastic Stiffness Coefficients for Bar-Insert
            Connections without a plate, Theoretical Results

Table 2.4-3 Theoretical elastic load limit and plastic load limit, for bar insert connections.

| $\ell$ | 1/2" | | 3/4" | | 1" | |
|---|---|---|---|---|---|---|
| | $P_E$ | $P_p$ | $P_E$ | $P_p$ | $P_E$ | $P_p$ |
| | | | Pinned End | | | |
| 9" | 55 | 93 | 184 | 313 | 436 | 742 |
| 7" | 70 | 119 | 236 | 402 | 560 | 954 |
| 5" | 98 | 167 | 331 | 564 | 785 | 1,336 |
| 3" | 164 | 279 | 552 | 940 | 1,309 | 2,226 |
| | | | Fixed End | | | |
| 9" | 110 | 186 | 368 | 626 | 872 | 1,584 |
| 7" | 140 | 238 | 472 | 804 | 1,120 | 1,908 |
| 5" | 196 | 334 | 662 | 1,128 | 1,570 | 2,672 |
| 3" | 328 | 558 | 1,104 | 1,880 | 2,618 | 4,452 |

## 2.4.4.2 Structural Angle Connections

The stiffness coefficients for the various structural angles were obtained by using the formulations described in Section 2.4.2 and the finite analysis method described in Section 2.4.3. The stiffnesses were obtained by averaging the results of loading nodes 21 through 25 for the computer generated solution. Table 2.4-4 lists the values obtained from classical structural analysis. Tables 2.4-5a and 2.4-5b list the values obtained for two runs of the finite element program. The first run indicated nodes at the bearing surface of the angle (Nodes 1-10) required fixing in the x direction. The results of the classical method and the second run of the computer analysis are plotted on Figure 2.4.9

It should be noted that throughout this study, all of the results listed in tables or plotted on graphs represent solutions for a structural angle connection 9 in. wide. This was done so that direct correlations can be made between the experimental and theoretical results.

The elastic load limit of a structural angle loaded vertically downward is written mathematically as

$$P_{yp} = \frac{\sigma_y w_E}{L},\qquad 2.4.18$$

where $w_E = \frac{bt^2}{6}$. The plastic load limit is written as

$$P_p = \frac{\sigma_y w_E}{L},\qquad 2.4.19$$

where $w_p = \frac{bt^2}{4}$. The moment arm length (L) depends on the mode of attachment and the direction of the load. Table 2.4-6 lists the calculated values of $P_{yp}$ for each angle tested experimentally. Note that the ratio of plastic load limit to elastic load limit is equal to 1.5 in the case of structural angles. Table 2.4-6 may be used to obtain the plastic load limit by multiplying the $P_{yp}$ figure by the shape factor 1.5.

Table 2.4-4    Theoretical elastic stiffness coefficients for structural angles, as calculated using Table 5.2-1 classical structural analysis.

| Angle (in. x in. x in.) | Case I Welded Loaded Upward | | Case II Bolted Loaded Upward | | | Case III Slotted Loaded Upward | | |
|---|---|---|---|---|---|---|---|---|
| | $L_1$ (in.) | k (kips/in) | $L_2$ (in.) | $L_1$ (in.) | k (kips/in) | $L_1$ (in.) | $L_2$ (in.) | k (kips/in) |
| 4 x 6 x 3/8 | 3.5 | 80.25 | 2.3125 | 3.5 | 26.75 | 3.5 | 1.562 | 34.25 |
| 4 x 6 x 1/2 | 3.5 | 190.23 | 2.250 | 3.5 | 64.75 | 3.5 | 1.500 | 83.25 |
| 4 x 6 x 5/8 | 3.5 | 371.50 | 2.187 | 3.5 | 129.25 | 3.5 | 1.437 | 166.50 |
| 6 x 8 x 1/2 | 4.5 | 89.50 | 3.250 | 4.5 | 28.25 | 4.0 | 2.000 | 51.00 |
| 6 x 8 x 3/4 | 4.5 | 302.00 | 3.125 | 4.5 | 97.75 | 4.0 | 1.875 | 178.75 |



Case I          Case II          Case III

K (kips/in.)

175

150    CASE II - Not Slotted

125    CASE II        CASE III

100    CASE III - Slotted

75

50

25

      2      4      6      8      10    L/t
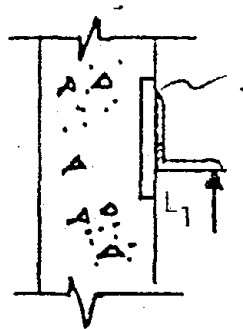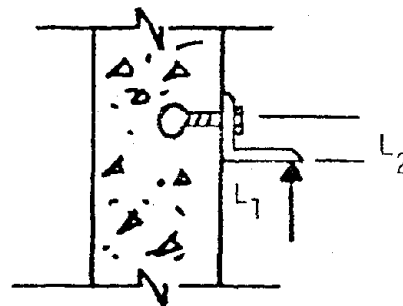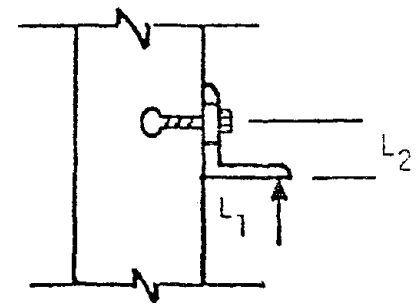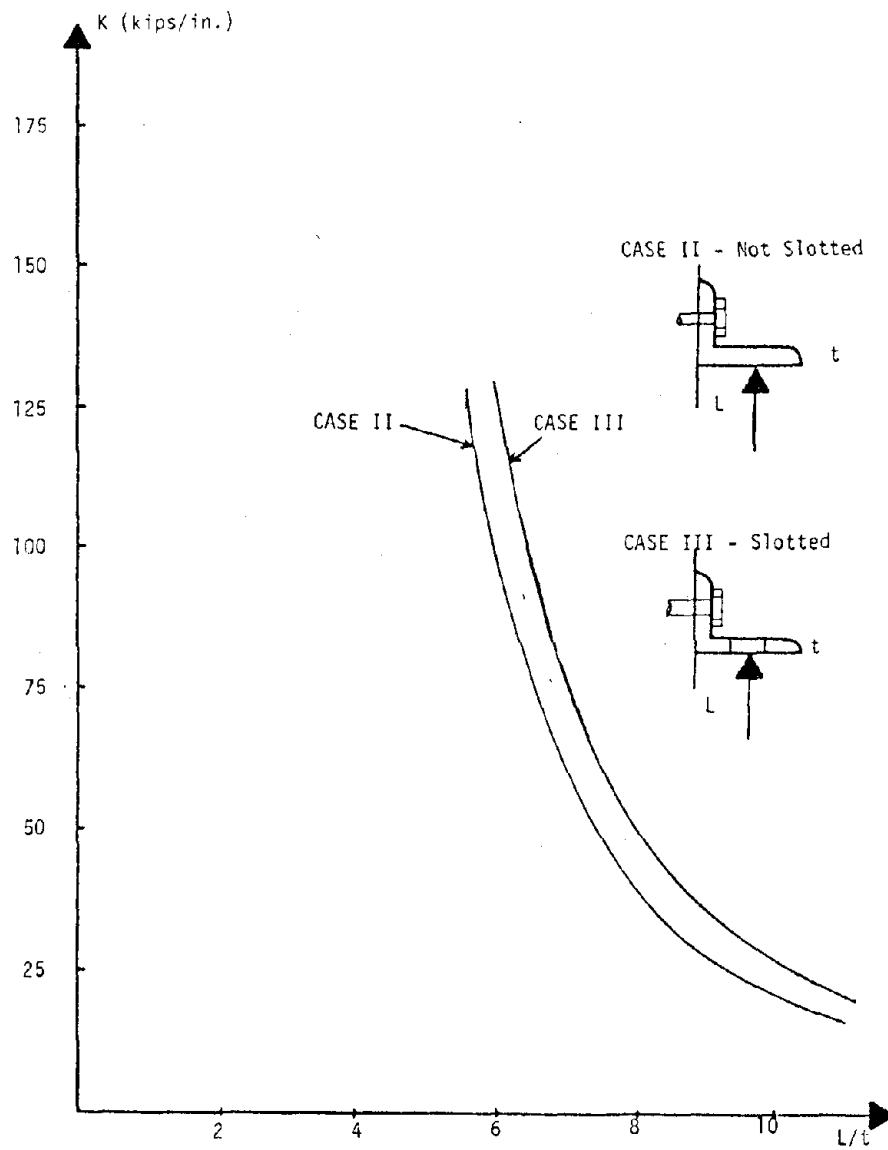
Figure 2.4.9 Elastic Stiffness Coefficients for Structural Angle Connections
              ( Classical Theoretical Results)

Table 2.4-5a.  Theoretical elastic stiffness coefficients as calculated
using finite element analysis (first computer run).

| Angle (in. x in. x in.) | Welded Loaded Vertically Upward | | Bolted Loaded Vertically Upward | |
|---|---|---|---|---|
| | $L_1$ (in.) | k(kips/in.) | $L_1$ (in.) | k(kips/in.) |
| 4 x 6 x 3/8 | 3.5 | 57.14 | 3.5 | 31.30 |
| 4 x 6 x 1/2 | 3.5 | 134.50 | 3.5 | 74.14 |
| 4 x 6 x 5/8 | 3.5 | 260.67 | 3.5 | 144.65 |
| 6 x 8 x 1/2 | 4.5 | 71.20 | 4.5 | 32.32 |
| 6 x 8 x 3/4 | 4.5 | 237.69 | 4.5 | 108.91 |

Table 2.4-5b.  Theoretical elastic stiffness coefficients as calculated
using finite element analysis (second computer run).

| Angle (in. x in. x in.) | Welded Loaded Vertically Upward | | Bolted Loaded Vertically Upward | |
|---|---|---|---|---|
| | $L_1$ (in.) | k(kips/in.) | $L_1$ (in.) | k(kips/in.) |
| 4 x 6 x 3/8 | 3.5 | 66.439 | 3.5 | 31.974 |
| 4 x 6 x 1/2 | 3.5 | 153.950 | 3.5 | 75.725 |
| 4 x 6 x 5/8 | 3.5 | 293.530 | 3.5 | 147.742 |
| 6 x 8 x 1/2 | 4.5 | 76.297 | 4.5 | 32.69 |
| 6 x 8 x 3/4 | 4.5 | 252.224 | 4.5 | 110.188 |

Table 2.4-6.  Elastic load limit for structural angle connections (theoretical) ($\sigma_y$ = 36 ksi).

| Angle (in. x in. x in.) | Case I | | Case II | | Case III | | | |
|---|---|---|---|---|---|---|---|---|
| | $\ell$ (in.) | $P_{yp}$ (lbs.) | $\ell$ (in.) | $P_{yp}$ (lbs.) | $\ell$ (in.) | $P_{yp}$ (lbs.) | $w_E$ | $w_p$ |
| 4 x 6 x 3/8 | 2.625 | 2,892 | 3.5 | 2,169 | 3.5 | 2,169 | .2109 | .3164 |
| 4 x 6 x 1/2 | 2.500 | 5,400 | 3.5 | 3,857 | 3.5 | 3,857 | .3750 | .5625 |
| 4 x 6 x 5/8 | 2.375 | 9,973 | 3.5 | 6,768 | 3.5 | 6,768 | .6580 | .9875 |
| 6 x 8 x 1/2 | 3.500 | 3,857 | 4.5 | 5,264 | 4.0 | 3,375 | .3750 | .5625 |
| 6 x 8 x 3/4 | 3.250 | 9,349 | 4.5 | 6,752 | 4.0 | 7,596 | .8440 | 1.2660 |

## 2.4.5 Energy Dissipation Characteristics

The total strain energy of a panel connection system may be conceptualized as shown in Figure 2.4.10 as simply the area under the load-deflection curve.  The area under the portion of the linear representation (that area which is lightly shaded on Figure 2.4.9 ), below the elastic load limit $p_E$ is the elastic energy, and is equivalent to half the potential of the applied loading, i.e.

$$U_E = \frac{1}{2} p_E d \qquad 2.4.20$$

where $p_E$ = load in the elastic range

d = deflection caused by the load $p_E$ and $U$ has the units force-length.

Equation 2.4.20 can be written as

$$U_E = \frac{1}{2} \int \frac{m^2}{EI} dx \qquad 2.4.21$$

for the internal elastic strain energy for the bending of a beam element where the axial and shear energy are small compared to the bending energy. The load displacement curve is non-linear from the elastic load limit to
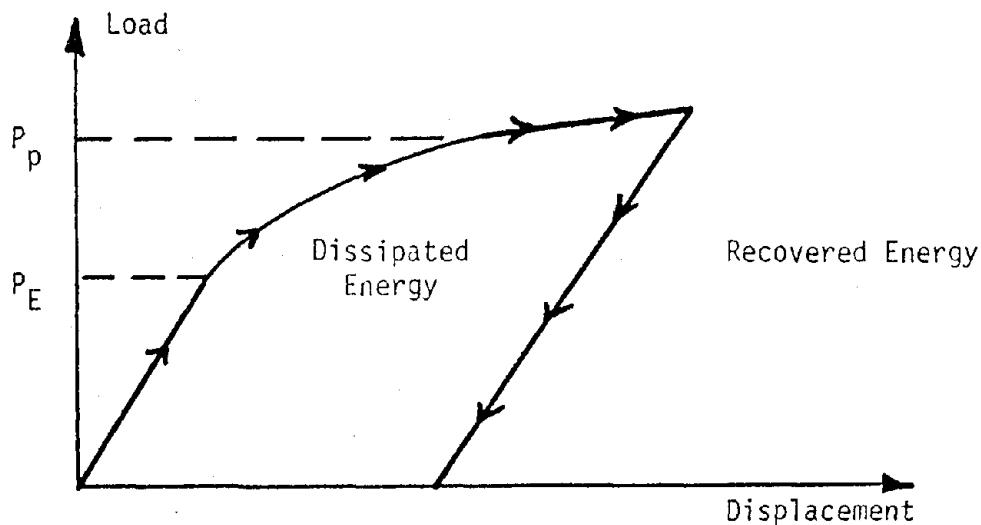
Figure 2.4.10  Energy dissipated and recovered.

the plastic load limit; therefore, it would be necessary to describe this curve mathematically, and to integrate according to equation 2.4.20 in order to find the total energy.  The load displacement curve may be idealized by assuming an elastic perfectly plastic relationship as shown in Figure 2.4.11.  This assumption was shown to be valid during the experimental study of the connection assemblies, i.e., the post-yield stiffness for each connection was found to be very low compared to the elastic stiffness.

The assumed elastoplastic force deflection curve is then easily analyzed in order to achieve the various energy dissipation values for the connection systems studied in the experimental section.  The total energy dissipation, therefore, for an elastic-perfectly plastic response is

$$U \text{ dissipated} = P_p (D_f - D_p), \qquad 2.4.21$$

where $D_p$ is the deflection cause by the initial $P_p$ loading and where $D_f$ is the final deflection obtained during the loading sequence.  All

Table 2.4-7. Energy dissipation equations.

---

## Bar Insert Connections

| Pinned | Fixed |
|---|---|
| $P_p = \dfrac{\sigma_y w_p}{2}$ | $P_p = \dfrac{2\sigma_y w_p}{2}$ |
| $k = \dfrac{3EI}{L^3}$ | $k = \dfrac{12EI}{L^3}$ |
| $D_p = \dfrac{P_p L^3}{3EI}$ | $D_p = \dfrac{P_p L^3}{12EI}$ |
| $D_p = \dfrac{1}{3}\dfrac{\sigma_y w_p L^2}{EI}$ | $D_p = \dfrac{2}{12}\dfrac{\sigma_y w_p L^2}{EI}$ |
| $U_{dissipated} = P_p(D_f - D_p)$ | $U_{dissipated} = P_p(D_f - D_p$ |
| $U_d = \dfrac{\sigma_y w_p}{L}\left(D_f - \dfrac{1}{3}\dfrac{\sigma_y w_p L^2}{EI}\right)$ | $U_d = \dfrac{\sigma_y w_p}{L}\left(D_f - \dfrac{1}{6}\dfrac{2\sigma_y w_p L^2}{EI}\right)$ |
| If $D_p <<< D_f$ the | If $D_p <<< D_f$ then |
| $U_d = \dfrac{\sigma_y w_p}{L} D_f$ | $U_d = \dfrac{2\sigma_y w_p}{L} D_f$ |

## Structural Angle Connections

| Pinned at Structure | Fixed at Structure |
|---|---|
| $U_d = \dfrac{\sigma_y w_p}{L} D_f$ | $U_d = \dfrac{2\sigma_y w_p}{L} D_f$ |
| (If $D_p <<< D_f$) | (If $D_p <<< D_f$) |

---

of the energy stored during the elastic deformation is by definition recoverable and, therefore, not dissipated.

The load necessary to produce plastic deformation in the fixed angle supports is extremely high and not likely to occur even under severe seismic loading. Table 2.4-7 produces the equations which identify the specific energy dissipation value for the connection configurations tested experimentally. The energy dissipated by a connection depends on the amount of deformation during which the connection experiences loads greater than the plastic load limit. The duration and magnitude of a seismically induced load on a curtain wall panel and the connections is found by analysis of the earthquake parameters for the specific building and panels in question.

This approach is very complex and not necessary for the writing of this paper. However, a simplistic approach using code requirements UBC,(1979),for panel design regarding accommodations for interstory drift will be used to identify the energy dissipation characteristics of a specific panel. The assumption used for analysis will be that an earthquake of moderate strength would produce approximately .25 g accelerations on the structure and 1% interstory drift and for a severe earthquake approximately 3% interstory drift. Therefore, the standard story height of 12 feet produces a drift from 1.44 in. to 4.32 in. for the assumed earthquake range. The elastic energy of a typical bar insert connection is small when compared to the total energy of the system when referring to interstory drifts ranging from approximately 1 in. to 5 in. Figure 2.4.12 illustrates this point by plotting the values obtained when applying the equations for $U_{dissipated}$ from Table 2.4-7, i.e.,

$$U_d = \frac{\sigma_y w_p}{L}\left(D_f - \frac{1}{3}\frac{\sigma_y w_p L^2}{EI}\right)$$

for the pinned end bar insert connection system. Note that the energy

dissipation for a fixed end bar insert connection is twice that of a

pinned end system. Also note that the second term of the expression

within the parentheses is the elastic energy recovered during the cycle.

Ignoring this term if $D_p <<< D_f$ and taking the energy dissipation for a

connection system as the product of the interstory drift times the plastic

load limit is a valid approach for obtaining a realistic solution. The

energy dissipation characteristics for bar insert connections and long-

legged thin (1/2 in. or less) structural angles is therefore identified

as the plastic load limit of the connection times the interstory drift

at the panel story. For those structural angles which are thicker than

1/2 in. and are relatively short-legged, the elastic energy is signifi-

cant and must be subtracted from the total energy for accurate dissipa-

tion values.
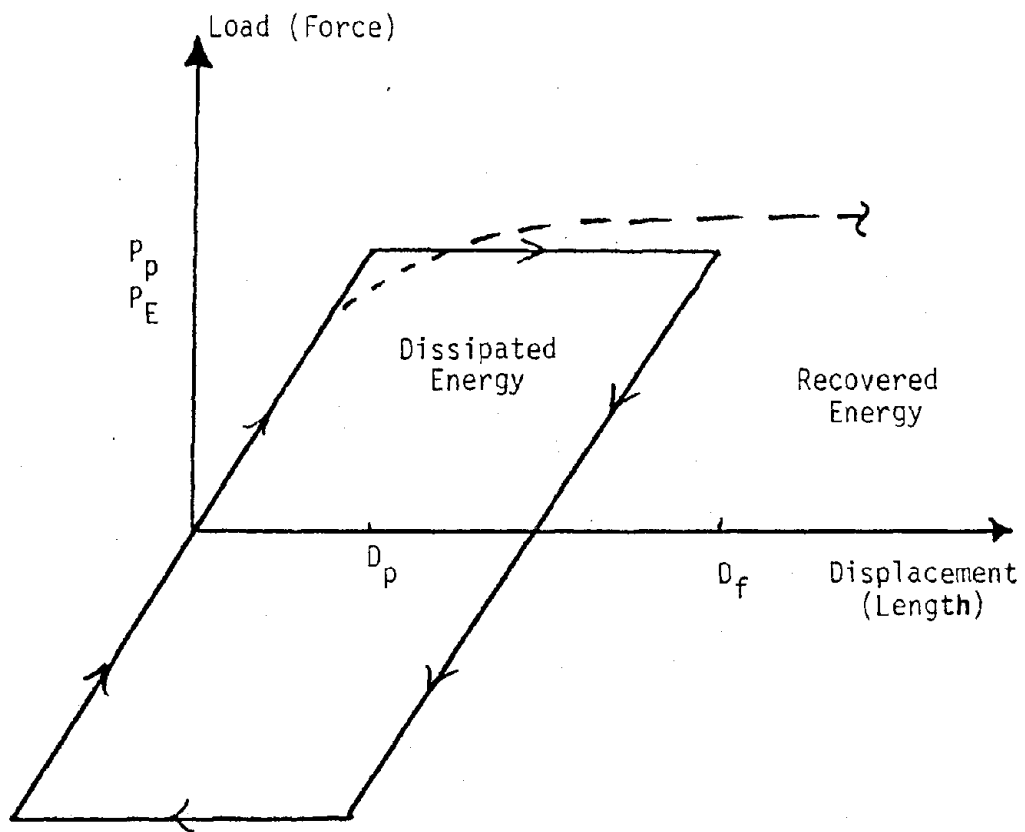
Figure 2.4.11   Elastoplastic idealized load/deflection curve,
complete cycle
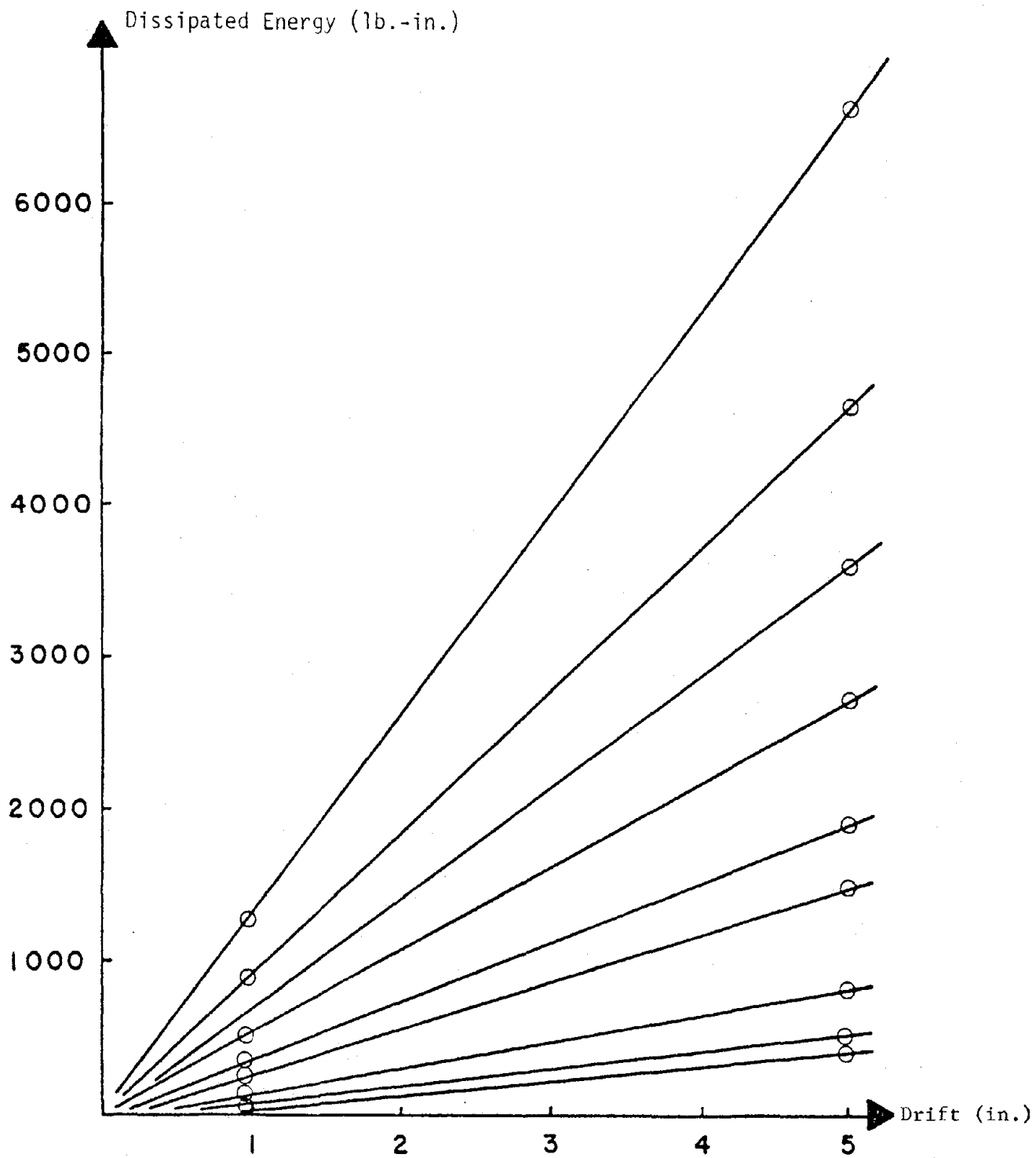
Figure 2.4.12 Energy Dissipation Values for Pinned End Bar-Insert
Connections

## 2.5 COMPARISON OF EXPERIMENTAL AND ANALYTICAL RESULTS

### 2.5.1 Bar Insert Connections

The discussion on the comparison of the experimental and analytical results is presented for each of the three basic types of connections studied; the bar insert connection, the slotted structural angles, and the fixed support (welded or bolted) structural angles. The idealizations used in the analysis of the connections (Sections 2.4.1, 2.4.2, and 2.4.3) obviously do not exist in reality and mathematical correlations must be identified in order to apply experimental results to future design situations. The comparison for bar inserts is based on the fixity obtained by the connection at the point of attachment at the panel and at the structural framework. Figure 2.5.1 illustrates the comparison of the experimental results and the analytical results for a bar insert connection with regard to stiffness for various $\ell/d$ ratios. The solid line plots are for those K values found theoretically assuming moment fixity for the fixed-end load application and zero moment fixity for the pinned end load application at the point of loading. The values obtained for bar-insert stiffnesses for the experimental study are probably those values which can be expected to occur in a panel connection system. The effect of the degree of fixity, therefore, can be seen as a function of the necessary $\ell/d$ of the bar insert to obtain a desired stiffness coefficient for the connection system. The reason for the difference between the theoretical solution and the experimental is that the assumptions used in the analytical study do not account for the various construction

factors (as discussed in Section 2.3) which increases the flexibility of the connection system. The finite element approach to analyzing the connection allows the investigator the ability of very careful modeling techniques in order to achieve values for the stiffness coefficients which are very close to those which can be obtained experimentally. This type of analysis is not necessary for bar insert connections generally, because of the simplicity of the system, i.e., single or double cantilevers. However, should a bar insert system be used in combination with other flexible connection plates or angles, a detailed analysis using finite element programs will give results that can be used directly without the use of a correction factor. Whichever method is used for predicting the stiffness coefficient of a bar insert connection system, it remains a matter of engineering judgment as to the exact value to use for design purposes.

The elastic load limit for bar insert connections tested experimentally are listed with the theoretical yield points in Table 2.5-1 for comparative purposes. The elastic load limit found experimentally is reasonably close to that which is predicted theoretically, which indicates a direct correlation exists and calculated values do not need adjustment for use in designing panel connections. The elastic and plastic load limits are obtained theoretically using the assumptions set forth in Section 2.4 of this paper. Those assumptions hold true for pure bending.

K/d ( kips/in./in. of bar diameter )

Pinned Experimental

Pinned Theoretical

Fixed Experimental

Fixed Theoretical

ℓ/d
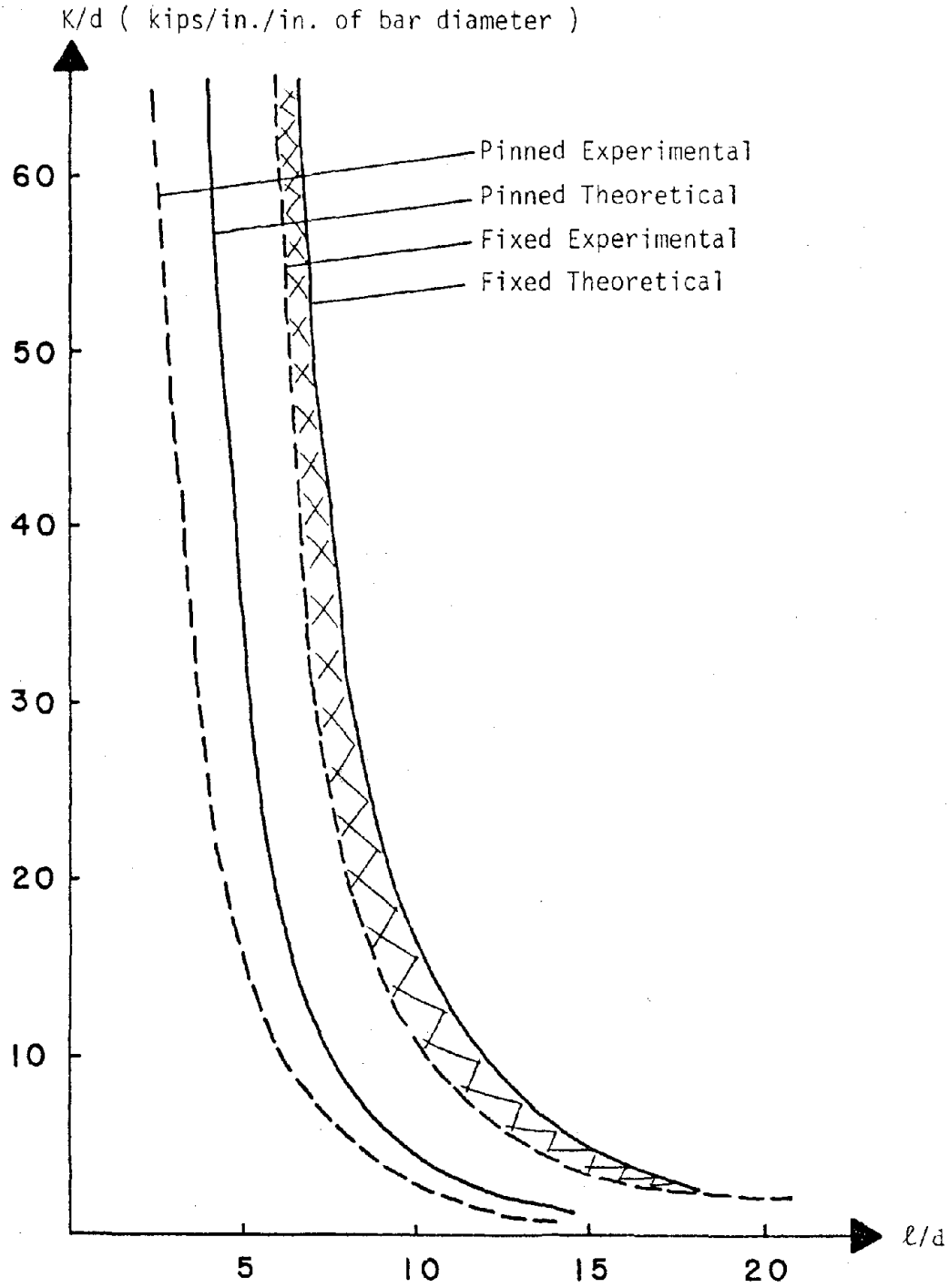
Figure 2.5.1 Elastic Stiffness Coefficients (presented for comparison) for both Experimental and Theoretical Results for Bar-Insert Connections

Table 2.5-1. Elastic load limits.  ($\sigma y$ = 60,000)

| Bar Insert Size | Pinned | | | Fixed | | |
|---|---|---|---|---|---|---|
| | Length $\ell$ in. | Exp. lbs. | Theor. lbs. | Length $\ell$ in. | Exp. lbs. | Theor. lbs. |
| 1/2" | 7 | 105.5 | 105.4 | 9 | 163 | 164 |
| 3/4" | 7 | 362.5 | 354.0 | 9 | 610 | 552 |
| 1" | 9 | 610.0 | 654.0 | 9 | 1,672 | 1,309 |

## 2.5.2 Structural Angle Connections, Fixed

The stiffnesses for the structural angle support connections (those welded securely to the panel and bolted to the actuator) are plotted vs. their $\ell/t$ ratio in Figure 2.5.2 for the loading situation described in the top right corner of the Figure.  Table 2.3-3 and 2.4-4 list the plotted values for the experimental and theoretical results, respectively.  The plot on Figure 2.5.2 incorporates values obtained from,

1) The theoretical solution as described in section 2.4.2

2) The finite element solution as described in section 2.4.3

3) The experimental results as they were obtained in the lab as described in Section 2.3

Note that the values obtained in all three circumstances plot out with the characteristic inverse cubic shaped curve.  This verifies the accuracy of each method for the determination of the stiffness factors, and aids in the process of comparing methodology and results.  Obviously, each experimental result is a good prediction of the performance of that specific connection system when used in exactly the same form on a con-

structed structure. The next best tool for predicting the stiffness for structural angles used as panel connectors is the use of the computer and finite element analysis methods. As shown on Figure 2.5.2 for welded angles and Figure 2.5.3 for bolted angles the experimental and finite element analytical curves are shaped similar to those found experimentally. This again indicates the accuracy of the analytical approach even though exact correlations have not been obtained. Table 2.5-2 is a composite of the values obtained experimentally and those found using the finite element analysis method.

Table 2.5-2.  Experimental and finite element results for the stiffness coefficient of structural angles.

| Angle Size | Welded | | Bolted | |
|---|---|---|---|---|
| | Experimental K (lbs/in) | F.E.M. K (lbs/in) | Experimental K (lbs/in) | F.E.M. K (lbs/in) |
| 4 x 6 x 3/8 | 70,195 | 57,142 | 28,586 | 31,306 |
| 4 x 6 x 1/2 | 75,721 | 134,495 | 64,794 | 74,142 |
| 4 x 6 x 5/8 | 223,671 | 260,669 | 102,986 | 144,656 |
| 6 x 8 x 1/2 | 71,526 | 71,194 | 49,586 | 32,327 |
| 6 x 8 x 3/4 | 131,497 | 237,690 | 84,667 | 108,916 |

Note the value for the stiffness coefficients of the 4 x 6 x 3/8 welded angle is obviously quite high for the experimental results when compared to the rest of the angles tested. This particular test result is too far off to be used, it is not feasible in this case for the experimental result to be higher than the calculated theoretical result. The same argument holds true for the 6 x 8 x 1/2 bolted angle results.
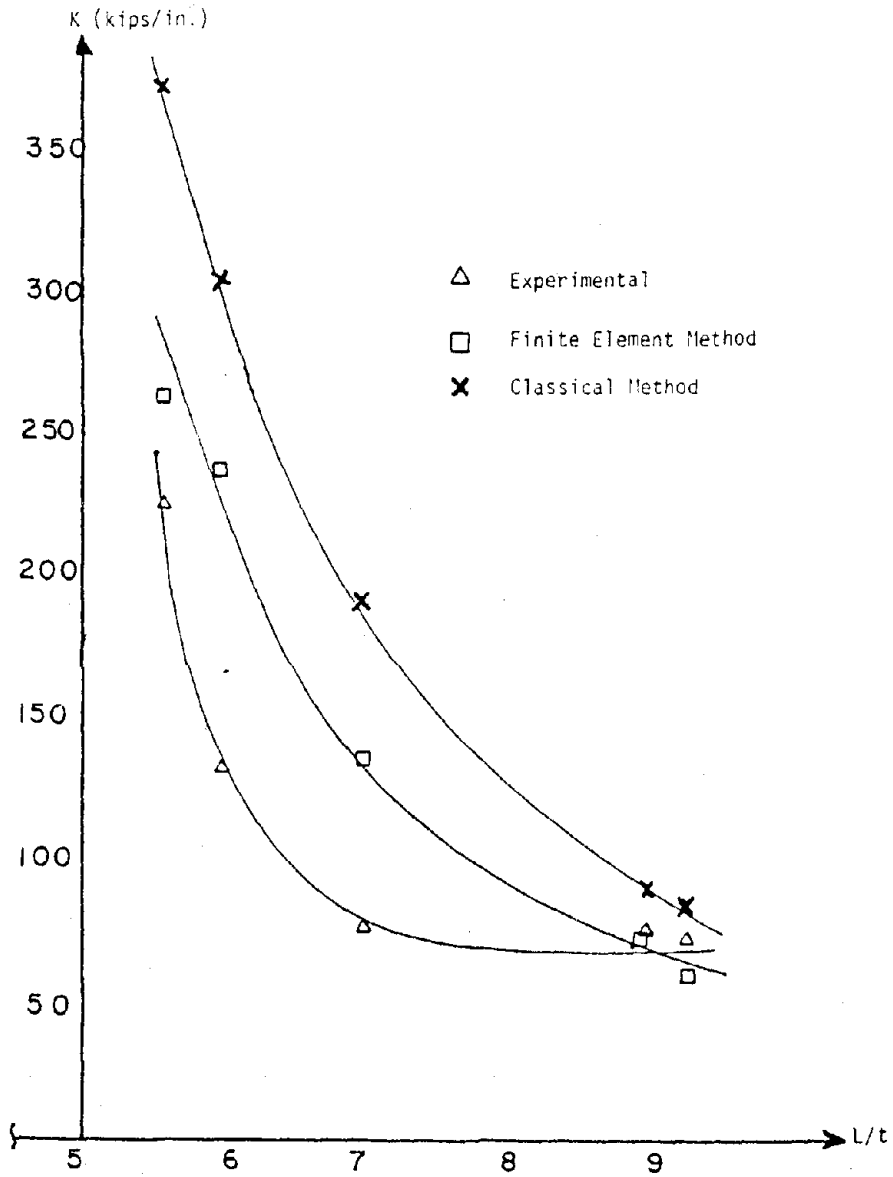
Figure 2.5.2 Elastic Stiffness Coefficient for Structural Angles Welded
to Anchor Plates. ( Experimental and Theoretical Results )
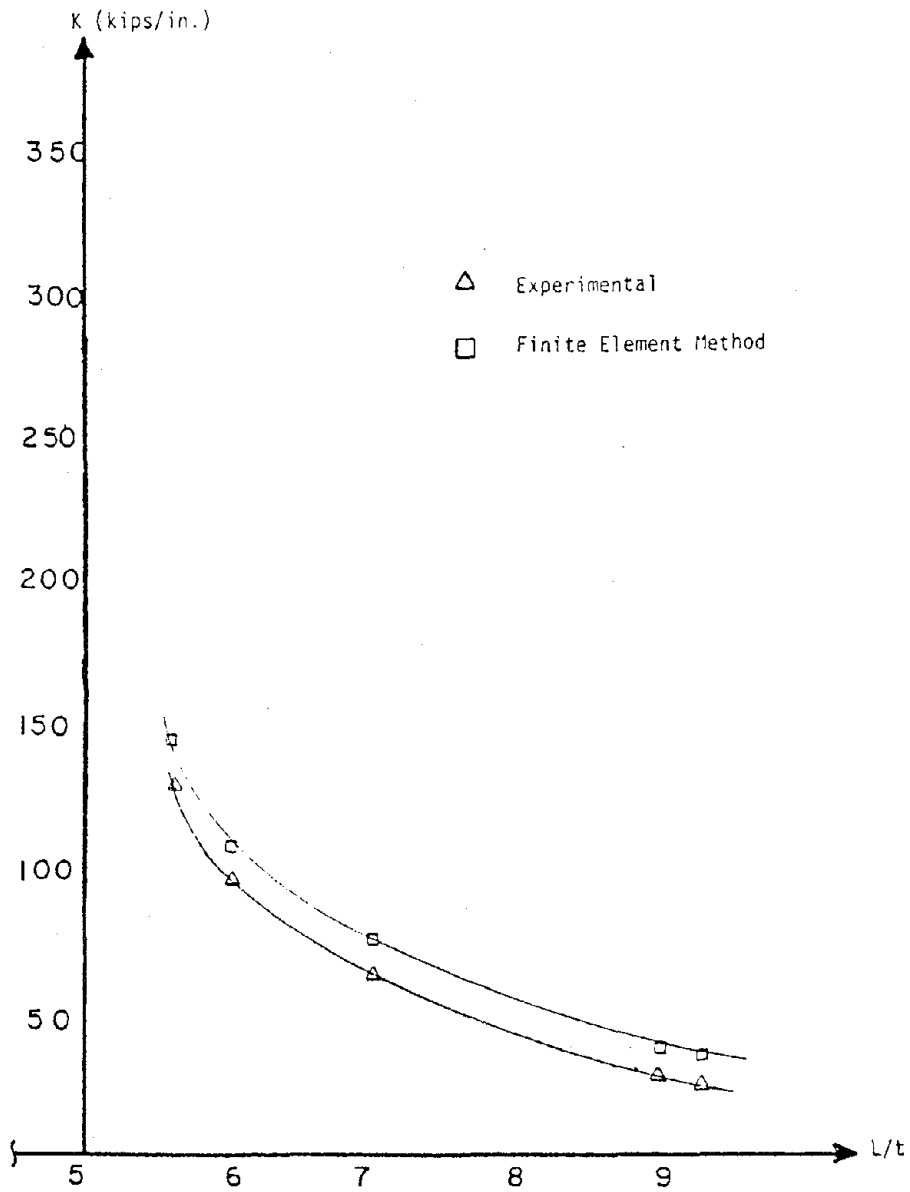
Figure 2.5.3 Elastic Stiffness Coefficients for Structural Angles bolted to the panels. (Experimental and Theoretical)

The model used for the finite element analysis was simplistic and a vast dissimilarity exists between the experimental results and those calculated in Section 2.4. The reasons for such variances lie with the complicated nature of the structural angle connection, and the very simplistic assumptions used to analyze the stiffness characteristics. For example, the torque on the bolts, the anchors for the inserts, and the inserts themselves are not modeled in any of the analytical studies, which accounts for part of the dissimilarity. The object of comparing the theoretical results and experimental results in this manner is to give the reader a basis with which to proceed for predicting stiffness values of connections which were not tested during the study. Further discussion of this will be presented in Section 2.6 of this paper.

There are other observations about the comparison of the finite element analytical results and experimental results that warrang additional comment. The deflection shapes witnessed by the investigator during the experimental testing of welded angles were simulated by the finite element run. The base of the analytical model pulled away from the anchor plate at the center line of the angle base in the same manner as did the lab tested angle. The output for the analytical run on the bolted angle connection also verified the investigator's experimental observation that the bolted angles showed translation at the base of the angle (nodes 11-15) and rotation at the angle corner (also nodes 11-15).

During that portion of the experimental study in which the angles were loaded past their elastic load limit it was noted where each connection formed the plastic zone. The analytical results from the Sap IV runs indicated that elements 5-8 experience the highest membrane stresses

and bending moments for bolted structural angles and elements 9-12 for welded structural angles. The plastic zones identified during the experimental study are in agreement with those found using Sap IV.

The structural angles were loaded horizontally (see Table 2.3-4 for the experimental results) to identify the stiffness properties in that direction. The stiffness and yield point for angles loaded laterally is so high compared to the expected earthquake induced loads that for analysis purposes complete rigidity may be assumed for the standard structural angles. For example, a 10,000 lb panel experiencing .4 g accelerations due to earthquake activity would induce only 2,000 lbs of lateral force in each of the two base support angles. (See Sessa, 1980) The stiffness factors for the angles tested ranged from 150,000 lbs/in. to 300,000 lbs/in. approximately, which indicates between .0133 in. and .0066 in. deflection would occur as a result of the lateral loads on the support angles. In general, the critical design parameter for lateral loads on an angle support is the shearing resistance of the hold down bolts.

## 2.5.3 Structural Angle Connections, Slotted

The stiffness coefficients obtained experimentally and those obtained through calculations using the structural analysis approach outlined in Section 2.4.2 are compiled here in Table 2.5-3 for comparison. The values obtained theoretically are within 30% of those obtained experimentally and can be used for predicting connection behavior. The stiffness values obtained theoretically are higher than the experimental values because the actual connection has several construction characteristics (as discussed in Section 2.3.4.2) which introduce increased flexi-

Table 2.5-3. Stiffness coefficients for the slotted angle connections (loaded vertically upward)

| Connection | Experimentally Obtained Values (lbs/in) | | | | | | Theoretical Values | | |
| | Slotted Structural Angles | | | | | | Slotted | | |
| | Insert Only | | | Insert with Plate | | | Loaded Vertically Up | | |
| Size (in. x in. x in.) | Vertical Loose | Vertical & Horizontal Loose | Both Tight | Vertical Loose | Vertical & Horizontal Loose | Both Tight | $\ell_1$ | $\ell_2$ | k (kips/in.) |
|---|---|---|---|---|---|---|---|---|---|
| 4 x 6 x 3/8 | 15,151 | -- | 22,763 | 27,964 | 26,562 | 31,250 | 3.5 | 1.562 | 34.25 |
| 4 x 6 x 1/2 | 28,782 | -- | 30,625 | 32,258 | 29,904 | 52,083 | 3.5 | 1.500 | 83.25 |
| 4 x 6 x 5/8 | 45,776 | -- | 47,169 | 105,042 | 93,552 | 129,533 | 3.5 | 1.437 | 166.50 |
| 6 x 8 x 1/2 | 40,952 | 37,513 | 54,347 | 40,322 | 37,878 | 52,083 | 4.0 | 2.000 | 51.00 |
| 6 x 8 x 3/4 | 62,662 | 54,704 | 111,940 | 88,967 | 80,906 | 125,000 | 4.0 | 1.875 | 178.00 |

bility in the system. The reason for using slotted angles is to dissoci-
ate the structure from the panel during a seismic loading situation by
allowing the structure to move without introducing forces to the panel.
The study has shown that as the structure moves, and the bolts subse-
quently move within the slotted holes of the angle, no load is induced to
the panel or the connection. This changes however if the interstory
drift of the structure is large enough to overcome the amount of movement
which the slot length is designed to accomodate. In that case the stiff-
ness of the slotted angle connection becomes critical due to the high
loads which the angle will withstand, and subsequently transfer to the
panel itself. If the seismic event is a magnitude greater than or equal
to an interstory drift which causes more movement than the slotted angle
can accomodate the slot bolts will be subjected to repeated impacts from
the angle as the building displaces.

The high stiffness obtained for these connections indicates that
very little additional displacement will be allowed when the bolt reaches
the end of the slotted hole. This implies the need for careful analysis
of the building response during seismic activity, increasing the stress
in the angles, the connection bolts and insert strength, and the ability
of the panel itself to withstand these transferred loads. Further
discussion on this subject is taken up in Section 2.6.

## 2.6   IMPLICATIONS FOR CONNECTION DESIGN

### 2.6.1 Connection Design Implications

The design of structural angle connections used as supports for the panels is based on the expected loads and the geometric properties of the system.  The information obtained from this study indicates that the angles are extremely stiff and allow little movement of the panel relative to the support attachments on the structural framework.  The controlling design criteria for these angles is the critical load induced laterally during an earthquake.  The angle designed to sustain these loads will usually meet the stiffness requirements to restrain lateral movements of the panel due to the lateral loads.  The high strength and stiffness for the common support angles may have an effect on the stiffness of the structural framework at the point of attachment.  The deep wide flange sections used as spandral beams, which are often oversized in order to accomodate the panels and their attachment requirements (as shown on the drawings listed in Table 2.1-1) and the integration of the composite floor construction produce a very rigid floor section upon which the precast panel would have little effect regarding additional stiffness.  However, for those systems which employ nominal framing for carrying curtain wall panels, the stiffness added by the panel support connections may be very significant.  For this type of panel system the design of the support connections is still controlled by the necessary load carrying capacity but close attention to the stiffness properties of the beam-panel system would allow the designer to make efficient use of

the structural framing steel. Note that ATC-3 does not allow connectors to be relied upon for added stiffness. The current design procedure for obtaining the moment capacity of structural angles (as discussed in Appendix A) is adequate for the needs of most precast panel systems.

The experimental study was limited to several representative types of structural support connections. A designer wishing to obtain a stiffness coefficient for a specific connection design not tested experimentally may find assistance from the comparisons made in section 6 of this paper between experimental values and theoretical values. Using the techniques employed by the author and applying a correction factor based on the results of this study and sound engineering judgment, would enable the designer to closely predict the stiffness coefficient of his connection design.

The design of flexible connections used to accommodate the interstory drift caused by the accelerations due to seismic activity is often controlled by the shear and tension applied to the connection. The critical load which determines the size of the bar-insert connection is the tension or pull out force. The size of the bar then determines the unbraced length of the bar necessary to produce the desired flexibility for accommodating interstory drift. A check is made to determine if the unbraced length will inhibit buckling of the bar used as the connector body under the expected normal loads to the panel. The length of the bar is selected to allow maximum flexibility in the lateral direction without sacrificing axial strength to resist buckling. The use of Figure 2.5.1 gives the designer the ability to estimate the flexibility of a bar insert connection for the controlling values of $\ell/d$.

There are situations when the desired flexibility is more than can be obtained with a bar insert connection due to geometric constraints or excessive normal loads due to wind, for example. In these cases, the use of slotted connections may be the best answer. The normal loads on the panel can be easily sustained with structural angles as shown in the experimental results of this study. The interstory drift may be accommodated by sizing the slots such that frame travel is less than one-half the slot length. The interstory drift problem may be alleviated by the use of horizontal slots only if care is taken in both design and construction to ensure free travel of the bolts through the slots. Vertical displacement due to the drift may be accommodated by vertically oriented slots. The slotted angle connection does not provide a mechanism for energy dissipation whereas the flexible bar insert connection does. This may be of little consequence when compared to the amount of energy induced by the ground accelerations for buildings with high natural frequencies, but for highrise structures with thousands of panels, the dissipated energy may be a significant contribution in the building response to seismic activity.

That portion of the study which investigated the dissociative type of connections, slotted angles and bar-insert connections, is of particular importance to the designers who choose panels which utilize those types of connections. Several observations which were made in the body of the text of this report are listed here to reemphasize the point for the designer.

1. A flexible bar-insert connection has a low elastic load limit, and a low stiffness coefficient. This low-stiffness coefficient allows

the framework to experience severe interstory drift without inducing large loads to the panel, and those loads which are induced are not going to cause any damage to the concrete of the precast panel (which has a $f_c' \geq 5000$ usually) or to the insert itself. It should also be noted that a steel face plate at the panel surface is not necessary to protect the concrete surface.

2. Slotted angles are extremely effective for dissociating the panel from the structure as long as the slots are lined up so the bolts travel smoothly through them. It is absolutely necessary to ensure that quality construction is maintained during the erection process so that the proper low friction washers are installed, and the bolts are correctly placed to ensure smooth travel. If the bolts become bound with the angle, the panel and spandral beam will experience severe loadings due to the high stiffness coefficients of the commonly used structural angles

3. The use of anchor plates and welded angles for bearing support connections is an acceptable method provided the welds used are adequate. The welded angle anchor plate system performed very well during the cyclic tests in the lab, and it can be expected to do so in the field provided quality construction is maintained.

4. The use of slotted connections must be predicated on an accurate dynamic response analysis of the entire structure for seismic activity. Should a slotted connection be used and a seismic event occur which has a magnitude sufficient to cause an interstory drift larger than the slots of the connection can accommodate, then severe impact loads are going to be put on the connection system, the panel and the spandral beam. This requirement, as well as the need for very close construction inspec-

tion indicates that the slotted angle is not as simple an answer to the connection design problem as is the flexible bar insert system.

5. The performance of the bar-insert flexible connection is dependent upon several construction aspects (as discussed in section 2.3.4.1of this paper) which require careful inspections to ensure proper installation. Faulty welds, loose nuts, lack of washers and poor alignment are all construction items which can drastically alter the performance of a bar insert connection and even (in this investigator's opinion) increase the possibility of catastrophic failure of the panel connection.

## 2.6.2 Safety Concerns

The safety concerns which were raised during discussions with members of the curtain wall panel industry (designers and fabricators) were:

1. brittle fracture of a flexible connection at the panel interface after a limited number of load reversals due to earthquake activity,

2. slotted angles rendered ineffective by movement of the structural framework that does not return to original orientation, i.e., bolt no longer centered in the slot after an earthquake,

3. slotted connections not properly aligned during construction.

4. welded connections lacking ductility.

During the limited cyclic loading sequence of this study several bar insert connections and structural angle (welded type only) connections were tested and none of these experienced any signs of brittle fracture. The one bar which did develop a crack was not properly

tightened into the insert. More tests are necessary in cyclic loading before a definitive statement can be made. However, it is the opinion of this investigator that even though moderate earthquakes are going to cause the loads necessary to yield the rods used in flexible connections, brittle fracture of the bars is unlikely unless thousands of repeated yieldings occur. Also it is much more disconcerting to the investigator that poor quality control during the construction phase of placing the panels is more likely to cause severe problems for the proper performance of the panel system than a brittle fracture failure after a limited number of load reversals.

The problem of slotted angles not returning to center after an earthquake can not be adequately addressed here, more cyclic tests will be needed by future investigators in order to fully answer this question on connection behavior. It is the opinion of the author, however, that proper design and dynamic response analysis will prevent this from occurring during a design earthquake on the building. It also seems that if the connector slot is initially centered during erection, and yielding has not occurred in the primary structure the connector will always be centered. And, should a maxi earthquake be experienced a noncentered slotted connection will be a minor worry of the building owner.

Proper alignment of slotted connections is a valid concern and can prove to be a prominent cause of inducing extremely high loads into the panel and spandral beam. Should a slotted angle bind for any reason, the stiffness which the connection then possesses is equal to that of a bearing support angle of equal dimension. Obviously the loads this type of connection can transfer are enormous and could cause severe damage should the panel and spandral beam not be adequately designed to accommodate them.

Again it must be emphasized that more cyclic tests should be run in order to address the concern about the fatigue susceptibility of welded connections. It is the belief of the author that properly designed and field inspected welded connections will result in an acceptable system.

## 2.7  CONCLUSIONS

The objective of this section was to investigate the energy dissipation characteristics and the stiffness characteristics of some of the most commonly used curtain wall panel connections.  These objectives were met and the results have led the author to the following conclusions regarding connection design and performance.

1.  Comparisons of analytical and experimental results from this study indicate that finite element analysis as well as careful structural analysis using classical methods can provide realistic estimates of the stiffness coefficients for curtain wall connections.

2.  The connection systems studied here have performed acceptably with respect to the strength of the ferrule inserts used in conjunction with threaded bars or bolted structural angles.  There were no failures of the inserts during any of the experimental tests.

3.  The in plane stiffness coefficients associated with the four basic ferrule inserts indicate that all of these inserts perform identically under similar in plane loading situations.

4.  Panel connections may be assumed to perform as ideally elastic perfectly plastic.

5.  The energy dissipation characteristics for a connection system can be based on the product of the interstory drift and the plastic load limit.

6.  The use of face plates with connections using single inserts and threaded bars is not necessary.  The insert and the concrete of the

panel do not need additional steel plates for response to in plane loads. A useful purpose of the face plate steel may be to increase the pull out resistance of the insert when designing for high loads normal to the panel surface.

7. Construction practices can play a major role in the behavior of curtain wall panels during a seismic event. Poor welding, loose nuts, untightened bolts, misaligned slotted angles are some of the items which can cause catastrophic failure of a panel under seismic loads.

8. During the cyclic tests that were conducted it was obvious that the concrete of the panels maintained its integrity. There was no spalling or cracking and all connections yielded prior to any damage to the panel. This is significant in that the most severe loads induced by a seismic event should cause little or no damage to the concrete surrounding the panel fastener. This is not to say that panel damage will not occur from other sources, such as impingement or projectile impact during a seismic event.

9. Anchor plates which use nelson studs or welded rebar for attachment are acceptable for attaching support angles and lateral connections. Proper sizing and welding gives this method a reliability equal to embedded inserts or anchor bolts. During the yielding phase of the experimental study each anchor plate remained in place and showed no signs of failure for all of the welded support connections tested.

In summary, the overall performance of the basic curtain wall connections tested during this experimental study was excellent. High-rise buildings, which make use of the precast panels for curtain walls, may be assumed to respond favorably during a severe seismic event.

Panels may be damaged but should, given proper construction practices,

remain on the building in one piece.

### 3.0 TASK II: ANALYTICAL INVESTIGATION OF CURTAIN WALL ASSEMBLAGES

## 3.1 Introduction

Recently, a large number of advances have been made in the theoretical and computational analysis of nonlinear structures and a number of general purpose computer programs for nonlinear analysis have been developed. Three excellent papers have been written which summarize the current solution methods available for nonlinear dynamic analysis (Argyris *et al.* 1979; Mondkar and Powell 1978; Bathe 1976). Many others have addressed the nonlinear dynamic analysis problem including Morris (1977), Clough and Penzien (1975), and Oden (1972). Most of the authors agree that the only generally applicable method for the analysis of arbitrary nonlinear systems is the numerical step-by-step integration of the coupled equations of motion in the time domain, although modal methods may be used for mildly nonlinear applications (Argyris *et al.* 1979).

Mondkar and Powell (1978) summarize the combinations of solution schemes presently used in computer programs for nonlinear static and dynamic analyses. The available schemes include the step-by-step solution, the Newton-Raphson iteration, the constant stiffness iteration, and an adaptable scheme in which the structural stiffness is reformed only when needed. In the step-by-step solution procedure, the load is applied in small steps and the structure is assumed to respond linearly within each step. In the Newton-Raphson iteration the structural stiffness matrix is reformulated at every iteration while in the constant stiffness iteration the stiffness matrix is only formed once. Many of these schemes and combinations of these schemes are presently being used. Some of these methods can be categorized as follows:

1. Step-by-step procedure with stiffness reformation at the end of every load increment within the step.

2. Newton-Raphson iteration within every time step.

3. Constant stiffness iteration within every time step and stiffness reformation at the end of every time step.

4. Constant stiffness iterations within every time step using the initial elastic stiffness throughout.

5. Step-by-step procedure in time with stiffness reformation at specified time intervals.

6. Constant stiffness iterations within each time step but the stiffness is reformulated if convergence is not obtainable in a specific number of constant stiffness iterations.

7. Mixed iteration procedure within each time step in which Newton-Raphson iterations are followed by constant stiffness iterations.

For more information about these schemes, refer to Mondkar and Powell (1978), Desai and Abel (1972), and Argyris *et al.* (1979).

No single scheme appears to be optimal for all types of nonlinear structures and each scheme may differ on the basis of accuracy and efficiency. Apparently, most of the authors believe that important development and research is needed in all areas of nonlinear finite element analysis, particularly relating to dynamic analyses.

This section presents the analytical methods used to develop the mathematical model used in Task II and provides the basis for the refined mathematical model to be developed in Task IV. The displacement method was selected for use in the analysis because it can provide a general solution method for most curtain wall-framing configurations and can be implemented on the computer. Traditional elements are used to idealize the structural framing while the two dimensional planar panel element developed by Briggs

(1980) is used to model the precast curtain walls. Two fundamental analytical capabilities are developed in this section: calculation of response due to static loading and calculation of response due to dynamic loading. In the static analyses, both linear and nonlinear material properties in the panel-frame connections are considered while the primary structure is assumed to behave linearly elastic. Only linear dynamic analysis capabilities are developed and are based on a lumped mass system to approximate distribution of masses.

A three dimensional computer program, SAPFAP, was developed to implement all of these analytical capabilities. SAPFAP is a modified version of SAP IV (Bathe *et al.* 1974), a general purpose static and dynamic analysis program. With this program, individual panel elements can be modeled into the structural system and the response of the system analyzed. Although this is a three dimensional program, it should be noted that only lateral stiffness contributions from the panel elements are considered. Computer models of the five full-scale laboratory tests conducted at the University of Idaho (Task III) are then developed using this program and are analyzed for static and dynamic response. With these models, the tests performed in Task III were analyzed completely and compared to the experimental values.

## 3.2 METHOD OF ANALYSIS

The purpose of this section is to present the theory and assumptions used to develop the analytical capabilities for predicting the interaction between structural framing and precast concrete panels. Four types of analysis methods are discussed: (1) linear static analysis, (2) nonlinear static analysis based on the nonlinear material properties of the panel-frame connections, (3) linear dynamic analysis, and (4) nonlinear dynamic analysis based on nonlinear panel-frame connections.

Because of the previous work done by Briggs (1976) and Mak (1977), the displacement method was selected as the basis for analysis. This previous work demonstrated that the panel element stiffness matrix derived by Briggs can be used successfully in the displacement method and can provide reasonable estimates of lateral stiffness contributions made by the precast curtain wall elements. The displacement method provides a general solution method for most curtain wall-framing configurations and can be used to predict dynamic response.

Included in this section is a discussion of a precast curtain wall element and the method used to predict the response of structural framing with precast panels due to static and dynamic loading conditions.

### 3.2.1 Precast Curtain Wall Element

The curtain wall element model developed by Briggs (1976) consists of a precast panel that is attached to the supporting structure at four distinct points. A panel-frame connection is typically composed of structural angle and bolts both of which have horizontal and vertical stiffnesses that are

much less than that of a precast curtain wall. Consequently, Briggs assumed the panel to be rigid while all the deformation associated with the panel assembly is attributed to the four connections. Thus, as the supporting structure is deformed and the panel moves, the distances between panel points remain constant while the supporting structure changes shape. The idealized panel element and panel-frame connection is shown in Figure 3.2.1.

All loads transferred between the panel assembly and the structural framing must be introduced through the panel connections. Any load distribution by contact between precast panels can cause inaccuracies in the analysis and should be noted when the panel stiffness is used in structural analysis. Briggs performed a kinematic analysis of the panel movement and developed the basis for determining the relative panel displacements that will result in the panels contacting each other.

Briggs developed both a two dimensional and three dimensional elemental stiffness matrix for precast curtain walls. For each panel-frame connection, there are six freedoms, three translational and three rotational. In the two dimensional model, only the two in-plane translational freedoms in the X and Y directions are considered as shown in Figure 3.2.2. For the three dimensional analysis, a more general elemental stiffness matrix was developed with six freedoms at each node as shown in Figure 3.2.3. Although the three dimensional model would be the most desirable in structural analysis, it is not used in the analysis being described for the following two reasons.

First, in the derivation of the stiffness matrix for the panel element, it is assumed that the stiffness of the connections are known for each freedom. These stiffnesses are determined from experimental and analytical data, and are based on the slope of load-deflection and load-rotation curves.

Precast Curtain Wall

Panel Connection
(Either Isolation or Integration)

(a)

Precast Curtain Wall

Supporting Structure

Panel Connection
(Either Isolation or Integration)

(b)
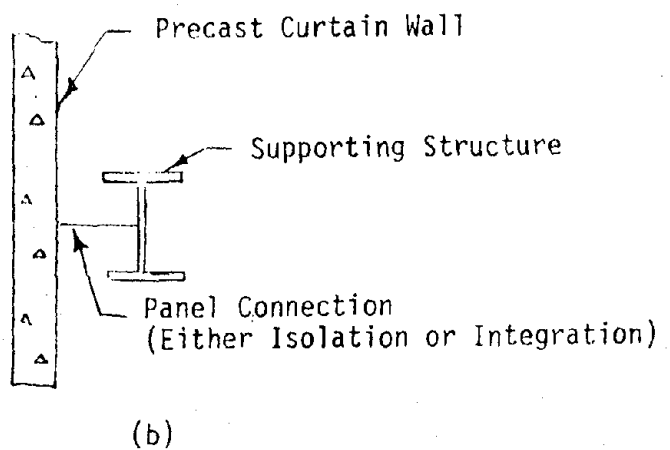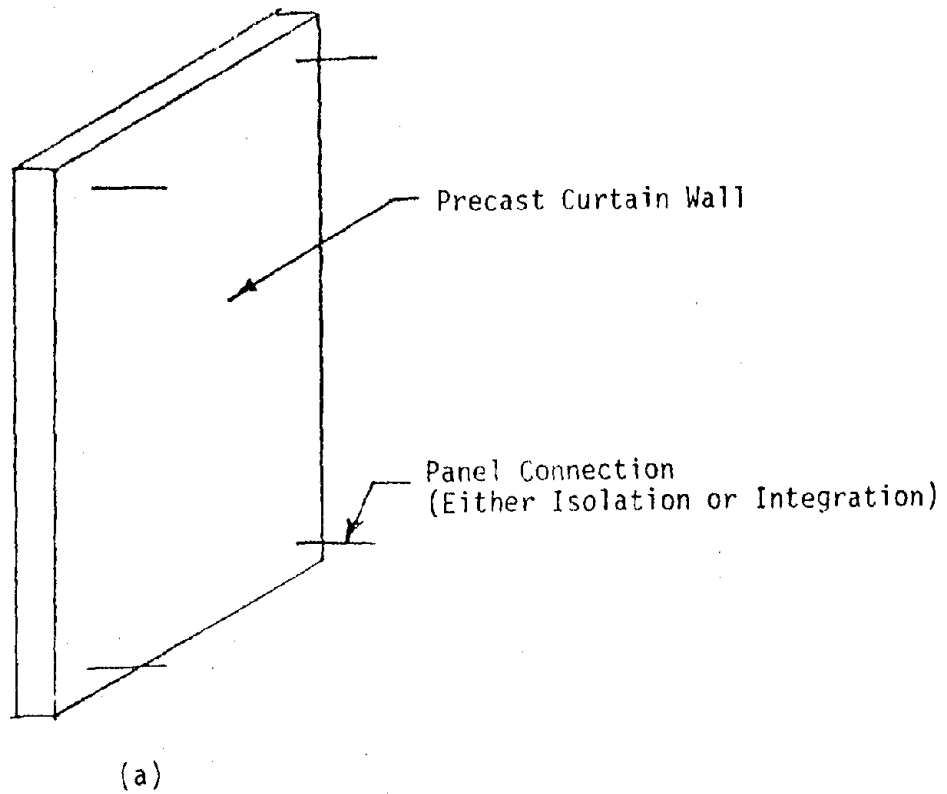
Figure 3.2.1. (a) Idealized Panel Element, (b) Idealized Structure-Panel
Connection (from Briggs 1976)
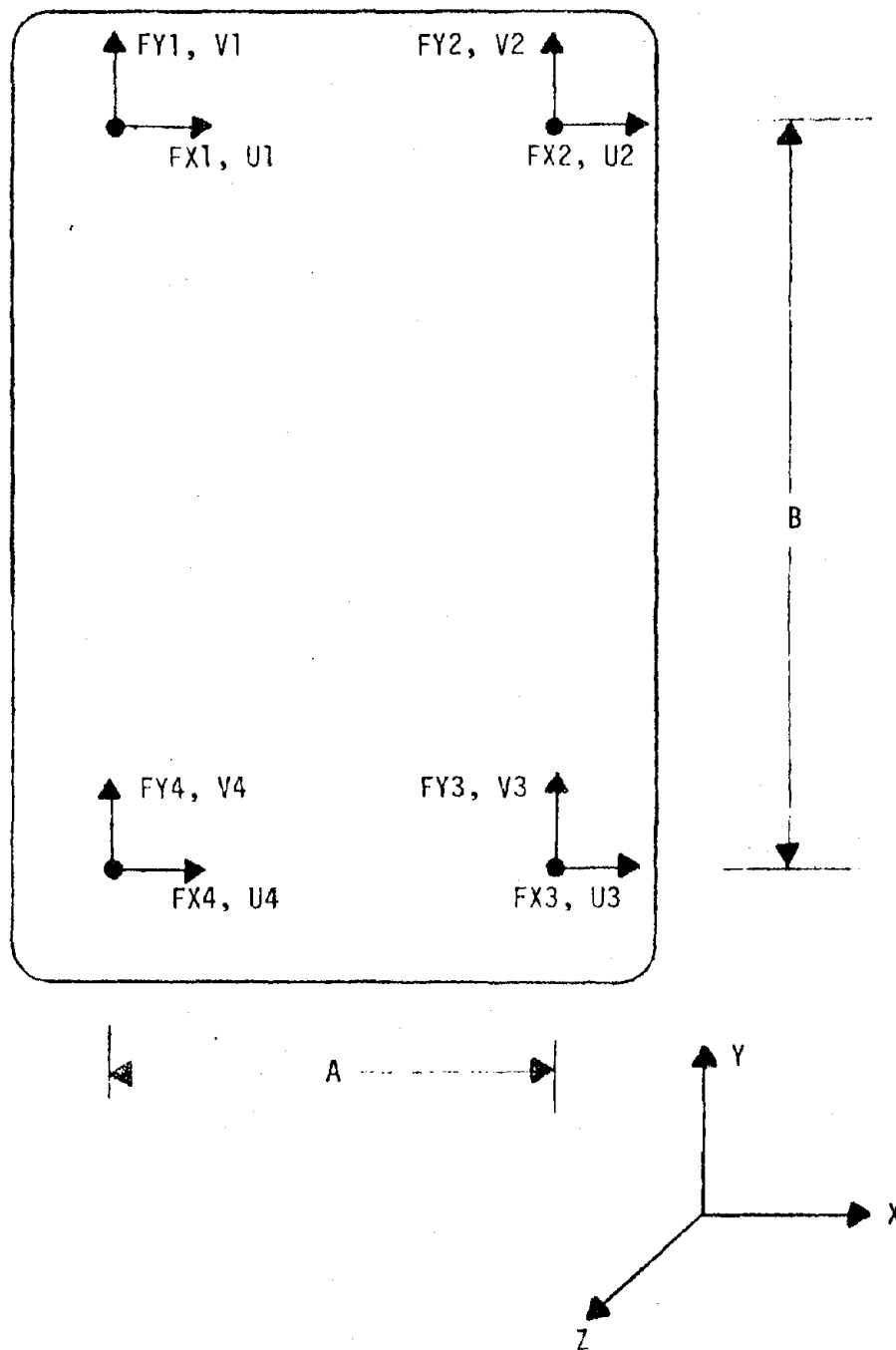
Figure 3.2.2. Model of Two Dimensional Panel Element (from Briggs 1976)
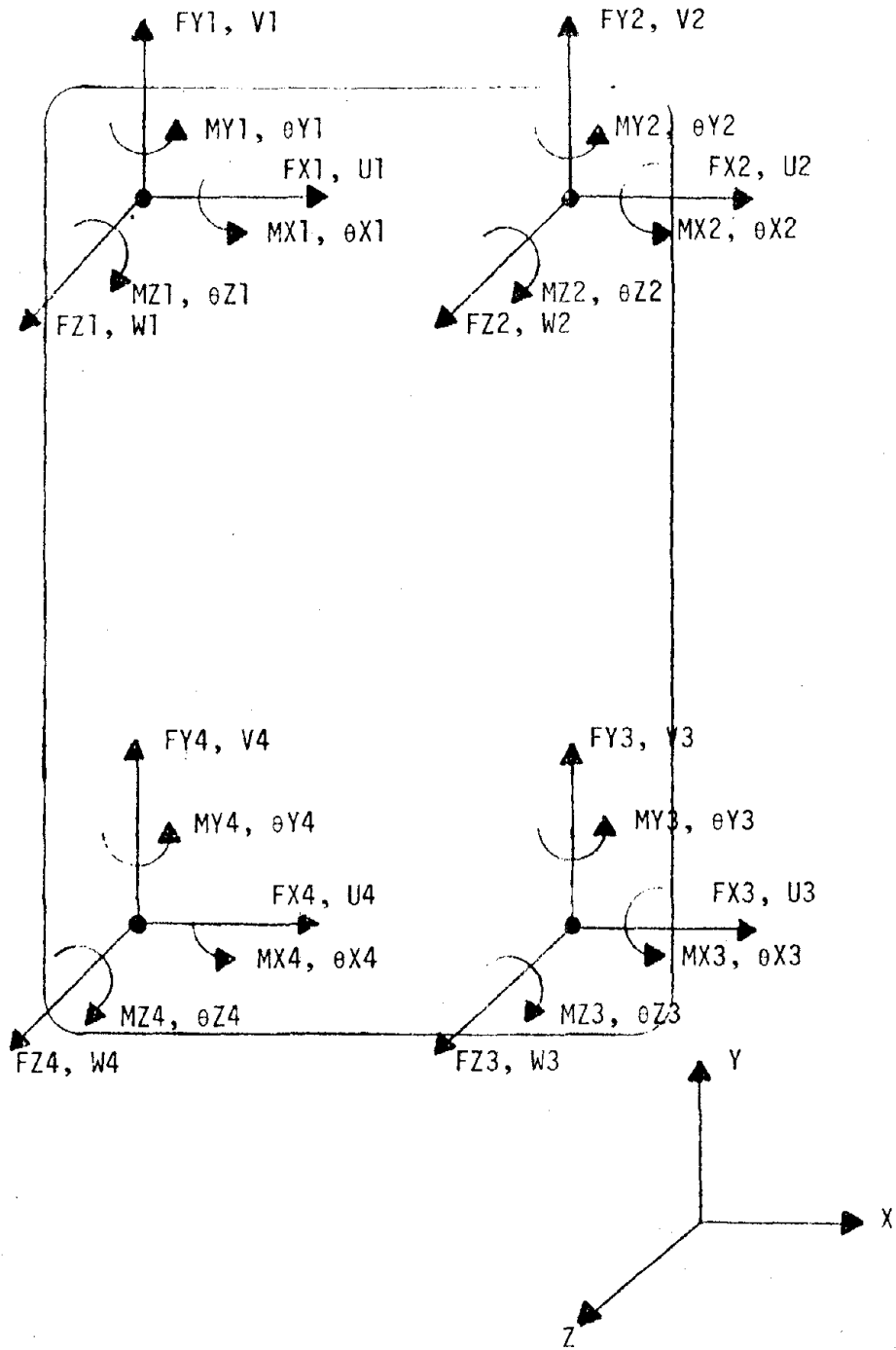
Figure 3.2.3. Model of Three Dimensional Panel Element (from Briggs 1976)

Presently, only load-displacement relationships for typical panel connections have been developed for the translational freedoms in the X and Y directions (Sessa 1980). Consequently, use of a complete three dimensional element would not be practical at this time.

The second reason the two dimensional model is used is that matrix inversion is required for the development of each panel elemental stiffness matrix. The two dimensional panel element requires inversion of an 8 by 8 flexibility matrix while the three dimensional model requires inversion of an 18 by 18 flexibility matrix as will be shown later on in this section. It can be shown that it takes approximately 10 times more computational effort (cost) to invert the 18 by 18 full flexibility matrix than the 8 by 8 matrix. Although inversion of an 18 by 18 matrix is not a large task, inversion of this size of matrix for many panel element stiffness matrices could be costly, particularly in nonlinear analysis where the stiffness matrices may have to be reformulated for each increment of load. Comparing the two and three dimensional panel element models leads to the conclusion that the two dimensional model is the most practical choice at this time for developing the panel element. It should be noted that the two dimensional model only considers the lateral stiffness (in-plane) contribution of the panel element and neglects the stiffness contributions perpendicular to the panel. A more in depth look at the limitations of the two dimensional model can be found at the end of this section.

Briggs developed the panel-element stiffness matrix using the flexibility-stiffness transformation method. (For more information about this method, see Gallagher (1975)). The two dimensional element is based on the freedoms shown in Figure 3.2.2 and incorporates all 8 freedoms in the following stiffness matrix.

$$\bar{k} = \begin{bmatrix} \underline{F}^{-1} & | & \underline{F}^{-1}\,\bar{\underline{R}}^{T} \\ \hline \bar{\underline{R}}\,\underline{F}^{-1} & | & \bar{\underline{R}}\,\underline{F}^{-1}\,\bar{\underline{R}}^{T} \end{bmatrix}$$

(3.2.1)

where

$$\bar{\underline{R}} = \begin{bmatrix} -1 & -1 & 0 & -1 & 0 \\ 0 & B/A & 0 & B/A & -1 \\ 0 & B/A & -1 & -B/A & 0 \end{bmatrix}$$

(3.2.2)

$\bar{k}$ = Panel elemental stiffness matrix in local coordinates

$\bar{\underline{R}}$ = Static equilibrium matrix

$\underline{F}$ = Flexibility matrix of the panel element supported at the U1, V1, and V2 freedoms (shown in Figure 2.4)

A = Width of panel (between connection points)

B = Height of panel (between connection points)

KX1 = Individual panel connection stiffness in the X direction for node 1

KY1 = Individual panel connection stiffness in the Y direction for node 1

It should be noted that this stiffness matrix is not arranged in a form traditionally used in matrix structural analysis but relates forces and displacements as follows.

$$\begin{bmatrix} FX2 \\ FX3 \\ FY3 \\ FX4 \\ FY4 \\ FX1 \\ FY1 \\ FY2 \end{bmatrix} = \bar{k} \begin{bmatrix} U2 \\ U3 \\ V3 \\ U4 \\ V4 \\ U1 \\ V1 \\ V2 \end{bmatrix}$$

(3.3.3)

By proper rearranging of rows and columns of the stiffness matrix and adding in zero values of stiffness for the stiffnesses in the Z direction, Equation 3.3.3 can be expanded into the following matrix equation. This equation describes the behavior of the panel in local coordinates in three dimensions considering

$$\underline{F} = \begin{bmatrix} \dfrac{1}{KX1} + \dfrac{1}{KX2} & \dfrac{1}{KX1} & 0 & \dfrac{1}{KX1} & 0 \\[4mm] \dfrac{1}{KX1} & \dfrac{1}{KX1} + \dfrac{B^2}{A^2 KY1} + \dfrac{B^2}{A^2 KY2} + \dfrac{1}{KX3} & \dfrac{B}{A KY2} & \dfrac{1}{KX1} + \dfrac{B^2}{A^2 KY1} + \dfrac{B^2}{A^2 KY2} & -\dfrac{B}{A \cdot KY1} \\[4mm] 0 & \dfrac{B}{A\, KY2} & \dfrac{1}{KY2} + \dfrac{1}{KY3} & \dfrac{B}{A \cdot KY2} & 0 \\[4mm] \dfrac{1}{KX1} & \dfrac{1}{KX1} + \dfrac{B^2}{A^2 KY1} + \dfrac{B^2}{A^2 KY2} & \dfrac{B}{A \cdot KY2} & \dfrac{1}{KX1} + \dfrac{B^2}{A^2 KY1} + \dfrac{B^2}{A^2 KY2} + \dfrac{1}{KX4} & -\dfrac{B}{A \cdot KY1} \\[4mm] 0 & \dfrac{-B}{A \cdot KY1} & 0 & -\dfrac{B}{A \cdot KY1} & \dfrac{1}{KY1} + \dfrac{1}{KY4} \end{bmatrix}$$

Figure 3.2.4. Flexibility Matrix of the Panel Element Supported at the U1, V1, and V2 Freedoms

only the panel connection stiffnesses in the local X and Y direction; that is, only the lateral stiffness contribution of panel element is considered.

$$
\begin{bmatrix} FX1 \\ FY1 \\ FZ1 \\ FX2 \\ FY2 \\ FZ2 \\ FX3 \\ FY3 \\ FZ3 \\ FX4 \\ FY4 \\ FZ4 \end{bmatrix} = \underline{\bar{k}}_{12 \times 12} \begin{bmatrix} U1 \\ V1 \\ W1 \\ U2 \\ V2 \\ W2 \\ U3 \\ V3 \\ W3 \\ U4 \\ V4 \\ W4 \end{bmatrix}
$$

(3.2.4)

To transform the stiffness matrix into global coordinates, the stiffness matrix in local coordinates must be multiplied by the transformation matrix and its transpose. (For example, see Cook (1974).)

$$
\underline{k} = \underline{T}^T \underline{\bar{k}} \underline{T}
$$

(3.2.5)

where

$$
\underline{T}_{12 \times 12} = \begin{bmatrix} \underline{L} & 0 & 0 & 0 \\ 0 & \underline{L} & 0 & 0 \\ 0 & 0 & \underline{L} & 0 \\ 0 & 0 & 0 & \underline{L} \end{bmatrix}
$$

(3.2.6)

$$
\underline{L} = \begin{bmatrix} l_1 & l_2 & l_3 \\ m_1 & m_2 & m_3 \\ n_1 & n_2 & n_3 \end{bmatrix}
$$

(3.2.7)

$\underline{T}$ = Coordinate transformation matrix

$\underline{L}$ = Matrix of direction cosines

$l, m, n$ = Direction cosines

The stress matrix in global coordinates is formed in a similar fashion; the stress matrix being defined as the matrix which directly yields panel

connection forces in terms of the nodal displacements

$$\underline{S} = \bar{\underline{k}} \ T \tag{3.2.8}$$

and

$$\underline{r} = \underline{S} \ \underline{d} \tag{3.2.9}$$

where

$\underline{S}$ = Stress matrix in global coordinates

$\underline{r}$ = Vector of elemental stresses (or internal loads)

$\underline{d}$ = Vector of elemental displacements

At this point, it is appropriate to identify some of the limitations of the two dimensional panel element developed by Briggs. As mentioned throughout this section, the two dimensional element only accounts for the planar or lateral stiffness contributions made by the precast curtain wall. Stiffness contributions made by the panel element other than those in the plane of the panel are neglected. Since the wind or an earthquake may load the structure from any direction, neglecting these additional stiffnesses in a three dimensional problem will lead to a less accurate prediction of the response of the structure. It should also be noted that Briggs neglected the rotational stiffness contribution made by individual panel connections in the two dimensional model. Significant rotational stiffness could arise in panel connections composed of structural angle but is likely to be small in flexible rod connections. The actual rotational stiffness contribution would require experimental and/or analytical investigations into each connection type. Neglecting this stiffness term leads to a slightly more flexible panel element.

There are also several limitations when applying the panel element. The panel element was derived with assumption that the connection pattern is

rectangular in shape as shown in Figure 3.25. Consequently, panels with non-
rectangular connection patterns cannot be analyzed using this element. A
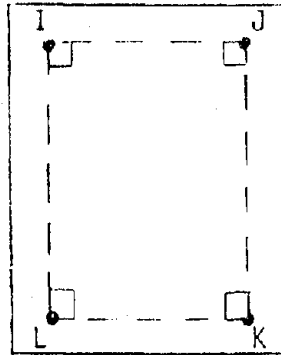


Figure 3.25. Perpendicular Panel Connection Pattern

numerical limitation involves connections with zero stiffness; for example,
the stiffness of a slotted connection if it is assumed that there is no fric-
tion between the connection and structural frame or the stiffness of an
elastic-perfectly plastic connection when loaded in the post yield state.
The panel stiffness matrix is formulated from the flexibility matrix given
in Figure 3.2.4. Note that all of the stiffness terms (KX1, KY1, etc.) are
in the denominator of each entry thus inputting a zero stiffness will cause
an entry to be undefined. An acceptable way to overcome this and obtain an
approximate solution is to enter a stiffness term of significant magnitude
less than the other connection stiffness terms for the zero stiffness value.
It has been shown that using a stiffness value equal to one thousandth of
the other connection stiffnesses will provide good results and will not intro-
duce numerical instabilities.

### 3.2.2. Linear Static Solution Method

The static analysis process consists of essentially three phases when using the displacement method (Bathe and Wilson 1976).

1. Calculation of the structural stiffness matrix and formation of the load vector.

2. Solution of the equilibrium equations.

3. Evaluation of elemental stresses.

Although the total solution may be subdivided into these phases, it should be realized that the implementation of one phase can have a pronounced effect on the efficiency of other phases when this method is applied to computer techniques.

A linear static solution requires the solution of the equilibrium equations

$$\underline{R} = \underline{K}\,\underline{D} \qquad\qquad (3.2.10)$$

where $\underline{R}$ equals the load vector, $\underline{K}$ equals structural stiffness, and $\underline{D}$ equals the displacement vector. The structural stiffness matrix is formed by the direct addition of the individual element stiffness matrices, i.e., enforcement of equilibrium. The structural stiffness matrix is given by

$$\underline{K} = \sum_{n=1}^{M} \underline{k}_n \qquad\qquad (3.2.11)$$

where $\underline{k}_n$ is the stiffness matrix for the nth element and M is the total number of elements. Elemental stiffness matrices for beam, truss, boundary, and panel elements are all merged into the same structural stiffness matrix. Beam, truss, and boundary elemental stiffness matrices are formed in the usual fashion described in finite element analysis books while panel elemental stiffness matrices are based on Equation 3.2.1 in Section 3.2.1. Formally elemental stiffness matrices, $\underline{k}_n$, are of the same order as the structural

stiffness matrix, $\underline{K}$. Nonzero entries in the elemental stiffness matrices occur only in those rows and columns that correspond to elemental degrees of freedom. The addition of the elemental matrices can therefore be performed by using the elemental matrices in compact form together with identification arrays which relate elemental and structural degrees of freedom (Bathe and Wilson 1976). Consequently, only the compacted elemental stiffness matrices (which are of order ·equal to the number of elemental degrees of freedom) and identification arrays need to be found, thus reducing storage requirements for a computer program.

The solution of Equation 3.2.10 involves the inversion of the structural stiffness matrix such that

$$\underline{D} = \underline{K}^{-1} \underline{R} \qquad (3.2.12)$$

where $\underline{K}^{-1}$ = the inverse of the structural stiffness matrix. It should be noted that the structural stiffness matrix is never inverted explicitly, but is solved with numerical methods. These numerical methods lead to a minimum number of operations to solve the equilibrium equation; i.e., there are no operations on entries in the structural stiffness matrix with zero elements. Once the displacements are known, the elemental stresses or internal forces can be calculated by multiplying the elemental stress matrix by the appropriate displacements as shown below:

$$\underline{r} = \underline{S} \underline{d} \text{ or } \underline{r} = \overline{k} \underline{T} \underline{d} \qquad (3.2.9)$$

where $\underline{r}$ equals the vector of elemental stresses (or internal forces), $\underline{S}$ equals the elemental stress matrix, and $\underline{d}$ equals the elemental displacement vector.

### 3.2.3. Nonlinear Static Solution Method

A nonlinear static analysis solution method was developed to account for the nonlinear material properties in the panel connections. It was assumed that the structural framing behaved linearly elastic. Four possible solution techniques were available to approximate the nonlinearity of the panel connections: (1) the incremental, (2) the iterative, (3) the initial strain, and (4) the·initial stress methods. (Each of these methods have been used extensively in the past and are outlined, for example in Desai and Abel (1972).) Although the incremental procedure is probably not as efficient as the iterative method in terms of computational efficiency, it was selected because of the convenient manner with which it could be programmed.

The incremental procedure is a varying stiffness method; that is, the stiffness matrix is updated after each load increment. The fundamental equations used to calculate linear static displacements and stresses (Equations 3.2.9 and 3.2.10 are used in an incremental form in the nonlinear analysis. To approximate the exact solution, the total load or load vector is subdivided into equal increments and then the structure is loaded one increment at a time. At the end of each load increment, the structural stiffness matrix is adjusted as necessary; that is, the nonlinearity is treated as piecewise linear. Consequently, smaller increments will result in a more accurate solution. Note that for each load increment, the structural stiffness matrix must be altered, the equilibrium equations solved, and stresses calculated. Thus, the more increments the load is broken up into, the greater the computational effort.

Since the stiffness is updated at the end of each increment, the predicted stiffness of the structure will be greater than the true stiffness of

the structure. This is shown for a structure where the load vector is divided

up into three increments as shown in Figure 3.2.6. With the higher estimated
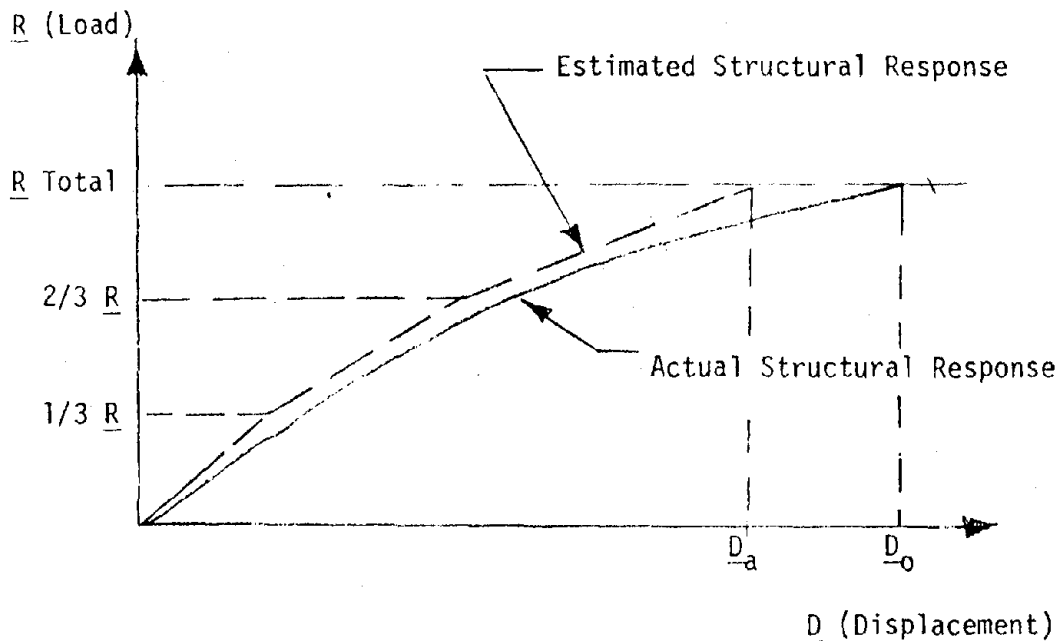


Figure 3.2.6. Estimated and Actual Structural Response for a Nonlinear Static
          Problem

stiffness used in analysis, the estimated displacement vector, $D_a$, will be

less than the actual displacement vector, $D_o$. Of course, this error can be

minimized by increasing the number of load increments.

The remainder of this section develops the procedure used to analyze

a structure with panels under static loads assuming the panel connections

are loaded in the nonlinear range. The analysis is based on the displacement

method as used in Section 3.2.2, but now the equilibrium equations are solved

incrementally and can be rewritten as follows:

$$R_i = K_i \, D_i \qquad\qquad (3.2.13)$$

where $R_i$ = load vector for increment "i"

$\qquad = R/N;$

N = number of load increments;

$\underline{K}_i$ = structural stiffness matrix for increment "i";

$\underline{D}_i$ = displacement vector for increment "i";

$\underline{R}$ = total load vector.

Solution of the first increment is essentially the same as a static linear solution. The structural stiffness matrix is formed by merging the beam, truss, boundary, and panel elemental stiffness matrices assuming the panel elements begin with linear properties. Formation of the load vector is the same as before only now each term is divided by the total number of increments, N. Once the structural stiffness matrix and incremental load matrix have been calculated, the displacements for the first increment can be solved for in the usual manner.

$$\underline{D}_i = \underline{K}_i^{-1} \underline{R}_i \qquad (3.2.14)$$

Again in an analogous manner, the elemental stresses for an increment can be calculated.

$$\underline{r}_i = \underline{s}_i \underline{d}_i \qquad (3.2.15)$$

where $\underline{r}_i$ = vector of elemental stresses for increment "i";

$\underline{s}_i$ = elemental stress matrix for increment "i";

$\underline{d}_i$ = elemental displacement vector for increment "i".

Note that the elemental stress matrix for the panel element is developed from the elemental stiffness matrix; thus, it too must be updated at the end of each increment.

At the end of each increment, the displacements and elemental stresses must be summed and stored.

$$\underline{D}_T = \underline{D}_T + \underline{D}_i \qquad (3.2.16)$$

$$\underline{r}_T = \underline{r}_T + \underline{r}_i \qquad (3.2.17)$$

where

$D_T$ = total displacement vector at the end of an increment (initially equal to zero);

$r_T$ = vector of elemental stresses at the end of an increment (initially equal to zero).

At this point the first increment is totally complete. To help visualize the entire procedure beyond the first increment, refer to Figure 3.2.7 which is a flow chart of the static nonlinear solution method.

To check if a panel element changes stiffness at the end of an increment, every vertical and horizontal load in the panel connections of an element must be compared to the experimental load-deflection curve (see Figure 3.2.8). It is checked to see if the actual load in the panel connection exceeds the yield load. If the actual load exceeds the yield load, the stiffness of that connector is modified to the new appropriate stiffness. For example, in Figure 3.2.9 (these graphs are based on the load-deflection curves from Figure 3.2.8), the actual load, PX, in the X-direction does not exceed the yield load $PX1_y$; therefore, the stiffness for the second increment will still be KX1. But the actual load, PY, in the connection in the Y-direction has exceeded $PY1_y$ but is less than $PY2_y$; consequently, the stiffness for the second increment will be KY2. This process is repeated for all four connections in each panel element. The results are then placed in a matrix that identifies the connection stiffness in each direction for all four connections in a panel element as described below.

$$KN = \begin{bmatrix} KXI \\ KYI \\ KXJ \\ KYJ \\ KXK \\ KYK \\ KXL \\ KYL \end{bmatrix} \qquad (3.2.18)$$

Comments

| | |
|---|---|
| $K = 1$ | |
| $\underline{K}_i = \sum\limits_{n=1}^{M} \underline{k}_n$ | Formation of structural stiffness matrix for linear increment |
| $\underline{R}_i = \underline{R}/N$ | Formation of incremental load vector |
| $\underline{D}_i = \underline{K}_i^{-1}\ \underline{R}_i$ | Calculation of incremental displacements |
| $\underline{r}_i = \underline{S}_i\ \underline{d}_i$ | Calculation of incremental stresses or internal forces for each element type |
| $\underline{D}_T = \underline{D}_T + \underline{D}_i$ <br> $\underline{r}_T = \underline{r}_T + \underline{r}_i$ | Summation of incremental displacements and elemental stresses |
| $K > N$ ? | |
| $K + K + 1$ | |
| $\underline{\Delta} = \Sigma \underline{k}_p - \underline{k}'_p$ | Formation of the structural stiffness correction matrix by subtracting the summation of the updated panel elemental stiffness matrices from the panel stiffness matrices from the previous increment |
| $\underline{K}_i = \underline{K}_i + \underline{\Delta}$ | Correction of the structural stiffness matrix for the next increment |
| END | |

Yes

No

Figure 3.2.7. Flow Chart of a Static Nonlinear Solution
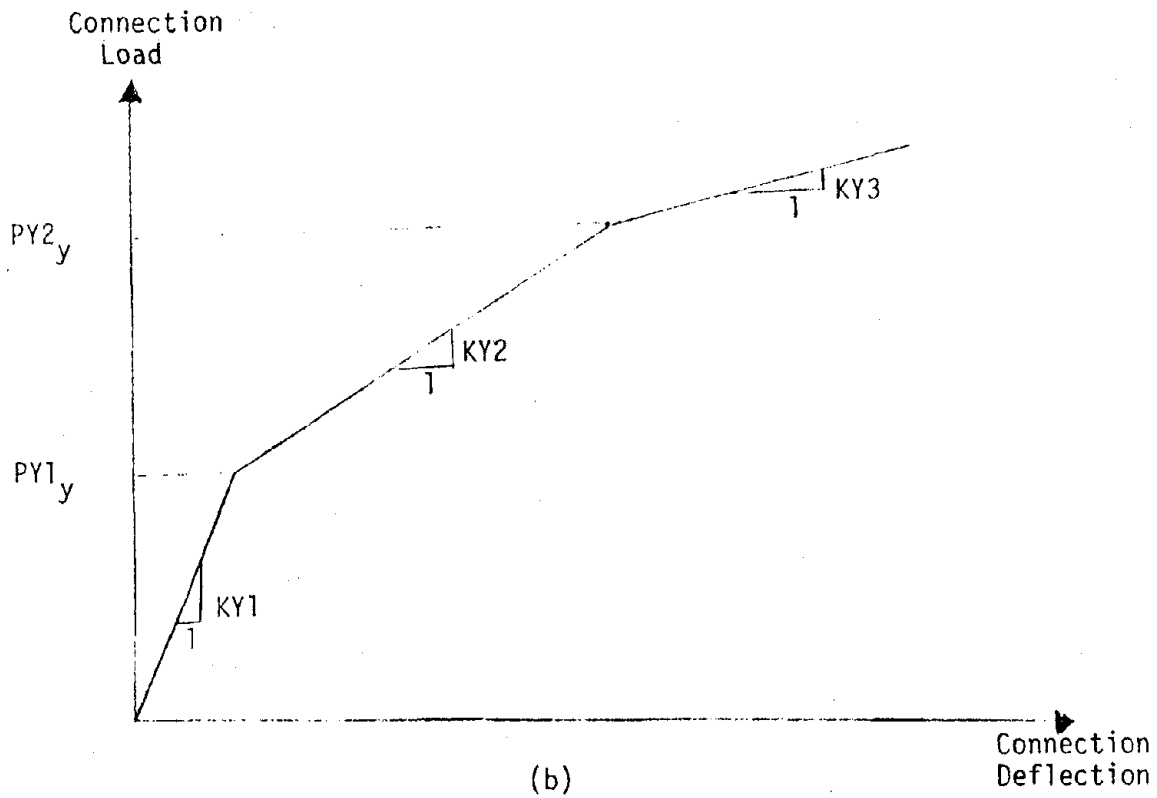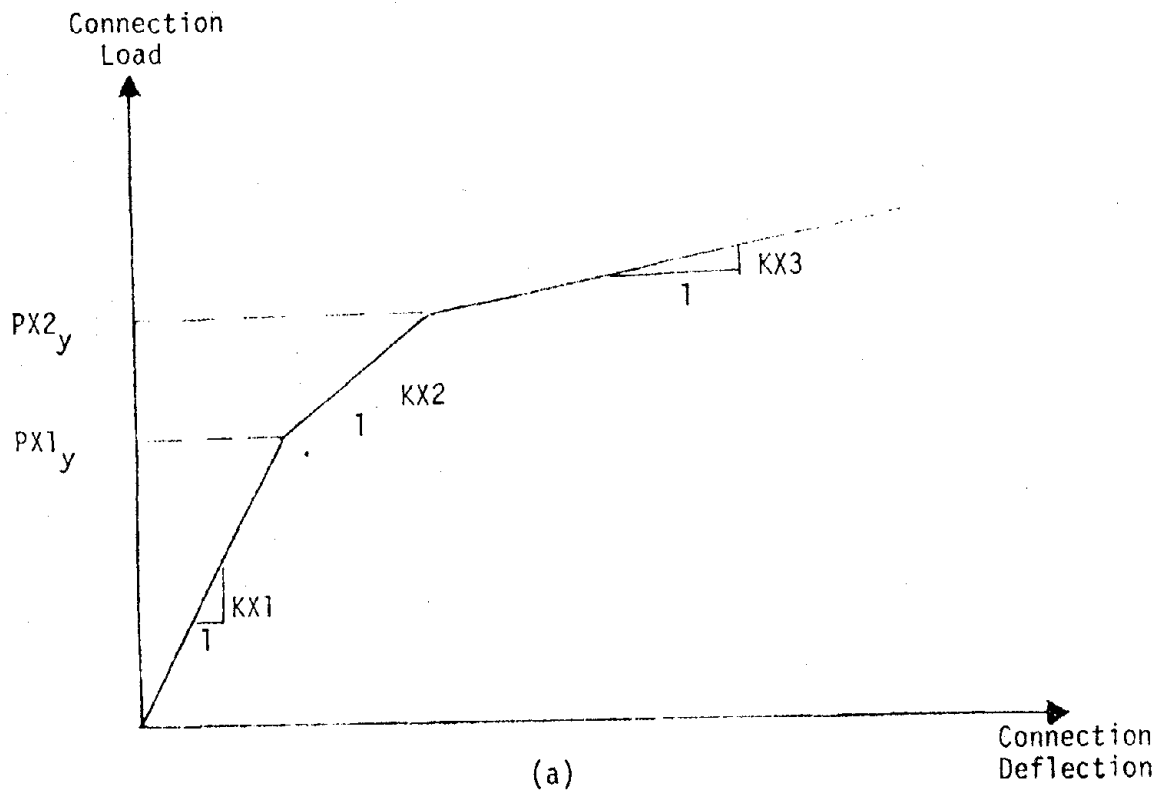
Figure 3.28. Typical Load Versus Deflection Curve for a Panel Connection
(a) X-Direction, (b) Y-Direction
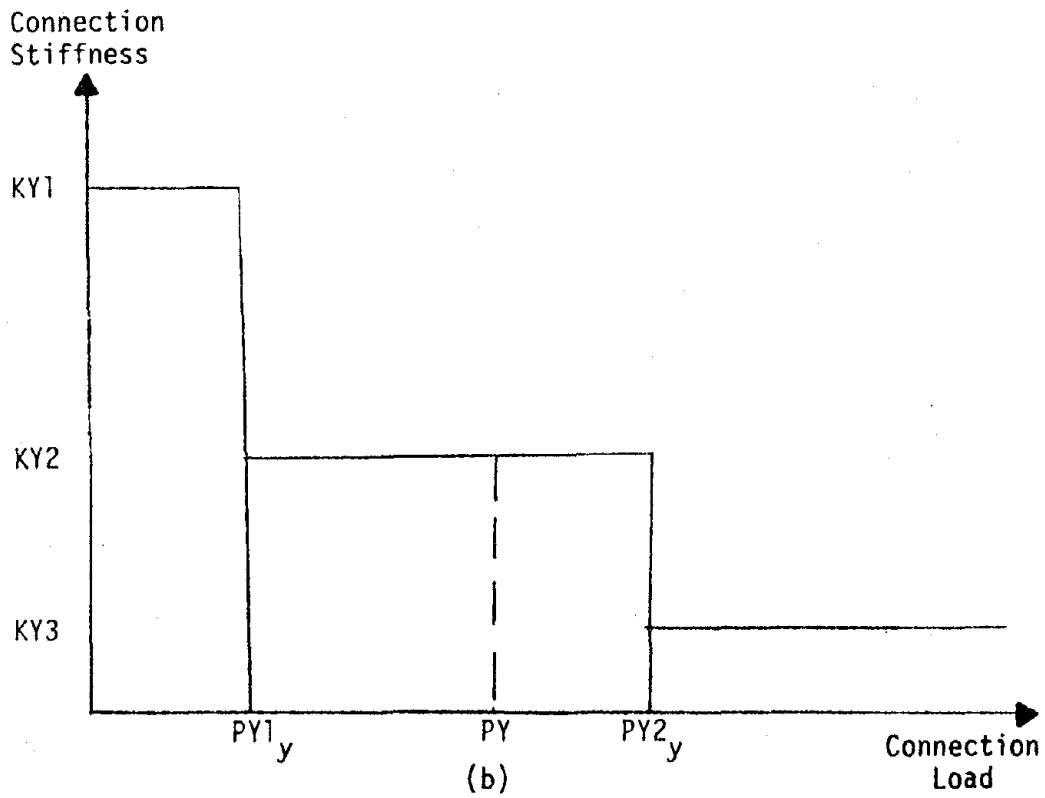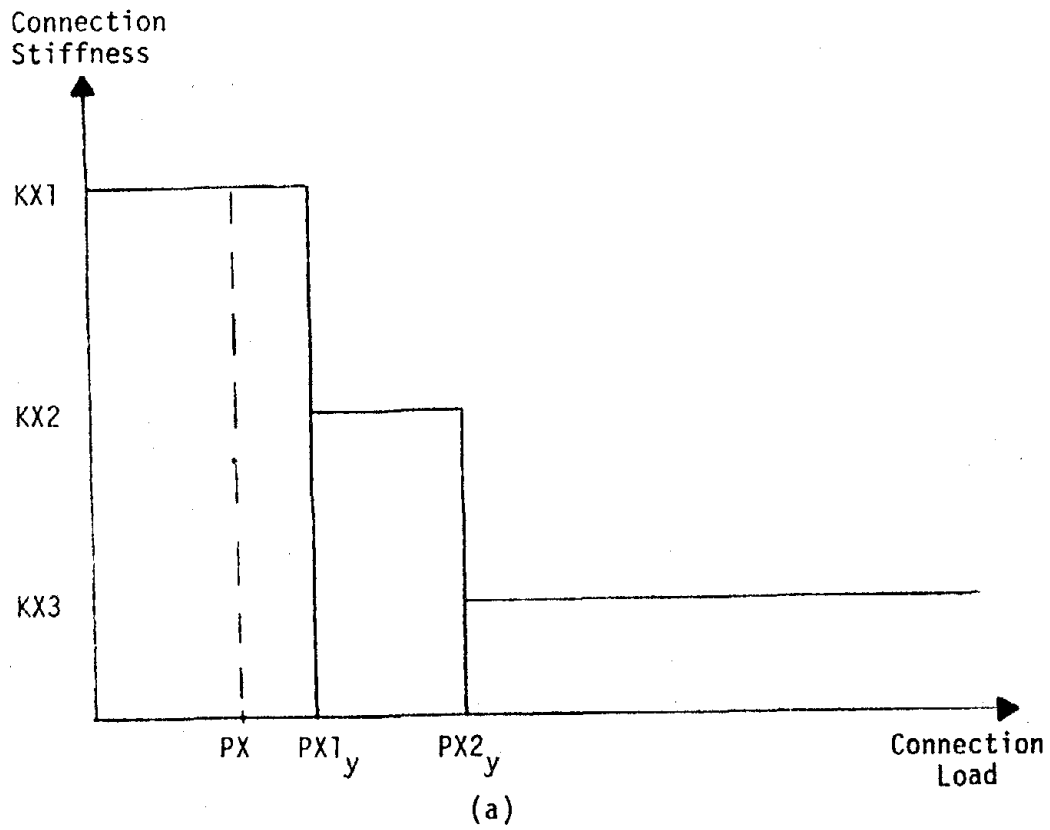
Figure 3.29. Typical Stiffness Versus Load Graphs for a Panel Connection
(a) X-Direction, (b) Y-Direction

where $\underline{KN}$ = stiffness storage matrix after connection stiffnesses have been updated;

KXI = updated connection stiffness in the X-direction for node I;

KYI = updated connection stiffness in the Y-direction for node I.

Connection stiffnesses from the previous increment are stored in the same fashion as the matrix $\underline{KN}$ and result in the matrix $\underline{KO}$

$$\underline{KO} = \begin{bmatrix} KXI' \\ KYI' \\ KXJ' \\ KYJ' \\ KXK' \\ KYK' \\ KXL' \\ KYL' \end{bmatrix} \cdot \qquad (3.2.19)$$

where $\underline{KO}$ = stiffness storage matrix for the previous increment;

KXI' = previous connection stiffness in the X-direction for node I;

KYI' = previous connection stiffness in the Y-direction for node I.

To determine whether or not any connection stiffnesses have changed, the updated stiffness storage matrix, $\underline{KN}$, must be compared to the previous stiffness storage matrix, $\underline{KO}$, for each panel.

$$\underline{KN} - \underline{KO} = \underline{Q} \qquad (3.2.20)$$

If $\underline{Q}$ is the null matrix (all zero entries), the connection stiffnesses for that panel did not change for that increment and thus no change of the structural stiffness matrix would be required. If the $\underline{Q}$ matrix is nonzero, the panel elemental stiffness and stress matrices must be modified for that panel element. The structural stiffness matrix then needs to be updated to account for the alteration of panel elemental stiffness matrices.

Complete reformation of the structural stiffness matrix would require a significant amount of computational effort. To minimize this effort, a structural stiffness correction matrix was developed to adjust the structural

stiffness matrix from the previous increment. Recall that the structural stiffness matrix is formed by the direct addition of the element stiffness matrices.

$$\underline{K} = \sum_{n=1}^{M} \underline{k}_n \qquad (3.2.11)$$

Equation 2.11 can be rewritten in terms of each different element type for the previous increment as shown below.

$$\underline{K}_i = \sum \underline{k}_{BM} + \sum \underline{k}_{TR} + \sum \underline{k}'_p \qquad (3.2.21)$$

where $\underline{k}_{BM}$ = element stiffness matrix for a beam element;

$\underline{k}_{TR}$ = element stiffness matrix for a truss element;

$\underline{k}p'$ = element stiffness matrix for a panel element for increment i.

For the next increment, the structural stiffness matrix only needs to be modified to account for the change in panel element stiffness. The beam and truss element stiffness matrices do not change, thus the structure stiffness matrix becomes

$$\underline{K}_{i+1} = \sum \underline{k}_{BM} + \sum \underline{k}_{TR} + \sum \underline{k}_p \qquad (3.2.22)$$

where $\underline{k}_p$ = updated panel element stiffness matrix for increment i + 1. The difference between the structural stiffness matrix between the i and i + 1 increments is given by the matrix $\underline{\Delta}$ or the structure stiffness correction matrix.

$$\underline{\Delta} = \underline{K}_{i+1} - \underline{K}_i = \sum (\underline{k}_p - \underline{k}'_p) \qquad (3.2.23)$$

or

$$\underline{K}_{i+1} = \underline{K}_i + \sum (\underline{k}_p = \underline{k}'_p) = \underline{K}_i + \underline{\Delta}$$

Now with Equation 3.2.23, the structural stiffness matrix for the next increment, $\underline{K}_{i+1}$, can be formed by merging in the $\underline{\Delta}$ matrix to the structural stiffness matrix of the previous increment. With $\underline{K}_{i+1}$ formed, the solution of

the next increment can be solved and the procedure repeated. Once all of
the incremental steps have been completed, the total displacement is given
by the vector $\underline{D}_T$, and the total elemental stresses are given by the vector
$\underline{r}_T$. (There is one vector of elemental stresses or internal loads for each
element.)

### 3.2.4. Linear Dynamic Analysis

The three basic analytical capabilities that were desired to predict
the response of linear systems under dynamic loading conditions were: (1)
calculation of natural frequencies and mode shapes, (2) calculation of response
due to forced dynamic loads, and (3) calculation of response due to loads in-
duced by ground acceleration. For multi-degree of freedom systems, solution
of the equations that provided these capabilities requires tremendous compu-
tational effort. The computer program SAPFAP was developed to minimize this
effort by modifying SAP IV (Bathe *et al*. 1974), an existing finite element
analysis computer program. (SAPFAP is discussed in detail in Section 3.3 and
Beers, 1980. Essentially no modifications were made to the dynamic por-
tion of SAP IV. The only change effecting the dynamic section of the program
was the addition of the panel element. Included in this section is an over-
view of the equations used in dynamic analyses and a discussion of modeling
and limitations of the panel element in these analyses.

### 3.2.4.1. Overview of Equations Used in Linear Dynamic Analysis

Just as in static analyses, the stress analysis process for dynamic
loading consists of the same three phases:

1. Calculation of the structural stiffness matrix, the mass matrix,
   the damping matrix, and the load vectors.

2. Solution of the equilibrium equations.

3. Evaluation of elemental stresses.

Evaluation of structural response due to dynamic loading conditions is based
on the three following equations:

1. Calculation of natural frequencies and mode shapes:

$$\underline{K}\, \underline{\emptyset} = \omega^2\, \underline{M}\, \underline{\emptyset}$$  (3.2.24)

where $\underline{K}$ = structural stiffness matrix;

$\underline{\emptyset}$ = mode shape matrix;

$\omega$ = natural free vibration frequency;

$\underline{M}$ = mass matrix.

2. Calculation of forced dynamic response:

$$\underline{M}\, \underline{\ddot{D}} + \underline{C}\, \underline{\dot{D}} + \underline{K}\, \underline{D} + \underline{R}(t)$$  (3.2.25)

where $\underline{C}$ = damping matrix;

$\underline{\ddot{D}}$, $\underline{\dot{D}}$, $\underline{D}$ = acceleration, velocity, and displacement vectors, respectively;

$\underline{R}(t)$ = vector of arbitrary time varying loads.

3. Calculation of response due to ground motion:

$$\underline{M}\, \underline{\ddot{D}}_r + \underline{C}\, \underline{\dot{D}}_r + \underline{K}\, \underline{D}_r = -\underline{M}\, \underline{\ddot{D}}_g$$  (3.2.26)

where $\underline{\ddot{D}}_g$ = ground acceleration vector;

$\underline{D}_r$ = relative displacement vector of the structure with respect to ground.

The structural matrices $\underline{K}$, $\underline{M}$, and $\underline{C}$ are formed by direct addition of
the element matrices as discussed in Section 3.2.2. Note that the structural
stiffness matrix, $\underline{K}$, is the same as the stiffness matrix used in static analy-
ses. SAP IV uses a diagonal mass matrix; therefore, a lumped mass analysis
is used where the structure mass is the sum of the individual element mass
matrices plus additional concentrated masses which are specified at selected
degrees of freedom (Bathe *et al.* 1974). The mass of each element is assumed

to be concentrated at each of its nodes such that the lumping of the element

mass to these points is determined by statics.  In practice, it is difficult,

if not impossible, to determine for general finite element assemblages the

element damping parameters, in particular because the damping properties are

frequency dependent (Bathe and Wilson 1976).  For this reason, the damping

matrix in SAP IV is constructed using the mass matrix and stiffnesses matrix

of the complete structure together with experimental results on the amount

of damping.  It should be noted that damping properties can be measured if

the structure exists.  For a more complete discussion of the assumptions used

in lumped mass analyses and the use of proportional damping, refer to Clough

(1968), Clough and Bathe (1972), Hurty and Rubinstein (1964), and Wilson and

Penzien (1972).  (Taken from Bathe *et al*. (1974).)

A complete discussion of the solution methods used to solve the equi-
librium equations for dynamic analyses is beyond the scope of this paper;
consequently, only a summary of the solution techniques available in SAP IV
will be given (Bathe *et al*. 1974).

1. Calculation of frequencies and mode shapes by the determinant
   search method.

2. Calculation of frequencies and mode shapes by the subspace itera-
   tion method.

3. Calculation of forced dynamic response or response due to ground
   motion by the mode superposition method.

4. Calculation of forced dynamic response or response due to ground
   motion by direct integration.

5. Calculation of response due to ground motion by a response spectrum
   analysis.

For more information about these solution methods, refer to Bathe *et al*.

(1974), Bathe and Wilson (1976), and Clough and Penzien (1975).  Once the

equilibrium equations are solved, a history of the displacements is known and

a history of the elemental stresses (or internal loads) can be calculated. With these histories, the critical stresses and displacements can be determined.

### 3.2.4.2. Use of the Panel Element in Linear Dynamic Analysis

The panel element is used just like any other element (beam, truss, etc.) in linear dynamic analysis. The only basic difference is the way that the mass of the panels is modeled. For the usual beam and truss elements, a diagonal mass matrix is formed where half of the mass of each element is lumped at each node. With the panel element, development of the mass matrix is not this straightforward. Usually four connections are used to attach the panels to the framing, two stiff load support (or bearing) connections which support most of the dead weight of the panel and two lateral (flexible or slotted) connections which nominally help hold the panel in place. For a more complete description and discussion of these connections, see Section 3.4.1.1 and work done by Sessa (1980) and the Prestressed Concrete Institute (1977). Since the bearing connections are significantly stiffer than the other two types of connections, the structure will see almost all of the mass effects of the panels through the bearing connections. Consequently, panel masses must be input as concentrated rigid body masses and mass moments of inertia at the nodes where the bearing connections are attached to the support structure.

Concentrating the panel masses and mass moments of inertia is a reasonable approach in determining the structural response of the system under dynamic loads, but the approach causes difficulty in calculating the loads in the panel connections. Since the masses are idealized to be at the node where the panel and supporting structure (say a beam element) are connected,

both the stiffness of the panel and beam element will be resisting the loads induced by the panel mass simultaneously. In reality, the loads due to the panel mass are first transferred through the panel connections and then into the supporting structure. Consequently, calculation of the loads in the panel connections based on concentrated masses and mass moments of inertia would underestimate the true loads in the connections. It should also be noted that in the derivation of the panel element, Briggs assumed that all the loads on the panel assembly were introduced through the supporting structure and not by forces on the panel itself. For these two reasons, calculation of the loads in the panel connections due to dynamic loads was not pursued.

## 3.2.5 Discussion of Nonlinear Dynamic Analysis

The primary concern in the nonlinear dynamic analysis for these types of structural systems is the nonlinear material behavior of the panel connections assuming the structural framing behaves in a linearly elastic fashion. The only generally applicable method for the analysis of nonlinear systems is the numerical step-by-step intergration of the coupled equations of motion in the time domain (Clough and Penzien 1975). The response history is divided into short, equal time increments, and the response is calculated during each increment for a linear system having the properties determined at the beginning of the increment. At the end of an interval, the properties of the structural stiffness and damping matrices are modified to conform to the state of deformation and stress at that time; thus, the nonlinear analysis is approximated as a sequence of successively changing linear systems.

In view of the complexity of the nonlinear dynamic analysis problem, development of an accurate solution method was not pursued. The reason being that the overall effect of the panel connection nonlinearity was anticipated to have a "weak" or minimal effect on the overall dynamic response; that is, the frequencies and deflections are primarily affected by the structural framing and not by the panel connections. To verify this assumption, a computer study was performed using linear dynamic analysis techniques to indicate approximately the effect of the panel connection nonlinearity on the response of the structural system.

The basic structure used in the analytical study was a single bay from a structure with two exterior precast panels. Each panel was attached to the support structure with bearing connections at the base and flexible rod connections at the top. The complete description of this structure and the analytical computer models used to perform the analyses can be found in Section 3.4 (Test Configuration II). A hypothetical horizontal ground motion was applied to the system with a ground acceleration equal to $\sin(20\,\pi t)$ in./sec$^2$ for a total of five seconds. The response of the structure was then calculated for these five cycles. Four basic tests were performed to indicate the significance of the stiffness and nonlinearity of the panel connections. The effect of the panel masses and mass moments of inertia were included for all four tests.

Test A:  The lateral stiffness contribution of the panel elements is totally neglected.

Test B:  The lateral stiffness contribution of the panel elements is included assuming the panel connections behave linearly elastic.

Test C:   The lateral stiffness contribution of the panel elements is included assuming the bearing connections provide full linear elastic stiffnesses and the flexible connections provide post-yield stiffnesses.

Test D:   The lateral stiffness contribution of the panel elements is included assuming the bearing connections provide full linear elastic stiffness in the horizontal direction, and the bearing connections in the vertical direction and the flexible connections provide post-yield stiffnesses.

These four tests were selected to bound the solution between the full linear elastic solution (Test B) and the solution with the panel connections in the post-yield state (Test D). The true response would be between Test B and Test D depending on the magnitude of the load in the connections at a specific time; that is, the connections could be either in the linear elastic or post-yield state.

Two basic criteria were used to evaluate the differences between analytical models A, B, C, and D:

1.   Comparison of the first five natural frequencies. See Table 3.2.1.

2.   Comparison of the displacements at nodes 11 and 13 for the U, V, and $\theta Z$ freedoms (see Section 3.4, Figure 3.4.18). Nodes 11 and 13 represent the points of attachment for the right bearing connection and the right flexible connection, respectively, for panel number 2. See Table 3.2.2.

After the data for each test was tabulated, the results of Tests B, C, and D were compared to Test A (the test where the panel element stiffness was neglected completely). This data is summarized in Tables 3.2.1 and 3.2.2. It should be noted that the damping was assumed to be zero; consequently, the magnitude of the displacements developed in this analysis may be slightly greater than an analysis assuming damping. It has been determined experimentally that the actual damping ratio of this system is approximately 5 percent. Displacements listed in Table 3.2.2 are the maximum values that occurred in the system during the five cycles of ground acceleration.

Table 3.2.1. Effect of Panel Stiffness and Panel Connection Nonlinearity on the Natural Frequencies of Test II. (Frequencies, $\omega$, are in Hz.)

| Frequency $\omega$ | Test A | Test B | % Change Relative to A | Test C | % Change Relative to A | Test D | % Change Relative to A |
|---|---|---|---|---|---|---|---|
| $\omega_1$ | 2.70 | 2.92 | +8.1% | 2.72 | +0.7% | 2.71 | +0.4% |
| $\omega_2$ | 7.35 | 7.87 | +7.1% | 7.37 | +0.3% | 7.36 | +0.1% |
| $\omega_3$ | 10.49 | 10.51 | +0.2% | 10.49 | 0.0% | 10.49 | 0.0% |
| $\omega_4$ | 14.57 | 14.62 | +0.3% | 14.57 | 0.0% | 14.57 | 0.0% |
| $\omega_5$ | 16.63 | 16.65 | +0.1% | 16.63 | 0.0% | 16.63 | 0.0% |

Table 3.2.2 Effect of Panel Stiffness and Panel Connection Nonlinearity on the Maximum Displacements of Nodes 11 and 13. (Displacements and rotations are expressed in inches and radians, respectively, and have been multiplied by $10^6$. Note that these are relative displacements between the ground and the total displacement.)

| Node | Freedom | Test A | Test B | % Change Relative to A | Test C | % Change Relative to A | Test D | % Change Relative to A |
|---|---|---|---|---|---|---|---|---|
| 11 | U | 1264 | 1215 | -3.9% | 1252 | -0.9% | 1261 | -0.2% |
| Lower left bearing connection point panel 2 | V | 82.72 | 66.23 | -19.9% | 81.51 | -1.5% | 82.34 | -0.5% |
|  | $\theta Z$ | 5.833 | 4.844 | -17.0% | 5.768 | -1.1% | 5.813 | -0.3% |
| 13 | U | 1264 | 1215 | -3.9% | 1252 | -0.9% | 1260 | -0.3% |
| Upper left flexible connection point panel 2 | V | 6.501 | 7.240 | +11.4% | 6.569 | +1.0% | 6.520 | +0.3% |
|  | $\theta Z$ | 6.291 | 4.869 | -22.6% | 6.189 | -1.6% | 6.260 | -0.5% |

The first two natural frequencies for the test structure were significantly increased over Test A, +8.1% and +7.1%, respectively (see Table 3.2.1), when the panel connections with completely linear elastic material properties were considered (Test B). Contrary to this, the stiffness of these panel elements provided minimal change to the higher natural frequencies ($\omega_3$, $\omega_4$, and $\omega_5$). Results from Tests C and D indicate that once the flexible connections reach a point' where the stiffness of the connections are in the post-yield range, the panel elements have virtually no effect on the natural frequencies of the structure as shown in Table 3.2.1.

When the linearly elastic panel element (Test B) is used, the maximum relative displacement between the ground and the total displacement in the horizontal direction of the structure is lowered by 3.9% which is in the direction of the ground motion. Note that the displacements of the two panel connection points for the positive V and $\theta Z$ freedoms are also effected by these stiffnesses. Although the percentage differences between Tests A and B appear to be high for these two freedoms, these changes are relatively insignificant when considering the magnitude of the structural response. Again, once the flexible connections are loaded into the post-yield range, the panel elements have virtually no effect on the maximum displacements of the structure.

Reviewing the four analytical tests conducted, there is evidence that the panel elements investigated provide approximately an eight percent increase in the first two natural frequencies and about a four percent decrease in the maximum horizontal displacement while loaded in the linearly elastic range. When the flexible connections are loaded into the post-yield range, the stiffness of the panel element has essentially no effect on the dynamic response

(frequencies and deflections) of the structure. As mentioned before, the true dynamic response will be somewhere between these two conditions. It is concluded that the overall effect of the panel connection nonlinearity has a "weak" or minimal effect on the overall structural response (frequencies and deflections), thus it is not recommended that nonlinear dynamic analyses of these types of structural systems be pursued.

## 3.3 DEVELOPMENT OF THE COMPUTER PROGRAM SAPFAP

A computer program was required for the solution of the equilibrium equations for the interaction between precast curtain walls and structural framing. Four basic analytical capabilities were required.

1. Linear Static Analysis

2. Nonlinear Static Analysis

3. Determination of Mode Shapes and Natural Frequencies of Linear Systems

4. Determination of Forced Dynamic Response of Linear Systems

Three possibilities were considered to develop these capabilities. The first option was to completely write the program without the aid of existing computer programs. Because of the complex nature of developing a program for static and dynamic analyses, this option could not have been completed within the time frame of the National Science Foundation project. Consequently, the second and third possibilities involved the modification of existing finite element analysis computer programs to accommodate precast curtain wall elements. ADINA (Bath 1977), a finite element program for Automatic Dynamic Incremental Nonlinear Analysis, was the top choice for modification because the nonlinear capabilities were already built into the program. Unfortunately, the cost of ADINA was prohibitive and there was concern that the program would not fit on the University of Idaho IBM 370/145 computer system. It was concluded that this was not a viable alternative. SAP IV (Bathe *et al.* 1974), a Structural Analysis Program for static and dynamic response of linear systems, was selected because the cost was reasonable, it could be conveniently modified, and it could be adapted to the University of Idaho IBM 370/145 computer system.

SAPFAP, a Structural Analysis Program for Frames with Panels, was developed by modifying SAP IV. This modification was done by adding new subroutines and by altering existing subroutines within SAP IV. The development of SAPFAP consisted of four stages.

1. Implementation of SAP IV on the University of Idaho IBM 370/145 computer and verifying the original program for accuracy.

2. Addition of new subroutines to SAP IV and modification of existing subroutines to accommodate the precast panel elements with linear material properties in the panel connections based on static loading conditions.

3. Modification of the program developed in stage 2 to accommodate panel elements with linear or nonlinear material properties in the panel connections for static loading conditions.

4. Modification of the program developed in stage 3 to accommodate the panel elements with linear material properties for dynamic loading conditions.

SAP IV consists of a relatively small main program with many supporting subroutines. Each subroutine carries out a specific portion of the analysis such as the formation of elemental stiffness matrices or the calculation of elemental stresses. Table 3.3.1 lists the subroutines used in a static linear analysis and the function of each of these subroutines. Eight element types are available in SAP IV, many of which were not used to predict the interaction between structural framing and curtain walls. (For example, a three dimensional brick element.) To save computer storage space, all subroutines relating to extraneous elements were deleted. (For a list of the subroutines and elements deleted, see Beers, 1980). Three dimensional beam, truss, and boundary elements were retained in the program to account for the structural system.

Addition of a panel element into SAP IV for the response of linear systems under static loads required the addition of two new subroutines,

Table 3.3.1. Summary of Subroutines Used in a Static Analysis

| Subroutine | Function |
| --- | --- |
| MAIN | Main program |
| INPUTJ | To input nodel coordinates and boundary conditions |
| ELTYPE | To direct program to different element types |
| PANEL | To direct formation of panel stiffness matrices, to direct calculation of elemental stresses, and to print elemental stresses |
| PSTIFF | To form panel stiffness and stress matrices |
| CALBAN | To calculate the bandwidth of the structural stiffness matrix |
| TRUSS | Similar to PANEL but for truss elements |
| RUSS | Similar to PSTIFF but for truss elements |
| BEAM | Similar to PANEL but for beam elements |
| TEAM, NEWBM | Similar to PSTIFF but for beam elements |
| INL | To input nodal loads and masses |
| ADDSTFF | To merge elemental stiffness matrices into the structural stiffness matrix |
| SOLEQ | To direct the solution of the equilibrium equations, printing of displacements, and calculation of elemental stresses |
| SESOL | To solve equilibrium equations |
| PRINTD | To print nodal displacements |
| STRESS | To direct calculation of stresses for all element types |
| STRSC | To calculate elemental stresses |

PANEL and PSTIFF, plus small modifications to some existing subroutines. A source listing of all new subroutines and all modified existing subroutines required to develop SAPFAP can be found in Beers (1980). The subroutine PANEL is analogous to the existing SAP IV subroutines TRUSS and BEAM. PANEL directs the formation of the panel elemental stiffness matrices and directs calculation and printing of panel element stresses, while the actual formation of the panel elemental stiffness and stress matrices is executed in PSTIFF. PSTIFF is analogous to the existing SAP IV subroutines RUSS and TEAM for truss and beam elements, respectively. A flow chart demonstrating the static linear solution and how PANEL and PSTIFF are situated in the program is shown in Figure 3.3.1. Summaries of the subroutines PANEL and PSTIFF are given in Tables 3.3.2. and 3.3.3, respectively.

Development of static nonlinear capabilities did not require the addition of any new subroutines once the panel element was merged into SAP IV. Significant changes were made in the subroutines MAIN, PSTIFF, PANEL, BEAM, TRUSS, PRINTD, and ADDSTFF. These subroutines were changed to allow the computer program to perform the incremental analyses required to approximate nonlinear material behavior in the panel-frame connections. Figure 3.3.2 shows the flow chart for a static nonlinear solution, while Tables 3.3.2 through 3.3.6 summarize the subroutines with significant changes. Again, the source listing in Beers (1980) shows the complete details of the changes.

Once the panel element was merged into SAP IV, no additional changes were required to extract mode shapes and natural frequencies. Consequently, this portion of SAP IV was adequate. To develop forced dynamic response capabilities, only minimal changes to the subroutine STRSD1 were required. Note that the program SAPFAP will not calculate the forces in the panel connections due to dynamic loads for the reasons discussed in Section 3.2.4. With
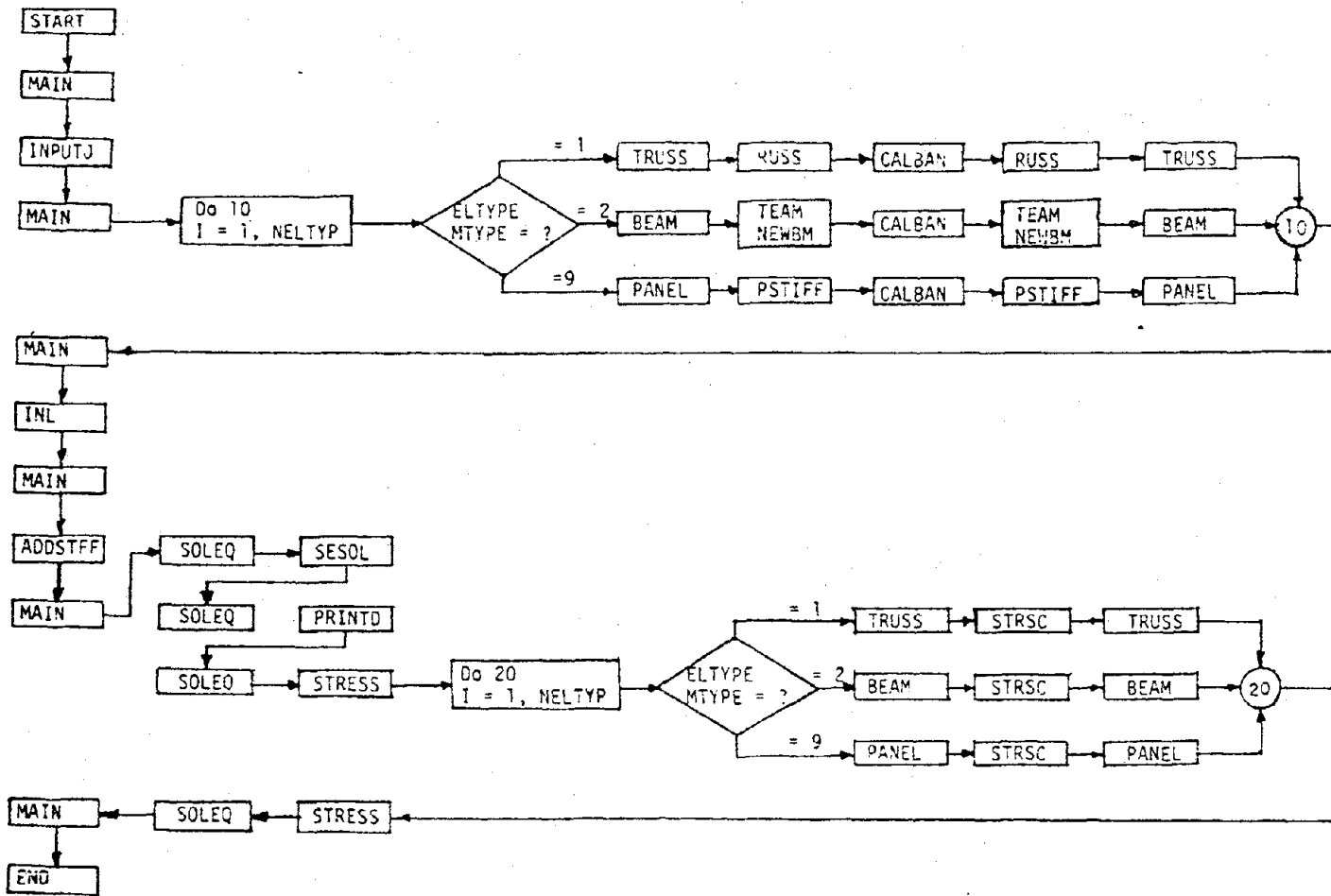
Figure 3.3.1. Flow Chart of a Static Linear Solution

Table 3.3.2. Summary of the Subroutine PANEL

---

Primary Function:  To direct formation of elemental panel stiffness matrices,

to direct calculation of elemental panel stresses, and

to print elemental panel stresses

Function in a Linear Solution:

1. To call PSTIFF for formation of the panel elemental stiffnesses and stress matrices

2. To call STRSC for calculation of panel stresses

3. To print panel stresses

Function in a Nonlinear Solution:

1. To call PSTIFF for formation of the initial panel elemental stiffness and stress matrices

2. To call STRSC to calculate incremental panel stresses

3. To print incremental panel stresses

4. To print summation of incremental panel stresses at the end of each increment

5. To save incremental and summation of incremental stresses on tape

---

Table 3.3.3. Summary of the Subroutine PSTIFF

---

Primary Function:  To form panel elemental stiffness and stress matrices

and to form panel elemental stiffness correction matrices

Function in a Linear Solution:

1.  To input and print panel element properties

2.  To form panel elemental stiffness and stress matrices

3.  To call CALBAN for the storage of panel stiffness matrices on tape and calculation of bandwidth

4.  To save stress matrices on tape

Function in a Nonlinear Solution:

1.  To perform the same duties executed in the linear solution for the first load increment

2.  To determine which panel connections changed stiffness after each load increment

3.  To calculate updated stiffness and stress matrices for the panel elements that change stiffness

4.  To form panel stiffness correction matrices

5.  To save stiffness, stress, and stiffness correction matrices on tape

---
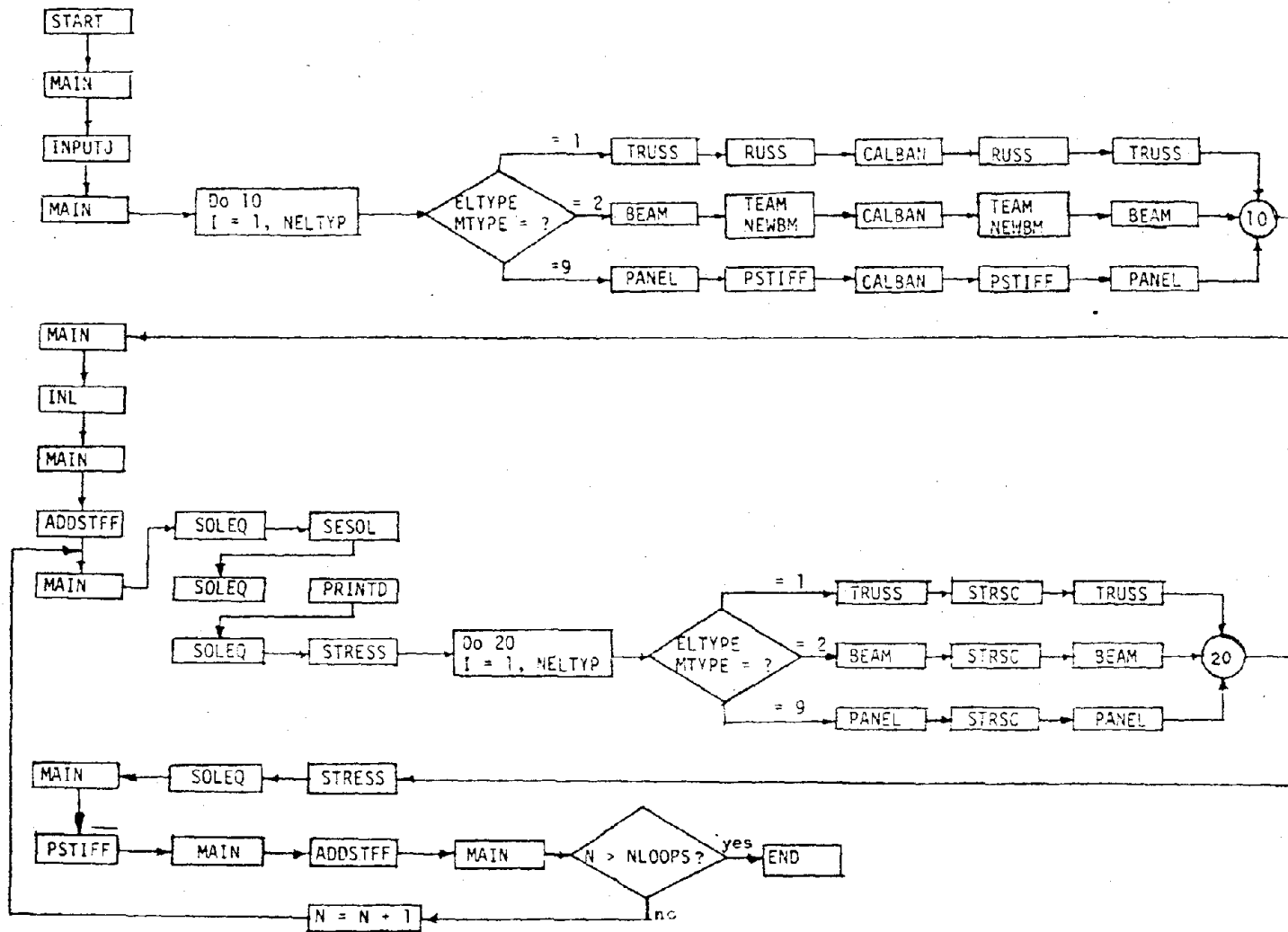
Figure 3.3.2. Flow Chart of a Static Nonlinear Solution

Table 3.3.4. Summary of the Subroutine ADDSTFF

---

Primary Function:  To merge elemental stiffness matrices into the struc-

tural stiffness matrix and to form the equilibrium equa-

tions in blocks

Function in a Linear Solution:

   1.   To input element load multipliers

   2.   To read load and mass matrices from tape

   3.   To read element stiffness matrices from tape and merge these
matrices into the structural stiffness matrix

   4.   To form equilibrium equations in blocks and save on tape

Function in a Nonlinear Solution:

   1.   To perform the same duties executed in the linear solution for
the first load increment

   2.   To read the equilibrium equations in blocks from tape

   3.   To merge panel elemental stiffness correction matrices into the
structural stiffness matrix

   4.   To reform the corrected equilibrium equations in blocks and save
on tape

---

Table 3.3.5. Summary of the Subroutine INL

---

Primary Function:  To input nodal loads and masses

Function in a Linear Solution:

    1.  To read nodal loads and masses and save on tape

Function in a Nonlinear Solution:

    1.  To input nodal loads and masses

    2.  To divide all nodal loads by the number of load increments

    3.  To save nodal masses and incremental loads on tape

---

Table 3.3.6. Summary of the Subroutine PRINTD

---

Primary Function:  To print nodal displacements

Function in a Linear Solution:

    1.  To print nodal displacements

Function in a Nonlinear Solution:

    1.  To print incremental displacements

    2.  To print summation of incremental displacements at the end of each increment

    3.  To save incremental and summation of incremental displacements on tape

---

the small change made to the subroutine STRSD1, all the dynamic capabilities of SAP IV are available to the user.

For an in-depth look at the changes required to implement SAPFAP, one should refer to the sourece listing showing all of the altered and new sub-routines in Beers (1980). Note that Beers (1980) provides a supplement to the SAP IV users manual for using the program SAPFAP and demonstrates an example problem including input and output.

3.4 APPLICATION OF SAPFAP TO FULL-SCALE TESTS

CONDUCTED AT THE UNIVERSITY OF IDAHO

Presently, at the University of Idaho, full-scale testing of the inter-
action between structural framing and precast curtain walls is being performed
for both static and dynamic loading conditions. The project is sponsored by
the National Science Foundation and is being carried out by the Civil Engineer-
ing Department at the University of Idaho. Presented in this section is a
brief description of the five different tests being conducted and the analy-
tical models developed to evaluate these tests. These analytical models were
used to analyze the tests under static loading conditions and to calculate
the natural frequencies and mode shapes. A summary of these analyses is pre-
sented in this chapter, along with a comparison of the first two natural fre-
quencies of Test I and the first three natural frequencies of Test II to the
measured natural frequencies.

### 3.4.1. Full-Scale Tests Conducted at the University of Idaho

### 3.4.1.1. Description of Test Facilities and Test Configurations

The three types of precast concrete panels that were used in the test-
ing program are: (1) the window box, (2) the column cover, and (3) the
spandrel cover panel. (A description of the geometry of the panels and the
different panel configurations used in the test program is presented at the
end of this section.) These five inch thick concrete panels were attached
to the supporting structure with four connections. The three types of panel-
frame connections that were used in the testing program are: (1) flexible,
(2) bearing, and (3) slotted. The flexible connection used in Test II consists

of a 3/4 in. diameter threaded steel rod and a 4 in. by 4 in. by 1/4 in.
steel angle. Ferrule loop inserts (3/4 in. diameter) with threaded holes
are cast into the panel to provide the connection between the rod and the
panels as shown in Figure 3.4.1. The rod is attached to the test frame by the
1/4 in. angle and bolts. Most of the weight of the panel is carried by the
bearing connections which are constructed out of 8 in. by 8 in. by 1/2 in.
steel angles; therefore, virtually none of the deadweight of the panel is
resisted by the flexible connection. Figure 3.4.2 shows how the bearing con-
nections are bolted to the test frame and panels. Slotted connections are
constructed similar to bearing connections except the bolt holes in the 8 in.
by 4 in. by 1/2 in. angle are slotted as shown in Figure 3.4.3. The bolts are
not tightened down; thus, there is minimum resistance in the plane of the
panel until a displacement of one inch is reached (Sessa 1980). With this
much displacement, the connection begins to provide full resistance. Note
that full stiffness is provided in the direction perpendicular to the panel.
For a more detailed discussion of these panel-frame connections, see work
done by Sessa (1980) and the Prestressed Concrete Institute (1977).

The general test configuration consists of one bay of a full-size
building with different configurations of panels attached. The University
of Idaho test facilities and the configuration for Test II are shown in
Figure 3.4.4. The test frame used to represent the single bay of the structure
consists of 4 W8 x 35 steel sections with moment resisting connections as
shown in Figure 3.4.5. At the bottom of the test frame are four lateral support
guides. These ball bearing guides prevent the test specimen from getting out
of plane during testing. Note that they may provide some resistance in the
plane of the test frame due to friction. Steel tubes (8 in. by 4 in. by 3/8

—— Ferrule Loop

W8 x 35

2 1/2"

3/4" Steel Rod

9 1/2"

4" x 4" x 1/4"
Steel Angle
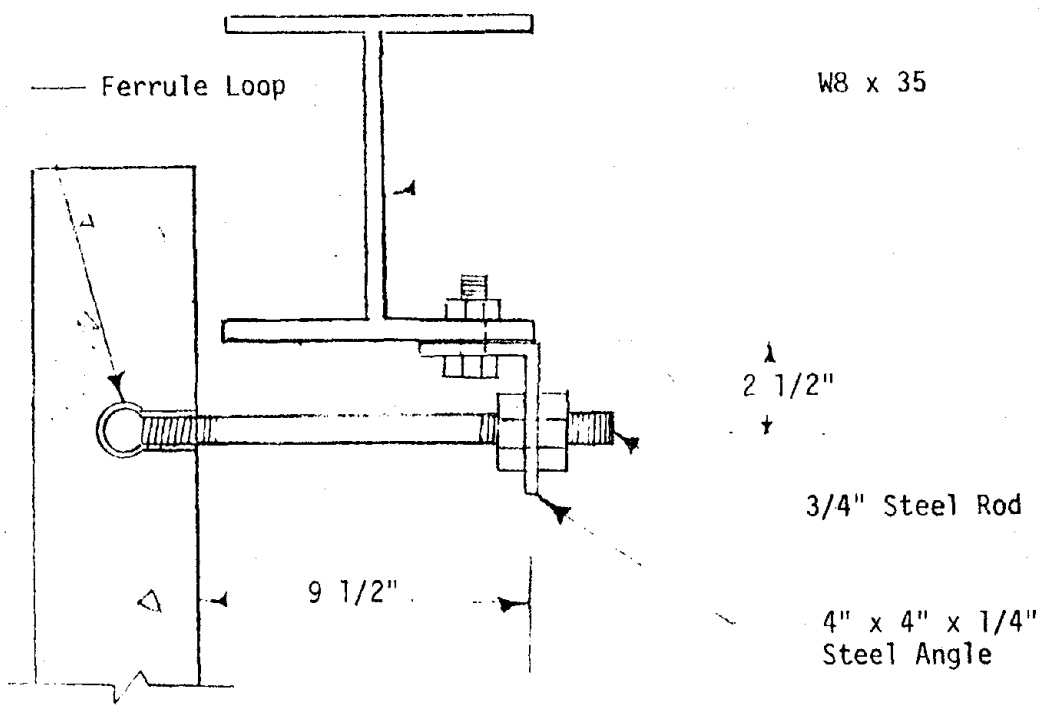
Figure 4.1.   Flexible Panel-Frame Connection

—— 9" x 9" x 1/2" Steel Plate

8" x 4 " x 1/2"
Steel Angle

2 1/2"

2 1/2"

8"

5 1/2"

2"
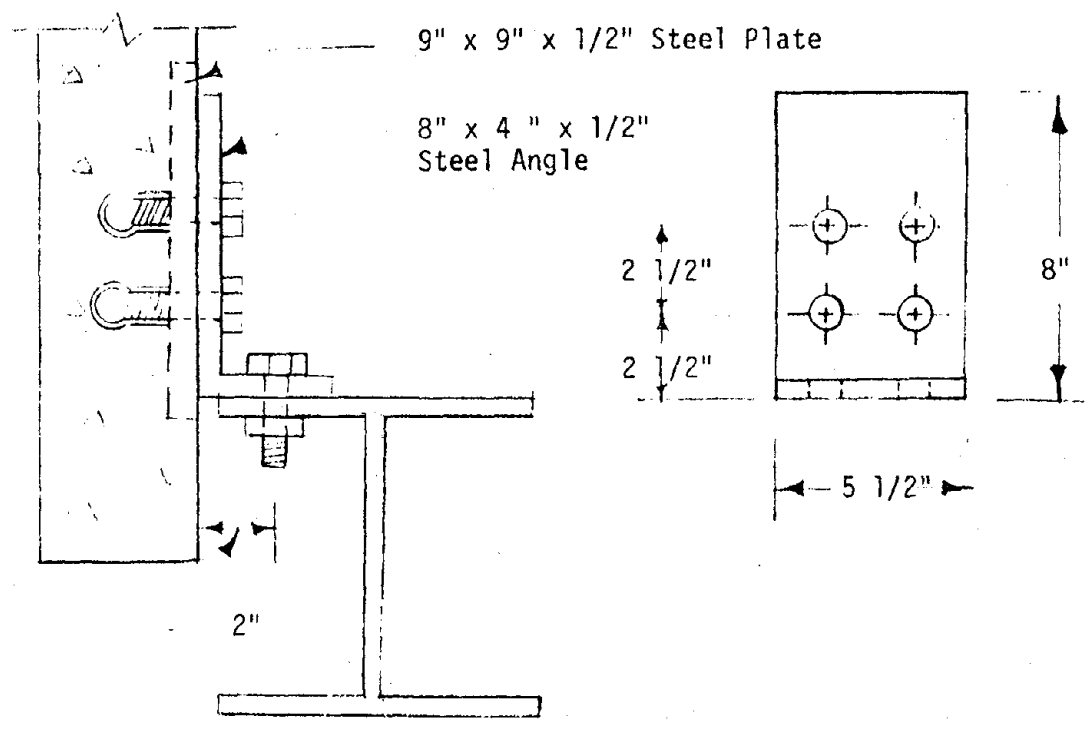
Figure 3.4.2. Bearing Panel-Frame Connection

W8 x 35

Ferrule Loop

B

8" x 4" x 1/2"

A    A

a) Connection Detail

4"

7/8" x 2"

8"

b) Section A-A

9"

c) Section B-B
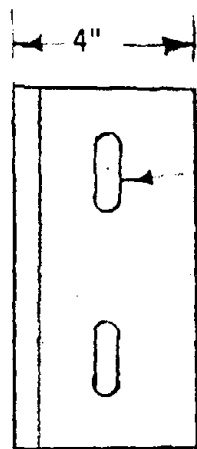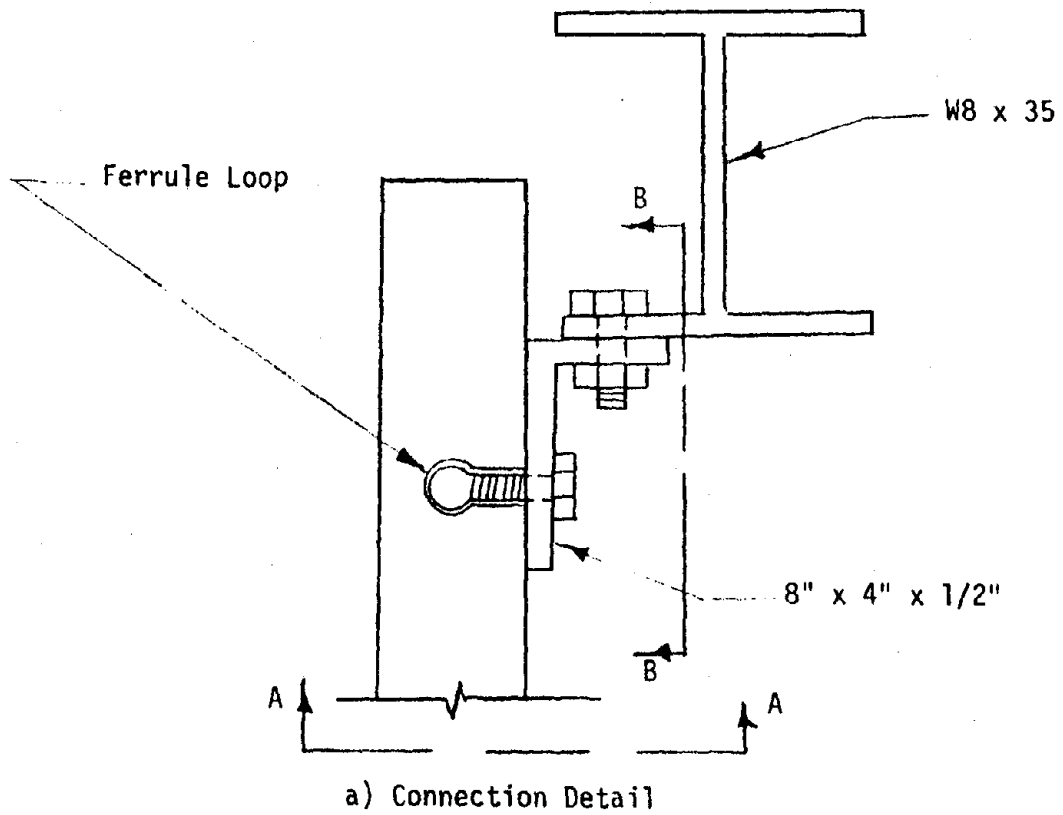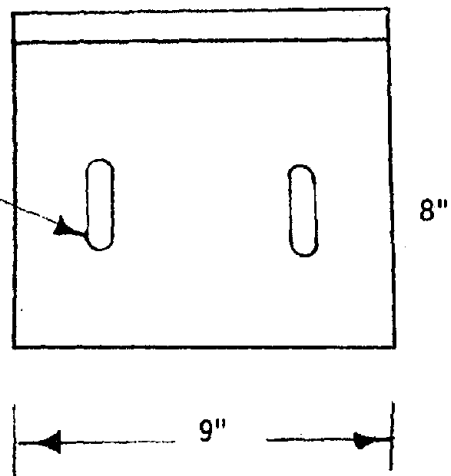
Figure 3.4.3. Slotted Panel-Frame Connection
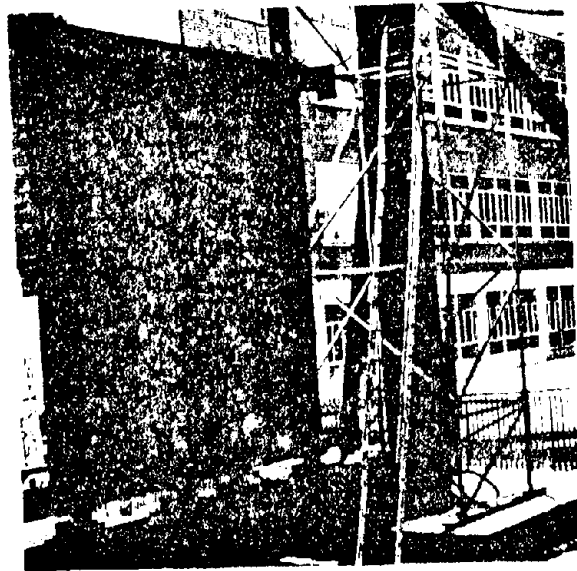
a) Test Configuration for Test II



b) Dynamic Loading Mechanism and Glide Assembly

Photo 3.4.1. Full-Scale Experimental Tests at the University of Idaho
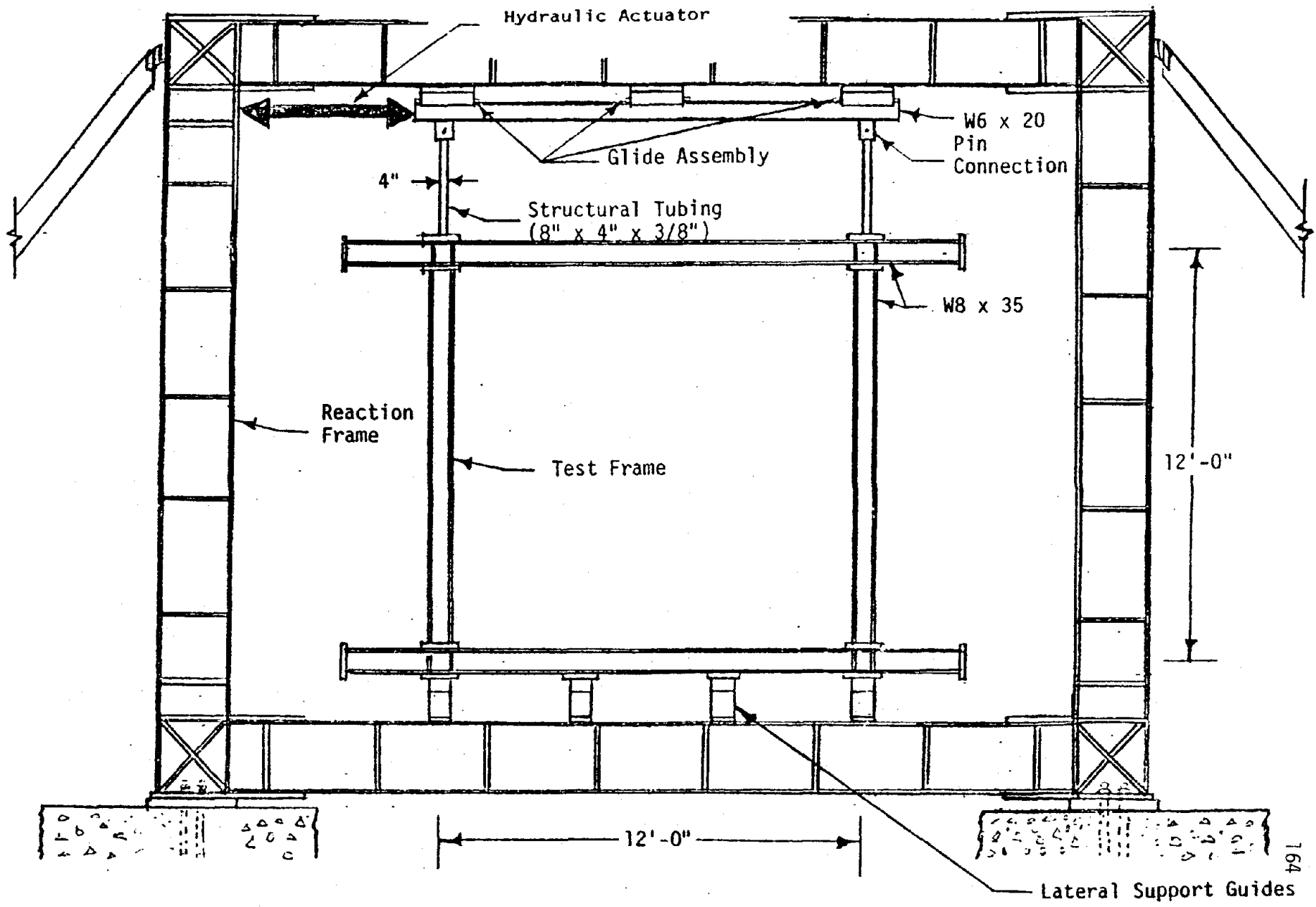
Figure 3.4.4. Test Facilities and Configuration for Test I

in.) connect the top of the test frame to the displacement control system with moment connections at the test frame and pin connections at the displacement control system. The displacement control system (see top of Figure 3.4.4) is used to dynamically load the test specimen and consists of a hydraulic actuator connected to a W6 x 20 steel beam suspended from a lubricated glide system.

An external reaction frame is used to support the test specimen and dynamic loading equipment as shown in Figure 3.4.4. The reaction frame is very stiff relative to the internal frame; consequently, the reaction frame is presumed to act as a stationary support for the test specimen. The actual response of the reaction due to the loading of the test specimen is addressed further by Thomas (1980).

Five different test configurations were used at the University of Idaho to determine the interaction between structural framing and precast panels. Each test consists of the test frame, one or more precast panels, and a combination of two to three connection types. A summary of the test configurations is listed below.

Test I:  Test frame without panels.  See Figure 3.4.4.

Test II:  Test frame with two 6 ft by 12 ft window box panels using flexible and bearing connections.  See Figure 3.4.5.

Test III:  Test frame with one 6 ft by 12 ft window box panel using flexible and bearing connections.  See Figure 3.4.6.

Test IV:  Test frame with one 6 ft by 12 ft window box panel using slotted and bearing connections.  See Figure 3.4.7.

Test V:  Test frame with two 3 ft by 14 ft column cover panels and two 4 ft by 9 ft spandrel cover panels using flexible, slotted, and bearing connections (articulated system).  See Figure 3.4.8.

Hydraulic Actuator

Flexible
Connection
(See Figure 4.1)

Bearing
Connection
(See Figure 4.2)

12'-0"

12'-0"

Lateral Support Guides
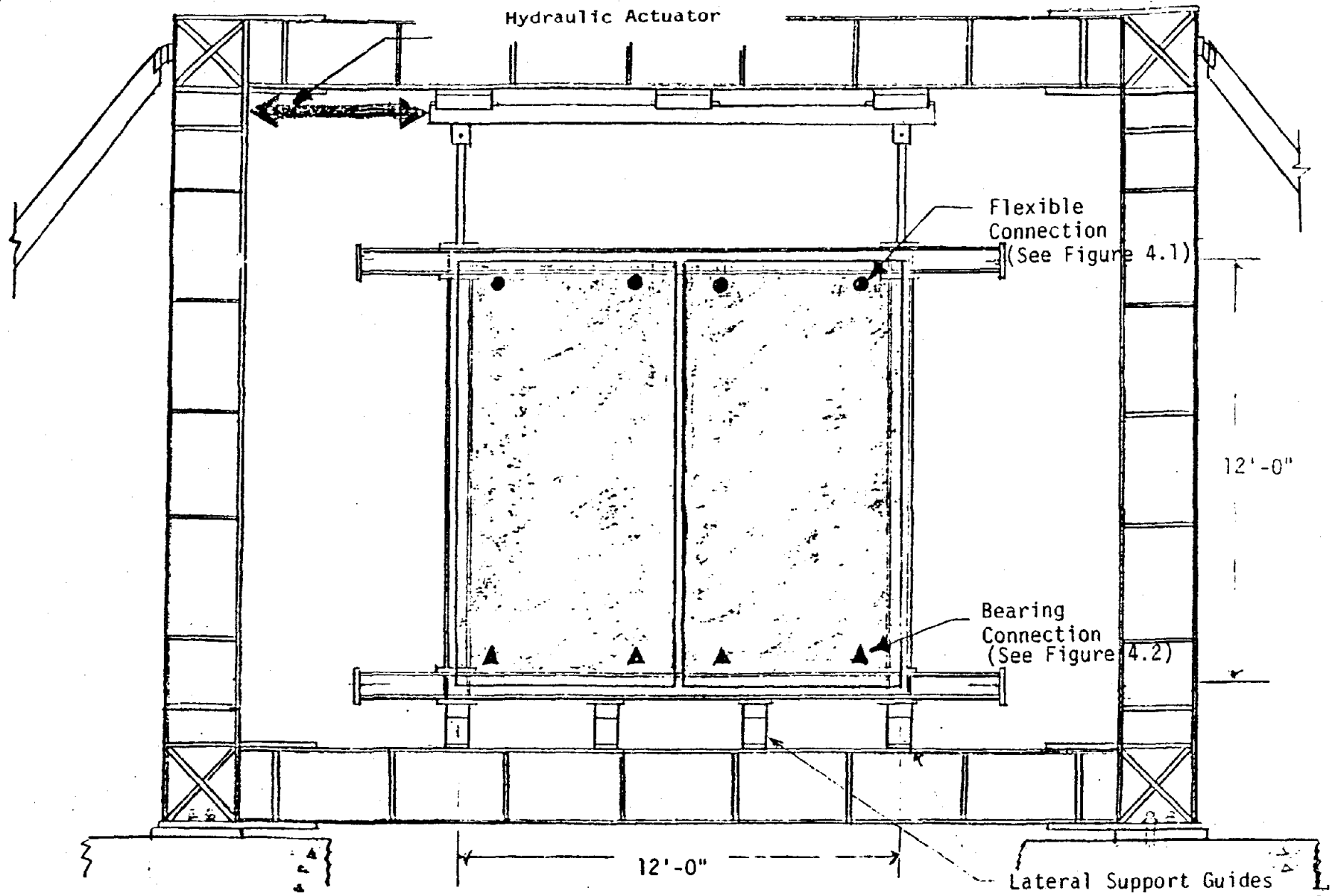
Figure 3.4.5. Configuration for Test II
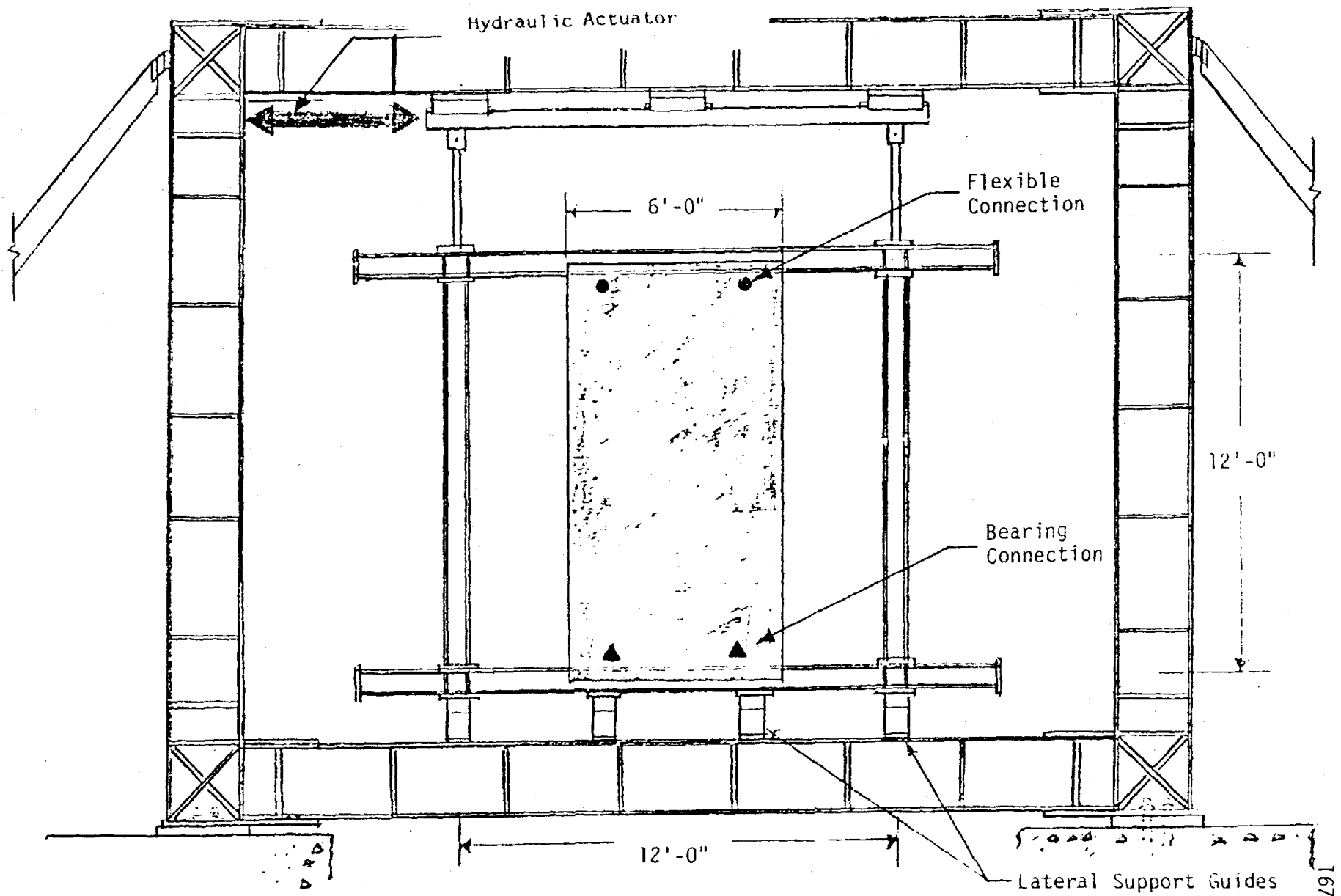
Figure 3.4.6. Configuration for Test III

Hydraulic Actuator

6'-0"

Slotted
Connection
(See Figure 4.3)

12'-0"

Bearing
Connection

12'-0"

Lateral Support Guides

168
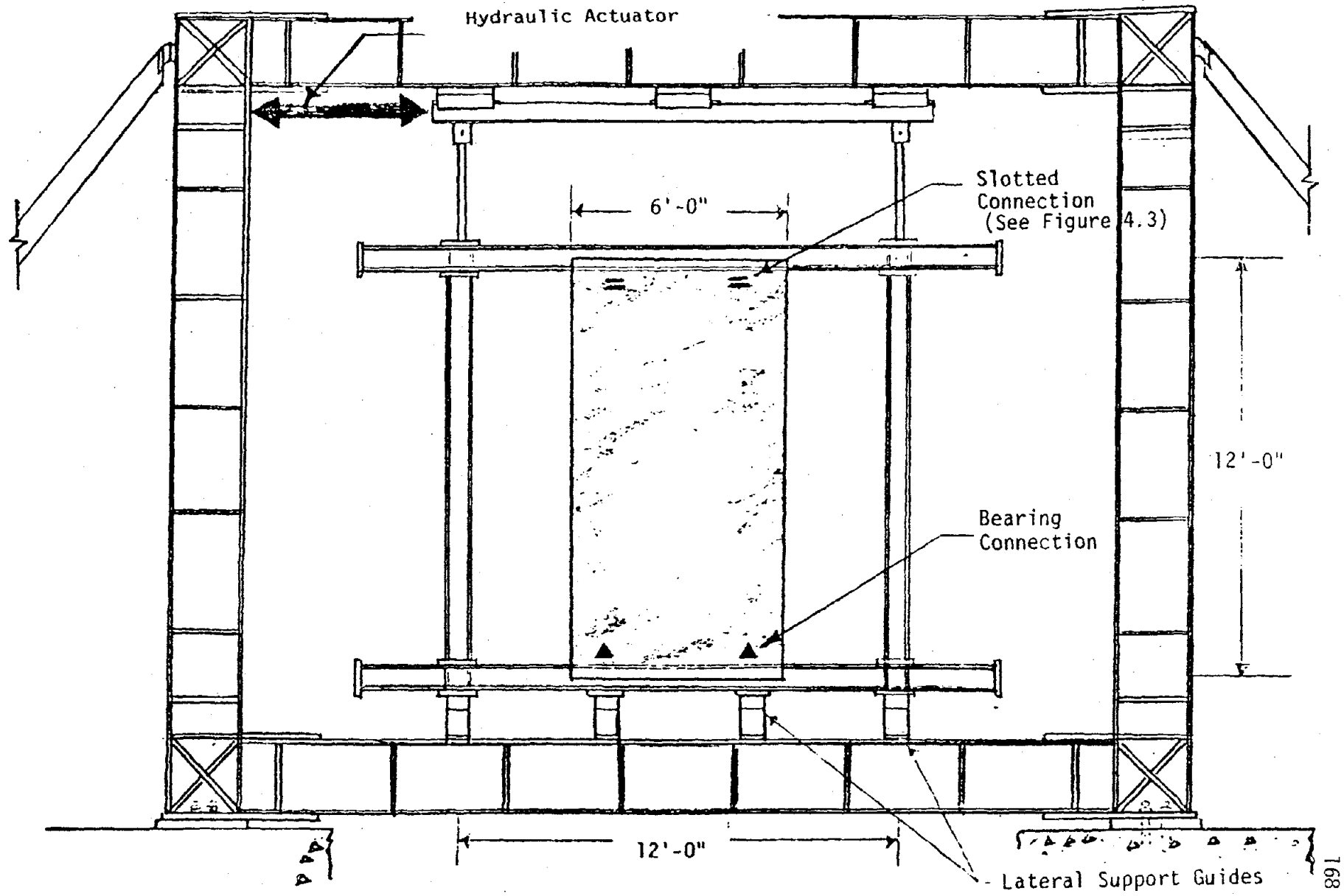
Figure 3.4.7. Configuration for Test IV
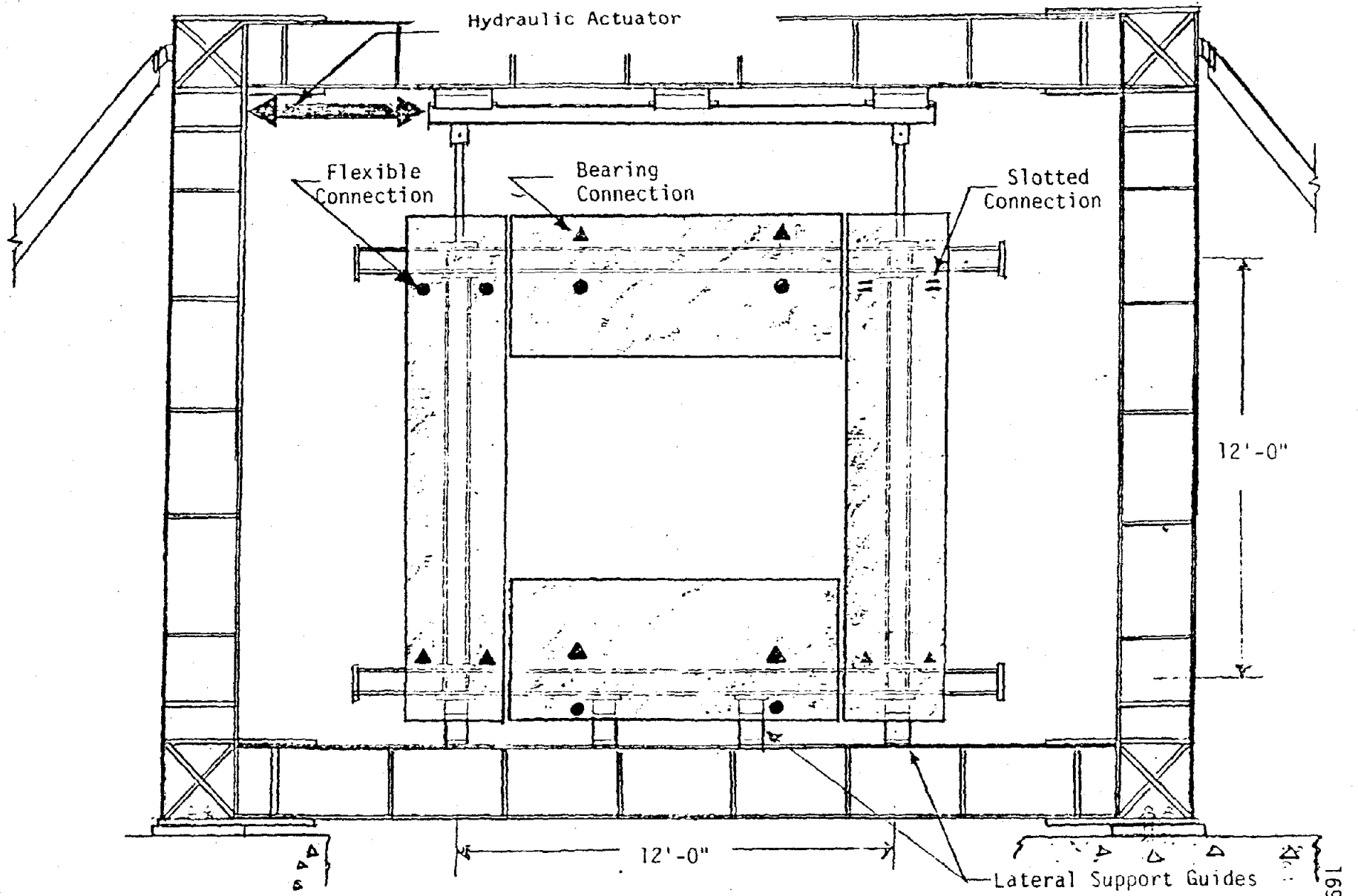
Figure 3.4.8. Configuration for Test V

### 3.4.1.2. Tests for Flexibility and Natural Frequencies

Experimental tests were run to determine the natural frequencies of the system and also to establish the flexibility coefficients. This was done before the system was tested for forced dynamic response. To determine the natural frequencies, each test specimen was excited with a sinusoidal input through a range of frequencies (swept sine technique). Maximum response (displacement and strain) occur at the damped natural frequencies; thus, they are easily identified by LVDT's (instruments used to measure displacement) and strain gages. Note that there is a possibility that the panel connection may be loaded into a nonlinear state during testing. This will slightly alter the natural frequencies; consequently, these connection stresses should be monitored during testing.

Static tests performed on each test configuration consisted of two parts. First, a horizontal static load was applied at point A (see Figure 3.4.9) and the displacements at A and B were recorded. The load was then increased and the resulting displacements recorded. Repeating this procedure for increasing loads provides displacement-load curves for each test specimen; thus, a measure of the flexibility. After this step was completed for a test specimen, the loading mechanism was moved to point B and the entire procedure repeated. Considering only horizontal loads and displacements at points A and B, the results of these tests can be summarized in a set of equations.

$$\begin{bmatrix} U_A \\ U_B \end{bmatrix} = \begin{bmatrix} F_{AA} & F_{AB} \\ F_{BA} & F_{BB} \end{bmatrix} \begin{bmatrix} P_A \\ P_B \end{bmatrix} \tag{3.4.1}$$

where $U_A$ = horizontal displacement at A;

$P_A$ = horizontal load at A;

$F_{AB}$ = flexibility coefficient.
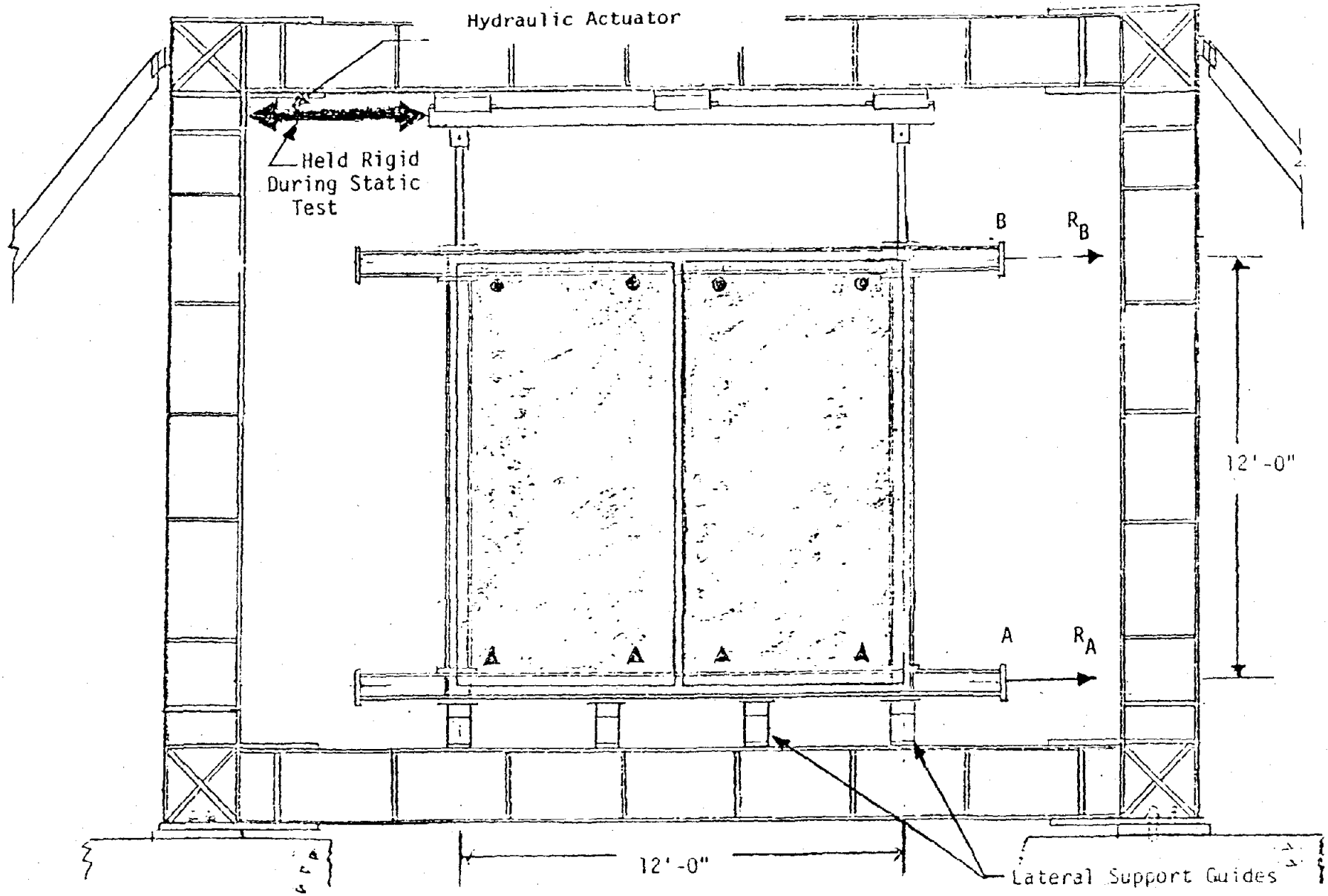
Figure 3.4.9. Static Test for Test II

The flexibility coefficient, $F_{AB}$, can be described as the displacement at A due to a unit load at B. Remember that for each step of the static test, the load was gradually increased and the displacements at A and B were recorded. Plotting these results leads to displacement-load curves for each freedom. For example, the coefficient $F_{AB}$ is determined from the displacement-load curve for the displacements at A due to increasing horizontal loads at point B. Figure 3.4.10 shows the results from a hypothetical test where the slope of the curve is the flexibility coefficient, $F_{AB}$.
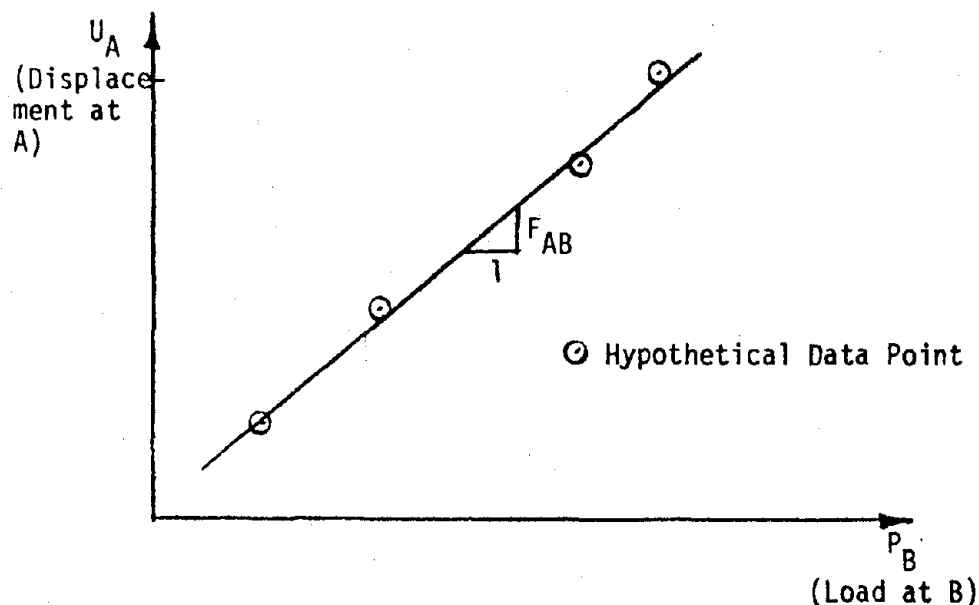


Figure 3.4.10. Hypothetical Displacement-Load Curve

Presently, only the determination of the first two natural frequencies for Test I and first three for Test II have been completed. These results were determined by the experimental procedure discussed previously and are tabulated in Table 3.4.1. Note that the effects of damping were neglected and the panel connections were not monitored to see if they went into a nonlinear state. For the time being, it was assumed that damping and the possibility

Table 3.4.1.Experimental Natural Frequencies for Tests I and II (Hz)

| Frequency | Test I | Test II |
|---|---|---|
| $\omega_1$ | 5.6 | 2.6 |
| $\omega_2$ | 21.0 | 7.4 |
| $\omega_3$ | -- | 10.0 |

of nonlinearity did not have a significant effect on the results. This can be checked in the future when more comprehensive tests are made. Data for static and forced dynamic response of Tests I and II has not been finalized at this time. Once these tests are completed, Tests III through V will be conducted.

### 3.4.2.Analysis of Full-Scale Tests Using SAPFAP

The computer program SAPFAP was utilized to analyze the tests done at the University of Idaho. The three basic elements used to model the five tests are beam, panel, and boundary elements. Beam elements were used to model the test frame, panel elements were used to model the precast curtain walls and connections, and a boundary element was used to simulate the hydraulic actuator. Nodes were established at points of support, connection points, and at enough intermediate points to describe the behavior of the test specimen under loading. Beam elements were modeled using actual lengths, not the clear span between members. This assumption appeared correct because the results obtained for some initial static and dynamic tests of the test frame indicated that the model was somewhat too stiff; therefore, using the clear span for the member lengths would only make the model less accurate. Since the loading is in the plane of the test frame, the W8 x 35 beams will bend

about their strong axis ($I = 126.0$ in.[4]) and the structural tubing will bend about the weak axis ($I = 21.4$ in.[4]). The input data for the panel elements required the stiffness properties for each panel-frame connection type. These properties were obtained from data and equations developed by Sessa (1980) and are presented in Figure 3.4.11. Note that in Test V, the spandrel panels are attached to the test frame on the upper and lower flanges of the test frame beams. (See Figure 3.4.8) Instead of using short rigid beam elements to model in distance between the center of the beam and the flanges, slave nodes were used for the panel connection points. Slave nodes can be used to model rigid links into the system for attaching diaphrams or panels to beam elements. Bathe *et al.* (1974) provides a more complete discussion of slave nodes.

### 3.4.2.1 Static Analysis

Since the displacement control system shown in Figure 4.10 is held rigid during the static tests, the top of the structural tubing is idealized as having a pin support at the displacement control system. Figures 3.4.12 through 3.4.15 present the computer models used to analyze each of the five tests under static loading. One thousand pound loads were applied individually one at a time in the horizontal direction at nodes 15 and 23 for Tests I through IV and at nodes 23 and 38 for Test V. These nodes are analogous to points A and B described in the previous discussion on the experimental tests. With the computer solution, the displacements are identified at nodes A and B and the flexibility coefficients for each test configuration were calculated. The flexibility matrices for the five tests are summarized in Table 3.10. The maximum bending stress and location of the maximum bending
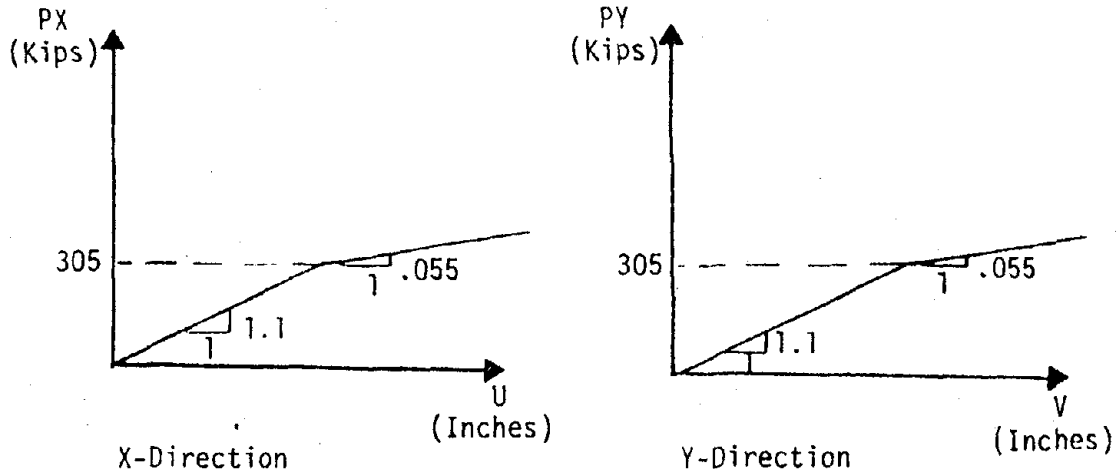
a) Flexible Connection: 3/4 in. Diameter Rod
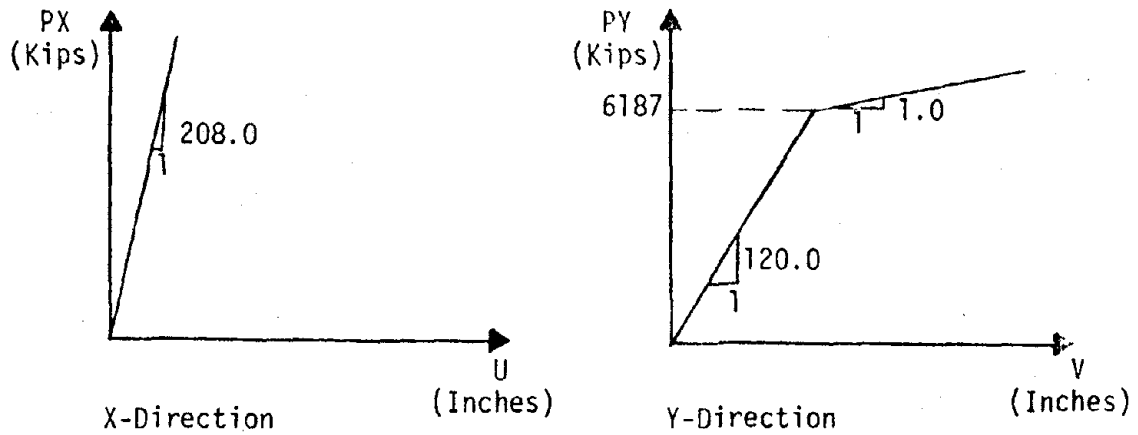
b) Bearing Connection: 8 in. by 4 in. by 1/2 in. Steel Angle
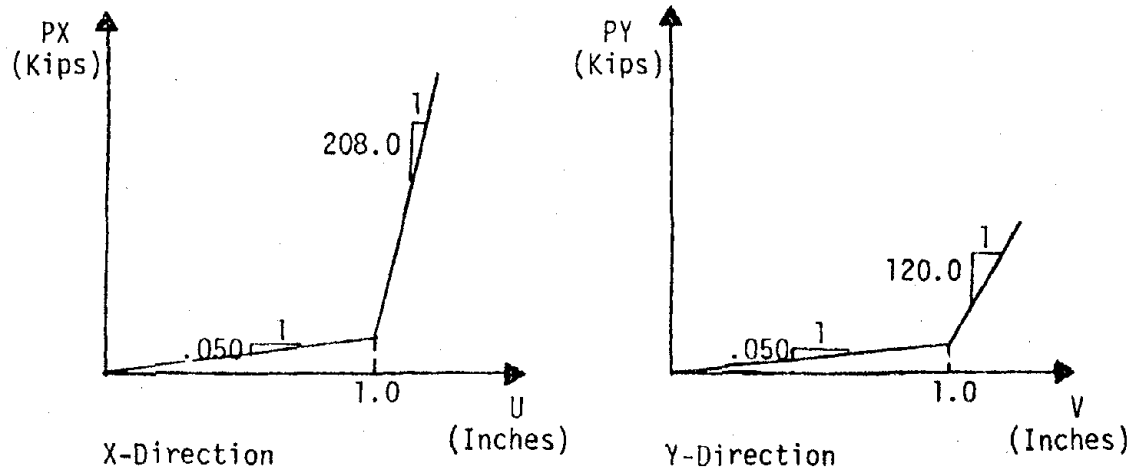
c) Slotted Connection: 8 in. by 4 in. by 1/2 in. Steel Angle

Figure 3.4.11. Idealized Load-Displacement Curves for Three Types of Connections

Figure 3.4.12. Computer Model for Test I: Static Loading

176
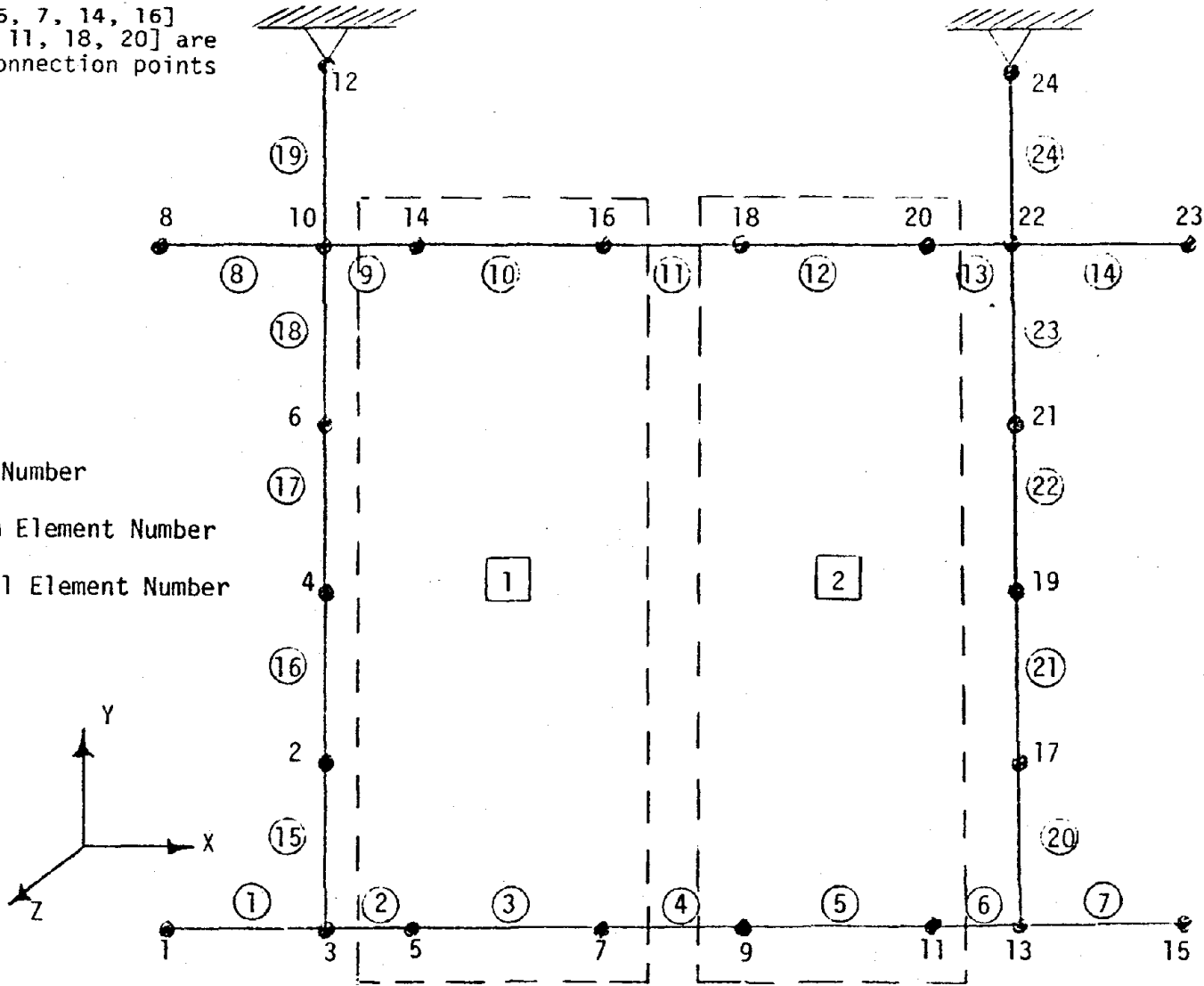
Figure 3.4.13. Computer Model for Test II: Static Loading

Nodes [7, 9, 16, 18] are panel connection points

LEGEND

1 - Node Number

(1) - Beam Element Number

[1] - Panel Element Number
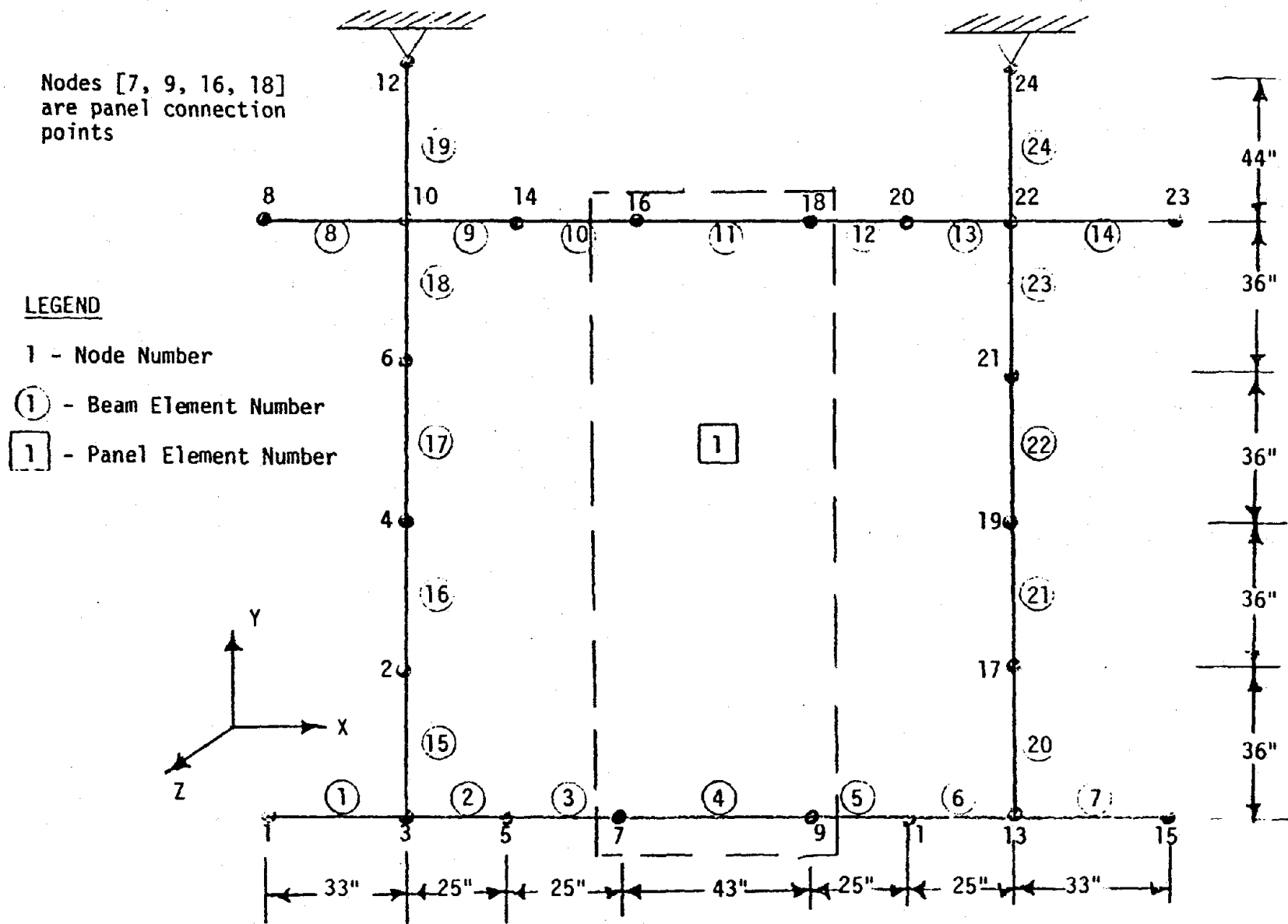
Figure 3.4.14. Computer Model for Tests III and IV: Static Loading

178

Nodes [3, 7, 10, 12],
[9, 13, 17, 21], [18,
20, 26, 28], and [27,
29, 34, 36] are panel
connection points
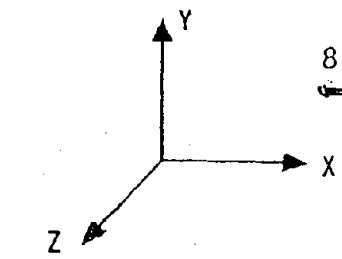
LEGEND

1 - Node Number

(1) - Beam Element
Number

[1] - Panel Element
Number
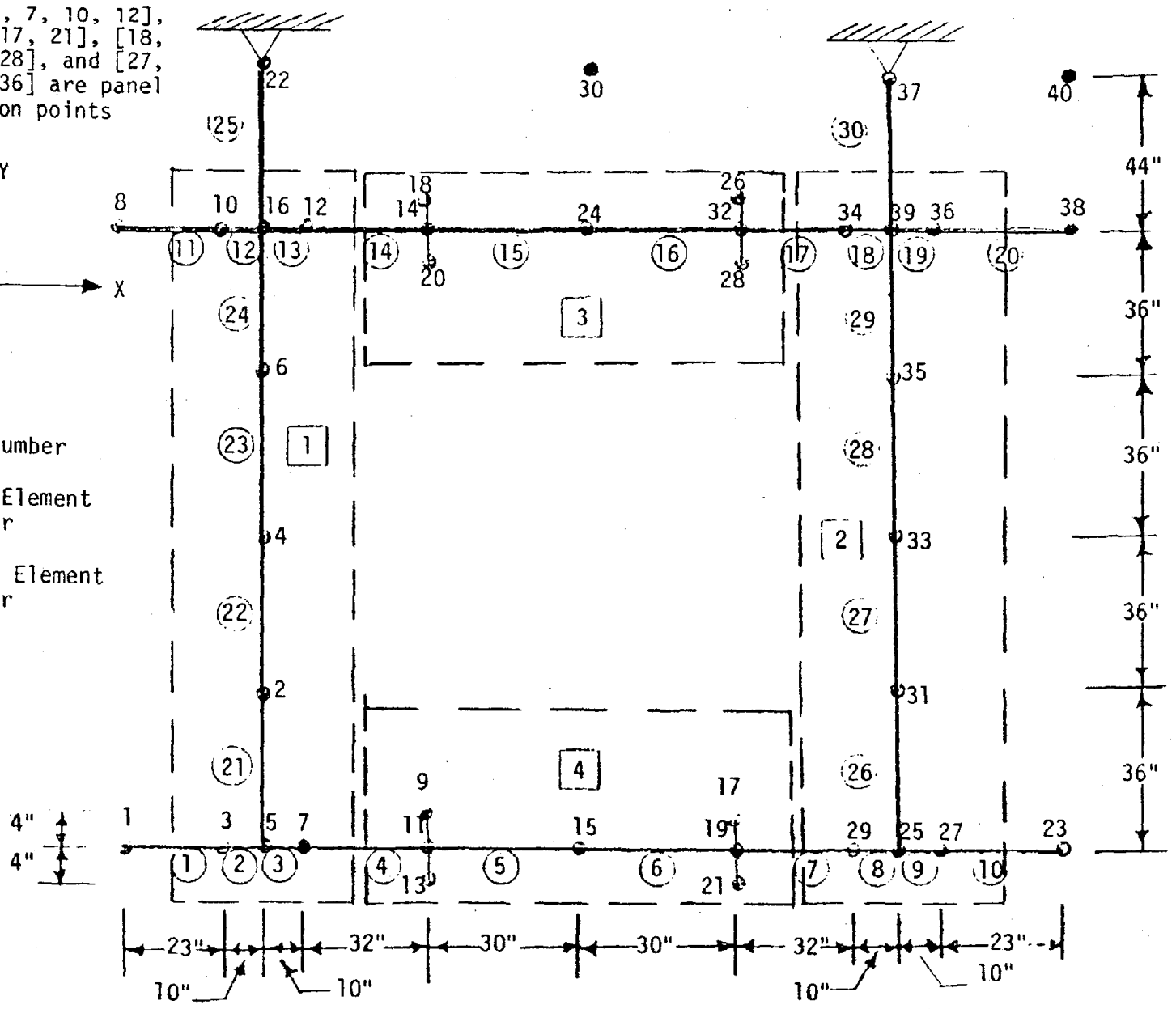
Figure 3.4.15. Computer Model for Test V:  Static Loading

Table 3.4.2. Theoretical Flexibility Coefficients Obtained from SAPFAP for Tests I through V

Test I:

$$\overline{F} = \begin{bmatrix} 126.74 & 41.46 \\ 41.46 & 30.39 \end{bmatrix} 10^{-6} \text{ in./lb}$$

Test II:

$$\overline{F} = \begin{bmatrix} 108.34 & 39.15 \\ 39.15 & 30.18 \end{bmatrix} 10^{-6} \text{ in./lb}$$

Test III:

$$\overline{F} = \begin{bmatrix} 113.58 & 39.76 \\ 39.76 & 30.16 \end{bmatrix} 10^{-6} \text{ in./lb}$$

Test IV:

$$\overline{F} = \begin{bmatrix} 125.41 & 41.25 \\ 41.25 & 30.34 \end{bmatrix} 10^{-6} \text{ in./lb}$$

Test V:

$$\overline{F} = \begin{bmatrix} 124.86 & 41.14 \\ 41.14 & 30.25 \end{bmatrix} 10^{-6} \text{ in./lb}$$

stress in the test frame due to the horizontal load at point A is summarized in Table 3.4.3 for each test while the maximum bending stresses in the structural tubing for the horizontal load at A is recorded in Table 34.4. A summary of the forces in each panel-frame connection under the same loading is given in Table 3.4.5. Note that the 1,000 pound load is a relatively small load on this system and none of the components are stressed close to their yield stress except·the bearing connections in the spandrel panels of Test V. (The high loads predicted in the spandrel panel connections may have resulted in incorrect use of the panel element, i.e., attaching panel elements to slave nodes. The results of full-scale tests will be able to verify the use of the panel element in this fashion.)

Results from Table 34.2 indicate that the configuration for Test II provides a measurable increase in the stiffness of the test frame. Considering the deflection and load at point A, Test II provides a 17% decrease in the deflection at point A over Test I, the bare frame. Using the same comparison, the configuration for Test III provides a 12% reduction in the deflection at point A over Test I. Configurations for Tests IV and V have little effect on the deflections of the test frame under static loads. In Test IV, the panel connections at the top are slotted connections; consequently, they provide minimal resistance when deformed. In Test V, the width of the column panels and height of the spandrel panel are very small, i.e., 20 in. and 8 in., respectively. With these small distances between connection points, the panels cannot resist as much load.

Reviewing the maximum bending stresses in the test frame (Table 3.4.3), Test II shows a 16% reduction in the maximum bending stress over the bare test frame (Test I), while Test III shows a 10% reduction in the maximum bending

Table 3.4.3 Maximum Bending Stress in the Test Frame Due to a 1,000 Pound
Load at Point A. (Note: Node 39 for Test V is the same as
node 22 for the other models.)

| Test | Maximum Moment (in.-lb) | Maximum Stress (psi) | Element | Node |
|------|------------------------|----------------------|---------|------|
| I    | 55,190                 | 1,775                | 13      | 22   |
| II   | 47,420                 | 1,525                | 13      | 22   |
| III  | 50,130                 | 1,612                | 13      | 22   |
| IV   | 54,820                 | 1,762                | 13      | 22   |
| V    | 54,330                 | 1,746                | 18      | 34   |

Table 3.4.4. Maximum Bending Stress in the Structural Tubing Due to a 1,000
Pound Load at Point A. (Note: Node 39 for Test V is the same
as node 22 for the other models.)

| Test | Maximum Moment (in.-lb) | Maximum Stress (psi) | Element | Node |
|------|------------------------|----------------------|---------|------|
| I    | 22,000                 | 2,056                | 24      | 22   |
| II   | 22,070                 | 2,062                | 24      | 22   |
| III  | 22,020                 | 2,057                | 24      | 22   |
| IV   | 22,020                 | 2,057                | 24      | 22   |
| V    | 21,840                 | 2,041                | 30      | 34   |

Table 3.4.5. Summary of Forces (lb) in the Panel-Frame Connections Due to a 1,000 Pound Load at Point A

| Test | Panel | Connector I | | | Connector J | | | Connector K | | | Connector L | | |
|------|-------|------|--------|--------|------|--------|--------|------|--------|--------|------|--------|--------|
| | | Node | X-Dir. | Y-Dir. | Node | X-Dir. | Y-Dir. | Node | X-Dir. | Y-Dir. | Node | X-Dir. | Y-Dir. |
| II | 1 | 14 | -53 | 5 | 16 | -53 | 3 | 7 | 60 | -355 | 5 | 46 | 352 |
| | 2 | 18 | -53 | 3 | 20 | -53 | 5 | 11 | 62 | -353 | 9 | 45 | 355 |
| III | 1 | 16 | -64 | 6 | 18 | -64 | -6 | 9 | 71 | -420 | 7 | 56 | 420 |
| IV | 1 | 16 | -5 | 0 | 18 | -5 | 0 | 9 | 13 | -32 | 7 | 3 | 32 |
| V | 1 | 10 | -17 | 2 | 16 | -17 | -1 | 7 | 18 | -238 | 3 | 15 | 238 |
| | 2 | 34 | -3 | 0 | 36 | -3 | 0 | 27 | 8 | -32 | 29 | -3 | 33 |
| | 3 | 18 | 4258 | 2 | 26 | -4270 | -2 | 28 | -17 | 0 | 20 | 28 | 0 |
| | 4 | 9 | 3137 | 2 | 17 | -3145 | -1 | 21 | -12 | 0 | 13 | 21 | 0 |

stress. Again, Tests IV and V indicate a minimum reduction of the bending stresses in the test frame.

Note that if the load on the structure is large enough, the flexible connections in Tests II and III will yield and only minimal additional stiffness will be provided. The example problem used in Beers (1980) evaluates the effect of nonlinearity in the connections for Test II and shows that the flexible connections will yield with a horizontal load between 3,750 lb and 7,500 lb at point A. At this load level, the flexible connections provide minimal stiffness; thus, the panel elements provide minimal additional stiffness to the test frame. Note that the yield load could be identified more accurately by increasing the number of increments used in the nonlinear analysis. A summary of the effects of this load on the structure is given in Beers (1980).

Reviewing the results of the five tests, it can be seen that the configurations for Tests II and III definitely provide additional stiffness to the overall structure and reduce the maximum bending moments in the test frame under static loads. Configurations used in Tests IV and V have essentially no effect on the stiffness of the test frame under static loading conditions.

### 3.4.22. Dynamic Analysis

The computer models developed for dynamic loading conditions are almost identical to those used for static loading except for the support conditions and the addition of concentrated masses to represent the panel elements and steel connection plates. Plates measuring 14 1/2 in. by 9 in. by 1 1/4 in. were used to provide the connection between columns and beams in the test

frame. (See Figure 3.4.4) These plates were also used to connect the beams of the test frame to the structural tubing while smaller plates were used for the lateral support guides and stiffness. All of the plates were modeled as concentrated masses at the node nearest to that plate. Although these masses are small relative to the mass of the panels and the test frame, they were significant in Test I, i.e., the test without the panels. Masses of the beam elements were idealized as concentrated masses, with half of the element mass lumped at each node. Dynamic properties of the panels were input as concentrated masses and mass moments of inertia. Since the flexible and slotted connections can only carry minimal loads relative to the bearing connections, the masses and mass moments of inertia were applied at the bearing connections. Note that the mass moments of inertia must be referenced to about the bearing connections and not the centroid of the panel. The masses and mass moments of inertia for the panels were distributed equally between the two bearing connections. Figures 3.4.16 through 3.4.19 demonstrate how the masses of the panel elements were distributed for the five tests and present the models used for dynamic analyses.

The glide assembly (see Figure 3.4.4)was idealized as beam elements supported by three roller supports while pin connections were input at the top of the structural tubing. The hydraulic actuator was modeled as a stiff boundary element as shown in Figures 3.4.16 through 3.4.19. The stiffness of the boundary element varies with the frequency used to load the system. This occurs from variations in the actuator load and displacement during different loading frequencies. An experimental test was performed to help develop the stiffness to be used in the boundary element for the computer model. The load in the actuator and the corresponding cyclic displacement was recorded
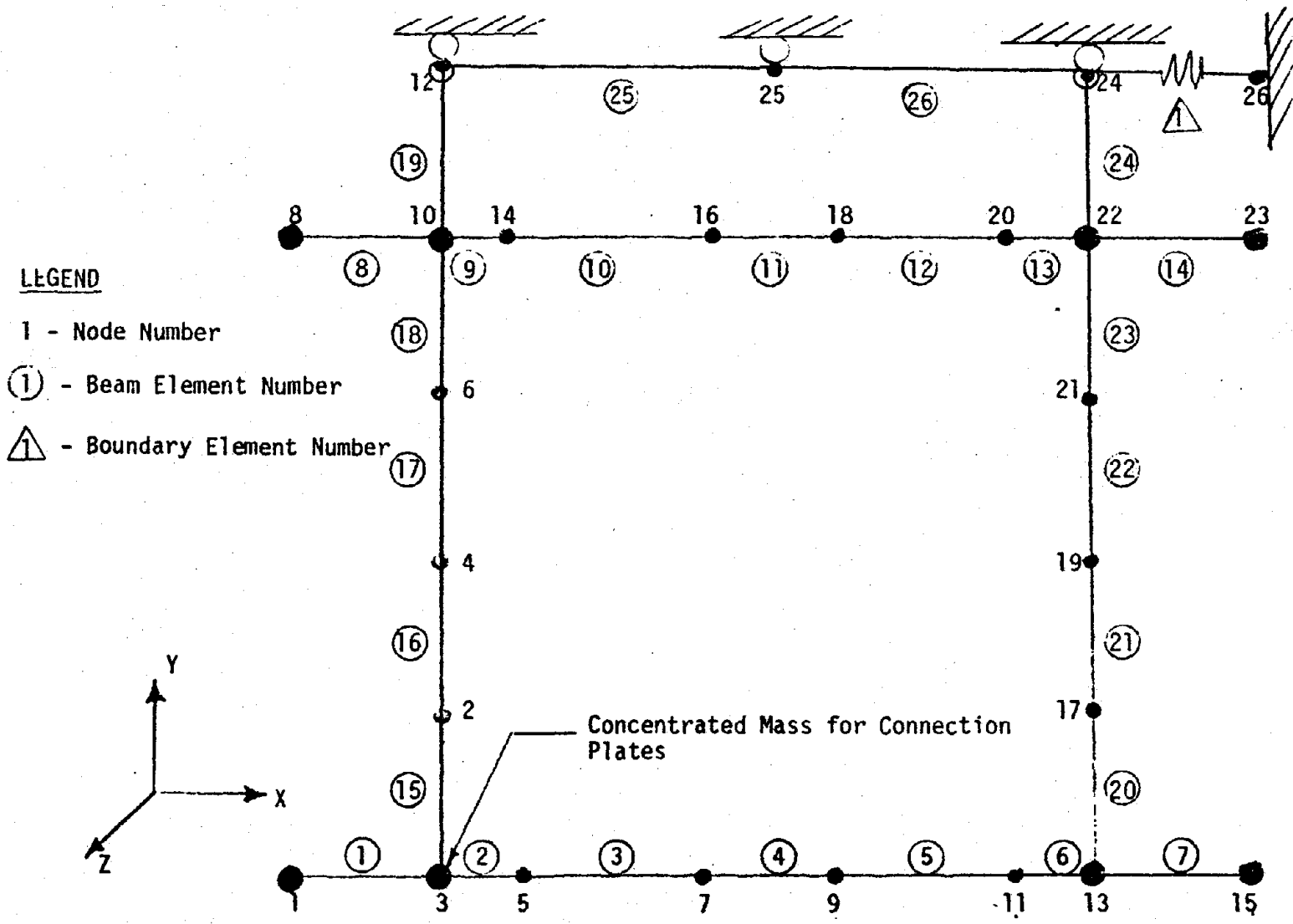
Figure 3.4.16. Computer Model for Test I: Dynamic Loading

LEGEND

1 - Node Number

① - Beam Element Number

☐ - Panel Element Number

△ - Boundary Element Number

─ 5.82 lb-sec$^2$
      in.

─ 42,472 lb-sec$^2$ in.
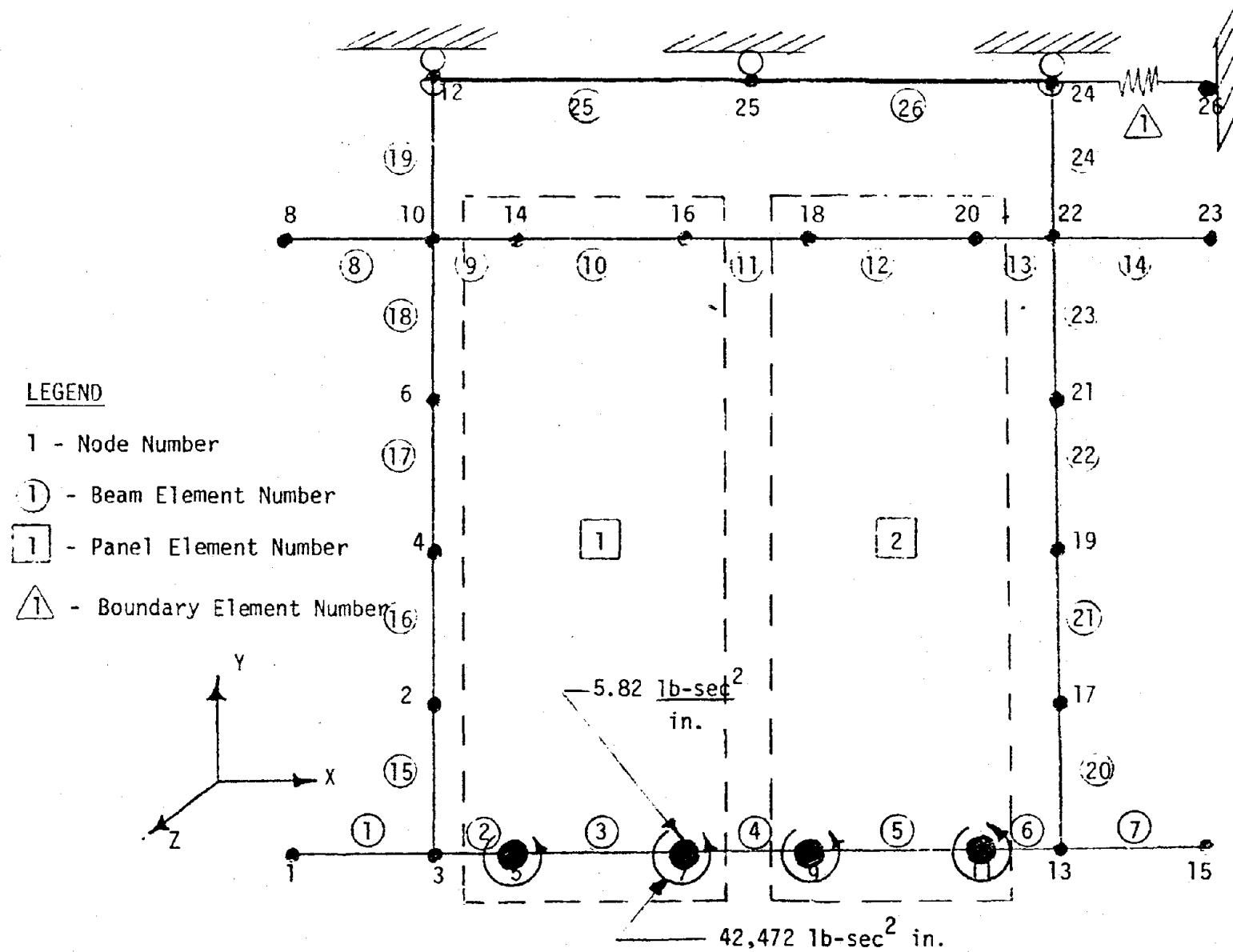
Figure 3.4.17. Computer Model for Test II:  Dynamic Loading

LEGEND

1 - Node Number

①  - Beam Element Number

☐1  - Panel Element Number

△1  - Boundary Element Number

5.82 $\frac{lb-sec^2}{in.}$

42,472 lb-sec$^2$ in.
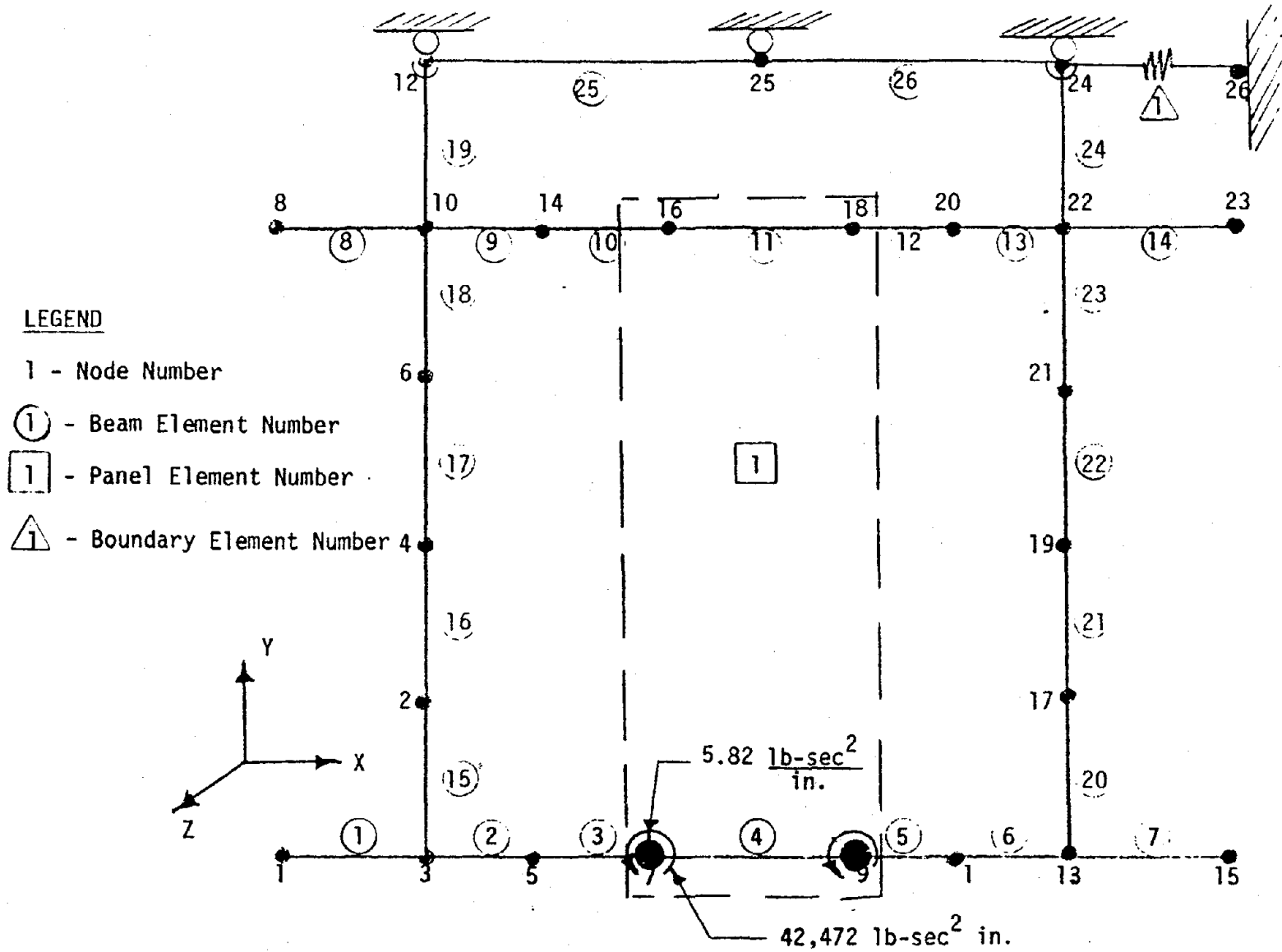
Figure 3.4.18. Computer Model for Tests III and IV: Dynamic Loading
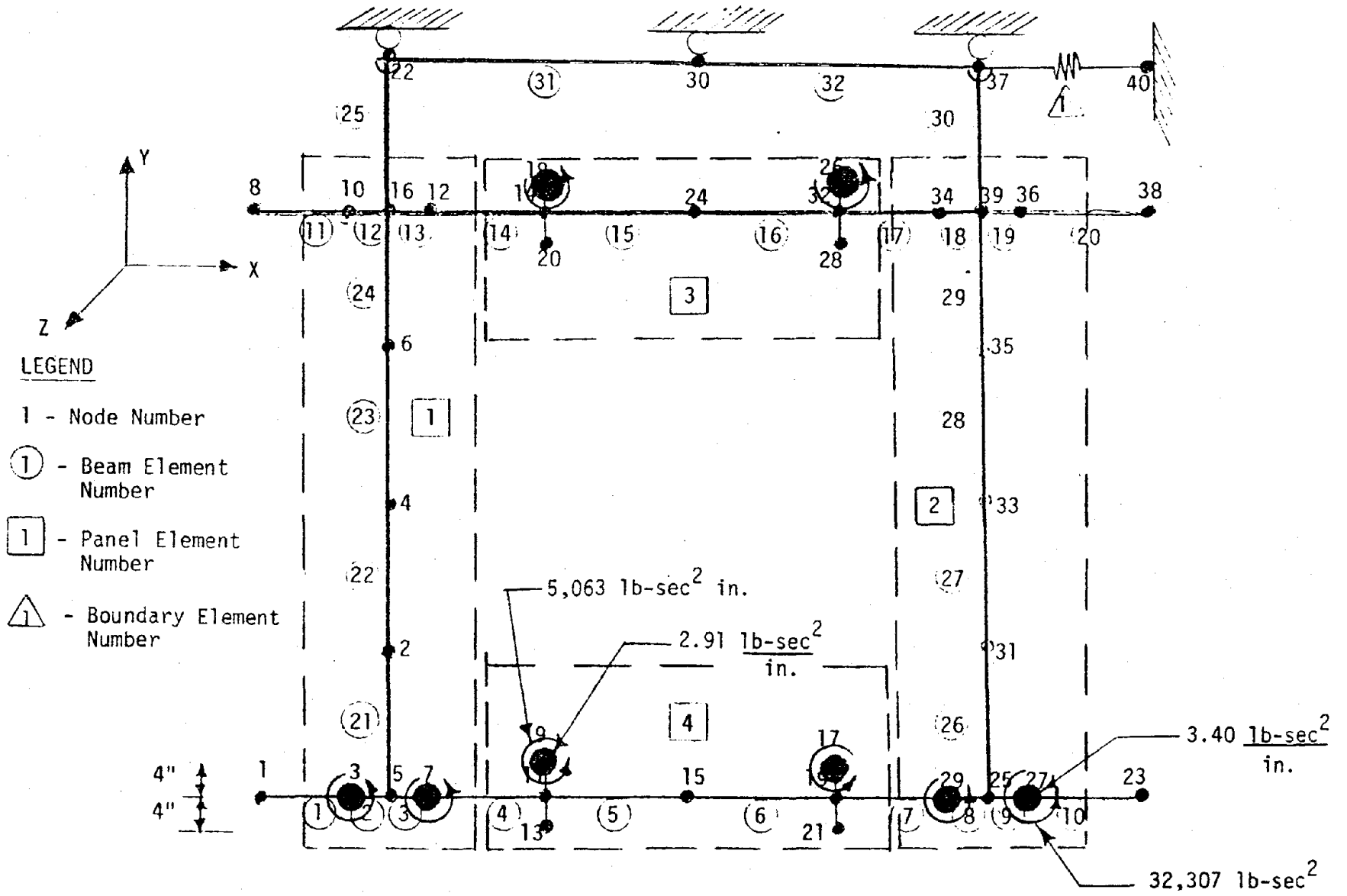
Figure 3.4.19. Computer Model for Test V: Dynamic Loading

for six different frequencies. The actuator (boundary element) stiffness was taken as the actuator load divided by the cyclic displacement. Results of the experiment are tabulated in Table 3.4.6 and plotted in Figure 3.4.20. For the frequencies between 1 and 10 Hz, the average stiffness of the actuator is about 25,000 lb/in. and for frequencies above 10 Hz, the actuator stiffness rises rapidly.

To simplify the computer analyses, two boundary element stiffnesses were developed, one for low frequency dynamic loading and one for high frequency dynamic loading. The stiffnesses of these two boundary elements were determined by fine tuning the boundary element stiffnesses in the analytical models such that they approximate the experimental data for the actuator stiffness and predict the first two natural frequencies of Test I and the first three natural frequencies of Test II. The measured natural frequencies are tabulated in Table 3.4.1. Using the appropriate computer model, the low frequency boundary element stiffness was modified until the analytical natural frequencies predicted the first natural frequencies of Test I and Test II. The resulting stiffness was 27,500 lb/in. which is very close to the experimentally obtained value for the actuator stiffness equal to 25,000 lb/in. The final analytical prediction of the first natural frequencies was 5.61 and 2.50 Hz for Tests I and II, respectively.

In the experimental stiffness-frequency comparison for the actuator, the actuator stiffness rises rapidly as the frequency exceeds 10 Hz. To simplify the analysis, the stiffness for the higher frequency boundary element was taken as 900,000 lb/in. or essentially rigid. A totally rigid element was not used because of the numerical instabilities that can arise (Cook 1974). Good estimations of the higher frequencies of Tests I and II were

Table 3.4.6.  Summary of Frequency-Load-Displacement Relationship for the
Hydraulic Actuator

| Frequency (Hz) | Load (lb) | Displacement (in.) | Stiffness (lb/in.) |
|---|---|---|---|
| 2.6 | 3,602 | .138 | 26,196 |
| 7.4 | 3,879 | .150 | 25,860 |
| 10.0 | 2,770 | .117 | 23,742 |
| 15.0 | 4,433 | .125 | 35,464 |
| 20.0 | 4,987 | .042 | 119,688 |
| 22.0 | 9,421 | .033 | 282,630 |
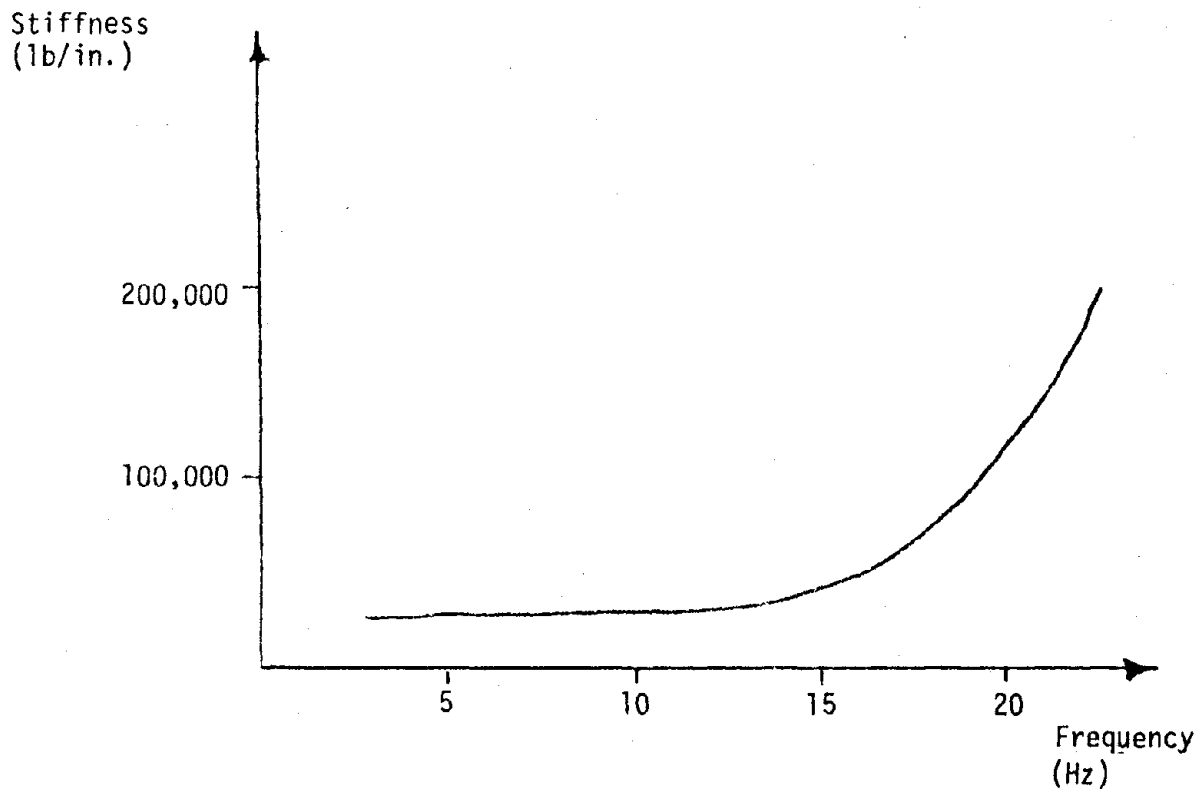


Figure 3.4.20.  Plot of Experimental Stiffness-Frequency Relationship for the
Hydraulic Actuator

obtained using the very stiff boundary element. The first five natural frequencies for all five tests are summarized in Table 3.15 using both the 27,500 lb/in. and the very stiff boundary elements. Except for Tests I and V, the predicted values of the second natural frequency is the same using the 27.5 or the 900 kip/in. boundary element stiffness for all tests. In Test I, the 900 kip/in. boundary element estimates the second natural frequency to be 22.7 Hz which is much closer to the experimental of 21.0 than 16.8, the prediction based on a stiffness of 27.5 kip/in. Both boundary elements provide good estimates of the second and third natural frequencies of Test II.

Based on the results demonstrated in Figure 3.32 and the comparisons made between predicted and experimental values of natural frequencies for both boundary elements, it is recommended for Tests I and II that the boundary element with a stiffness of 27.5 kip/in. be used for determination of natural frequencies and forced dynamic response when the actuator is operating at frequencies less than 7 Hz. When the operating frequency is between 7 and 10 Hz, it appears that both boundary element stiffnesses will provide acceptable results. For operating frequencies greater than 10 Hz, the 900 kip/in. or very stiff boundary element appears to provide more accurate results for Tests I and II. When using these models in the future to predict the response of Tests III, IV, and V, it is recommended that the load-cyclic displacement be monitored for the actuator for each test configuration as demonstrated in Table 3.14 and Figure 3.32. These tests will indicate the approximate behavior of the actuator and provide guidelines for selecting the correct boundary element stiffness or stiffnesses.

Table 3.4.7. First Five Natural Frequencies for the Tests Conducted at the University of Idaho. (Predicted values are given for both a boundary element stiffness of 27.5 kip/in. and 900 kip/in. and frequencies are expressed in Hz.)

| Frequency | Stiffness | Test I 27.5 | Test I 900 | Test II 27.5 | Test II 900 | Test III 27.5 | Test III 900 | Test IV 27.5 | Test IV 900 | Test V 27.5 | Test V 900 |
|---|---|---|---|---|---|---|---|---|---|---|---|
| $\omega_1$ | | 5.61 | 6.89 | 2.50 | 2.92 | 3.22 | 3.78 | 3.11 | 3.60 | 2.69 | 3.00 |
| $\omega_2$ | | 16.8 | 22.7 | 7.87 | 7.87 | 10.0 | 10.0 | 9.96 | 9.96 | 5.99 | 6.32 |
| $\omega_3$ | | 36.9 | 45.7 | 10.2 | 10.5 | 13.9 | 14.2 | 13.43 | 14.0 | 7.56 | 7.81 |
| $\omega_4$ | | 45.2 | 65.8 | 14.6 | 14.6 | 15.8 | 21.4 | 15.69 | 21.1 | 17.2 | 17.2 |
| $\omega_5$ | | 65.8 | 77.2 | 15.5 | 16.6 | 23.3 | 23.4 | 23.3 | 23.3 | 17.8 | 17.9 |

3.5  Prediction of Panel Connector Forces

This section presents a linear dynamic analysis to determine the resultant forces in the panel connectors due to seismic loading conditions. The response due to seismic excitation of the structural model is determined with the finite element program SAPFAP (Beers, 1980) using the mode-super-position method. The response of the structural model is then used to generate excitation for analysis of the architectural system.

Connector response is determined analytically for the modeled test assembly described as Test II (Section 3.4.1.1) for seismic loading conditions as recorded on the University of California, Berkeley; Earthquake Engineering Center accelerograms. Acceleration records taken from the tapes are used to provide excitation to the analytic model to find its response to various seismic loading conditions. Records that were used included ground acceleration time histories as well as acceleration records taken from upper stories of buildings during a recent earthquake. This was done in an effort to find the maximum forces transmitted by the connectors at various levels of high-rise buildings. The earthquake records used in this analysis are summarized and discussed in Section 3.6.

3.5.1  Method of Analysis

The section discusses the solution of the response of Test II to seismic loading conditions, and the corresponding response in the panel connectors. The modeled sample structure includes panel elements as developed by Briggs (1976) to include the effect of the interaction between the structural framing and the precast cladding. Response of the analytic model is determined using the finite element program, SAPFAP (Beers, 1980), for several different earthquake accelerograms (see Section 3.6). Total response in the panel connectors are found in two parts.

1.  Forces in the panel connectors caused by differential displacement between the panel connection points on the structural framing are found first. The displacement histories for the connection nodes determined by the solution of the interactive panel frame model are multiplied by the panel stiffness matrix to give these forces.

2.  The finite element program (SAPFAP) used in the determination of the response of the interactive panel-frame model does not account for the effect on the panel connectors of the eccentricity of the panel relative to the framing. The panel element (Briggs, 1976) used in the modeled structure is massless. Lumped translational and rotational masses are used at panel bearing points to account for the mass of the panels. A second analysis is required then, to determine response of the bearing connectors as they resist the inertia of the panel mass as the panel moves with the framing during seismic excitation. This portion of the analysis uses the response of the interactive panel-frame model to generate excitation for a model of the panel and its bearing connectors.

Resultant forces in the connectors are then determined by superimposing the force response caused by differential displacement between panel connection points with the force response caused by movement of the panel mass.

3.5.2  Idealization and analysis of Structural Framing with Panel Elements

The analysis of the sample frame for dynamic loading conditions becomes cumbersome because of the number of freedoms associated with the problem. The numerical solution for the eigenvalue problem will contain as many natural frequencies as the system has degrees of freedom. The test frame, idealized for finite element analysis, can be discretized into elements as shown in Figure 3.4.17.

The idealized frame contains a boundary element at the upper right to account for the stiffness of the hydraulic actuator used to excite the structure (Beers, 1980). Lumped masses are placed at nodes where beam connections are made to account for the additional mass at those points and are input to the model in the concentrated load, mass section of input to the program. Nodes, beam and panel elements are input to the model as shown with the given coordinates. The panel elements are in the positions shown but there are some restrictions and limitations in the element that should be observed.

The panel element incorporates the connectors into the formulation of the element properties so there are no real connector elements in the model of the test bay other than their stiffness contributions to the panel element. The panel element is assumed to be rectangular in shape and the configuration of the connectors is also assumed to be rectangular and connected at four discrete points to the framing. It is input to the SAPFAP program as directed by Beers (1980). The panel element that has been incorporated into the SAPFAP program is a two dimensional element (Briggs, 1976) and the formulation of the element flexibility matrix includes only stiffness contributions from the connectors in the translational freedoms in the plane of the panel. No rotational contributions from the connectors are included, resulting in an element that is more flexible than the actual structure. The formulation of the panel element assumes a rigid panel and that all deformation in the element must occur in the connectors. (Sessa's (1980) experimental work upholds this assumption). The formulation of the panel element does not include calculation of the element mass matrix. Lumped translational and rotational mass coefficients need to be calculated and input at bearing connection points as shown in Figure 3.4.17. Detailed discussions of the forumulation and implementation of the panel element is available in Briggs (1976) and Beers (1980).

The equations of motion for the test structure are written in matrix notation as,

$$[M]\{\ddot{x}\} + [C]\{\dot{x}\} + [K]\{x\} = \{0\}.$$

The mass matrix here uses lumped masses rather than a consistent mass formulation. Analytic results have shown (Zienkiewicz, 1975) that the lumped mass formulation will generally give better analytic results than the consistent mass formulation. The damping is assumed to be viscous for the structure and the matrix [C] is formulated as a linear combination of the stiffness and mass matricies as,

$$[C] = \alpha[M] + \beta[K]$$

where $\alpha$ and $\beta$ are determined experimentally (Clough and Penzien, 1975).

3.5.3  Response to Arbitrary Time Dependent Loading

Consider the same frame assembly as was discussed in the last section with the addition of the acceleration function A(t) applied to the structure as shown in Figure 3.5.1. The matrix equations to be solved are the same for the homogeneous case except that the right hand side of the equation now contains the forcing function. The forcing function becomes the mass matrix, [M], multiplied by the applied accelerations. The system equations of motion, written in matrix form become,

$$[M]\{\ddot{x}\} + [C]\{\dot{x}\} + [K]\{x\} = -[M]\{A(t)\}.$$

Solution of this problem is generally accomplished by one of two methods. The first method is mode-superposition, and the second method is by direct integration of the system equations of motion.

Mode-superposition (Clough and Penzien et al., 1975) procedes first by mathematically uncoupling the equations of motion. This method is used to determine the response of the structure for each solution time step by
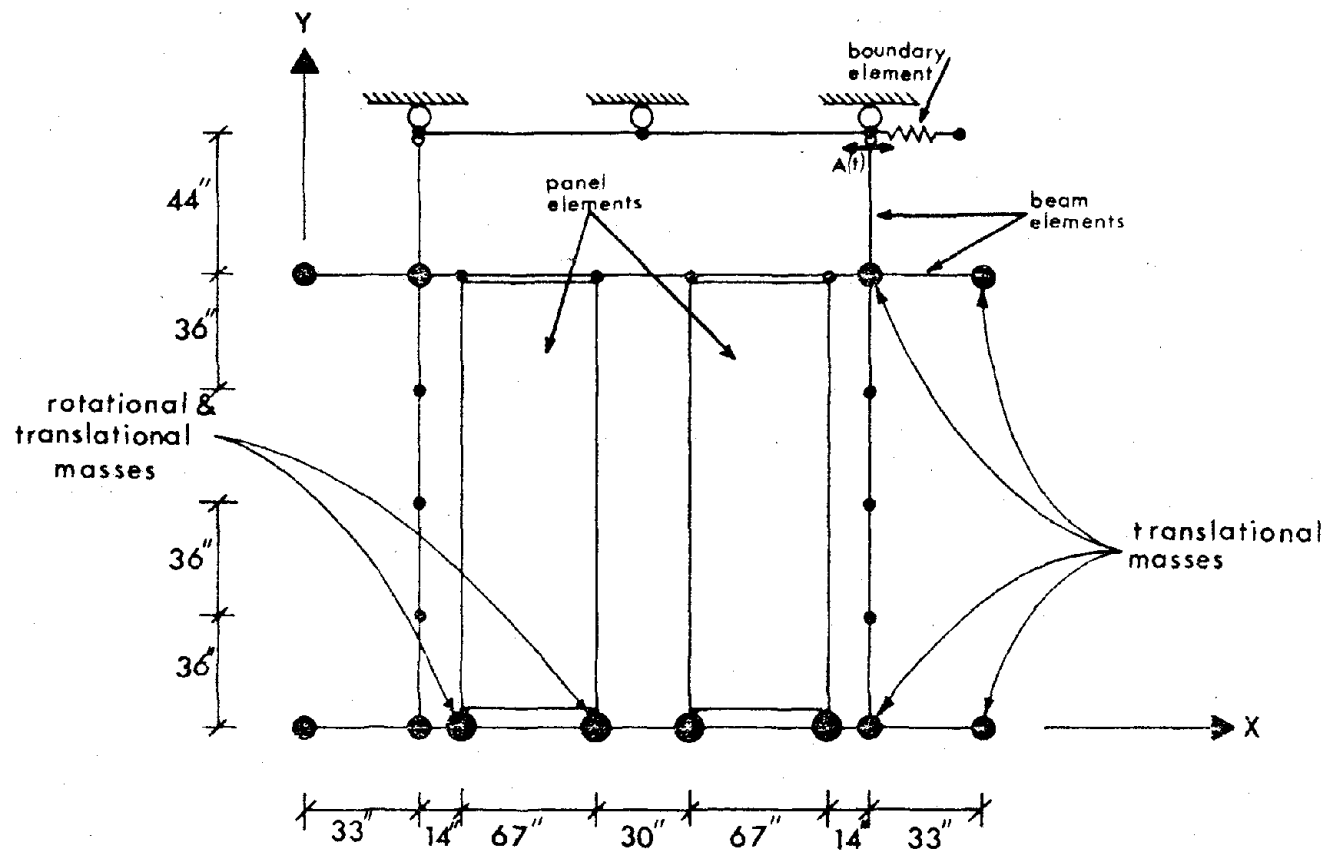
Figure 3.5.1. Idealized Test Frame with Applied Acceleration

superimposing the calculated response of each natural frequency of the system to the forcing function at that point to determine the total response for the system at each step. The method can be used to evaluate the response of a linear structure for which N modes and N associated mode shapes have been determined; furthermore, the damping matrix can be expressed by modal damping ratios. The homogeneous problem for free undamped vibrations is solved for the frequency vector $\omega$, and the mode-shape matrix $\theta$.

Each mode-shape vector, $\phi_n$, is used in turn to compute the generalized mass and generalized load for each mode,

$$M_n = \phi_n^T m \phi_n \qquad P_n(t) = \phi_n^T p(t).$$

The uncoupled equations of motion can then be written for each mode using the generalized mass and force matricies for that mode together with the modal frequency $\omega_n$ and a specified value of the modal damping ratio, $\xi_n$. The general response expression is given by the Duhamel integral for each mode as

$$Y_n(t) = \frac{1}{M_n(\omega)_{Dn}} \int_0^t P_n(\tau) e^{-\xi_n \omega_n (t-\tau)} \sin \omega_{Dn}(t - \tau) dt.$$

When the response for each mode $Y_n(t)$ has been determined, the displacements expressed in geometric coordinates are given by the coordinate transformation,

$$v(t) = \Phi Y(t)$$

which can be written as,

$$v(t) = \phi_1 Y_1(t) + \phi_2 Y_2(t) + \phi_3 Y_3(t) + \ldots.$$

The response represents the superposition of the various modal contributions. For most types of structural loading the greatest contributions to the response come from the lowest modal frequencies with the contributions decreasing for the higher modes which are quickly damped out by the structure.

It is,therefore, not usually necessary to include all of the natural frequencies in the modal superposition method; hence the series can be truncated at any desired point of accuracy. It should also be kept in mind that the idealization of the structure makes the iterative eigenvalue calculation of the higher modal frequencies less accurate since the stiffness of the idealized structure is overestimated. For this reason it is usually wise to limit the number of modes considered in the dynamic response by mode-superposition.

The elastic force response can be found directly from the equation,

$$f_s(t) = kv(t) = k\Phi Y(t)$$

which gives the internal elastic forces which resist the deformation of the structure.

Direct integration methods of solution for the forced response dynamic problem are based on the assumption of linear acceleration between solution time steps.

The direct integration technique used in the SAP IV program is the Wilson-$\theta$ (Clough and Penzien, 1975) method, which is unconditionally stable. This method is based on the assumption that the acceleration is linear over an extended computation interval. The extended time step $\gamma$ is defined by $\gamma = \Delta t\theta$ where $\Delta t$ is the normal time step and $\theta$ is amount that the time step is extended. The acceleration increment $\Delta v(t)$ is calculated by the linear acceleration procedure (Clough and Penzien, 1975) applied to the extended time step. From this the increment $v(t)$ is found for the normal time step $\Delta t$ by linear interpolation. For values of $\theta > 1.37$ the method becomes unconditionally stable. The SAP IV program uses a value of $\theta = 1.4$.

The performance of the Wilson-$\theta$ method is dependent on the size of the extended time step. The numerical errors introduced are in the form of an artificial change of period and a reduction in amplitude. The amplitude

decay can be viewed as additional damping acting on the structure along with the damping characteristics of the system. Any response components for which $\Delta t/T > 1/4$ will be quickly damped out. A solution time step should be chosen so that $\Delta t/T < 1/10$ where T is the period of the highest frequency included in the analysis. This selection will introduce little amplitude decay in the frequency range of interest and will effectively truncate frequency responses when $\Delta t/T > 1/4$.

From the above discussion it can be seen that direct integration and mode-superposition should yield approximately the same solution to an input function provided a short enough time step is used for the direct integration solution. Direct integration is heavily dependent on the time step for a good solution but it should also be recognized that the solution will reflect the accuracy of idealization in the finite element model. For a solution time step of 0.02 seconds the highest frequency that should be included in the Direct Integration solution is $f = 1/T = 0.1/0.02=5$ Hz and frequency response over 12.5 Hz will be quickly damped out. The eigenproblem solution for the sample structure shows that only the first three natural frequencies are below 12.5 Hz. See Table 3.5.1.

3.5.4  Analytic Response of Example Structure to Seismic Loading

The response of the example structure to an arbitrary time dependent loading is determined analytically with the SAPFAP program. Acceleration records are taken from earthquake records as described in Section 3.6 and input to the modeled structure as ground accelerations. Acceleration records are input to the model horizontally at node 24. Response of the modeled test structure is calculated by the mode-superposition method using a 0.02 second solution time step.

**Table 3.5.1**     **First Ten Natural Frequencies of Analytic Structural Model**

Frequency (Hz)
(from analytic results)

| | |
|---|---|
| $f_1$ | 2.907 |
| $f_2$ | 7.865 |
| $f_3$ | 10.5 |
| $f_4$ | 14.62 |
| $f_5$ | 16.64 |
| $f_6$ | 21.96 |
| $f_7$ | 32.04 |
| $f_8$ | 59.42 |
| $f_9$ | 60.44 |
| $f_{10}$ | 69.03 |

| Mode | Frequency Ratios ($f_i/f_1$) |
|---|---|
| 1 | 1.0 |
| 2 | 2.71 |
| 3 | 3.61 |
| 4 | 5.03 |
| 5 | 5.72 |
| 6 | 7.55 |
| 7 | 11.02 |
| 8 | 20.44 |
| 9 | 20.79 |
| 10 | 23.75 |

Displacement time histories for nodes at a panel element connection point are output on cards with the Fortran statements shown in Rains (1980). The stiffness matrix for the same panel is output on cards to be used in the solution for the connector stresses. These output cards are used in the analysis for the connector response.

3.5.5 Solution for Forces in Connectors

This section discusses the idealization for finite element analysis of the architectural panel system and the solution for resultant forces in the panel connectors. Cards output from the analysis of the combined system are used to determine the response of the architectural system.

Forces resulting from differential movement in the panel connection points are calculated directly from the response found in the solution of the problem outlined above. The elastic resisting forces are found by multiplying the total displacement vector of the panel element by the panel element stiffness matrix for each output solution time step as shown by the equations below.

$$[Kp]\{xp\} = \{Fp\}$$

where [Kp] is the element stiffness matrix, {xp} is the element displacement vector and {Fp} is the elastic force vector. Forces in the flexible, top connectors are assumed to vary linearly until yield occurs, and then remain constant (i.e., they display a linear elastic perfectly plastic constitutive relationship). The bearing connectors are assumed to behave in a linear elastic fashion; hence nonlinear deformation will not be included in their analysis. Forces in the connectors resulting from differential movement in the panel connection points are determined by the programing listed in Bains (1980). Forces in the flexible, top connectors are assumed to vary linearly until yield occurs, and then remain constant (i.e., they display a

linear elastic perfectly plastic constitutive relationship). The bearing connectors are assumed to behave in a linear elastic fashion; hence nonlinear deformation will not be included in their analysis. Forces in the connectors resulting from differential movement in the panel connection points are determined by the programing listed. The bearing connectors are assumed to support the entire mass of the panel. Response of the top connectors is assumed to result only from differential movement of the panel connection nodes. The model of the panel and bearing connectors is set up and input to the SAP IV program and uses both plane stress and beam elements. The model of the architectural panel includes only analysis in the plane of the panel and is totally constrained against out of plane motion (i.e., two translational and one rotational freedoms are included in the analysis). The model used in this portion of the analysis is shown in Figure 3.5.2.

The model of the architectural panel and its bearing connectors is analyzed using excitation generated by motion of the entire structure. Displacement histories from the bearing connectors of one panel are numerically differentiated to give acceleration histories in the two translational freedoms at both points. The approximations (James, Smith, and Wolford, 1977) to the derivatives of the displacement history are developed from Taylor series expansions. Forward-difference approximations are used to determine the second derivative for the first two terms. Expressions with errors $O(h^2)$ are used for these two terms.

$$Y_i'' = -Y_{i+3} + 4Y_{i+2} - 5Y_{i+1} + 2Y_i/h^2$$

where h is the time step and y is the displacement function. Central-difference approximations to the second derivative are used for terms, 3 thru N-2, where N is the total number of terms. Expressions with errors $O(h^4)$

plane stress
elements

forcing functions

beam
elements

48"

48"

48"

2"

4"

14.5"    42.5"    14.5"
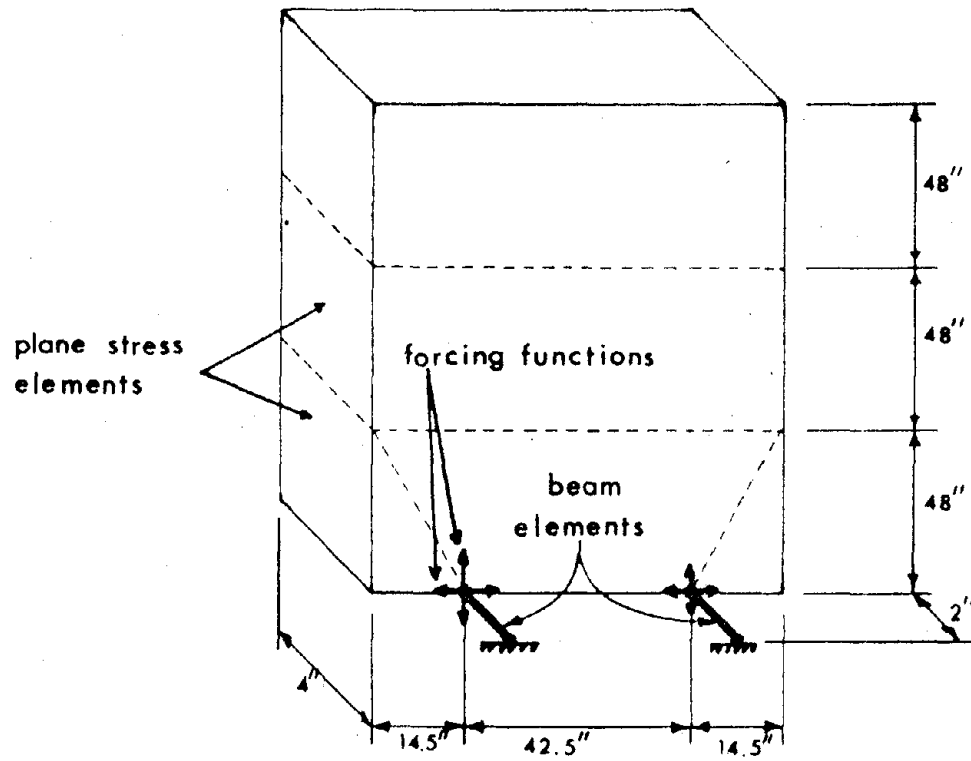
Figure 3.5.2.        Idealized Architectural Panel

are used, which gives;

$$Y_i'' = -Y_{i+2} + 16Y_{i+1} - 30Y_i + 16Y_{i-1} - Y_{i-2}/12h^2.$$

The last two terms in the series use a backward-difference approximation
to the second derivative with errors $O(h^2)$, and are represented by:

$$Y_i'' = 2Y_i - 5Y_{i-1} + 4Y_{i-2} - Y_{i-3}/h^2.$$

The acceleration histories calculated from the displacement histories
are then applied as forcing functions to the end of the beam elements at
their junction with the plane stress elements in the model of the architectural
system as shown in Figure 3.5.2. The forcing function used here is found
by multiplying the accelerations obtained by the differentiation process
by the translational mass at that point (i.e., 1/2 the total panel mass).
The SAP IV program provides for a scaler multiplier for any input forcing
function; hence the mass coefficient is input as this scaler. All freedoms
are fixed for the protruding ends of the beam elements. This can be justified
by examining the equations of motion between the framing and the panel.

$$m(\ddot{X} - \ddot{X}p) + Ky = 0$$

where,

$\ddot{X}$ is the acceleration at the framing end of the bearing connector,

$\ddot{X}p$ is the acceleration at the panel end of the bearing connector,

m is the mass of the panel, and

y is the differential displacement between the panel and the framing.

The forcing function can be assumed to be the acceleration
of the panel times 1/2 the panel mass. Note that inputing the force to the
panel assumes that the base of the panel moves with the same motion as the
bearing connection points. It was necessary to formulate this portion of
the analysis in this way in order to obtain a solution to the eigenvalue
problem because of SAP IV limitations.

Forces resulting from differential displacement between panel nodal points are assumed to act on the connector at its point of attachment to the structural framing. Output from the analysis of the architectural panel system includes the shear forces in the two principal directions at the ends of the beam elements representing the bearing connectors. These forces are superimposed with forces resulting from differential displacement between connection nodes to obtain the total response in the connectors.

3.6  Earthquake Data Used to Excite Analytic Model

3.6.1  Description of Earthquake Data

The acceleration records used to excite the analytic model are described in this section. The digitized records were recorded during earthquakes over the past several decades and contain acceleration, velocity, and displacement records, as well as computed Fourier spectra and spectral response data for each record. The computer tapes of these records were obtained from the University of California, Berkeley, Earthquake Engineering Center. A list of these records is shown in Table 3.6.1.

The strong motion earthquake records contain accelerograms and spectral data from various strong-motion earthquakes from 1933 through the February 9, 1971 San Fernando earthquake. Earthquake records chosen for use in the analysis were selected using basically two considerations. First, records were chosen that exhibited high amplitudes in the absolute acceleration response spectra corresponding to experimentally determined natural frequencies of the test assembly. Second, displacement records were chosen on the basis of high amplitudes and fast changes in displacement, thus giving large acceleration.

Earthquake records that were used, include response from two buildings recorded during the San Fernando, California earthquake of February 9, 1971, and from ground motion records taken during the El Centro, California earthquake of May 18, 1940. The specific records from the Berkeley tapes used in the analysis are from the El Centro earthquake; El Centro Site Imperial Valley Irrigation District, north-south component, and from the San Fernando earthquake; Jet Propulsion Lab., basement and ninth floors, north-south component, Pasadena, California and CalTech, Milikan Library, basement and tenth floors, north-south component, Pasadena, California.

These acceleration time histories were used to provide ground acceleration
to the modeled structure.  The acceleration records are read from the tapes
then output on computer cards to be used as input to the analytic model of
the test bay.  The acceleration record is applied to the node 24 shown in
Figure 3.4.17 as a ground acceleration.

Displacement records and the Absolute Acceleration Response Spectra
for each of the records mentioned are shown in Figures 3.6.1 thru 3.6.10.
The earthquake response spectra data as given on the tapes has been prepared
as discussed in Nigam and Jennings (1969).  Fortran programs written to
read data from the earthquake tapes and process it for graphing or output
on cards for use as input to SAP IV and SAPFAP are listed and discussed in
Rains (1980).

Examination of the absolute acceleration response spectra for each
record show peaks in all cases at approximately the period of the first
natural frequency of the analytic model (T1 = 1/f1 = .34 seconds, f1 = 2.91 Hz,
from Table 3.5.1.  These records should excite the first mode of the
structure and result in maximum response to the seismic loading.

# Table 3.6.1

STRONG MOTION EARTHQUAKE ACCELEROGRAMS - STANDARD DATA
CHRONOLOGICAL INDEX OF EARTHQUAKES

| NO. | YEAR | EARTHQUAKE | MAG. | DATE | TIME, PST | DATA REPORT REF. |
|---|---|---|---|---|---|---|
| 1 | 1933 | Long Beach, Calif. | 6.3 | 3/10 | 1754 | B021, V314, V315 |
| 2 | 1933 | Los Angeles, Calif. | 5.4 | 10/2 | 0110 | B022, B023 |
| 3 | 1934 | Ferndale, Calif. | | 7/6 | 1449 | U294 |
| 4 | 1934 | El Centro, Calif. | 6.5 | 12/30 | 0552 | B024 |
| 5 | 1935 | Helena, Mont. | 6.0 | 10/31 | 1138(MST) | B025 |
| 6 | 1935 | Helena, Mont. | | 10/31 | 1218(MST) | U295 |
| 7 | 1935 | Helena, Mont. | | 11/21 | 2058(MST) | U296 |
| 8 | 1935 | Helena, Mont. | | 11/28 | 0742(MST) | U297 |
| 9 | 1937 | Ferndale, Calif. | | 2/6 | 2042 | U298 |
| 10 | 1938 | El Centro, Calif. | 3.0 | 4/12 | 0825 | T274 |
| 11 | 1938 | El Centro, Calif. | 5.0 | 6/5 | 1842 | T275 |
| 12 | 1938 | El Centro, Calif. | 4.0 | 6/6 | 0435 | T276 |
| 13 | 1938 | Ferndale, Calif. | 5.5 | 9/11 | 2210 | B026 |
| 14 | 1940 | El Centro, Calif. | 6.7 | 5/18 | 2037 | A001, T277-T285 |
| 15 | 1941 | Ferndale, Calif. | 6.4 | 2/9 | 0145 | B027 |
| 16 | 1941 | Santa Barbara, Calif. | 5.9 | 6/30 | 2351 | U299 |
| 17 | 1941 | Ferndale, Calif. | 6.4 | 10/3 | 0813 | U300 |
| 18 | 1941 | Los Angeles, Calif. | 5.4 | 11/14 | 0042 | V316, V317 |
| 19 | 1942 | El Centro, Calif. | 6.5 | 10/21 | 0822 | T286 |
| 20 | 1949 | Hollister, Calif. | 5.3 | 3/9 | 0429 | U301 |
| 21 | 1949 | Seattle, Wash. | 7.1 | 4/13 | 1156 | B028, B029 (Olympia) |
| 22 | 1951 | El Centro, Calif. | 5.6 | 1/23 | 2317 | T287 |
| 23 | 1951 | Ferndale, Calif. | 5.8 | 10/7 | 2011 | A002 |
| 24 | 1952 | Kern County, Calif. | 7.7 | 7/21 | 0453 | A003-A007, V318 |
| 25 | 1952 | Tehachapi, Calif. | | 7/23-31 | ---- | U302, U303, U304 |
| 26 | 1952 | Ferndale, Calif. | 5.5 | 9/22 | 0441 | B030 |
| 27 | 1952 | San Luis Obispo, Calif. | 6.0 | 11/21 | 2346 | V319 |
| 28 | 1953 | El Centro, Calif. | 5.5 | 6/13 | 2017 | T288 |
| 29 | 1954 | Taft, Calif. | 5.9 | 1/12 | 1534 | B031 |
| 30 | 1954 | Hollister, Calif. | 5.3 | 4/25 | 1233 | U305 |
| 31 | 1954 | El Centro, Calif. | 6.3 | 11/12 | 0427 | T289 |
| 32 | 1954 | Eureka, Calif. | 6.5 | 12/21 | 1156 | A008, A009 (Ferndale) |
| 33 | 1955 | San Jose, Calif. | 5.8 | 9/4 | 1801 | A010, U306 |
| 34 | 1955 | El Centro, Calif. | 4.3 | 12/16 | 2117 | T290 |
| 35 | 1955 | El Centro, Calif. | 3.9 | 12/16 | 2142 | T291 |
| 36 | 1955 | El Centro, Calif. | 5.4 | 12/16 | 2207 | T292 |
| 37 | 1956 | El Centro, Calif. | 6.8 | 2/9 | 0633 | A011 |
| 38 | 1956 | El Centro, Calif. | 6.4 | 2/9 | 0725 | A012 |
| 39 | 1957 | Port Hueneme, Calif. | 4.7 | 3/18 | 1056 | V329 |
| 40 | 1957 | San Francisco, Calif. | 3.8 | 3/22 | 1048 | V320 |
| 41 | 1957 | San Francisco, Calif. | 5.3 | 3/22 | 1114 | A013-A017, V321 |
| 42 | 1957 | San Francisco, Calif. | 4.4 | 3/22 | 1815 | V322-V327 |
| 43 | 1957 | San Francisco, Calif. | 4.0 | 3/22 | 1627 | V328 |
| 44 | 1960 | Hollister, Calif. | 5.0 | 1/19 | 1926 | U307 |
| 45 | 1960 | Ferndale, Calif. | 5.7 | 6/5 | 1718 | U308 |
| 46 | 1961 | Hollister, Calif. | 5.7 | 4/8 | 2323 | A018, U309 |
| 47 | 1962 | Eureka, Calif. | 5.0 | 9/4 | 0917 | V330 |
| 48 | 1965 | Olympia, Wash. | 6.5 | 4/29 | 0729 | B032, U310 (Seattle) |
| 49 | 1965 | Castaic, Calif. | 4.0 | 7/15 | 2316 | V331 |
| 50 | 1966 | Parkfield, Calif. | 5.6 | 6/27 | 2026 | B033-B039, U311 |
| 51 | 1966 | El Centro, Calif. | 6.3 | 8/7 | 0936 | T293 |
| 52 | 1966 | Sacramento, Calif. | 6.3 | 9/12 | 0841 | V332 |
| 53 | 1967 | Eureka, Calif. | 5.8 | 12/10 | 0407 | B039, U312 (Ferndale) |
| 54 | 1967 | Hollister, Calif. | 5.2 | 12/18 | 0925 | U313, V333 |
| 55 | 1968 | Borrego Mtn., Calif. | 6.4 | 4/8 | 1830 | A019, A020, B040, Y370-Y381 |
| 56 | 1970 | Lytle Creek, Calif. | 5.4 | 9/12 | 0630 | W334 through N367 |
| 57 | 1971 | San Fernando, Calif. | 6.4 | 2/9 | 0600 | C041 through S243 |
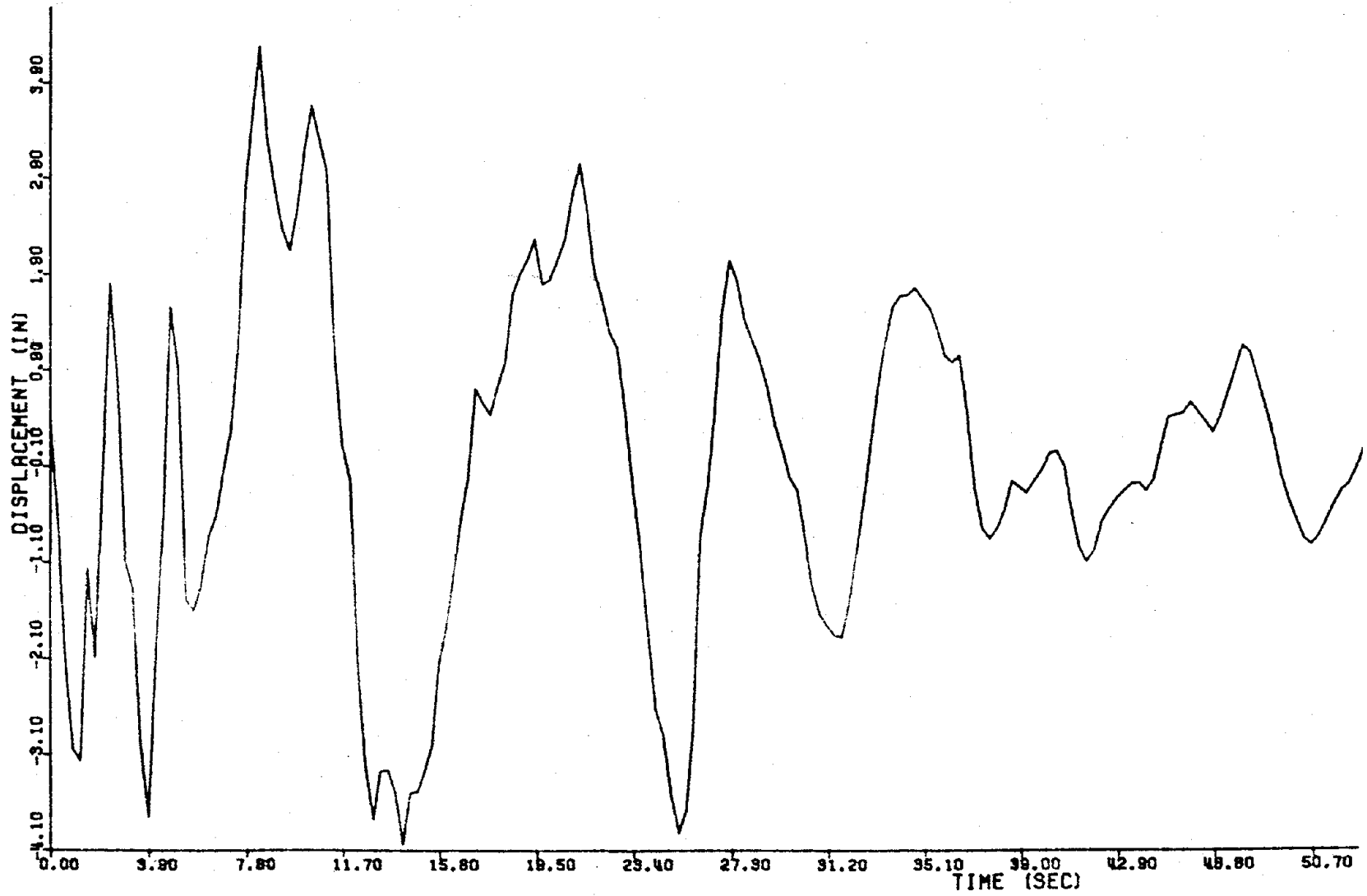
Figure 3.6.1    Displacement History
El Centro Earthquake

Figure 3.6.2    Absolute Acceleration Response Spectra
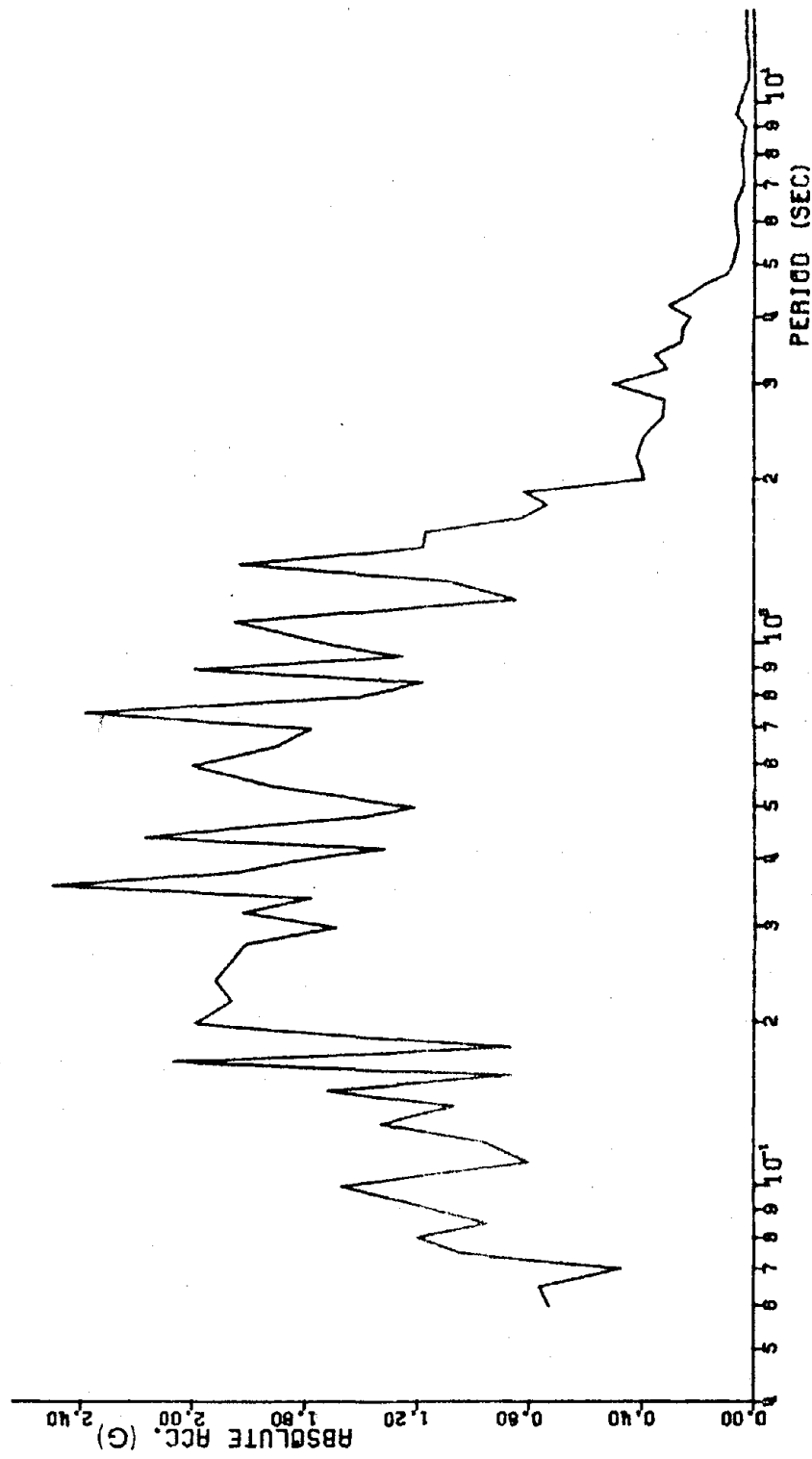
El Centro Earthquake

Figure 3.6.3    Displacement History
San Fernando Earthquake, basement,
Caltech, Millikan Library

Figure 3.6.4    Absolute Acceleration Response Spectra
                San Fernando Earthquake, basement,
                Caltech, Millikan Library

Figure 3.6.5.    Displacement History
San Fernando Earthquake, 10th floor,
Caltech, Millikan Library
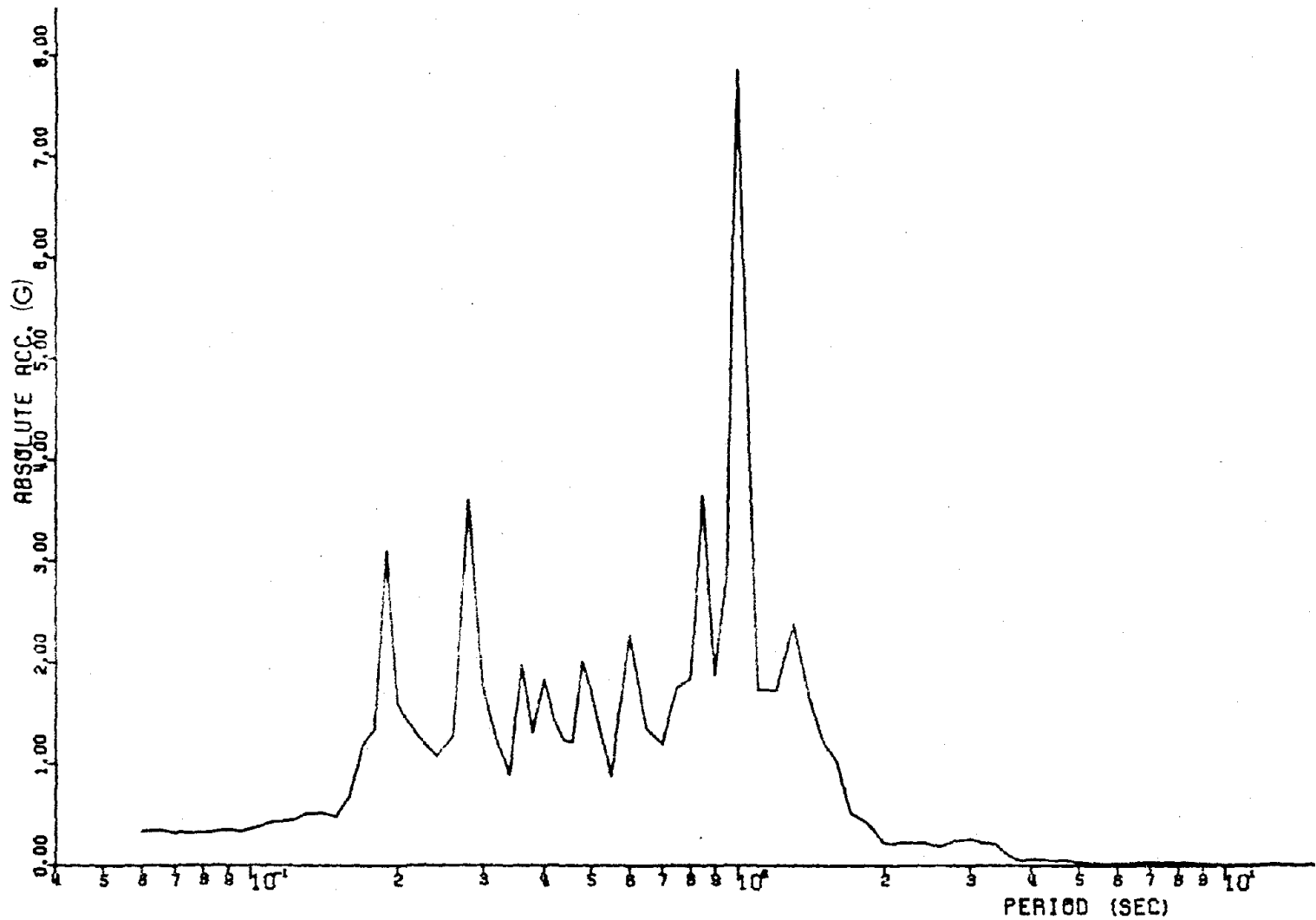
Figure 3.6.6.     Absolute Acceleration Response Spectra
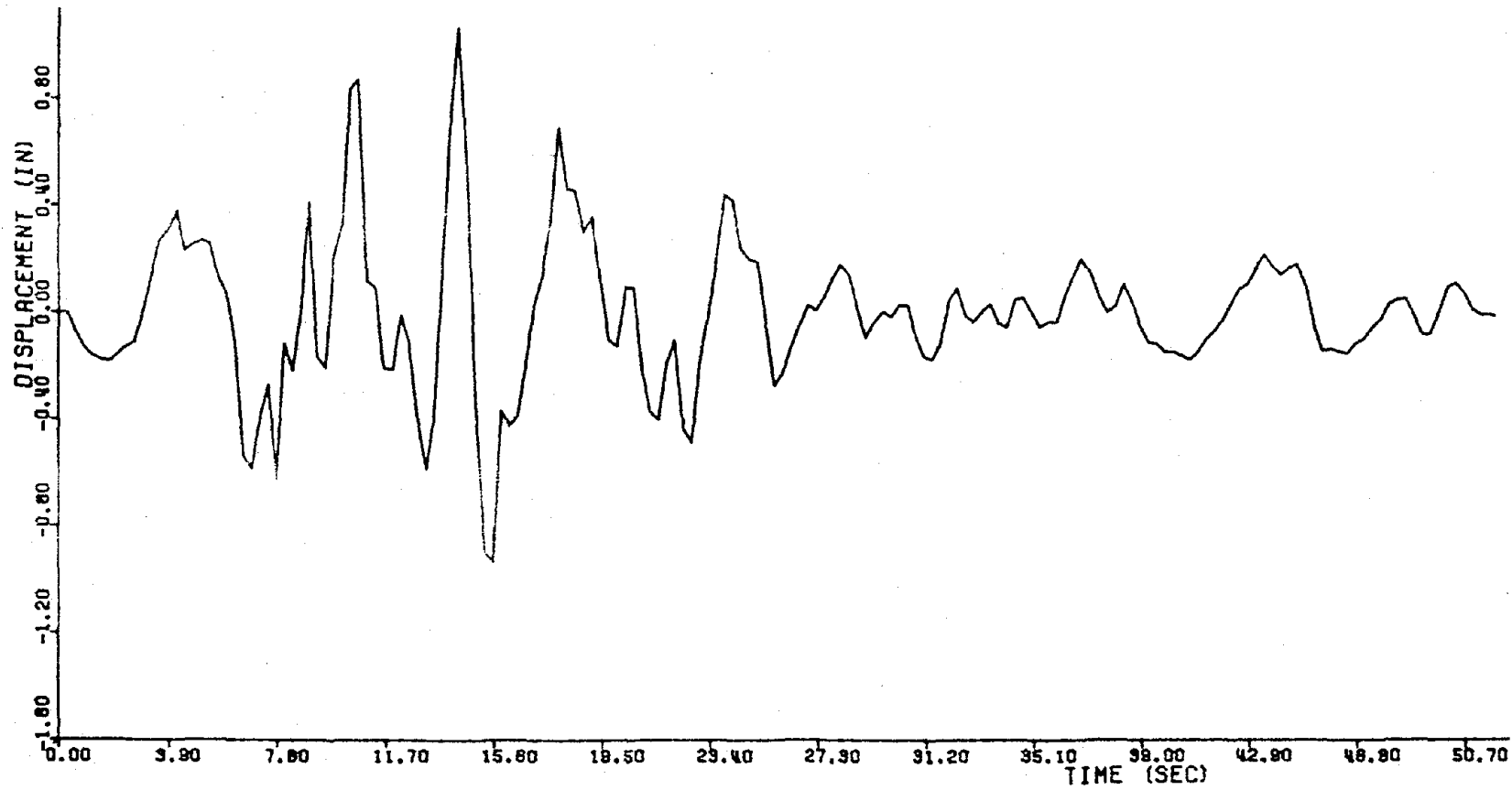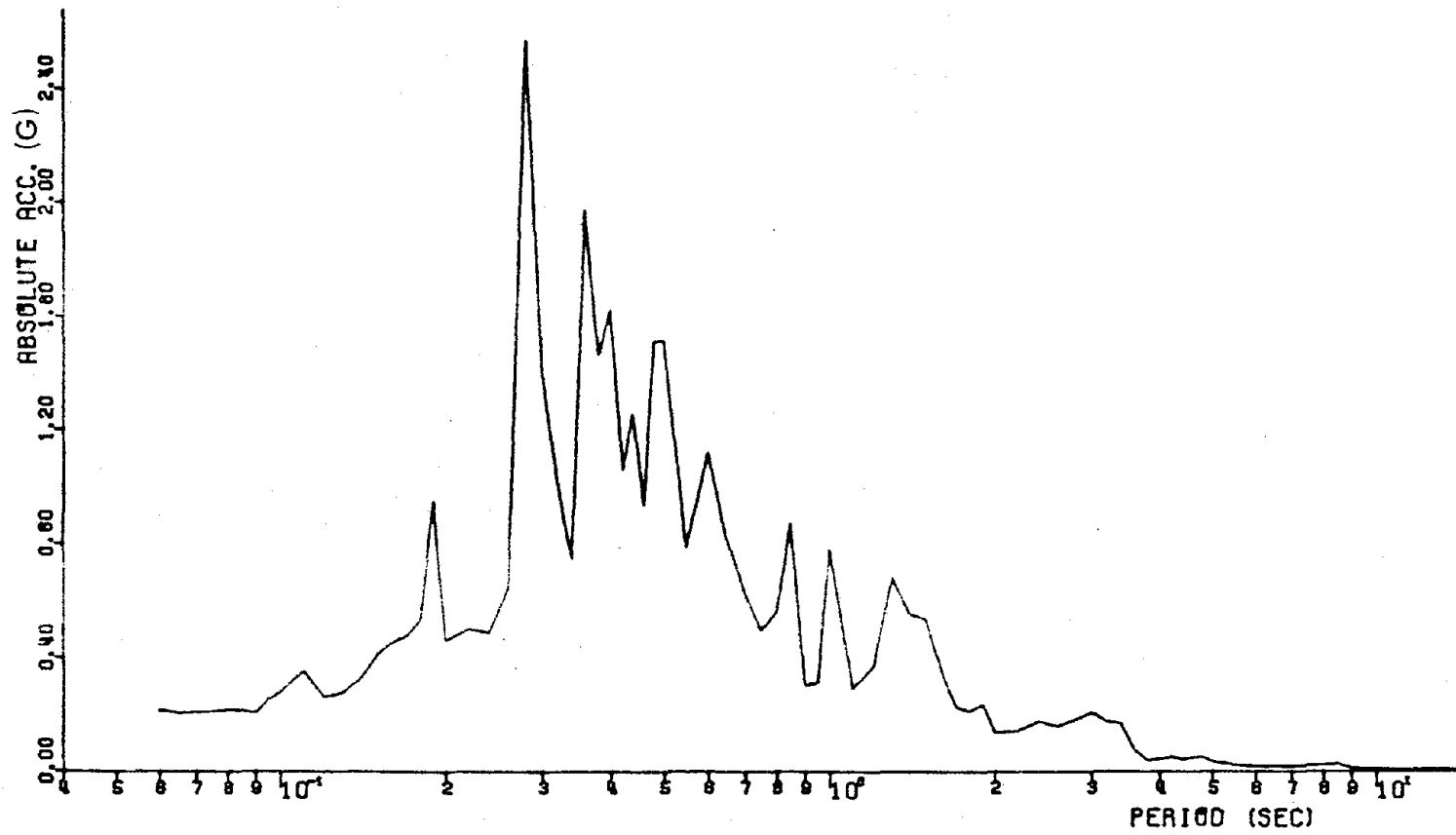San Fernando Earthquake, 10th floor,
Caltech, Millikan Library

Figure 3.6.7.    Displacement History
San Fernando Earthquake, basement,
Jet Propulsion Lab

Figure 3.6.8.   Absolute Acceleration Response Spectra
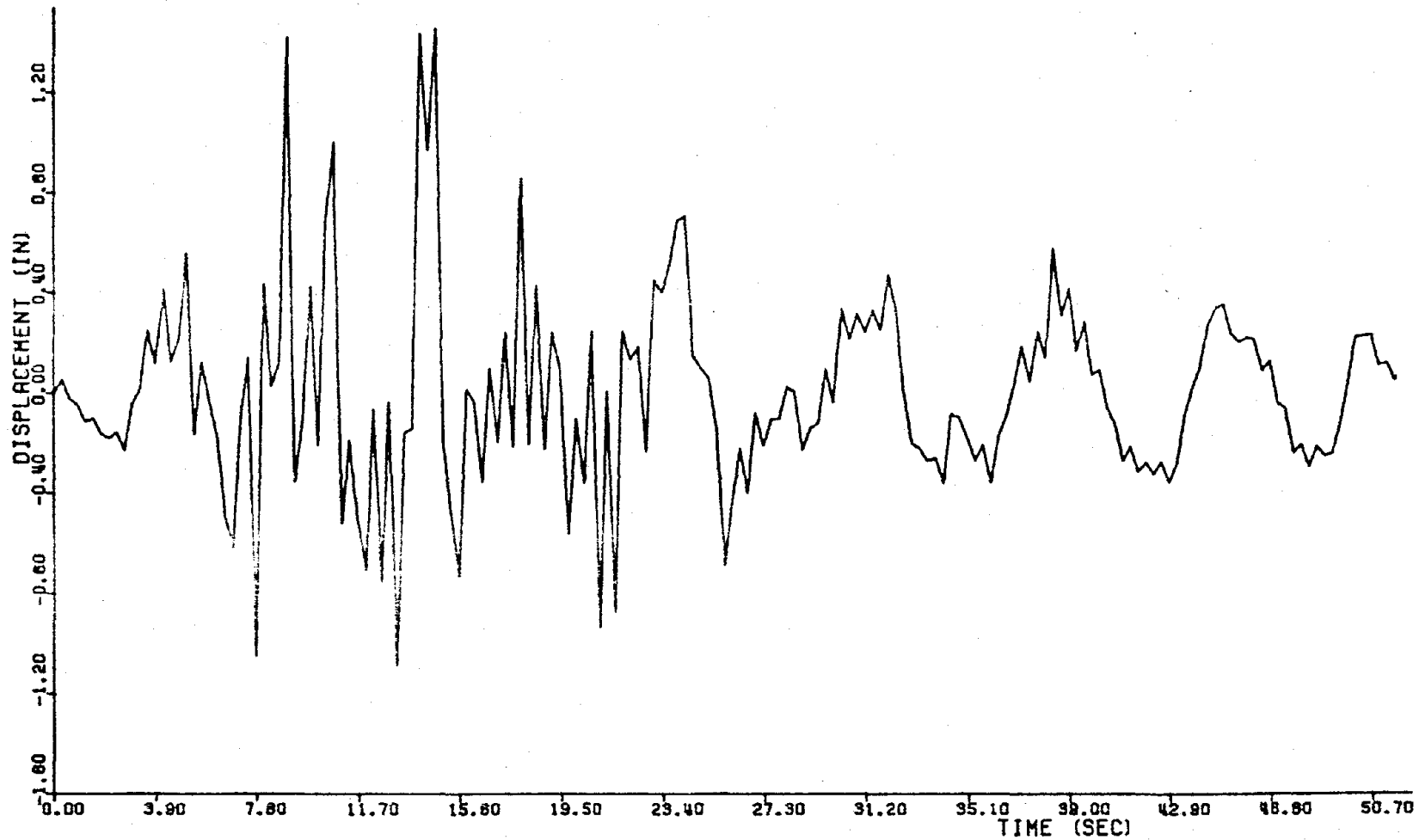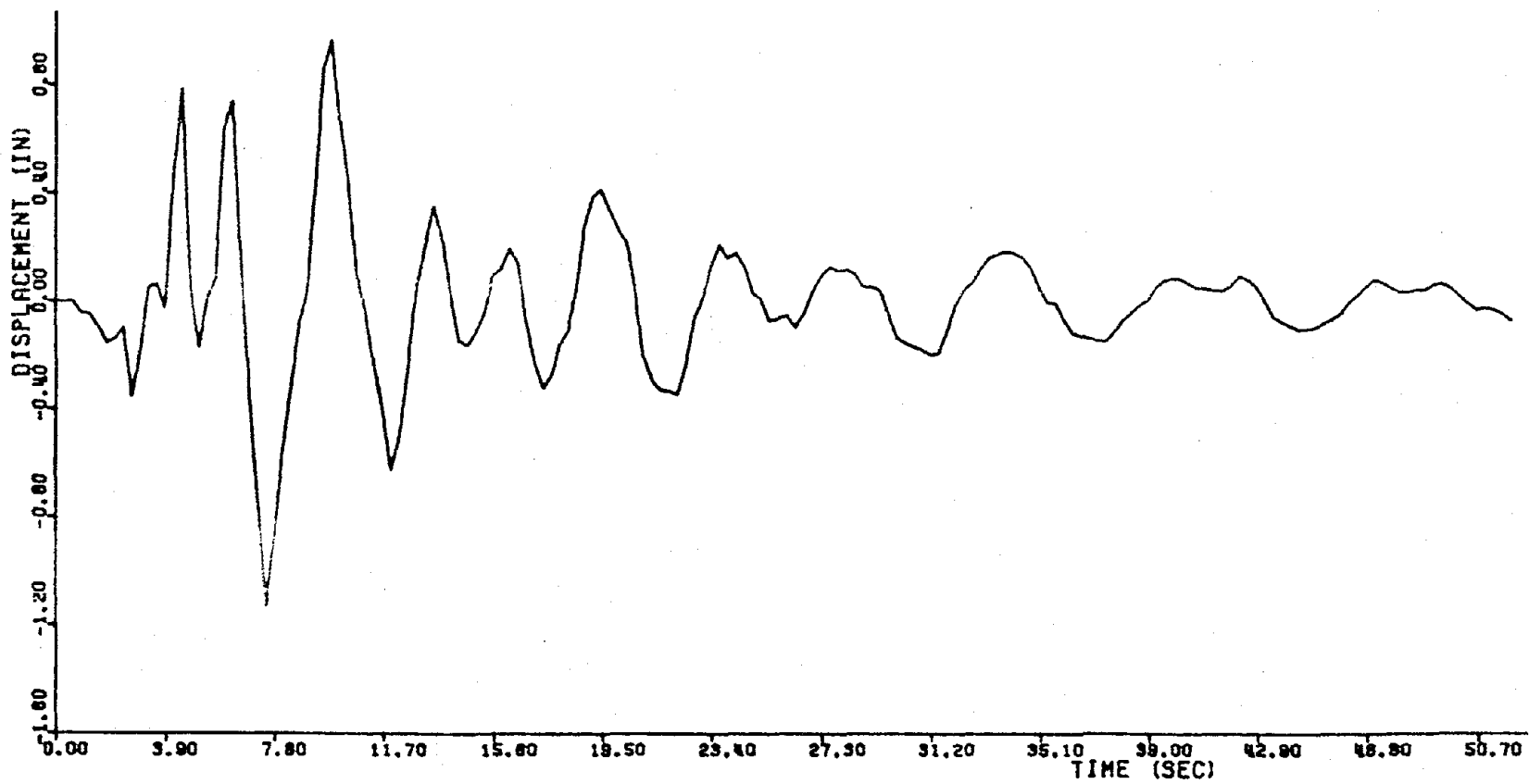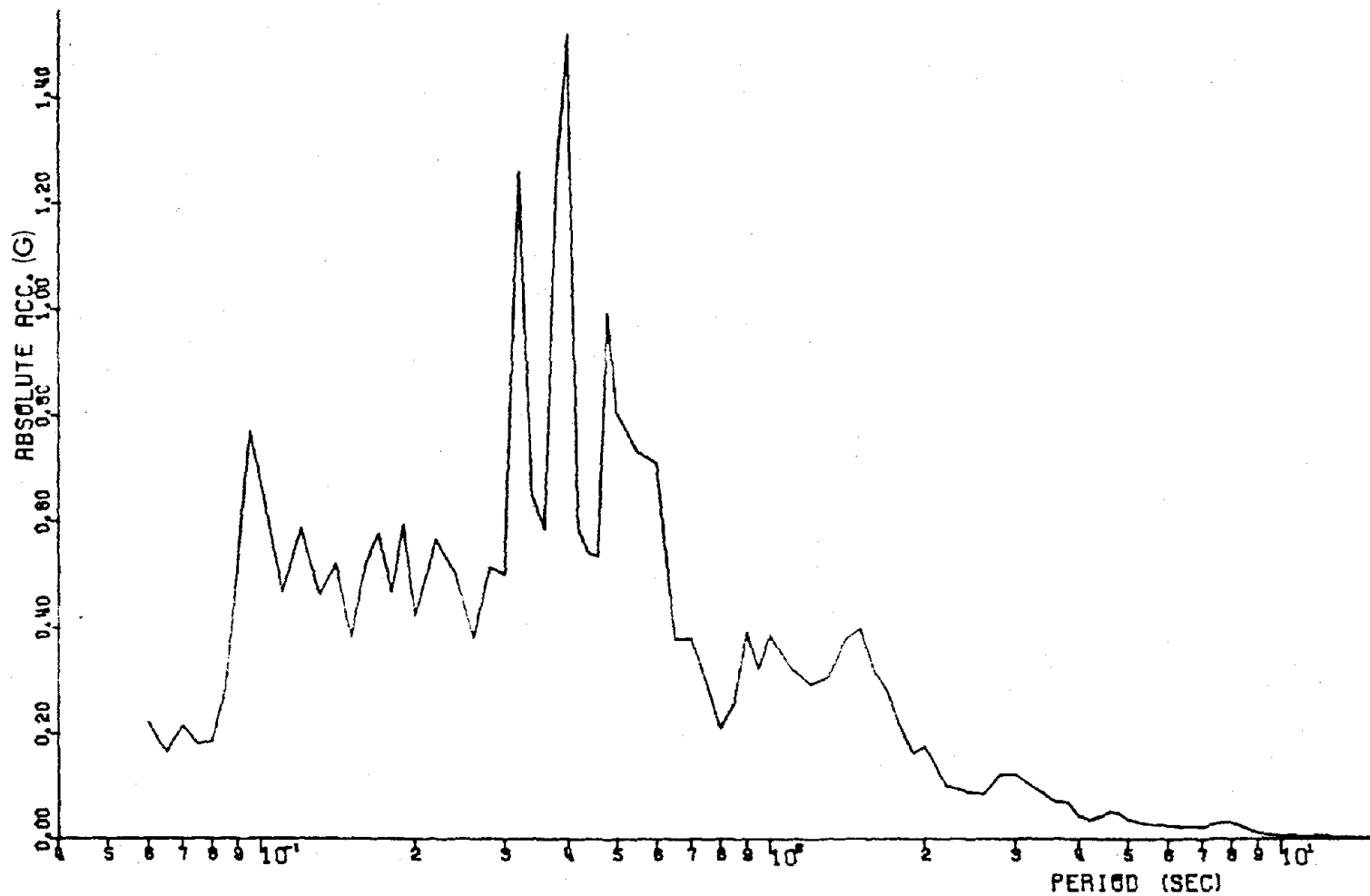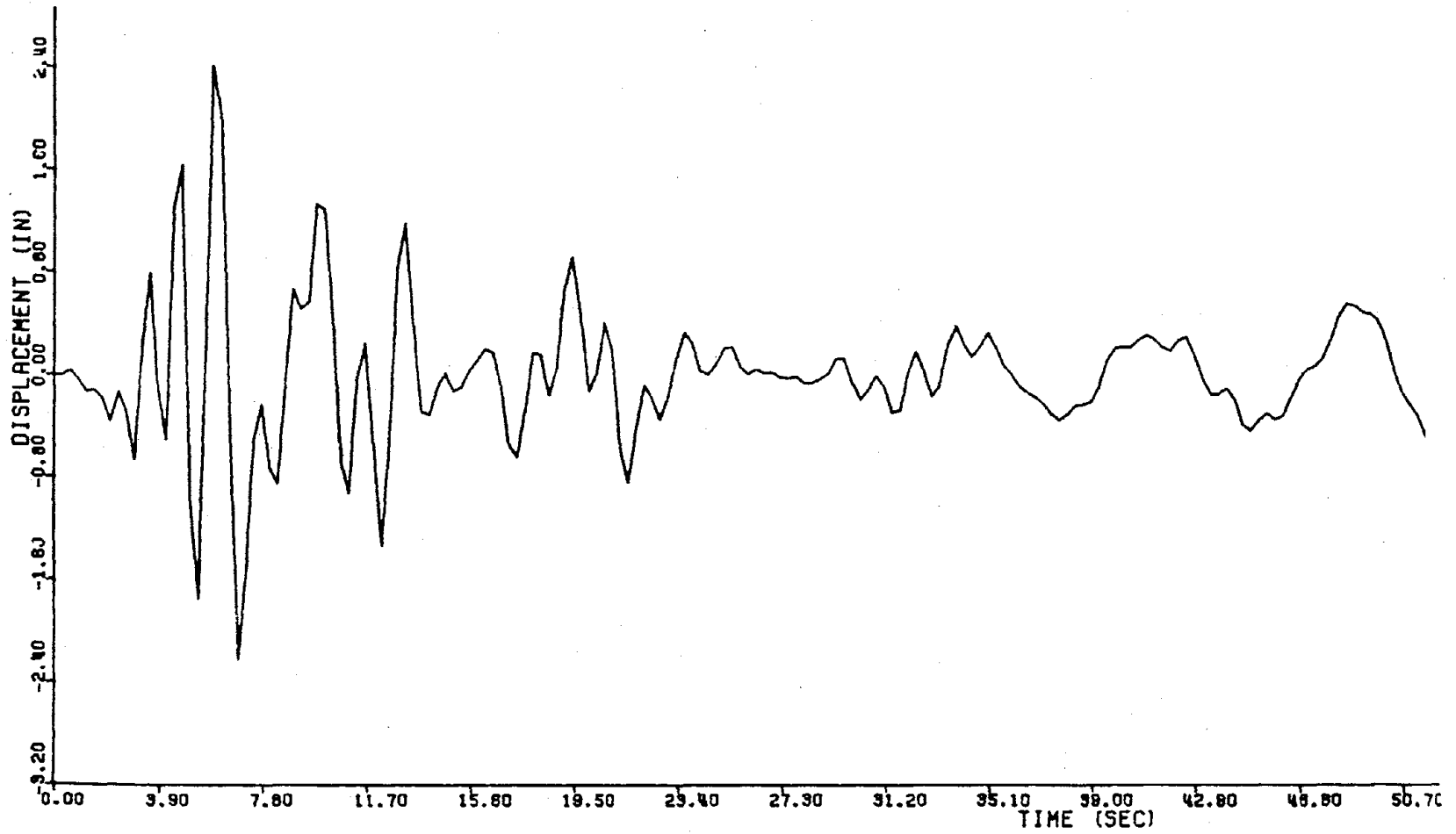San Fernando Earthquake, basement,
Jet Propulsion Lab

Figure 3.6.9.    Displacement History
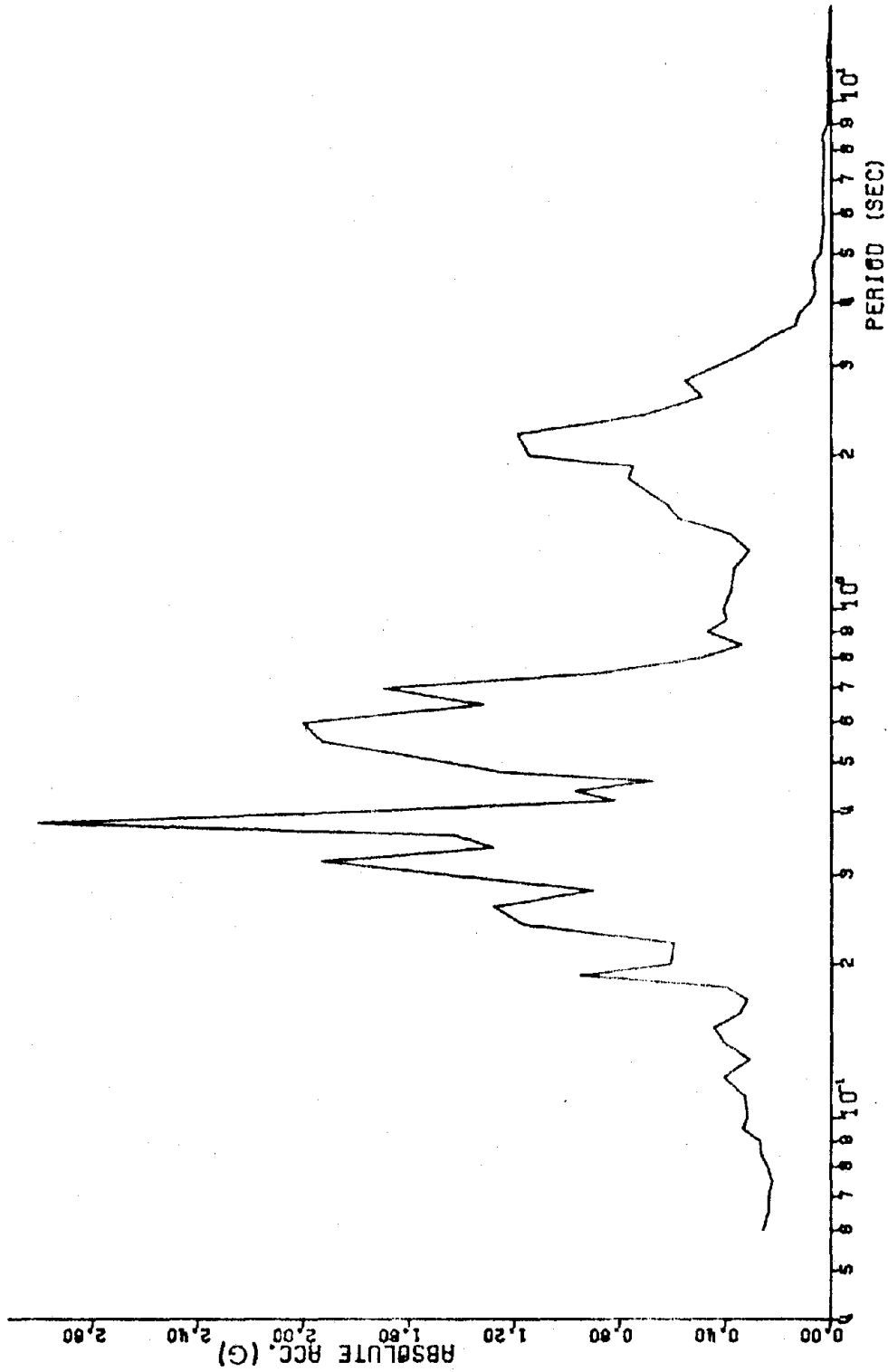San Fernando Earthquake, 9th floor,
Jet Propulsion Lab

Figure 3.6.10    Absolute Acceleration Response Spectra
San Fernando Earthquake, 9th Floor,
Jet Propulsion Lab

3.7  Results of Analytic Study of Panel Connectors

This section discusses the maximum response of the panel connectors
determined by the analytic models discussed earlier.  Tabulated results of
maximum displacement response, elastic forces in the connectors, and accel-
erations at bearing points are given for each earthquake record used in the
analysis.  Comparison is made between response determined at different
building story levels where they are included in the analysis (i.e., from
the records of the San Fernando earthquake).

3.7.1  Response of Interactive Panel-Frame Model

Maximum displacement response of the modeled test frame are given
in this section.  Only the maximum response in the panel connection nodes
are included in the summary to show response that can be generated by an
earthquake and to aid in illustrating the forces that can be induced in
panel connectors as a result of differential movement between panel connection
nodes.

It should be kept in mind that large deflections shown for response to
records G108 and G109 (basement and 10th floors of the Caltech, Millikan
Library) appear to be exhibiting first mode response.  Recall that these two
records exhibit peaks in the absolute acceleration response spectra nearest
the period of the first mode of the analytic model.  Figure 3.7.1 summarizes
the maximum displacements for all connection nodes and includes maximum
rotations at the panel bearing points.  Numbering of panel nodes and orient-
ation of axes are shown at the bottom of Figure 3.7.3.

Results show that interstory drift as great as 1.4 inches can occur
in the analytic model.  Maximum rotations at bearing points are quite small
from all response records, indicating that even though rotational stiffness

**Figure 3.7.1**     **Maximum Displacements at Panel Connection Points (in)**

| * | Record | | | | |
|---|---|---|---|---|---|
| | A001[a] | 6108[b] | 6109[c] | 6110[d] | 6111[e] |
| $X_1$ | .4819 | .7208 | .8675 | .3677 | .5951 |
| $Y_1$ | .03493 | .05226 | .0628 | .02657 | .04307 |
| $X_2$ | .482 | .721 | .8677 | .3667 | .5952 |
| $Y_2$ | .02546 | .03809 | .04577 | .01937 | .03139 |
| $X_3$ | 1.283 | 1.92 | 2.306 | .9758 | 1.582 |
| $Y_3$ | .01937 | .02903 | .0345 | .01467 | .02379 |
| $\theta z_3$(rad) | .00145 | .00218 | .00259 | .0011 | .00178 |
| $X_4$ | 1.283 | 1.919 | 2.305 | .9756 | 1.581 |
| $Y_4$ | .01795 | .0269 | .03196 | .0136 | .0204 |
| $\theta z_4$(rad) | .000868 | .0013 | .00154 | .00066 | .00107 |
| Interstory Drift | .8011 | 1.199 | 1.4383 | .6091 | .9868 |

*Panel node numbering is shown in Figure 3.7.3

[a]El Centro earthquake, May 18, 1940

[b]San Fernando earthquake, Feb. 9, 1971, basement, Caltech, Millikan Library

[c]San Fernando earthquake, Feb. 9, 1971, 10th floor, Caltech, Millikan Library

[d]San Fernando earthquake, Feb 9, 1971, basement, Jet Propulsion Lab

[e]San Fernando earthquake, Feb. 9, 1971, 9th floor, Jet Propulsion Lab

of the panel connectors is not included in the analysis, the results are not
significantly affected by their exclusion.  Note however, that this has
been found true only in the model studied in this section.

3.7.2  Elastic Response in Panel Connectors

Response in the panel connectors has been calculated and maxima
are summarized for the five earthquake records used to excite the analytic
model.  Differential displacement between connection points can be seen to
make significant contributions to the overall response of the panel connectors.
The largest elastic forces in the bearing connectors are in the vertical
direction, indicating that relatively small differential vertical displacement
between bearing points may cause high loads in integrative bearing connectors.
Forces in the flexible top connectors are seen to be largest in the horizontal
direction which results from interstory drift.  Results show little response
in the vertical direction in the top connectors.  Maximum elastic forces
found in the connectors for each response history are tabulated in Figure 3.7.2.

Results show that upper stories of buildings may be the most significant
in terms of panel connector forces caused by differential displacement bet-
ween connection nodes.  Both cases in which excitation was from two different
floors of a building show that maximum response is in the upper floors
(Records G109 and Gill).  These high elastic forces are caused by the large
differential displacement and interstory movement associated with the response
determined in the analysis of the test frame model.

Figure 3.7.2     Maximum Elastic Forces in
Panel Connectors   (lb)

Flexible Connections(1&2), Number of Times
Yield Exceeded[b]

| | Record | | | | |
|---|---|---|---|---|---|
| * | A001 | G108 | G109 | G110 | G111 |
| $FX_1$ | 1 | 49 | 67 | $471.0$[a] | 22 |
| $FY_1$ | $56.1$[a] | $84.1$[a] | $101.0$[a] | $42.8$[a] | $69.4$[a] |
| $FX_2$ | 1 | 49 | 68 | $471.0$[a] | 22 |
| $FY_2$ | $31.0$[a] | $45.4$[a] | $55.7$[a] | $23.6$[a] | $38.2$[a] |

[a] Yield not Exceeded, Maximum Load in Lbs.

[b] Yield = 616.0 lbs

Bearing Connections (3& 4)

| | Record | | | | |
|---|---|---|---|---|---|
| * | A001 | G108 | G109 | G110 | G111 |
| $FX_3$ | 379.0 | 566.0 | 1660.0 | 373.0 | 1470.0 |
| $FY_3$ | 4080.0 | 5980.0 | 7370.0 | 3110.0 | 5030.0 |
| $FX_4$ | 379.0 | 566.0 | 681.0 | 288.0 | 628.0 |
| $FY_4$ | 4100.0 | 6020.0 | 7410.0 | 3130.0 | 4790.0 |

*Panel node numbering is shown in Figure 4.3

3.7.3  Accelerations at Panel Bearing Points

Acceleration histories are determined by the numerical differentiation of the displacement histories of the panel bearing points.  Results from this portion of the analysis indicate that accelerations at bearing points can be as high as 1.79.  Again, in both cases where records were taken from upper stories of buildings, accelerations were greater at the upper stories than at the basement level of the same buildings.  Maximum accelerations at bearing nodes are shown in Figure 3.7.3.

3.7.4  Response in Connectors Due to Panel Inertia

A short analysis was performed to establish that the developed model of the architectural system would in fact give results that seem reasonable and to verify that the method of solution described does yield reasonable results.  The first 480 steps (9.58 seconds) of the acceleration record from the 10th floor of the Caltech, Millikan Library (Record G109) were input to the panel-frame model using a 0.02 second solution time step and response at every solution time step was output.  Acceleration histories of the bearing connectors were calculated and input to the architectural model using the shortened time step.  Results from this solution appeared reasonable.  Maximum values are shown in Figure 3.7.4.

Due to the capacity of the SAP IV program and the massive amount of data required to do a complete history analysis with a 0.02 second solution time step, it was not feasible to continue the analysis in the manner out-lined.  It is this authors opinion, however, that the analysis could be carried to completion with good results by setting up tape storage files and outputing data to these instead of on cards and expanding the program capacity size.  The SAP IV program capacity is controled by the size of the vector

Figure 3.7.3.    Maximum Accelerations at
                 Bearing Points

Accelerations ( in/sec$^2$ )

| | Record | | | | |
|---|---|---|---|---|---|
| | A001 | G108 | G109 | G110 | G111 |
| $AX_3$ | 367.0 | 559.0 | 660.9 | 280.0 | 440.72 |
| $AY_3$ | 5.6 | 8.2 | 9.945 | 4.19 | 6.65 |
| $AX_4$ | 367.0 | 559.7 | 661.0 | 280.0 | 440.8 |
| $AY_4$ | 5.2 | 7.85 | 9.22 | 3.93 | 6.145 |
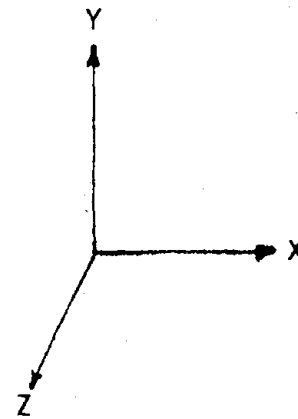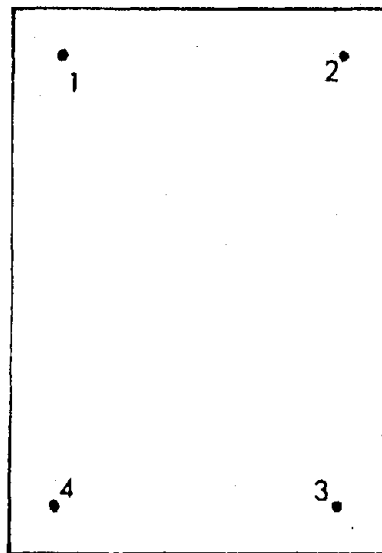


Numbering of Panel Connection Points

matrix 'A' and the variable 'MTDT' which are both dimensioned in the sub-
routine 'MAIN' in the first few lines of the program. Both are identified
in the program as being in control of the program capacity by COMMENT
statements.

Results from the analysis of the architectural system showed maximum
forces in the bearing connectors that were exceedingly high. This portion
of the analysis used a solution time step of 0.1 seconds for a mode-super-
position analysis. The use of this time step proved to be too large to
yield good results. The time step of 0.1 seconds was initially chosen
because it would allow approximately the first 48 seconds (480 points for
each of four acceleration histories) of the acceleration response calculated
from the displacement response of the panel bearing points. These accel-
eration histories were input to the SAP IV program without altering the
program capacity. The 0.1 second solution time step also cut down on the
number of computer cards required for data to hold the acceleration time
histories.

3.7.5 Maximum Combined Response in Bearing Connectors

Maximum combined response in the bearing connectors is found by
superimposing time history response determined for both cases assumed to
represent the total forces in the bearing connectors. Superposition of
force response histories for the first 9.5 seconds of response calculated
from only the 10th floor of the Caltech, Millikan Library has been found.
Results from calculations of the acceleration histories of the bearing points
show maximum accelerations in this portion of the record; therefore, it is
assumed that maximum combined response in the bearing connectors will be
found here. Maximum combined response in the bearing connectors for this

portion of the record are shown in Figure 3.7.4 . Maximum horizontal loads seen by individual bearing connectors are 5339.0 lbs. Maximum vertical loads in the bearing connectors are 6623.5 lbs., noting that the horizontal and vertical maxima do not occur simultaneously. In contrast UBC requirements for Fp which is applied to the center of gravity of the panel, is required to be 1920.0 lbs. divided between all of the panel connectors (see Figure 3.7.5 for the calculation of Fp).

Figure 3.7.5.        Uniform Building Code
                     Force Design Requirements for
                     Panel Connectors


$F_P = Z \ I \ C_P \ W_P$

> $I = 1.0$ for the entire connector assembly
>
> $Z = 1.0$ for seismic zone 4
>
> $C_P = 0.3 \times 1.3333 = 0.4$
>
> $W_P = 4800.0$ lbs


$F_P = (\ 1.0\ )(\ 1.0\ )(\ 0.4\ )\ (4800.0\ ) = \underline{1920.0 \ lbs}$


$F_P$ is applied laterally to the center of gravity
of the panel

## 3.8 SUMMARY AND CONCLUSIONS

### 3.8.1 Summary

The purpose of this analytical study was to predict the interaction between structural framing and precast curtain walls. The method of analysis used was based on the displacement method where the structural framing was idealized as beam, truss, and boundary elements and the precast curtain walls were idealized as two dimensional panel elements. The two dimensional panel element developed by Briggs (1976) consists of a rigid panel with four discrete connections between the panel and the structural framing. Only the planar stiffness contribution of the panel elements are considered and the rotational stiffnesses of the individual panel connections are neglected.

The three analytical methods developed to predict the response of structural framing with precast curtain walls are:

1. Linear static analyses.

2. Nonlinear static analysis assuming the structural frame behaves linearly elastic and the panel-frame connections behave with material nonlinearity. A piece-wise linear incremental method is used to approximate the nonlinearity effects of the panel-frame connections.

3. Dynamic linear analysis based on the methods used in SAP IV, an existing finite element analysis computer program developed by Bathe *et al.* (1974).

These analytical capabilities were developed by incorporating the planar panel element into SAP IV plus modifying the static solution to accommodate

the nonlinear effects. SAPFAP, the resulting program, has input, output, and computational efficiency similar to that of SAP IV.

Two dimensional computer models using SAPFAP were developed to idealize five full-scale structural framing-curtain wall tests. The test configurations represent a single bay of a structure and were based on a structural frame with different combinations of panel configurations and panel-frame connections. Each test configuration was analyzed for a horizontal in-plane load and the relative lateral stiffnesses compared. Results indicate the lateral stiffness contribution of the panel element depends on the type of panel-frame connection used and the geometry of the panels. These results were further verified by comparison of the first five natural frequencies of each test. An analytical study was also performed on a test configuration with two window box panels attached to the structural frame with an integrative connection system to approximate the effect of the panel connection nonlinearity on the behavior of the system under dynamic loading. Results of these studies demonstrate that these panels provide approximately an eight percent increase in the lateral stiffness to the system while loaded in the linearly elastic range, as evidenced by higher natural frequencies and by lower maximum displacements. Once the connections are loaded into the post-yielding range, the additional lateral stiffness provided by the panel elements is negligible for the system analyzed.

## 3.8.2 Conclusions

Based on the results of the analytical study, it can be concluded that:

1. A viable method has been developed to predict the interaction between structural framing and precast curtain walls for both dynamic and static loading.

2.  Panel configurations using the integrative panel connection system (i.e., bearing and flexible connections in these studies) provide additional lateral stiffness to the system while panel configurations using the isolation connection system (i.e., bearing and slotted connections) provide negligible additional lateral stiffness.

3.  Window box panels (Tests II and III) using the integrative panel connection system provide more lateral stiffness to the structure than the articulated panel system (Test V).

4.  Structural configurations using the integrative panel connection will provide additional lateral stiffness to the system while loaded in the linear elastic range but will supply negligible additional stiffness once connections are loaded into the post-yield range.

5.  The overall effect of the panel connection nonlinearity has a "weak" or minimal effect on the overall structural response, thus it is not recommended that nonlinear dynamic analyses of this problem be pursued to predict frequencies and deflections.

6.  Forces in panel connectors caused by differential displacement between panel connection points can be analytically predicted; furthermore, forces in panel connectors due to panel inertia can be analytically predicted as a post analysis to response determined by an interactive panel-frame model.

The three dimensional panel elemental stiffness matrix developed by Briggs (1976) could be incorporated into the computer program SAPFAP to analyze the contribution of all the stiffness components of the panel element on a three dimensional structure. Note, this would require additional experimental and analytical data for the various panel-frame connections to represent the stiffness properties for each panel connection freedom.

## 4.0 TASK III: FULL-SCALE LABORATORY TESTS OF CURTAIN WALL ASSEMBLAGES

### 4.1 Introduction

This task involved full scale laboratory testing of curtain wall assemblages. At the time the project was funded, the University of Idaho did not have a test facility to conduct the tests required in Task III. For this reason, it was necessary to design and build a facility for static and dynamic testing of the full scale curtain wall assemblages. In addition, it was necessary to upgrade the present data acquisition and analysis capabilities in order to investigate the behavior of these assemblages subjected to earthquake excitation. A PDP-11/03 computer was purchased by the Department of Civil Engineering, and the proper data acquisition and analysis hardware and software were designed, produced and implemented to meet the objectives of the project. This section describes the design of the reaction frame and the data collection system; furthermore, the test results obtained from the facility are presented.

## 4.2 DESIGN

### 4.2.1 Preliminary Concept

The requirement to construct a reaction frame grew from the need for a test facility to carry out a set of experiments. Various configurations of a typical structural unit (1 bay) from a high rise building, called a "unit cell" were to be tested. The preliminary concept of the unit cell shown in Fig. 4.1 consisted of full sized spandrel beams, columns, and architectural precast concrete panels. The objective was to determine the effect of the panels and their connections on the stiffness and dynamic response of the unit cell.

The reaction frame was required to accommodate the unit cell, provide reaction points for the cell and load application system, and not interact with the unit cell either statically or dynamically. The reaction frame design was begun using these initial requirements.

### 4.2.2 Design Criteria

Establishing design criteria is an important step in the design process. Proper design criteria help to define the problem and provide a basis for judging the acceptability of a design. For the reaction frame, the
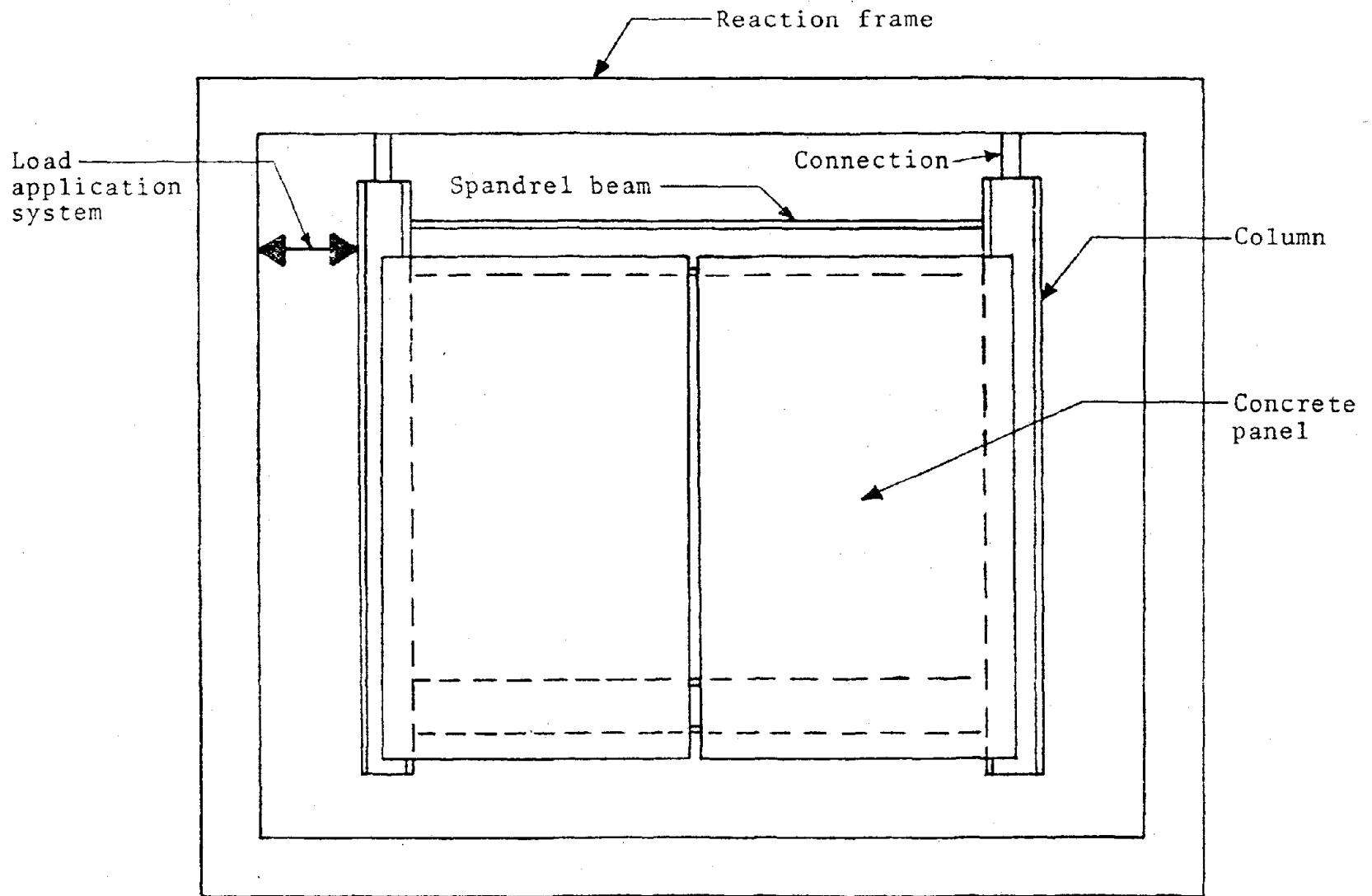
Fig. 4.2.1--Pre-design concept of the unit cell and reaction frame in the preliminary stage

critical design criteria were considered to be the frame location, size, deflections, strength, dynamic response, foundation conditions, and cost. Each of these criteria is treated separately in subsequent sections.

## 4.2.2.1 Location

The reaction frame was to be built on the University of Idaho campus. Test applications of the reaction frame were to involve full scale dynamic tests of the unit cell described in Section 4.2.1. Since equipment such as fork lifts and cranes would be required to lift the individual items comprising the unit cell into the reaction frame, the location of the reaction frame would have to provide working space for this lifting equipment, in addition to the space required for construction of the reaction frame itself.

## 4.2.2.2 Size

In determining the dimensions of the reaction frame, consideration was given to the full size unit cell, the load application system, the monitoring devices, and interior connections to the reaction frame. From preliminary estimates of the space required for these items, the centerline dimensions were set at 20 ft high by 25 ft long.

## 4.2.2.3 Deflection

In the test program to be conducted, experimental displacements would be measured to determine the static and dynamic response of the unit cell. If a significant

component of the experimentally generated data was due to displacement of the reaction frame, the data would not represent the true response of the unit cell. For this reason, the maximum displacement at any point in the reaction frame would have to be small in relation to the unit cell displacement. From consideration of typical inter-story stiffness in steel frame buildings and the mass of the concrete panels, an average unit cell displacement was estimated to be from 1.0 to 2.0 inches. The maximum displacement of the reaction frame was set at an order of magnitude less (0.1 to 0.2 in.) to avoid interference with the measured response of the unit cell. It was assumed that this small displacement would not introduce significant error into the tests.

### 4.2.2.4 Strength

The working stress method (e.g., Salmon and Johnson 1971) was used to determine the design stress levels for the structural steel in the reaction frame. In this method, stresses computed under the action of service loads are compared with predesignated allowable values. In this case, allowable stresses were taken from the American Institute of Steel Construction specifications (AISC-1977).

Allowable concrete stresses were determined from the ultimate strength design concept. In this method, service loads are increased by the so-called load factor to obtain the desired maximum strength and the concrete is designed

to meet these ultimate strength requirements. The design procedure and ultimate strength values were taken from "Building Code Requirements for Reinforced Concrete" (ACI 318-77).

## 4.2.2.5  Dynamic Response

For the dynamic response of the unit cell to be accurately represented in the testing program, the cell would have to be isolated from the dynamic response of the reaction frame; however, the subject of vibration isolation is too broad to be discussed extensively here. In general terms, if the natural frequencies of the reaction frame were close to experimental test frequencies, the reaction frame could display resonance and introduce a spurious response into the experimental data.

The reaction frame was a multi-degree-of-freedom system, so no quantitative criteria relating to allowable natural frequencies of the frame could be determined. This was because in a multi-degree-of-freedom system, the ways in which dynamic loads are applied (i.e., point of application, direction, etc.) as well as the loading frequency could contribute to resonant response of the system. For the reaction frame, these relationships were too complex to be evaluated in the pre-design stage. However, a single-degree-of-freedom model provided an estimate of how resonant response in the reaction frame might be avoided. For a single-degree-of-freedom system, the dynamic magnification

factor is only 1.01 if a periodic loading frequency is 0.10 of the natural frequency of the system. It was recognized in the pre-design stage that a detailed dynamic analysis may have to be performed if test frequencies approached natural frequencies of the reaction frame. A detailed description of a dynamic analysis of the reaction frame under test conditions is contained in Section 4.4.

### 4.2.2.6 Foundation Conditions

Soil conditions at the reaction frame site and the reactive forces generated during tests were considered in the design of the footings. These parameters would dictate the size and type of footings to be used. Specifically, three potential problems were to be obviated:

1. Settlement or uplift of the reaction frame.

2. Interference with the load carrying capabilities of existing foundations in the immediate area.

3. Vibration transmission to adjacent buildings.

### 4.2.2.7 Cost

The project budget allowed for a total cost of around $20,000. The major items contributing to the cost of the reaction frame were structural steel, fabrication, erection, excavation, reinforcing steel, and concrete.

## 4.2.3   Design Development

### 4.2.3.1   Preliminary Design

The steel plate box-type cross section shown in
Fig. 4.2.2 was initially investigated for the reaction frame.
Some of the experimental test loads would be slightly out of
plane with the reaction frame.   This cross section would be
efficient in resisting the torsion induced by these
eccentricities.   A closed box section has far more resist-
ance to torsion than an open section.

The frame was to be situated in the Gauss Engineer-
ing Laboratory (GEL).   Limited space at this location made
the bracing system shown in Fig. 4.2.3 necessary.   Resistance
to sidesway in the frame was provided by pretensioned high
strength steel rods.   This bracing system had several in-
herent disadvantages.   First, the pretensioned rods
required large and expensive anchor connections and, second,
the rods would have to be removed when the test configura-
tion was changed.

Lack of space in GEL also made special erection pro-
cedures necessary.   Although there is an overhead crane rail
system in the building, the individual weight of the items
to be erected exceeded the capacity of this crane system.
Therefore, the use of an overhead crane would have required
cutting a hole in the roof of the lab.   In addition, very
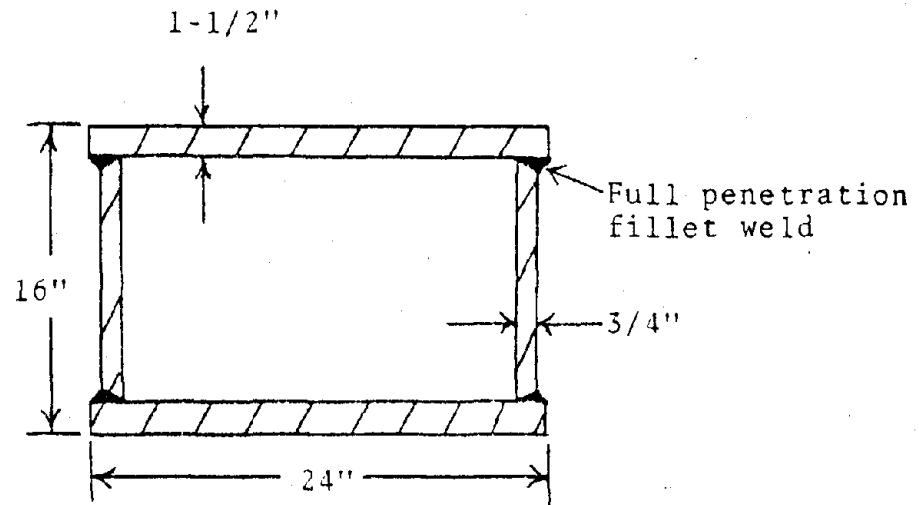little room was available to operate a fork lift.   In

Fig.4.2.2--Box-type cross section used
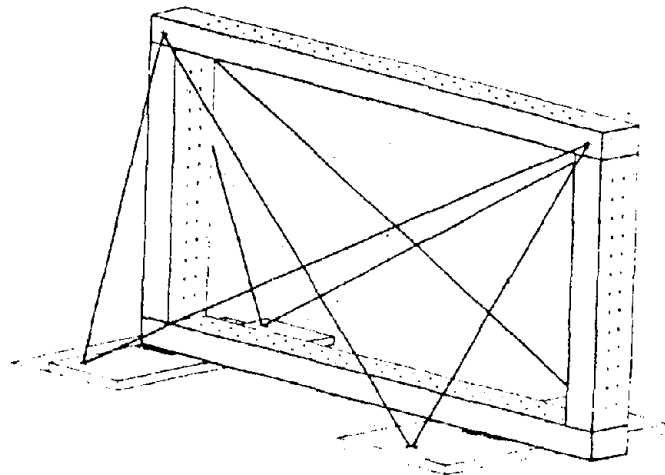in the preliminary design



Fig.4.2.3--High strength steel rod bracing system
used in the preliminary design

general, it was obvious that erecting the frame in GEL would introduce many onerous problems.

The cost of the preliminary design solution was found to be $36,000, exceeding the cost criterion of $20,000 by 80%. The most expensive parts of the design were the bracing system, the welds, the quantity of steel, and the special erection procedures. With these problems in mind, a new design was begun.

## 4.2.3.2 Final Design

The high cost of the preliminary design required reevaluation of the proposed site of the reaction frame. It was decided to locate the reaction frame outdoors, south of Buchanan Engineering Laboratory (Fig. 4.2.4). This decision reduced the cost in several ways. First, no special erection techniques were required at this location and, second, there was ample room for cranes and other construction equipment (see Fig. 4.2.4). The pretensioned rod bracing system was replaced with a simpler external system (Fig. 4.2.5). The axial stiffness of the braces themselves provided resistance to sidesway in the frame eliminating the need for pretensioning.

A new cross section was then determined for the reaction frame. It was decided to use two wide flange sections welded together side by side as shown in Fig. 4.2.6. By using this cross section rather than the box section, the weight of the frame was reduced by more than 50%, thus
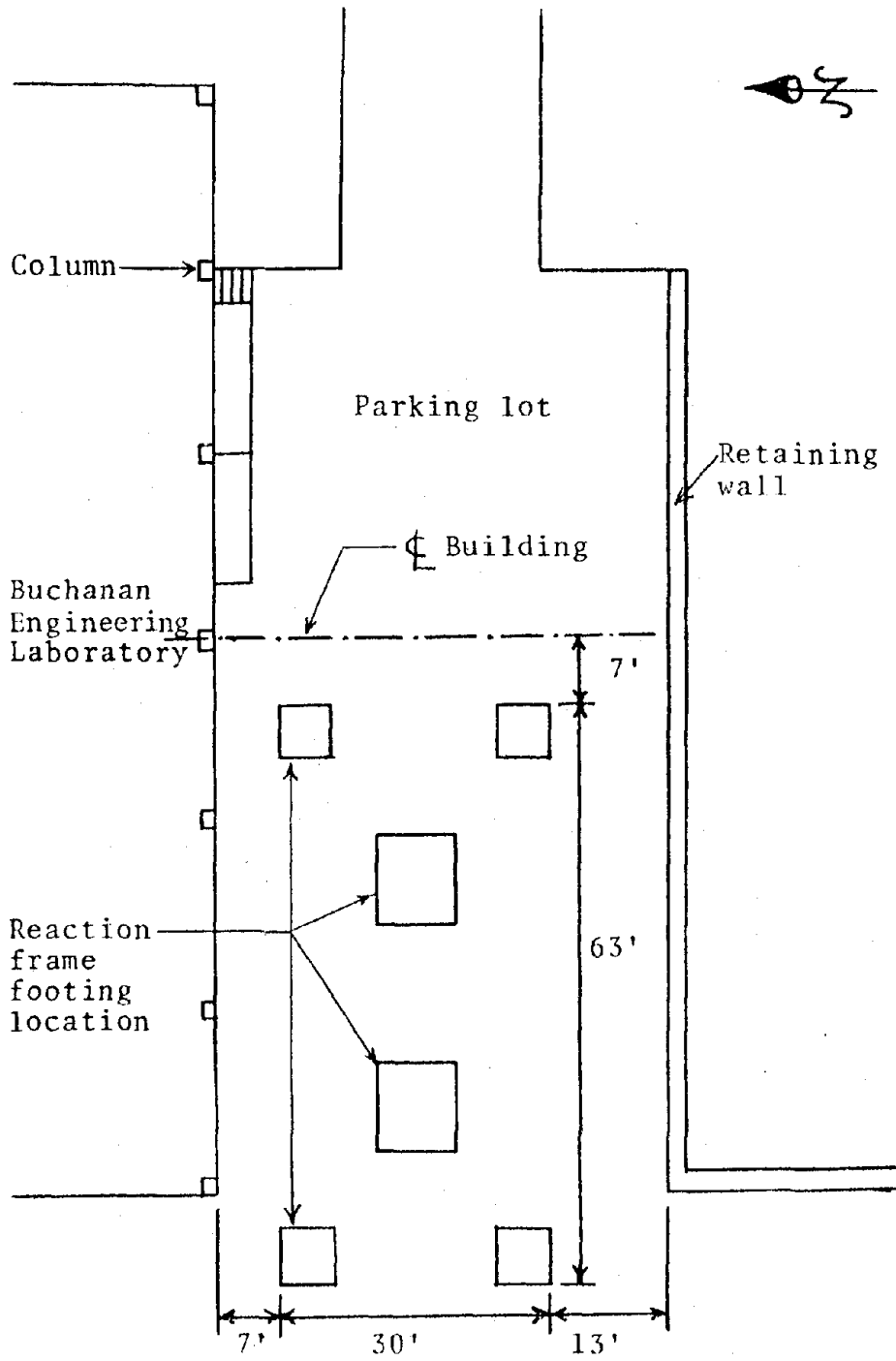
Fig.4.2.4--Plot plan showing location of reaction frame
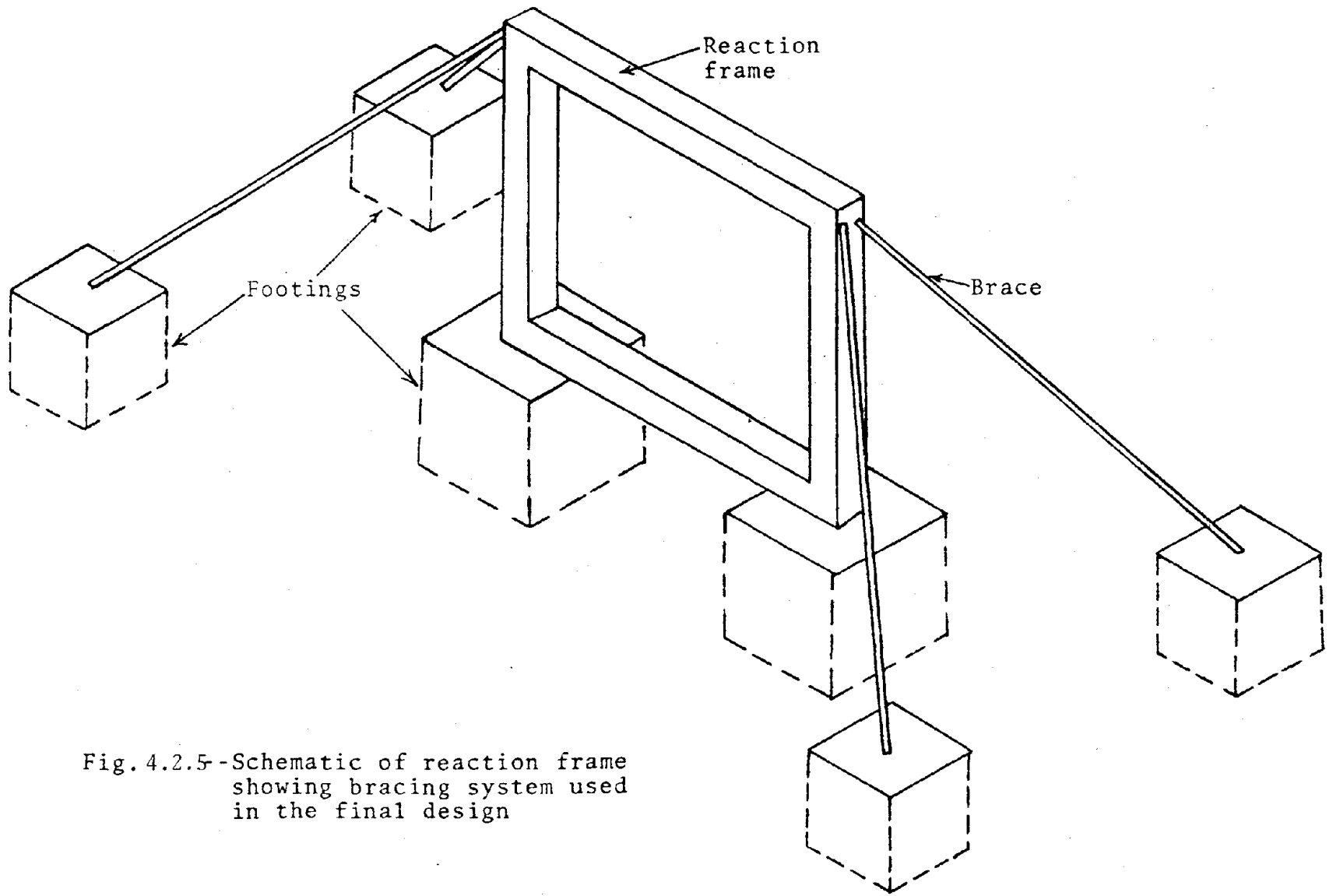for the final design

Fig. 4.2.5--Schematic of reaction frame
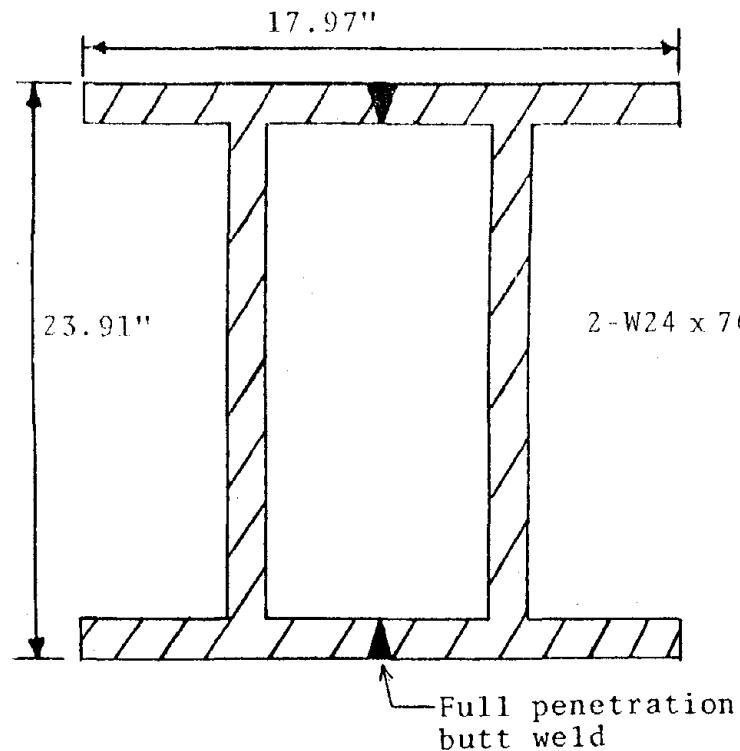showing bracing system used
in the final design

Fig.4.2.6--Cross section built from two wide
flange shapes used in final design

greatly reducing material costs. In addition, wide flange
members were readily available to fabricators in the area.
Another advantage to making the section from wide flange
shapes can be seen by contrasting Figs.4.2.2 and 4.2.6. As
shown, the box section required four welds and the wide
flange section required only two. Although the welding
procedure is different for a butt weld than for a fillet
weld, it was still found that welding costs were greatly
reduced for the wide flange section. Finally, adequate

(though reduced) torsional rigidity was maintained with the wide flange section because the central portion of the section formed a closed "box" shape. The section properties for the steel plate box section used in the first design 'and the wide flange section of the final design are summarized in Table 4.2.1.

Table 4.2.1-Comparison of section properties in preliminary and final designs

| Design | $A$ (in.$^2$) | $I_{xx}$ (in.$^4$) | $S_x$ (in.$^3$) | $I_{yy}$ (in.$^4$) | $S_x$ (in.$^3$) | $J$ (in.$^4$) |
|---|---|---|---|---|---|---|
| Preliminary | 91.5 | 4072 | 509 | 5660 | 472 | 4100 |
| Final | 44.8 | 4200 | 350 | 1070 | 119 | 1190 |

The reaction frame was then built using this latter design. The cost of structural steel, fabrication, and erection was approximately $16,000. The foundation cost was roughly $5,000, bringing the total cost of the reaction frame to about $21,000. This figure exceeded the cost criterion by only 5%, an acceptable amount. A conceptual drawing of the reaction frame as it was designed is shown in Fig. 4.2.7.

## 4.2.4  Design Procedure

The purpose of this section is to describe the procedure and techniques used in the development of the final

Fig.4.2.7--Conceptual drawing of reaction frame

design. Some steps in this procedure were done many times,
e.g., computer analyses. Others, such as the design of
details, were completed only when the design was thought to
be a viable solution. Each time specific design solutions
are cited, the reference is to the final design.

## 4.2.4.1 General Procedure

The design procedure began by assuming a cross sec-
tion with an adequate moment of inertia to meet the maximum
deflection criterion of between 0.1 and 0.2 in. displacement
(Section 4.2.2.3). Since the gross dimensions of the frame
had previously been established (Section 4.2.2.2), the next
step was to assume a bracing system that would stabilize the
frame and prevent sidesway. Next, an analysis of the pro-
posed configuration was performed.

Analyses of the design configurations were accom-
plished using a finite element computer program called
SAP IV (Bathe et al. 1973). The program was developed at
the University of California, Berkeley, and implemented at
the University of Idaho on an IBM 370/145 computer system.
Both the static and dynamic capabilities of SAP IV were
utilized in the design of the reaction frame. The computer
analysis provided values of stress and deflection which were
compared with the predetermined design criteria of strength
and allowable displacement.

Before construction drawings were prepared, design
details such as the reaction points, rigid frame knees,

footings, base plates, and anchor bolts had to be finalized. Static analysis, dynamic analysis, and detail design considerations are described in subsequent sections.

## 4.2.4.2 Static Analysis

SAP IV uses the well known stiffness method (e.g., Cook 1974) to solve the static equilibrium equations

$$\underline{K}\ \underline{u} = \underline{R} \qquad\qquad (4.2.1)$$

where $\underline{K}$ is the stiffness matrix, $\underline{u}$ is the nodal displacement vector, and $\underline{R}$ is the nodal load vector. In the idealization of the reaction frame, beam elements were used for the main portion, and truss elements for the bracing members. An elevation of the three-dimensional model used in the static analysis is shown in Fig. 4.2.8. Nodal points were numbered to minimize the bandwidth of the stiffness matrix, and hence reduce the cost of computer runs. A large number of nodal points were used in the model of the frame to represent the effects of the weight of the frame in the analysis. SAP IV uses the weight density given as input data to determine point nodal loads (no moments) due to gravity. Since a large number of nodal points were used in the model, the deflection and stresses due to the dead weight of the frame were closely approximated. In general, for a structure such as the frame, dead weight effects do not constitute a
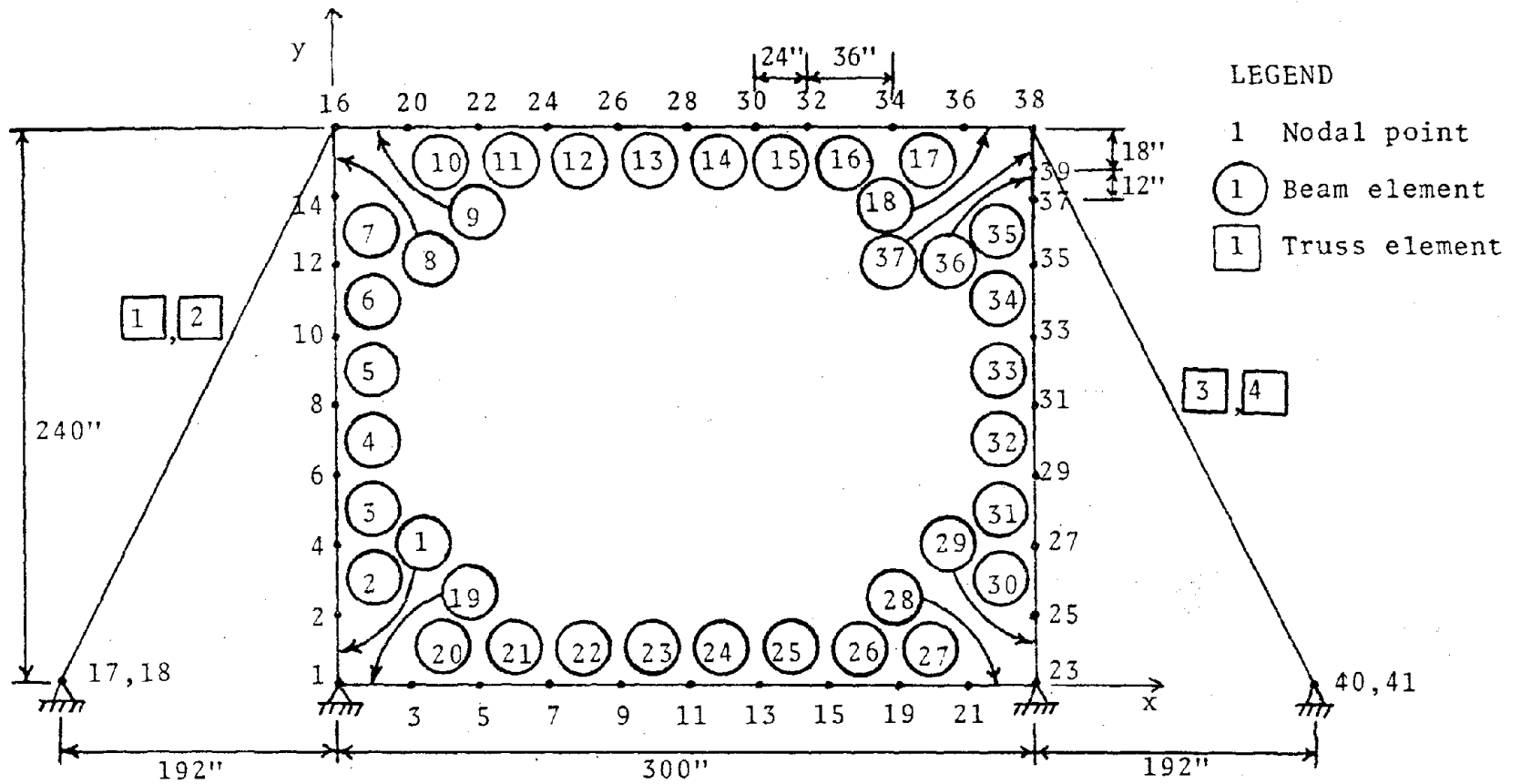
Fig. 4.2.8 -Three-dimensional computer model used in analyses of reaction frame.
Note:  All nodes spaced at 30" unless shown otherwise.

significant portion of the total static response. However, the large number of beam elements were justified for the sake of completeness and because it was anticipated that the same model would be used in dynamic analysis (Section 4. 2.4.3).

Initially the loads that would be applied to the unit cell during tests were not known. However, from considering typical interstory stiffness in high rise buildings and the anticipated capabilities of the load application system, an upper bound was estimated at 75,000 lb. Using this value and the principles of statics, the distribution of the load through the unit cell (Fig. 4.2.1) was calculated. The resultant static design load pattern is shown in Fig. 4.2.9.

The nodal point data, element data, and loads were input to SAP IV. The solution yielded values of displacement and stress that were compared to the design criteria described in Section 4.2. For the reaction frame, the maximum deflection constraint of from 0.1 to 0.2 in. was the critical criterion. The maximum static displacement was found to be 0.113 in. Specific computer results and corresponding design calculations are in Thomas (1980).

### 4.2.4.3 Dynamic Analysis

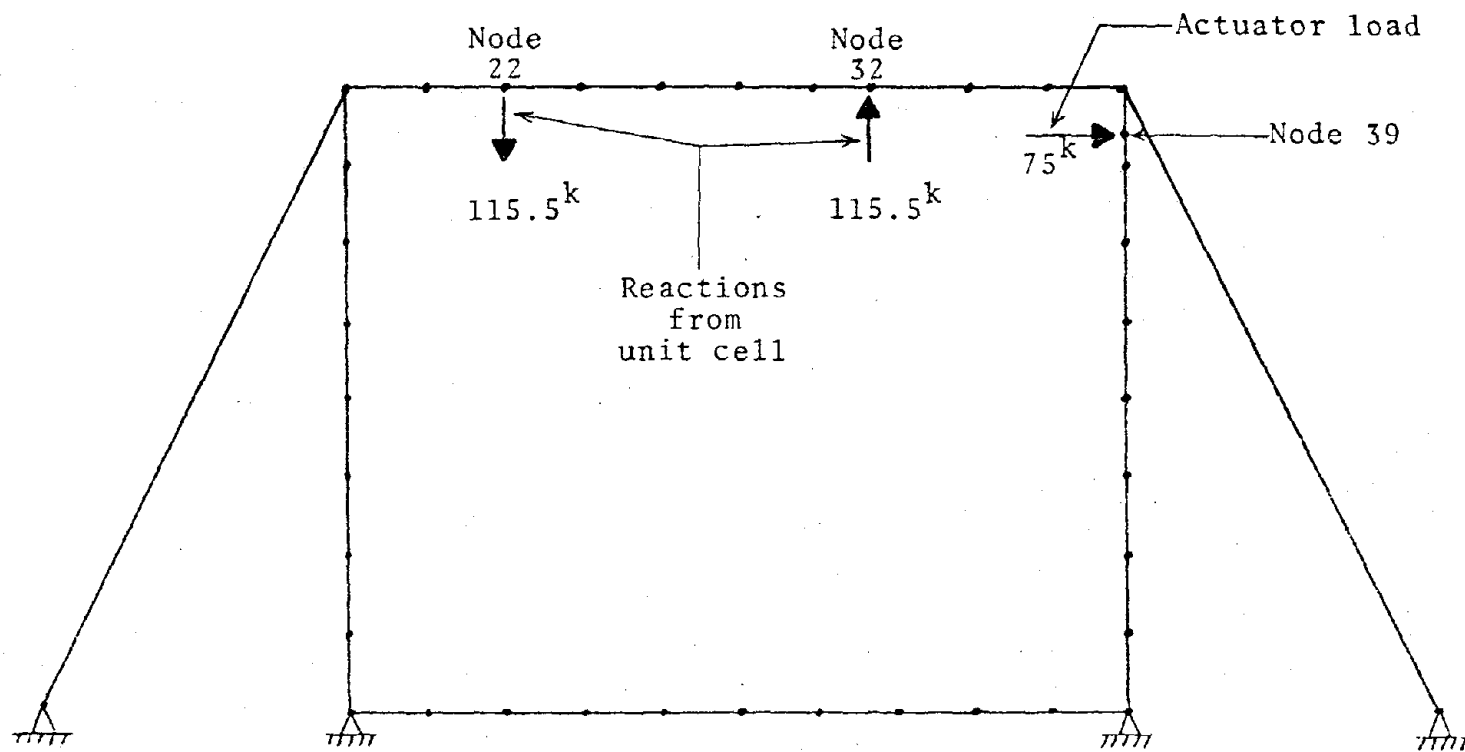SAP IV offers the following four types of dynamic analyses to the user:

Fig.4.2.9--Loads used in static analysis

1. Natural frequency calculations only.

2. Natural frequency calculations followed by response history analysis by mode superposition.

3. Natural frequency calculations followed by response spectrum analysis.

4. Response history analysis by direct integration.

The dynamic analysis of the reaction frame was carried out by utilizing the second option. Under this option, two problems are solved during each computer run as stated above. Natural frequencies and corresponding mode shapes are first calculated, then this information is used in a response history analysis that is carried out using mode superposition.

SAP IV represents the mass of a structure with a diagonal mass matrix. In other words, the mass of each element is assumed to be concentrated in point masses at each of the nodal points. The distribution of the mass to the nodal points is determined by statics (Clough and Penzien 1975). This technique is known as a lumped mass idealization (Fig. 4.2.10). Because the mass is assumed to be concentrated at the nodal points, a large number of nodal points are required in the model to accurately represent a uniformly distributed mass. Such a model was used in the static analysis (Fig.4.2.8) of the reaction frame to represent the effects of dead weight. The same model was used in dynamic analysis, but in this case the effect of a uniformly distributed mass was represented.
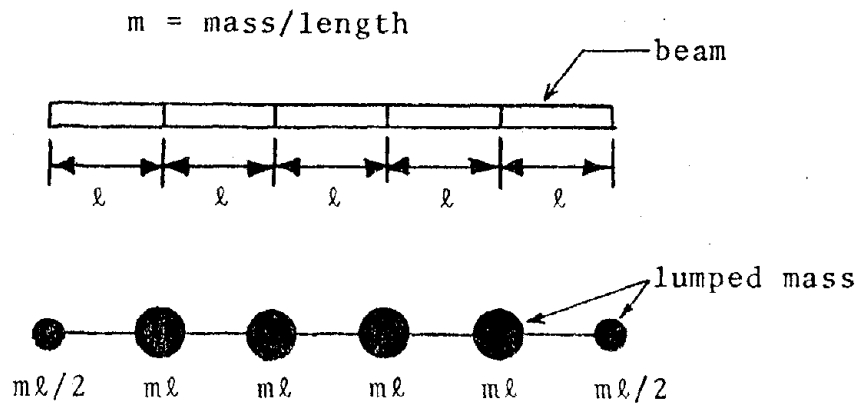
m = mass/length

beam

ℓ   ℓ   ℓ   ℓ   ℓ

lumped mass

mℓ/2   mℓ   mℓ   mℓ   mℓ   mℓ/2

Fig.4.2.10--Lumped mass idealization

## 4.2.4.3.1  Calculation of Natural Frequencies and Mode Shapes

The determination of natural frequencies and corresponding mode shapes involves the solution of the generalized eigenvalue problem

$$\underline{K}\ \underline{\phi} = \omega^2\ \underline{M}\ \underline{\phi} \qquad\qquad (4.2.2)$$

where $\omega$ is the free vibration frequency, $\phi$ is the mode shape vector, and $\underline{M}$ is the diagonal mass matrix for the structure. Two methods are used in SAP IV for the solution of the eigenvalue problem.  When the stiffness matrix can be held in high speed storage, a determinant search technique is carried out.  For systems with large order, for which the stiffness matrix cannot be contained in high speed storage,

a subspace iteration is required (Bathe and Wilson 1976).
In the reaction frame model used, the bandwidth of the
stiffness matrix was kept small with proper nodal numbering
techniques.    Therefore, the determinant search method was
used.

The first part of the computer run yielded fre-
quencies and mode shapes for the p lowest eigenpairs (vibra-
tion modes), where p was specified by the user.   The size
of p was determined from consideration of the significant
modal components contributing to the dynamic response (see
Section 4.2.4.3.2).  The first five modal shapes for the re-
action frame are shown in Figs. 4.2.11-4.2.15. These greatly
exaggerated figures show the shape the reaction frame would
take in free vibration at the natural frequency correspond-
ing to that mode shape.

4.2.4.3.2   Response History Analysis
by Mode Superposition

The governing equations for any general dynamic
response are

$$\underline{M}\,\underline{\ddot{u}} + \underline{C}\,\underline{\dot{u}} + \underline{K}\,\underline{u} = \underline{R}(t) \qquad (4.2.3)$$

where $\underline{C}$ is the damping matrix and $\underline{R}(t)$ is the dynamic load-
ing vector.   When mode superposition (Clough and Penzien
1975) is used it is assumed that the structural response
of a dynamically loaded system can be adequately described
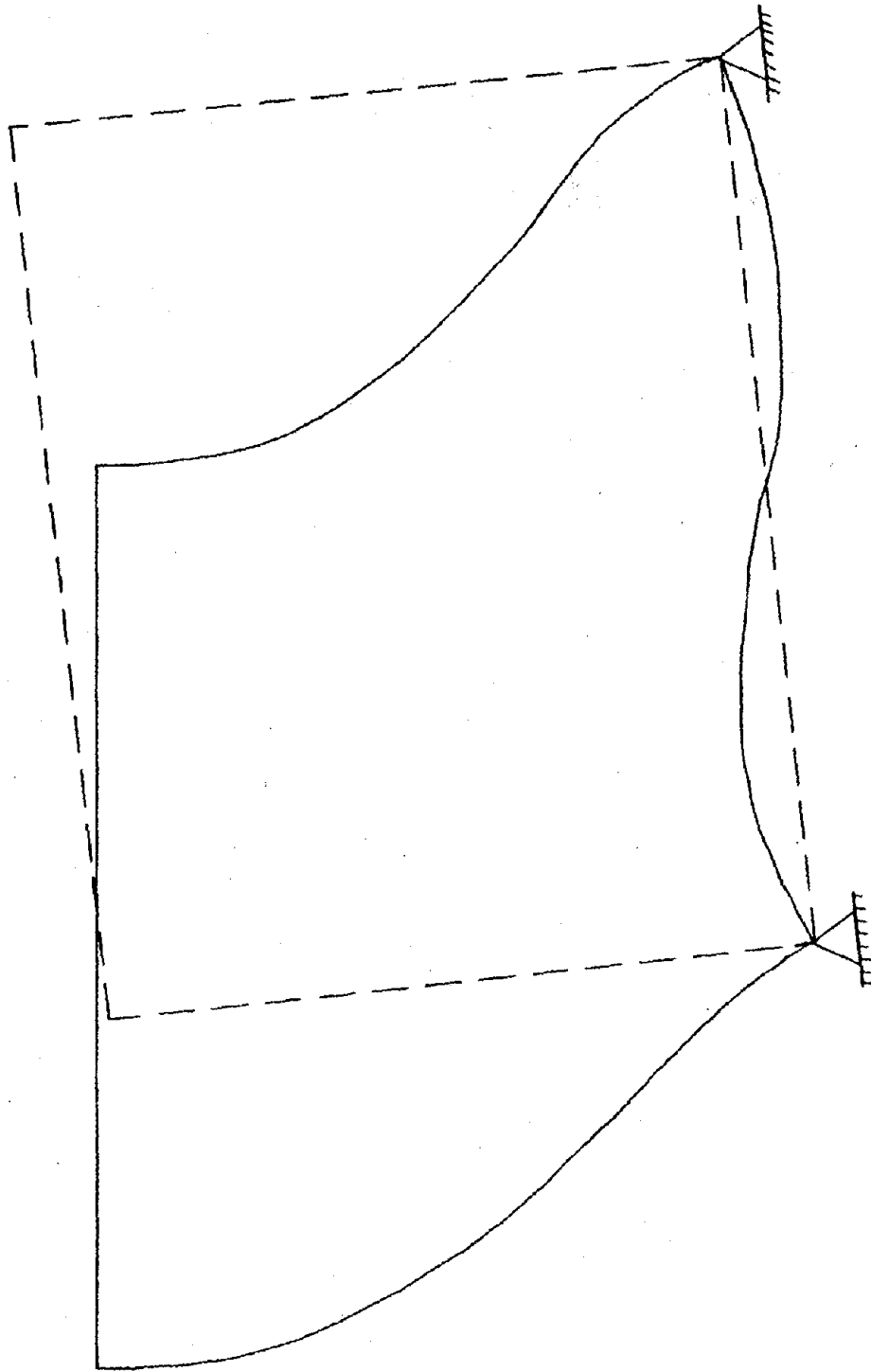by the p lowest vibration modes.   In the analysis of the

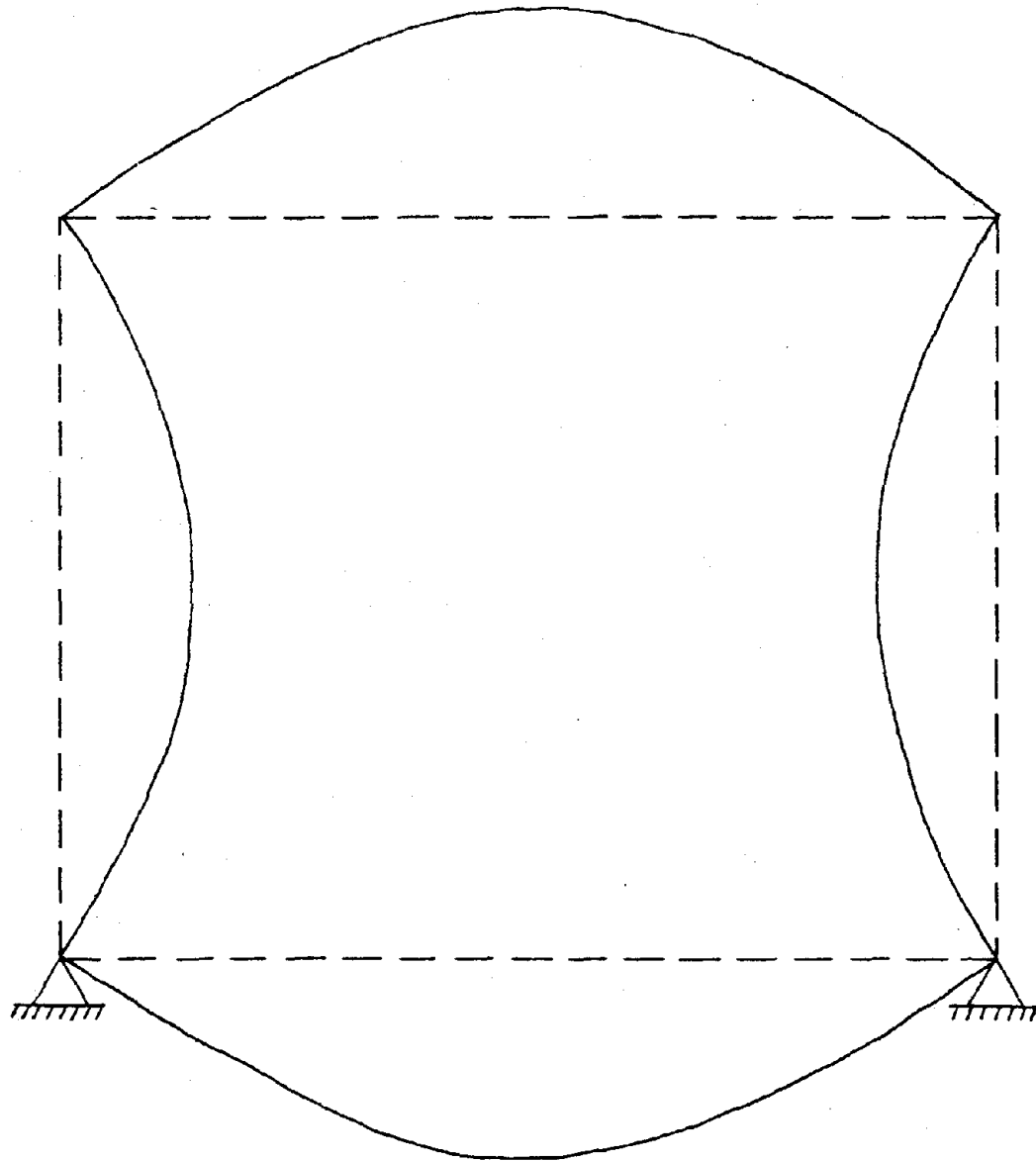Fig. 4.2.11--First vibration mode shape;   frequency = 37.68 Hz

Fig. 4.2.12--Second vibration
      mode shape; fre-
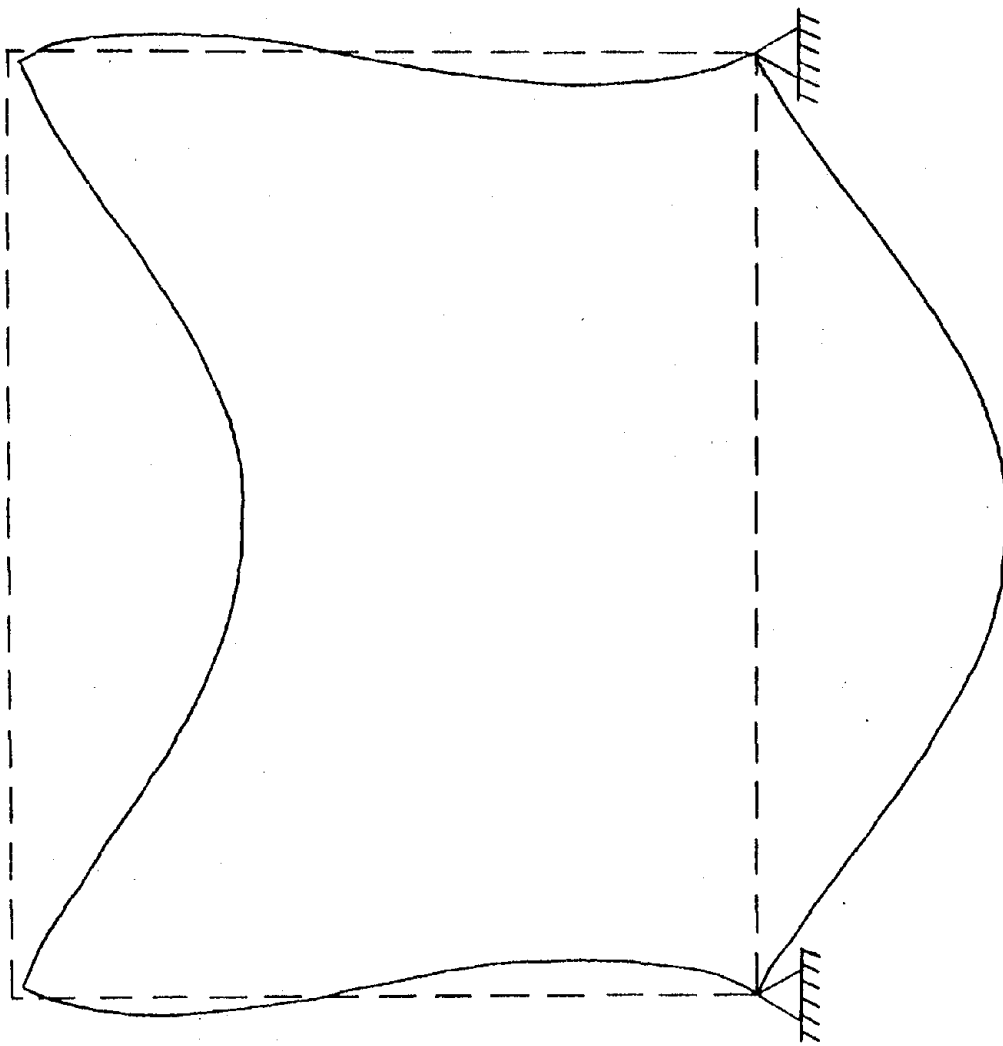      quency = 38.40 Hz

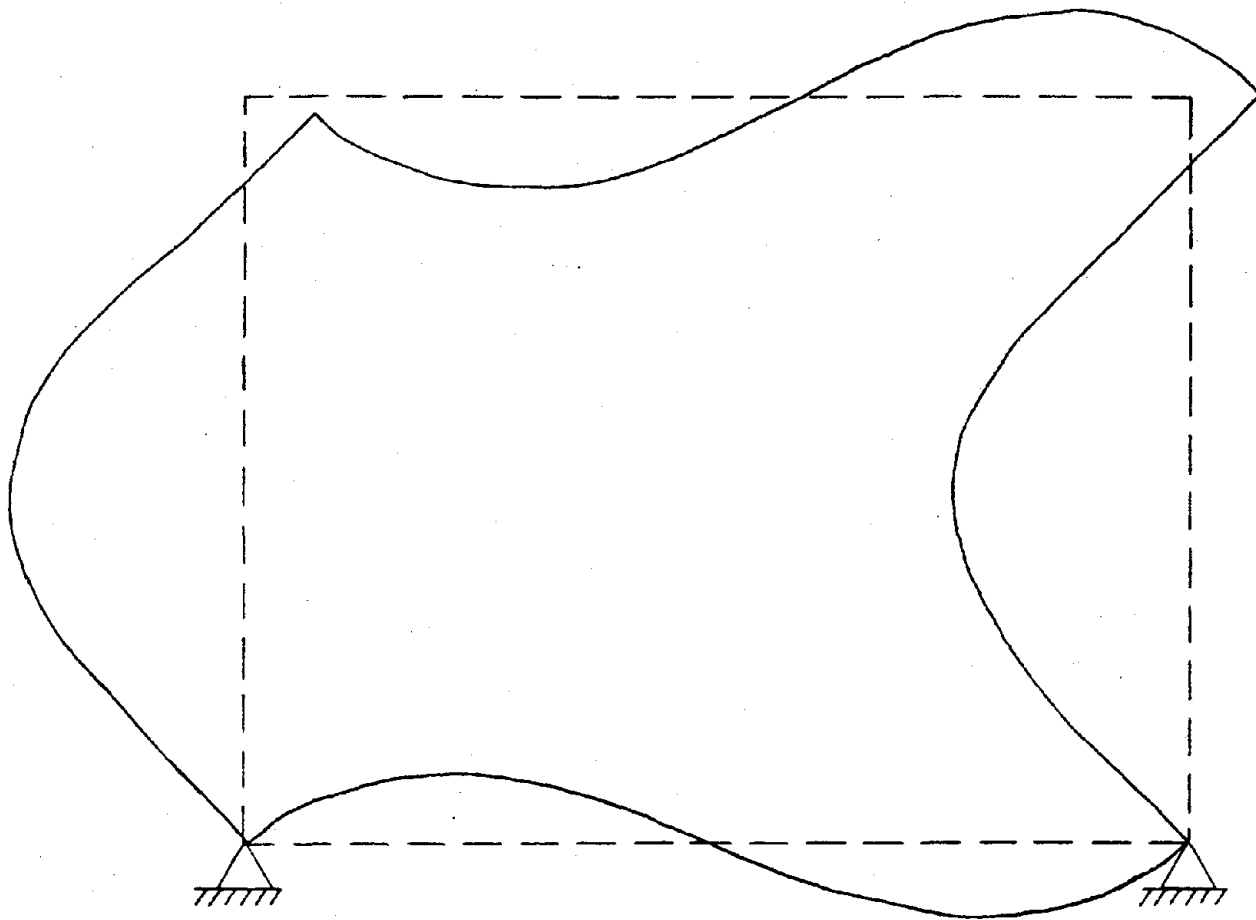Fig. 4.2.13 - Third vibration mode shape; frequency = 49.82 Hz

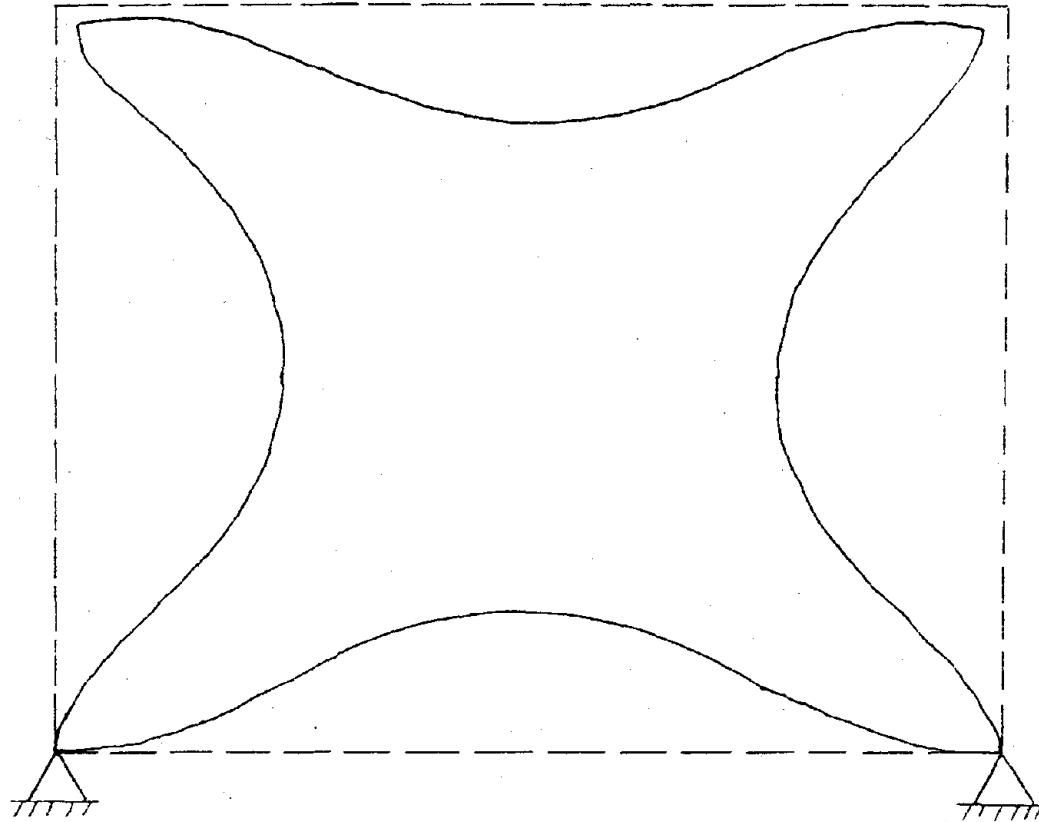Fig.4.2.14--Fourth vibration mode shape; frequency = 75.88 Hz

Fig.4.2.15 -Fifth vibration mode shape; frequency = 82.20 Hz

reaction frame it was assumed that the first ten vibration modes would be sufficient.

In general, the basic energy-loss (damping) mechanisms in a structural system are seldom well understood. .For this reason, damping properties must usually be determined experimentally after a structure has been built. However, in the design of the reaction frame it was recognized that the maximum dynamic response would generally be less in a damped system than in an undamped system. For this reason, $\underline{C}$ was assumed to be null in the dynamic analysis of the reaction frame.

SAP IV solves the above equations by the Wilson $\theta$ method (Bathe and Wilson 1976), which is an unconditionally stable step-by-step integration scheme. This method is a modification of the linear acceleration method (Clough and Penzien 1975) in which the acceleration is assumed to be linear over the computational time step $\Delta t$. The linear acceleration method is an acceptable numerical integration scheme as long as a short enough computational time step is used. This method is only conditionally stable, however, and it will become numerically instable if it is applied to modal response components having periods of vibration less than approximately 1.8 times the time interval. On the other hand, the Wilson $\theta$ method is based on the assumption that the acceleration varies linearly over an *extended* time step $\theta \Delta t$. The linear acceleration assumption for both

methods is depicted graphically in Fig. 4.2.16. For a value of $\theta$ = 1 the Wilson $\theta$ method is identical to the linear acceleration method, but for $\theta$ > 1.37 (usually taken as 1.40; Bathe and Wilson 1976), the Wilson $\theta$ method becomes unconditionally stable.

The time step required to adequately represent the dynamic response depended on the characteristics of the dynamic loading and on the periods of vibration of the reaction frame. The necessary time step to approximate the significant aspects of a dynamic loading situation could easily be established from a consideration of the nonlinear and rate change properties of the loading. Therefore, the choice of time step would primarily depend on the natural periods of vibration in the reaction frame. In general, a time increment-to-period ratio of 0.1 or less is a good rule of thumb for obtaining reliable results (Clough and Penzien 1975). In mode superposition this ratio applies to the highest vibration frequency which contributes significantly to the dynamic response.

The forcing function used in the dynamic analysis of the reaction frame was a sine wave function with the amplitude of the static design loads. This load form was chosen because it was known during the design process that at least some of the test loads would be sinusoidal. The loads (Fig. 4.2.17) were applied at the same nodal points as
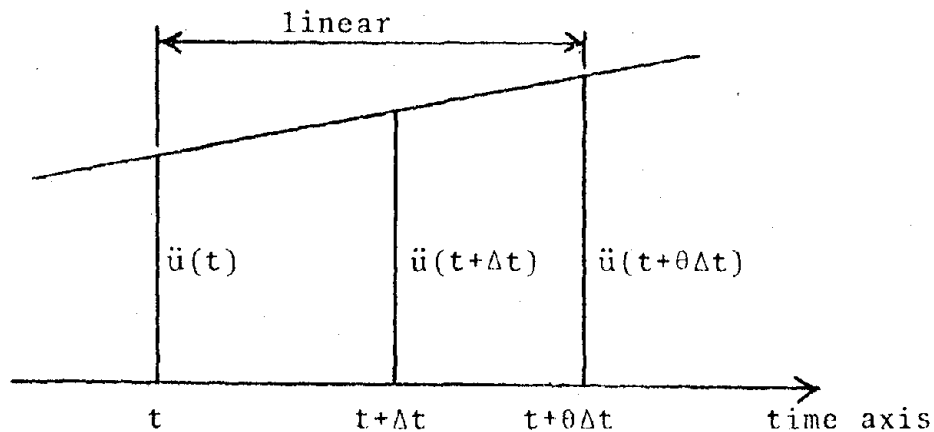
Fig. 4.2.16--Linear acceleration for normal
and extended time steps

they were in the static load case and the direction changed

simultaneously with the input sine wave.

The loading frequencies that were to be used in the

tests were not known during the design of the reaction

frame, but preliminary calculations showed that the first

natural frequency of the unit cell would be about 2 Hz.

Since this frequency condition would expose the frame to the

most severe design loads, this frequency was used in the

design dynamic analysis.

By considering the contribution of the

natural vibration modes to the response of the reaction

frame as previously discussed, a time increment of .0015 was

chosen. This accurately represented the effects of the

first three vibration modes and approximated the effects of

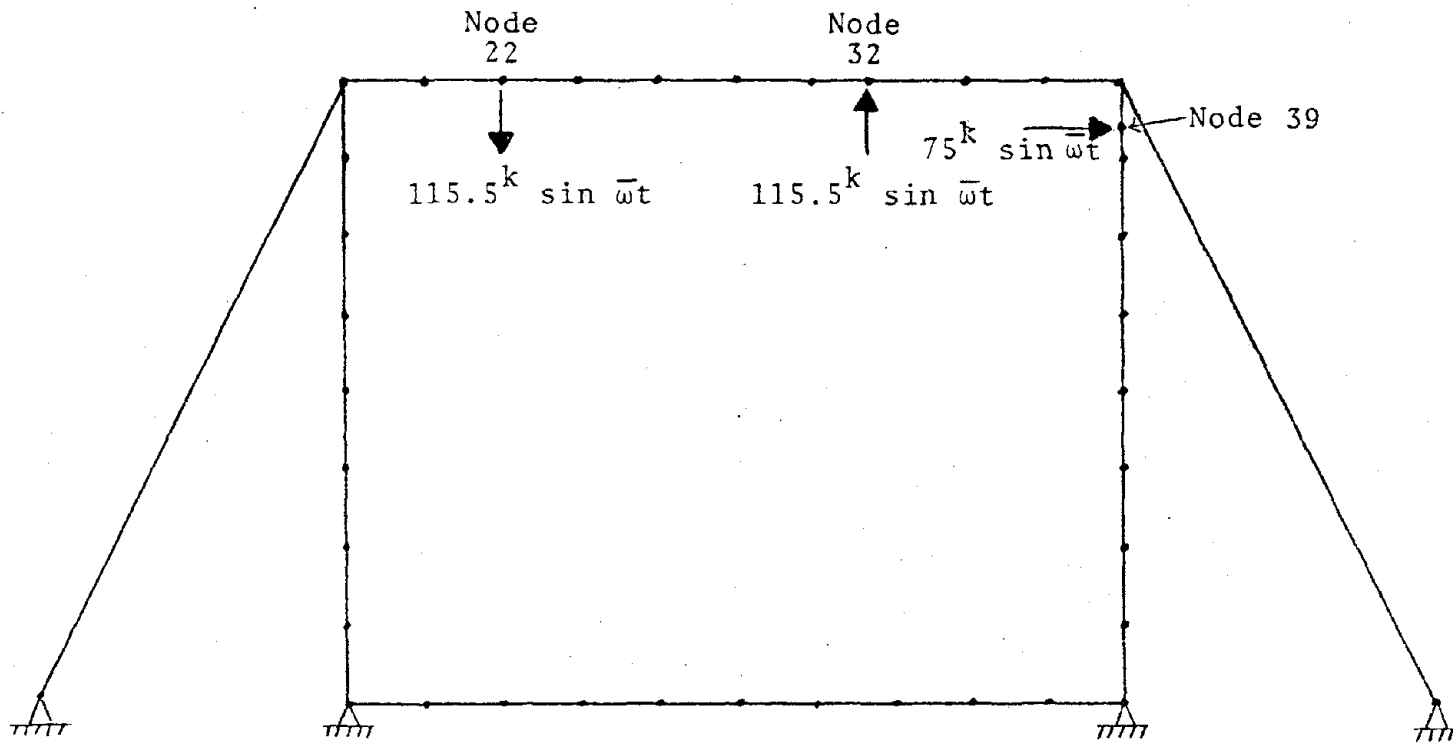the fourth and fifth. One thousand increments were used

Fig. 4.2.17-'-Loads used in dynamic analyses

giving a loading duration of 1.5 seconds for three cycles. This was believed to be long enough to determine the maximum response of the frame under the dynamic loads.

Since the loading frequency (2 Hz) was so low with ·respect to the lowest natural frequency of the reaction frame (37.68 Hz), it was expected that the maximum dynamic response of the frame would be quasi-static. Table 4.2.2 compares some of the static and dynamic analysis results. The values were chosen from the points of maximum response in the static analysis. As shown in Table 4.2.2, the dynamic parameters only slightly exceed the static values in one case, and in three of the parameters the dynamic result is less than the dynamic value. Basic theory shows that the dynamic response of the reaction frame could not be less than the response that would be produced by static application of the same load. Closer observation of the computer printouts revealed that in some cases the dynamic response was slightly less than the static response and in others it was slightly larger. These differences were attributed to the fact that different algorithms were used by SAP IV to accomplish the static and dynamic analyses. Therefore, it was concluded that the dynamic response to the design loads was quasi-static as expected.

It was recognized in the design stage that additional dynamic analyses may have to be carried out as specific test conditions were encountered.

Table 4.2.2--Comparison of static and dynamic design analyses
for selected parameters

| Element or node | Parameter | Static result | Maximum dynamic result |
|---|---|---|---|
| Truss [1] | Axial force | $30.21^k$ | $29.99^k$ |
| Truss [3] | Axial force | $34.60^k$ | $36.13^k$ |
| Node 22 | y displacement | .05" | .04" |
| Node 32 | y displacement | .11" | .11" |
| Beam (16) | Moment | $3947^{"-k}$ | $3055^{"-k}$ |

However, no further analyses were done during the initial
design. This decision was based on two considerations.
First, it was thought that the design loads had been con-
servatively estimated. The actual reaction frame would
probably never be exposed to such severe loading conditions.
Secondly, the first natural frequency of the reaction frame
was considerably higher than the anticipated full scale test
loading frequencies.

## 4.2.4.4  Detail Design

In order to complete the design procedure, it was
necessary to consider the details of the reaction frame.
Details to be designed were the reaction points, rigid from
knees, and footings. The soil conditions at the proposed

frame site and structural interference with adjacent

buildings were also considered in the final design stage.

Each of these items is discussed in detail in the sections

that follow.

4.2.4.4.1 Reaction Points

During the actual tests, the unit cell and the load

application system had to be connected to the reaction

frame. The reactive forces generated in the tests would be

transferred to the reaction frame through these connections

at "reaction points." During the design of the reaction

frame, the exact location of these points was not known, and

the precise type of connection to be used had not been

determined. For these reasons, an adaptable system of re-

action points had to be devised. Figure 4.2.18 shows the

method that was used. The reaction points were spaced at

three foot intervals around the entire reaction frame.

Closer spacing would have been more adaptable, but by spacing

the reaction points at three feet, a more economical solution

was obtained. If a connection was desired between reaction

points, the adjacent points could be bridged with a steel

plate. Therefore, connections were possible at any point

around the reaction frame.

Special features of the reaction points were the web

stiffeners and the holes in the flange of the reaction frame.

The stiffeners were located on the outside flange at each

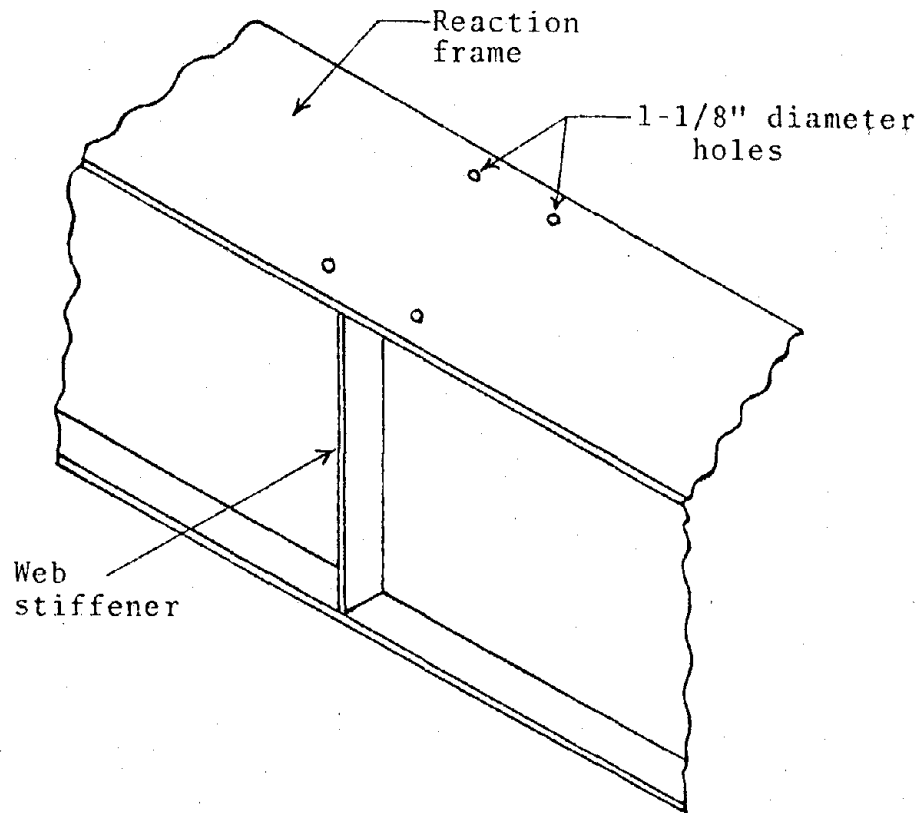reaction point to help distribute concentrated loads and

Fig.4.2.18--Reaction point for connections
to reaction frame

prevent local buckling of the cross section. The holes allowed connections to be bolted rather than welded to the frame; therefore, any connection could be accomplished without damaging the reaction frame.

## 4.2.4.4.2 Rigid Frame Knees

Complete transfer of moments around the corners of the reaction frame was required. This was accomplished as shown in Fig. 4.2.19. Internal forces were transferred from beam to column and vice versa through the one inch plates. Web stiffeners were supplied in the corner region to help resist induced shear forces in the web at full moment capacity. Stiffeners were situated perpendicular to the flange, 12 inches from the corner, and a pair of diagonal stiffeners were located inside the corner region. The construction drawings (Thomas, 1980) show use of an increased plate thickness rather than implementation of the diagonal stiffeners. This is because the diagonal stiffeners were decided upon after the bid had been awarded. Use of diagonal stiffeners was found to be less expensive than the increased plate thickness.

## 4.2.4.4.3 Footings

The design of the footings was based on a consideration of the reactive forces transferred from the reaction frame to the footings. The footing dimensions shown in Fig. 4.2.20 were calculated using the maximum uplift forces
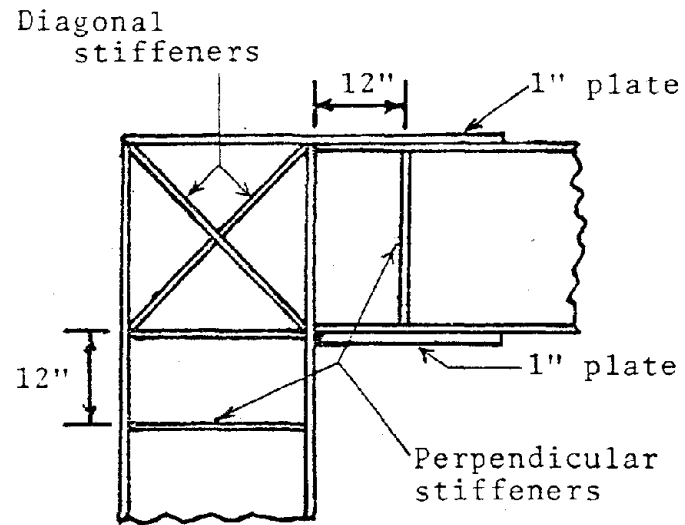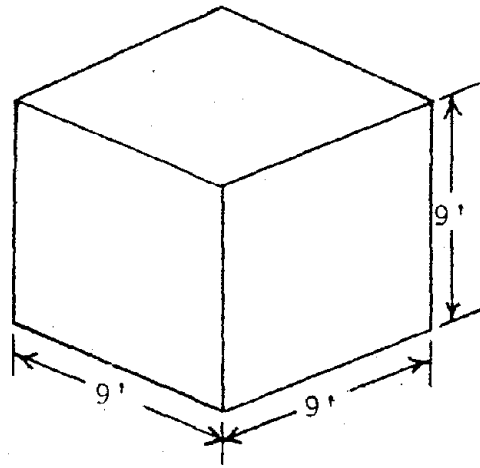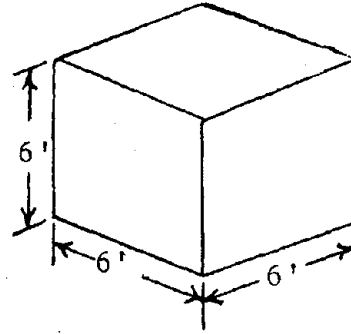
Fig.4.2.19--Rigid frame knee; complete transfer of
internal forces.  Note:  Detail showing
welds and plate sizes can be found in
Appendix C.

(a) Frame footing        (b) Brace footing

Fig.4.2.20--Dimensions of reaction frame footings

determined by the computer analysis. The density of concrete was taken to be 150 pcf. ACI code (ACI 318-77) specifications required that only temperature reinforcing in the top of the footings was required. However, a "cage" of reinforcing steel was provided as shown in Fig. 4.2.21 to contain the concrete and to allow the footings to function as units. The base plates and anchor bolts were designed using standard procedures (PCI 1971, p. 6-18, 6-23). A cross shaped arrangement of rebar                was used to tie the anchor bolts to the steel cage.

## 4.2.4.4.4  Soil Conditions and Structural Interference

Before the Buchanan Engineering Laboratory was built, a boring log was made at the existing southwest corner of the lab, and this boring provided a useful estimate of the soil properties at the proposed site of the reaction frame (Fig. 4.22). This log indicated that the soil was of high quality. As shown, the average penetration resistance N was 28 blows/ft indicating a very stiff clay with an unconfined compressive strength of from 2.00 to 4.00 tons/ft$^2$ (Lambe and Whitman 1969). This was more than adequate strength to carry the loads imposed by the reaction frame. In addition, calculations (Thomas, 1980) showed that settlements in adjacent buildings due to the reaction frame would be virtually nonexistent.
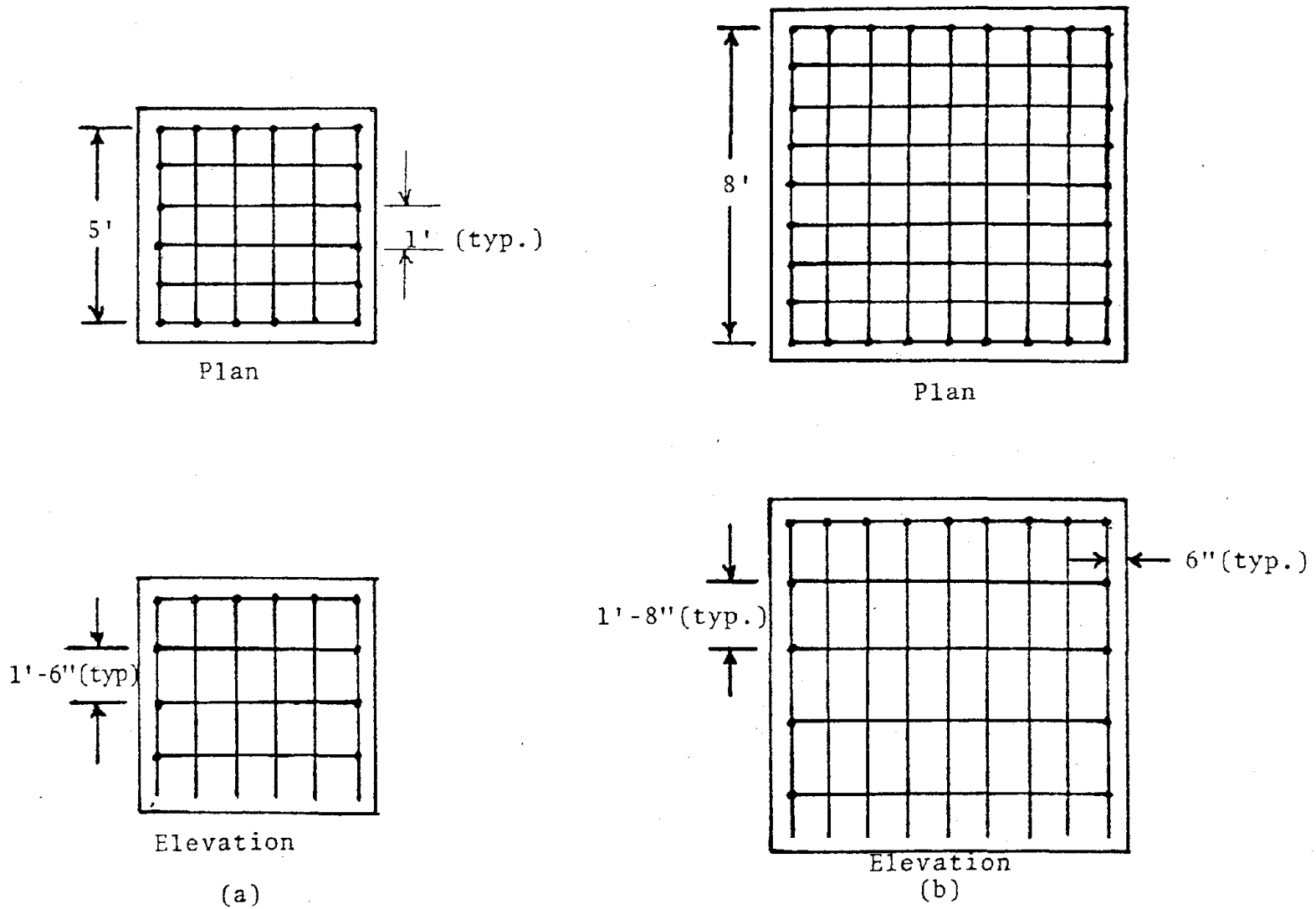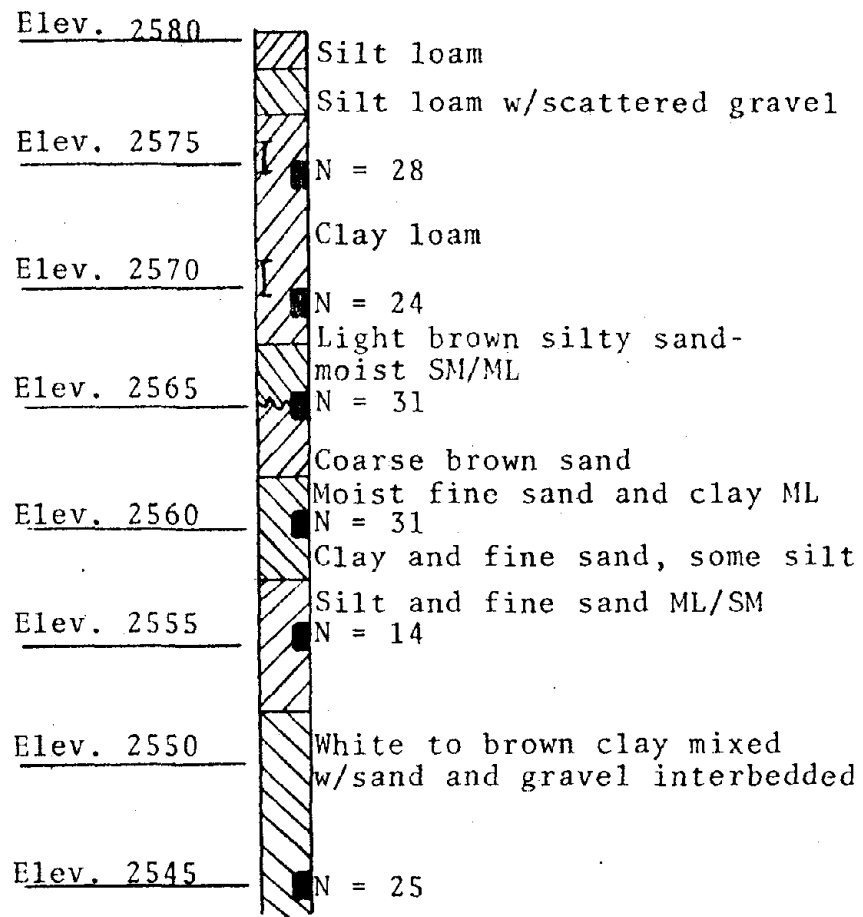
Fig.4.2.21--Steel reinforcement in reaction frame for (a) brace footings and (b) frame footings. Note: All reinforcement is #4 rebar.

Fig. 4.2.22 -- Boring log used to estimate soil properties
at reaction frame site

Problems with vibration transmission to existing buildings in the immediate area were not expected. This expectation was based on the relative weights of the footings and reaction frame, the properties of the soil, and the magnitude of the anticipated loads. The subject of vibration transmission is too broad to be discussed here. Notable books on the subject include those by Barkan (1962), Major (1962), and Harris and Crede (1961). During actual tests, an attempt to measure vibrations induced in adjacent buildings was made. An accelerometer was taken to various locations in the buildings, vibrations were monitored, and no measurable transmission of vibration could be detected.

### 4.2.5 General Comments and Capacities

In this chapter the concepts, criteria, techniques, and procedures used in the design of the reaction frame were described. In conclusion, the following general capacities relating to the reaction frame are presented for the reader:

1.  The total allowable moment for the reaction frame cross section is approximately 700 ft-kips. This value was determined from working stress design (AISC 1977), and the rigid frame knees were designed with this capacity in mind.

2.  The reaction points were designed for a maximum concentrated load of 115.5 kips; however, a greater capacity could be realized by increasing the bearing length of the load. If a concentrated load in excess of 115.5 kips is anticipated, each individual case should be analyzed for overstressing at the reaction points.

3.  The maximum axial compressive force for each brace member is 81 kips (AISC 1977), and the allowable tensile force is 310 kips.

4.  The concrete in the footings has a design compressive strength of 3000 psi (see Section 3.3). With this strength, the pullout capacity of each anchor bolt was calculated to be 370 kips.

For additional information, Thomas (1980) contains the specific design calculations, and the computer printouts used in the design.

## 4.3 EXPERIMENTAL STUDY

### 4.3.1 Description of Test Equipment

A testing program was conducted at the University of Idaho with the test facility shown in Fig. 4.3.1 and Photo 4.3.1. The facility represents the steel framing from one bay of a typical high rise building. The test frame, representing spandrel beams and columns, is made from four W8 x 35 steel beams formed into a rigid square frame (12' x 12'). The test frame is hung with 8" x 4" x 3/8" structural steel tubes which are pin connected to the glide strut as shown in Fig. 4.3.1. The glide strut is a W6 x 20 steel beam that is free to slide horizontally through the lubricated glide assembly shown in Fig. 4.3.2. The glide assembly is connected to the reaction frame at three locations as shown in Fig. 4.3.1. The outer connections provide reaction points for the test frame while the inner connection furnishes lateral support to the glide strut. Lateral support at the bottom of the test frame is provided by four ball bearing lateral support glides (Fig. 4.3.3) which were designed to allow free movement in the plane of the test frame.

A hydraulic load actuator is mounted between the reaction frame and the end of the glide strut. The actuator dynamically displaces the glide strut, thus displacing the test frame. Loads are automatically controlled by an MTS control console to cause the displacement specified by the test operator.

Precast concrete panels are hung on the test frame, emulating the various ways in which these types of panels
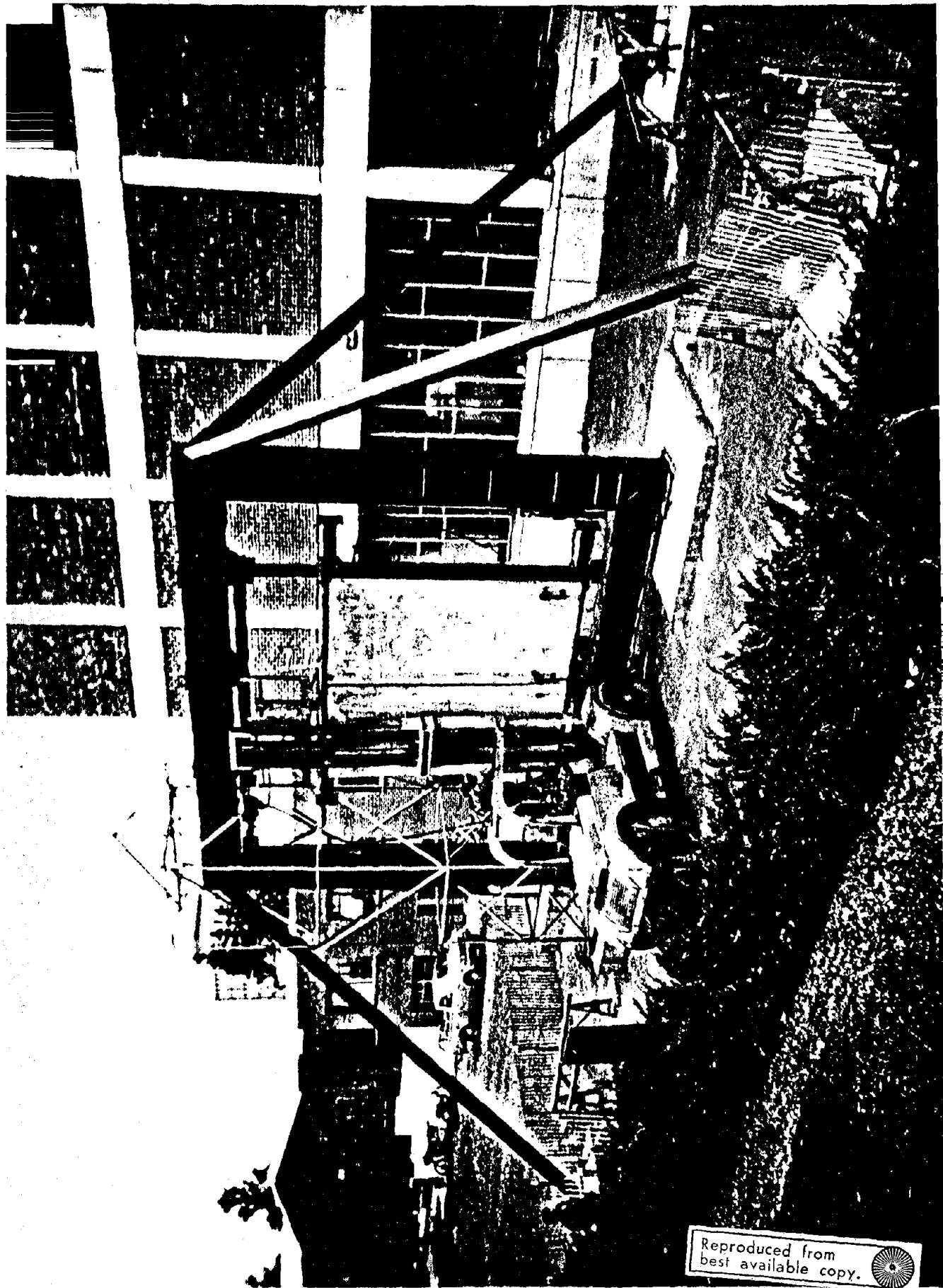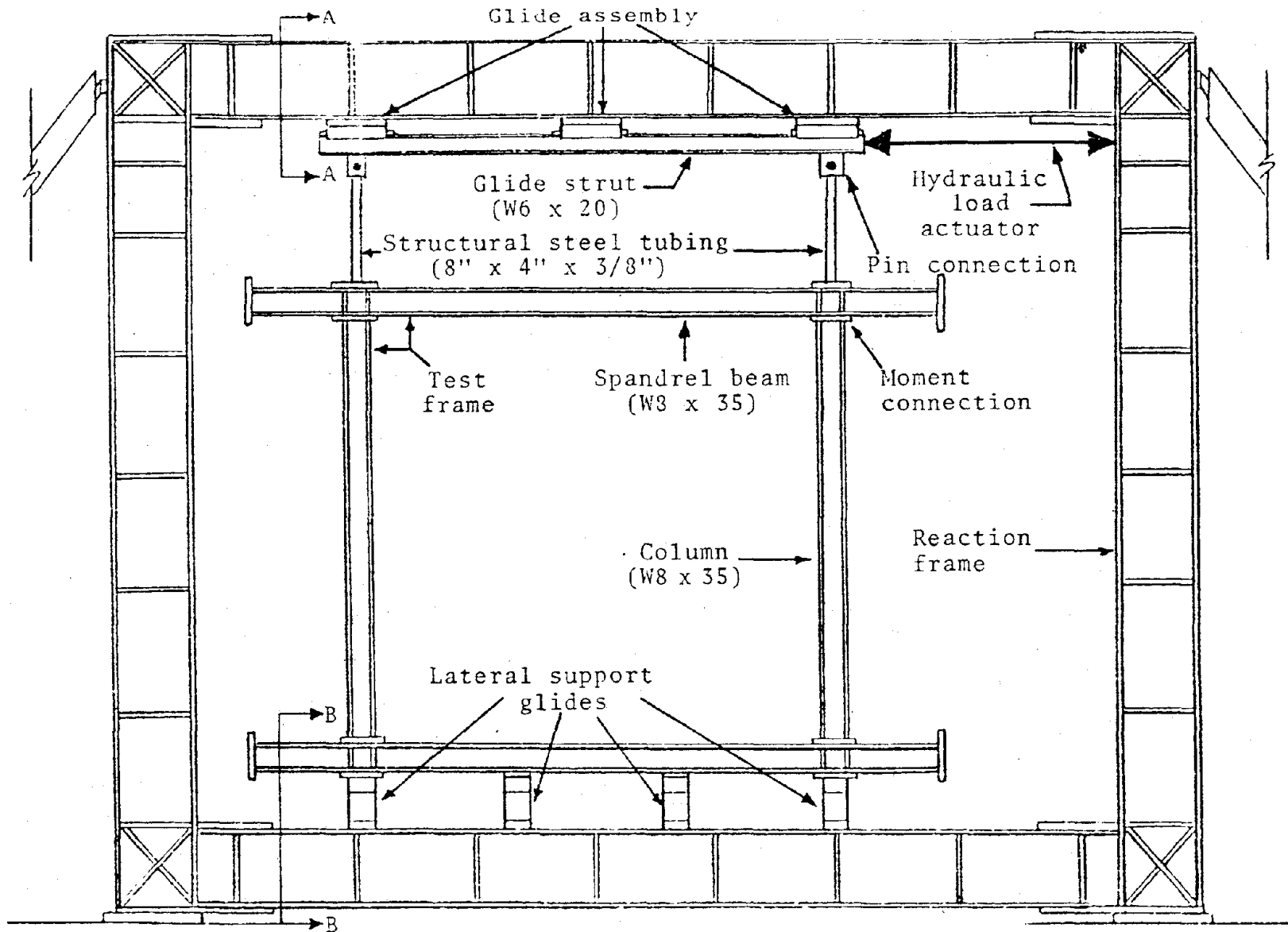
Photo 4.3.1  Test Facility With Assemblage Installed.

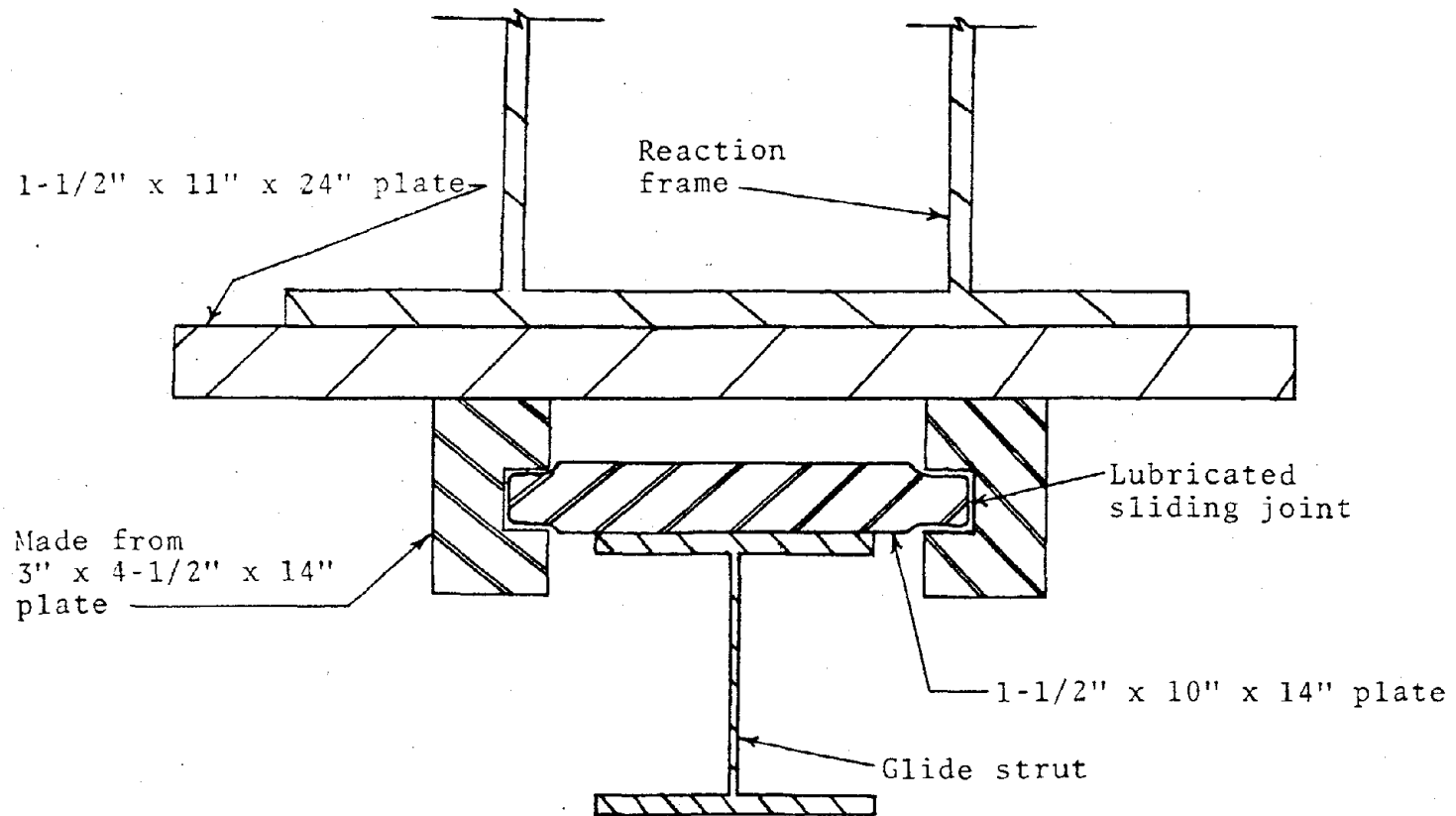Fig.4.3.1--Test facility representing steel framing in one bay of a high rise building

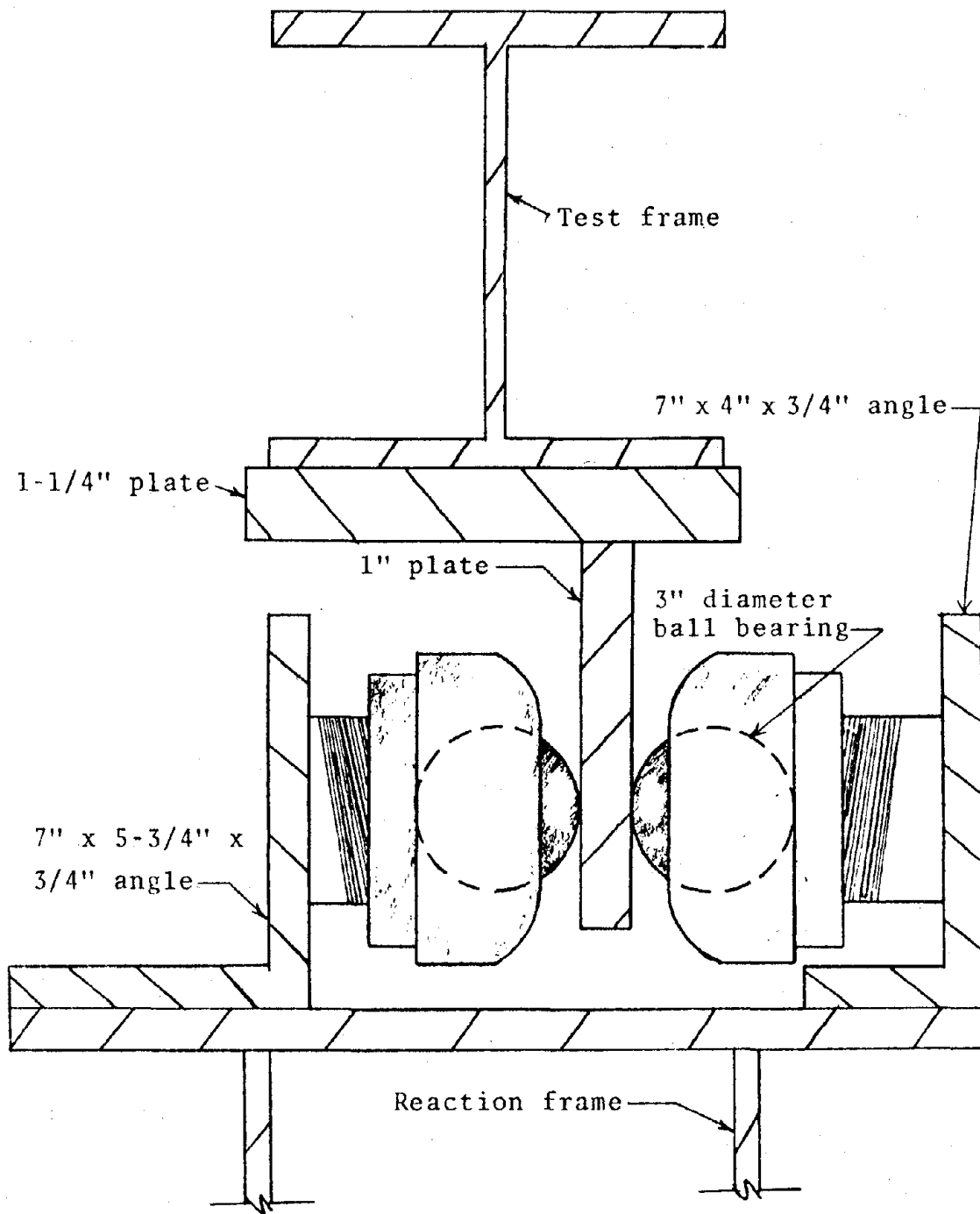Fig. 4.3.2-Detail showing lubricated glide assembly; Section A-A in Fig. 4.3.1

Labels in figure:
1-1/2" x 11" x 24" plate
Reaction frame
Lubricated sliding joint
Made from 3" x 4-1/2" x 14" plate
1-1/2" x 10" x 14" plate
Glide strut

Fig. 4.3.3--Detail showing lateral support glide system;
Section B-B in Fig. 4.3.1.

Steel
rods
(3/4")

6' x 12' Concrete
panels

Bearing
angles
(8"x4"x
1/2")
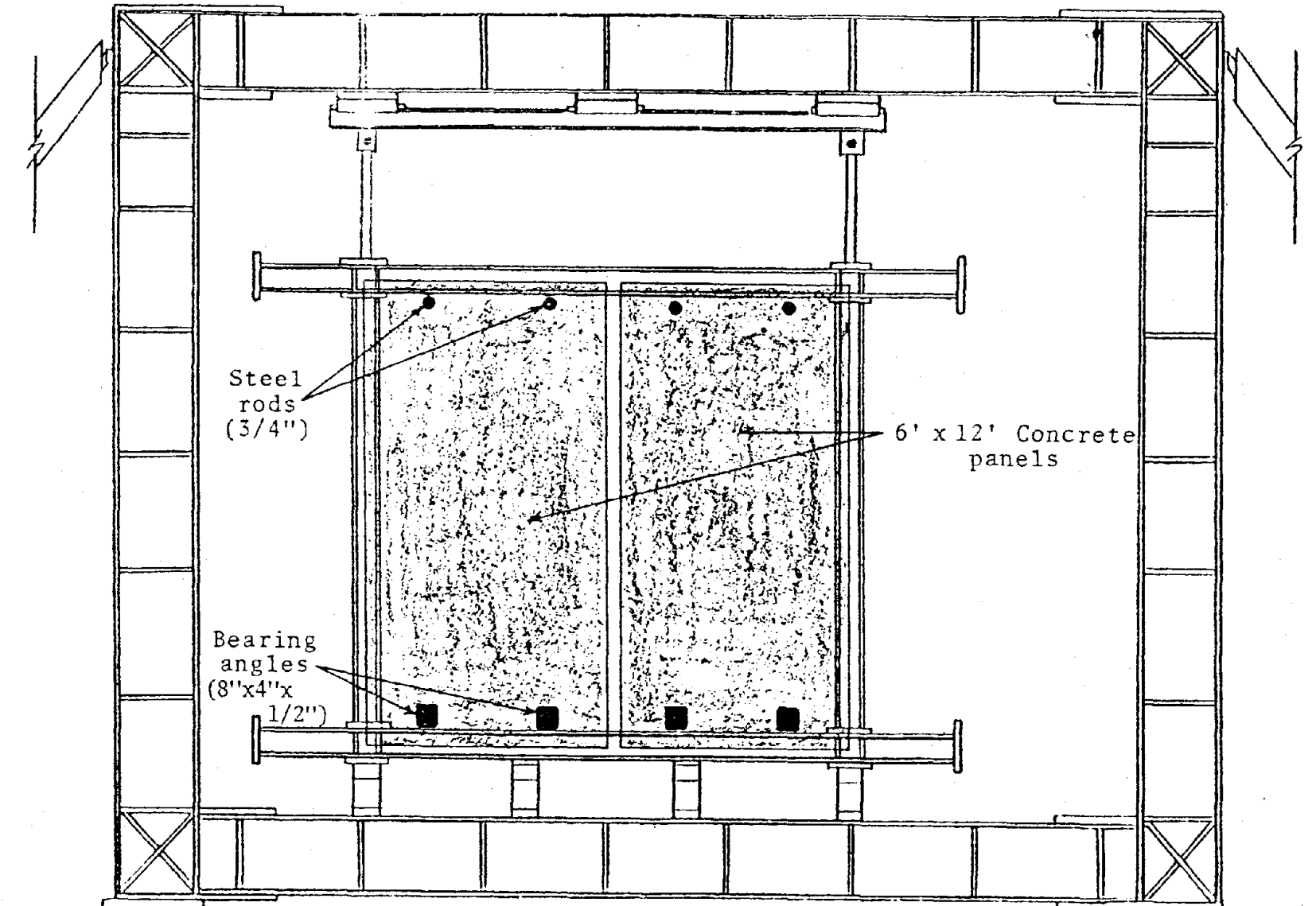
Fig.4.3.4--Test configuration used in the experimental study of the reaction frame

are used in high rise buildings. The test configuration used
in this study is shown in Fig. 4.3.4. Two 6' x 12' panels
are mounted on the test frame, each connected at four locations
as shown. The weight of the panels is supported by 8" x 4"
x 1/2" bearing angles at the bottom, and the top connections are
3/4" diameter steel rods. Beers (1980) presented a summary of
other test configurations considered at the University of Idaho.

### 4.3.2 Data Collection and Analysis System

### 4.3.2.1 PDP 11 Microcomputer

A Digital Equipment Corporation (DEC) PDP 11V03-L
microcomputer is used for data collection and analysis. This
system is used to collect data from the seismic tests because of
its ability to sample dynamic data at very fast rates and then
process the data after it is collected. This microcomputer has
64K (K = 1024) bytes of CPU memory and is equipped with two
RX02 format diskettes (floppy disks) which contain 250K of
storage each. In a typical configuration, the left floppy disk
contains the RT11 operating system, plus all of the system
programs, while the right disk contains user programs (i.e. the
data collection and analysis programs discussed in Section 4.3.3).
The data that is collected from the seismic tests is stored on
the right floppy disk to later be accessed by the data analysis
programs.

## 4.3.2.2  KWV11 Programable Real-Time Clock

The KWV11 is a DEC programmable clock/counter that pro-
vides a variety of means for determining time intervals or count-
ing events. The clock has a resolution of 16 bits and can be
driven from any of five internal crystal-controlled frequencies
(100Hz to 1MHz), from a line frequency input or from a Schmitt
trigger fired by an external input. The KWV11 can be operated
in any of four programmable modes:  (1) single interval; (2)
repeated interval; (3) external event timing; or (4) external
event timing from zero base. For the seismic tests, the clock
is set at a rate of 100kHz (milliseconds), and the repeated
interval mode is used. When the clock overflows (e.g., if the
clock is set at a rate of ten milliseconds using the repeated
interval mode, this will occur when ten milliseconds have
elapsed after the clock interval began) the clock sets an
interupt which signals the A/D board to start sampling.

## 4.3.2.3  MP1216-PGA Analog to Digital Board

The MP1216-PGA Burr-Brown analog to digital (A/D)
board samples a DC voltage signal at specific intervals which
are set by the real-time clock, and then converts the signal to
a digital value. This unit is a 16 channel differential-ended
(user strapable as 32 single-ended) analog input system with a
software programmable amplifier with gains from one to 1024.
The input range is $\pm$10V for a gain of one, and $\pm$10mV for a
gain of 1024. The gain for each channel is set individually
allowing each channel to have a different gain which gives the
user flexibility, for instance, the accelerometer signal is

±250mV and the strain gage signal is ±10mV so both channels can be input simultaneously with this feature. The A/D board requires 370 s for each conversion; therefore, if the user is sampling only one channel, a sampling rate of 2500Hz is possible, but if the user is sampling 16 channels, then a sampling rate of approximately 150Hz per channel is possible. The MP1216-PGA is a 12-bit A/D converter which can be operated in either interrupt or polling mode. In the interrupt mode, when the conversion is complete, the A/D gates an interrupt "vector" onto the PDP 11 bus returning control to the microcomputer. In the polling mode, the microcomputer must periodically scan the "STATUS" Register of the A/D to determine if the conversion is complete. For optimization of time, the data collection of the seismic test data is carried out in the interrupt mode.

## 4.3.2.4  Sensor Types and Locations

All of the strain gages used are Micro Measurements 120 ohm gages, and measure the strain that occurs in their axis of orientation. Shaevitz Model 5000 HPA LVDT's with a linear displacement range of ±5in are used to measure horizontal displacements of the frame. A Kinemetrics VM-1 vibration monitor is used with a Kinemetrics FBA-3 triaxial force-balance 1 G accelerometer to measure the accelerations of the panel. The locations of the sensors are shown in Figs. 4.3.5 while a description of what each sensor measures, along with the name used for reference in this project is included in table 4.3.1.
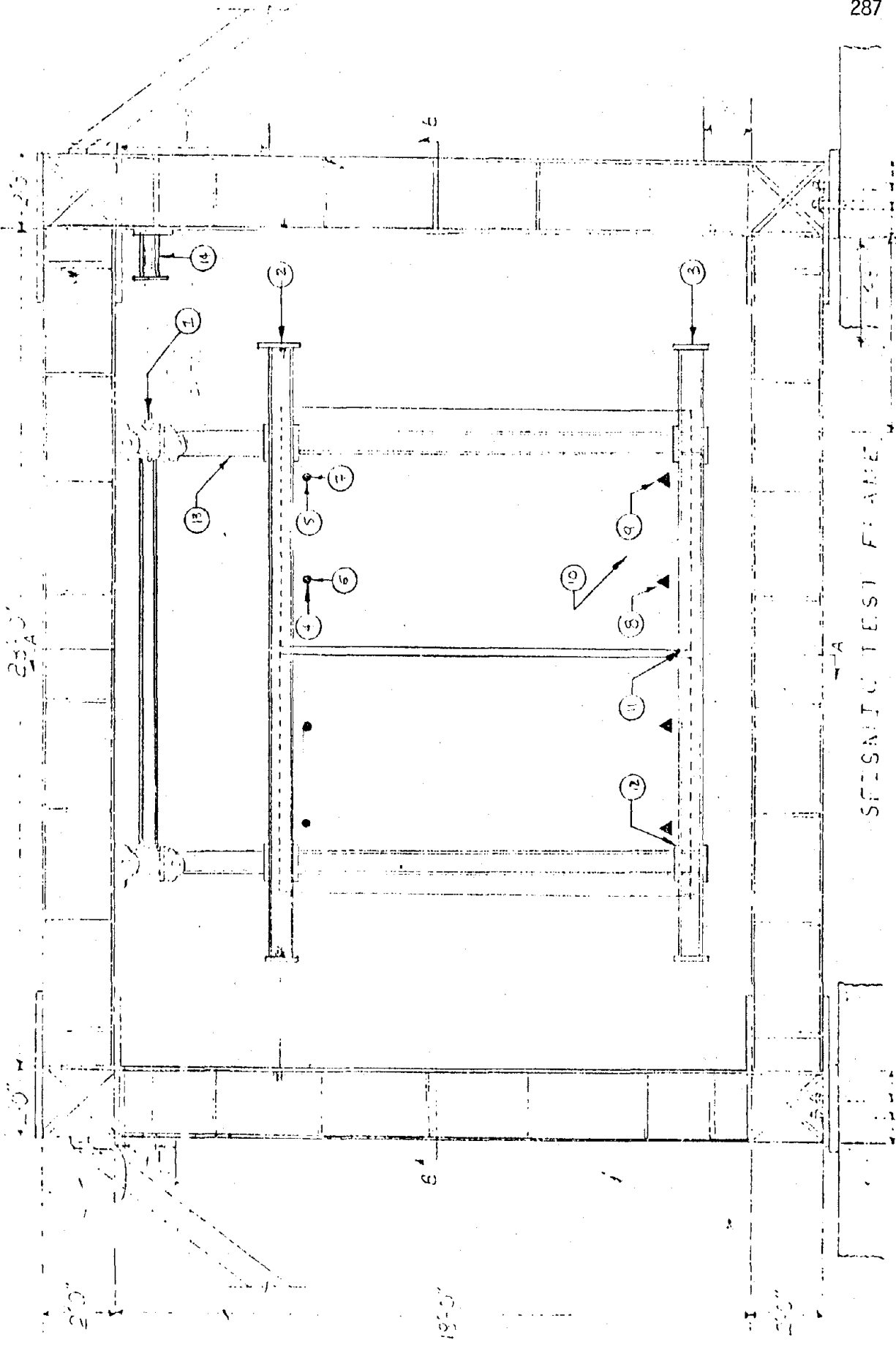
Figure 4.3.5  Location of Sensors

| SENSOR NUMBER | TYPE | QUANTITY THAT SENSOR MEASURES | PROJECT NAME |
|---|---|---|---|
| 1 | LVDT | Horizontal Displacement | Top LVDT |
| 2 | LVDT | Horizontal Displacement | Middle LVDT |
| 3 | LVDT | Horizontal Displacement | Bottom LVDT |
| 4 | STRAIN | Horizontal Bending (Rod) | Left Horizontal |
| 5 | STRAIN | Horizontal Bending (Rod) | Right Horizontal |
| 6 | STRAIN | Vertical Bending (Rod) | Left Vertical |
| 7 | STRAIN | Vertical Bending (Rod) | Right Vertical |
| 8 | STRAIN | Out-of-Plane Bending (Vert Leg) | Left Angle |
| 9 | STRAIN | Out-of-Plane Bending (Vert Leg) | Right Angle |
| 10 | ACC. | Horizontal Acceleration | Accelerometer |
| 11 | STRAIN | Vertical Bending | Back up Bottom C. |
| 12 | STRAIN | Vertical Bending | Back up Bottom Lt. |
| 13 | STRAIN | Horizontal Bending | Right Noodle |
| 14 | STRAIN | Axial | Glide Strut |

Table 4.3.1 DESCRIPTION OF SENSORS
Information Pertaining to the Various Sensors

### 4.3.3   Computer Software

The computer software involved is of two types:
(1) the data collection programs; and (2) the data analysis
programs.  The data collection main program is written in
FORTRAN with a subroutine written in DEC machine language
(MACRO).  This subroutine is written in MACRO since the real-
time clock and the A/D boards when driven in MACRO are approxi-
mately twice as fast as the FORTRAN instructions.  This is true
because there is not as much overhead involved.  That is, a
FORTRAN statement when converted results in several MACRO state-
ments to carry out the command;  however, these resulting MACRO
statements do not optimize time as efficiently as when the
program is initially written in MACRO.  It is very important
in data collection to minimize the time involved in running the
program.  This results in more time for the A/D board to make
conversions and allows faster sampling rates.  Computation time
is not as crucial in data analysis as in data collection;
therefore, the data analysis programs are all written in FORTRAN.

### 4.3.3.1   The Data Collection Programs

RIGHT1 is the name of the main program and CSTAR1 is
the MACRO subroutine that controls both the real-time clock
and the A/D boards.  A flowchart of RIGHT1 and its interaction
with CSTAR1 plus a listing of the programs and a user's guide
for the programs is contained in Wicher (1980).  The A/D
board samples the analog signals from the sensors which are in

the + 20 mV range; therefore, with 12-bit resolution, the full scale value of 40 mV is divided by 4096, resulting in an A/D resolution of 9.8 V. The analog signals are calibrated in inches/mV for the displacement sensors, and strain/mV for the strain sensors so the digital voltage values that are sampled can later be converted to displacement and strain, respectively. The sampled digital values are stored on the double density diskette (floppy disk). A double density diskette contains 974 blocks of storage, where one block is 513 bytes, allowing 256 interger values to be stored in one block. The programs designed for data acquisition and analysis require approximately 110 blocks of storage, resulting in 860 blocks of storage being available for sampled data. The data acquisition programs were designed to sample at 125 Hz per channel, and at this sampling rate there is approximately 110 seconds of storage on the floppy disk. The program is set up with a double buffered array so that samples are being stored in one buffer while the data in the second buffer is being transferred to the disk.

### 4.3.3.2  The Data Analysis Programs

The data analysis programs are of two types: (1) the Power Spectral Density (PSD) programs; and (2) the exceedance programs. The Power Spectral Density programs compute the PSD values according to standard procedures, and the Exceedance programs compute discrete strain or displacement levels and the number of times they are exceeded.

4.3.3.2.1  The Spectral Density Programs

All of the data analysis programs are written in
FORTRAN since the ease of writing the programs in FORTRAN (com-
pared to MACRO) outweighs the loss in computer efficiency.  A
flowchart of the PSD main program, the associated subroutines,
plus a listing and a user's guide for these programs is contained
in Wicher (1980).  The data is read from the disk by blocks,
the data for the first sweep is transferred into the appropriate
array, and then converted into the appropriate units, (i.e.,
units of strain for strain gages, and units of inches for the
displacement transformers).  The mean of the data is then
computed and subtracted out to remove any D.C. value than might
occur in the data.  This is done to avoid difficulties with the
spectral density becoming very large at zero frequency.  A
Hanning window is now applied to the data to smooth the result-
ing PSD spectrum.  The discrete Fourier transform of the data
is then computed with the aid of an FFT algorithm after the
discrete Fourier transform has been computed, the PSD values
can be generated as follows:

$$S(n/NT) = |X(f)|^2 \qquad (4.3.1)$$

where S(n/NT) is the PSD value, X(f) is the complex Fourier
coefficient, n is the number of the sampled point, N is the
total number of points sampled, f is the associated frequency,
and T is the sampling interval.  Consecutive PSD sweeps are

averaged successively to improve the accuracy of the PSD curve. The associated frequency $(\omega_n)$ at which the averaged PSD point occurs is calculated, and the PSD value and it s frequency are stored in a data file on the floppy disk to be either listed, or plotted later.

### 4.3.3.2.2  The Exceedance Programs

The exceedance programs are set up to measure the number of times strain and displacement values exceed a reference value.  A flowchart for the exceedance programs, plus a listing and a user's guide for the programs is contained in Wicher (1980).  The exceedance programs read the data for a given channel from the floppy disk and convert the data into the appropriate units.  The program then sets a reference value and checks to see how many data values exceed this value. Subsequently, the program sets a new reference value, which is an increment of ten higher than the previous reference value, and scans the data again for values exceeding this reference value.  Both the reference value and the number of times it is exceeded are stored on the floppy disk in a data file.

### 4.3.4  Experimental Results

### 4.3.4.1  Time-Displacement Functions

Two different time-displacement functions were used as excitation for the test frame facility.  A 2 Hz sine wave was input for a check of the Power Spectral Density (PSD)

program. The other time-displacement record that was input was the displacement history that occurred during the San Fernando Earthquake of February 9, 1971, on the 9th floor of the Jet Propulsion Lab as recorded by the Earthquake Engineering Center at the University of California, Berkeley. Figure 4.3.6 is a time-displacement plot of the 2 Hz sine input as it was recorded by the microcomputer. This plot is not a perfect sine wave, although two cycles per second does occur. The units of displacement are in 1/1000 of an inch; therefore, the discontinuties of the curve are only 5/1000 of an inch. The microcomputer sampling rate was not an even interval of 2 Hz and is the reason the record is not uniform. The seismic record was chosen since it exhibited high amplitudes in the absolute acceleration response spectra (Fig. 4.3.7) corresponding to experimentally determined natural frequencies of the test assembly (Table 3.4.1). Figure 4.3.8 is the actual displacement history input by the hydraulic system while Fig. 4.3.9 is the time-history record that the microcomputer recorded. The two records do not correspond exactly due to the hydraulic system's inability to follow the displacement history exactly.

4.3.4.2  Discussion of the 2 Hz Power Spectral Density Curves

The PSD curve for the left angle (Fig. 4.3.10) shows a small spike at 2 Hz and two larger spikes, one at approximately 5 Hz and the other at 7.5 Hz which is approximately the experimental second natural frequency of the test assembly. The

right angle PSD curve (Fig. 4.3.11) shows spikes 2 Hz, 3.5 Hz, and 7 Hz, with the largest spike at 3.5 Hz. Therefore, again both the forc ing function and the 2nd mode components show up and with the 3.5 Hz being the major component. The first mode of the frame is approximately 3 Hz, so due to the poor resolution of the PSD curve, the 3.5 Hz spike means that the first mode of the frame is being excited. For the left rod in horizontal bending, the PSD curve (Fig. 4.3.12) has the major spike at 2 Hz and a secondary spike at 3.5 Hz showing that the primary mode of the frame is again being excited. The horizontal bending curve of the right rod (Fig. 4.3.13) reflects the left horizontal bending with the magnitude of the 2 Hz component being larger. Both the left and right rods in vertical bending (Figs. 4.3.14 and 4.3.15) have the major spike occuring at 2 Hz, with the magnitude of the right vertical bending component being one and a half times larger than the left. The back-up frame bottom center curve (Fig. 4.3.16) shows spikes at 2, and 3.5 Hz and encompasses the frequencies between the two spikes. Back-up frame bottom left (Fig. 4.3.17) again shows spikes at 2, and 3.5 Hz with the larger magnitude occurring at 3.5 Hz. The right noodle, middle LVDT, top LVDT, and accelerometer curves (Fig. 4.3.18, 4.3.19, 4.3.20 and 4.3.21 respectively) show only one spike at 2 Hz. This provides a check for the PSD program because the top LVDT records the input and as shown by Fig. 4.3.6 is approximately 2 Hz.

### 4.3.4.3  Discussion of the Seismic PSD Curves

The seismic PSD curves are the result of the data
that was collected from the test frame facility which was ex-
cited by displacement history of the San Fernando Earthquake on
the 9th floor of the Jet Propulsion Lab.  Both the left and
right angle PSD curves (Fig. 4.3.22 and 4.3.23) show major
spikes at 3.5 Hz, 7.5 Hz, and 14.5 Hz with the 3.5 Hz spike
being the largest in magnitude.  The fourth analytical natural
frequency of the test frame is 14.6 Hz.  The magnitudes of the
spikes of the left angle PSD curve are much larger than the right
angle.  The left rod and right rod horizontal bending curves
(Fig. 4.3.24 and 4.3.25) show a minor spike at 2 Hz with a
major spike at 3.5 Hz and encompassing the area inbetween.
Therefore, for this seismic record the majority of the energy
associated with both the left and right horizontal bending is
between these two spikes.  The PSD curve for vertical bending
(Fig. 4.3.26) of the left rod has only one major spike which
occurs at 3.5 Hz, while the curve for vertical bending of the
right rod (Fig. 4.3.27) shows a major spike at 2 Hz and a
slightly smaller spike at 3.5 Hz.  Furthermore, this 2 and 3
Hz combination is present in both the back-up frame bottom
center and bottom left curves (Fig. 4.3.28 and 4.3.29).  The
major spike is 2 Hz for the bottom center channel while
3.5 Hz is the major spike for the bottom left.  The first mode
is the only component of the right noodle that is excited during
the seismic activity according to Fig. 4.3.30.  Both the middle

and top LVDT curves (Fig. 4.3.31 and 4.3.32) show the only major spike to be 2 Hz. This is very beneficial since it helps to explain the 2 Hz component which appears in the other curves. The 2 Hz component when it appears on the top LVDT curve means this is the frequency at which the majority of the energy input into the system occurs. The accelerometer curve (Fig. 4.3.33) has only one major spike which occurs at 3.5 Hz. The first mode of the frame is when the frame goes into single curvature, and since the accelerometer is located near the bottom of the panel, the first mode of the frame has been excited.

The PSD curves shown are not known to be the exact PSD curves of the data. To insure these curves are the exact curves, two changes should be applied to the PSD process: (1) different windows should be applied; and (2) different lengths of the window should be applied. A Hanning (Cosine) window was used in this analysis due to its popularity in structural dynamics situations. To insure that the Hanning window is indeed the window that should be used in this analysis other windows need to be applied to show which window gives the most desireable results. Each spectral window weights each data value differently; therefore, the shapes of the PSD curves due to different windows are different. One window may be the appropriate window to apply in seismic situations while another is the appropriate window to use in wind analysis. Other popular windows are: (1) Hamming; (2) parzen; (3) cosine; and (4) Half Cycle Sine. All of these windows should be applied to

the same data and then the window that produces the desired result should be used. Different window lengths need to be applied, because the length of the window controls the resolution of the resulting PSD curve. As an experiment, the PSD curve for the backup frame bottom left (Fig. 4.3.17) was shifted ahead by a quarter cycle. This was done to try to find the location of any hidden peaks due to poor resolution in the vicinity of 1 Hz. The two curves have the same general shape, suggesting that there are no hidden peaks. The resolution was then increased (i.e. the window length was increased) to approximately 0.5 Hz and a definite peak occurred at 0.5 Hz. Therefore, it shows that to ensure the presence of both frequency content and peak locations, different window lengths need to be applied.

4.3.4.4   Discussion of Exceedance Data

The exceedance analysis indicates the maximum values of strain and displacement that occurred during the tests and is very important because it shows if a rod has gone into the inelastic range. The exceedance information also indicates if the excitation was input at the appropriate amplitude by monitoring the exceedance value recorded by the top LVDT. The maximum value of each sensor for the San Fernando seismic excitation was recorded. The left rod in horizontal bending reached a stress value of 59 kips per square inch (Ksi), which is in the post yield range, while the right rod in

Figure 4.3.6  The 2 Hz Sinusoid
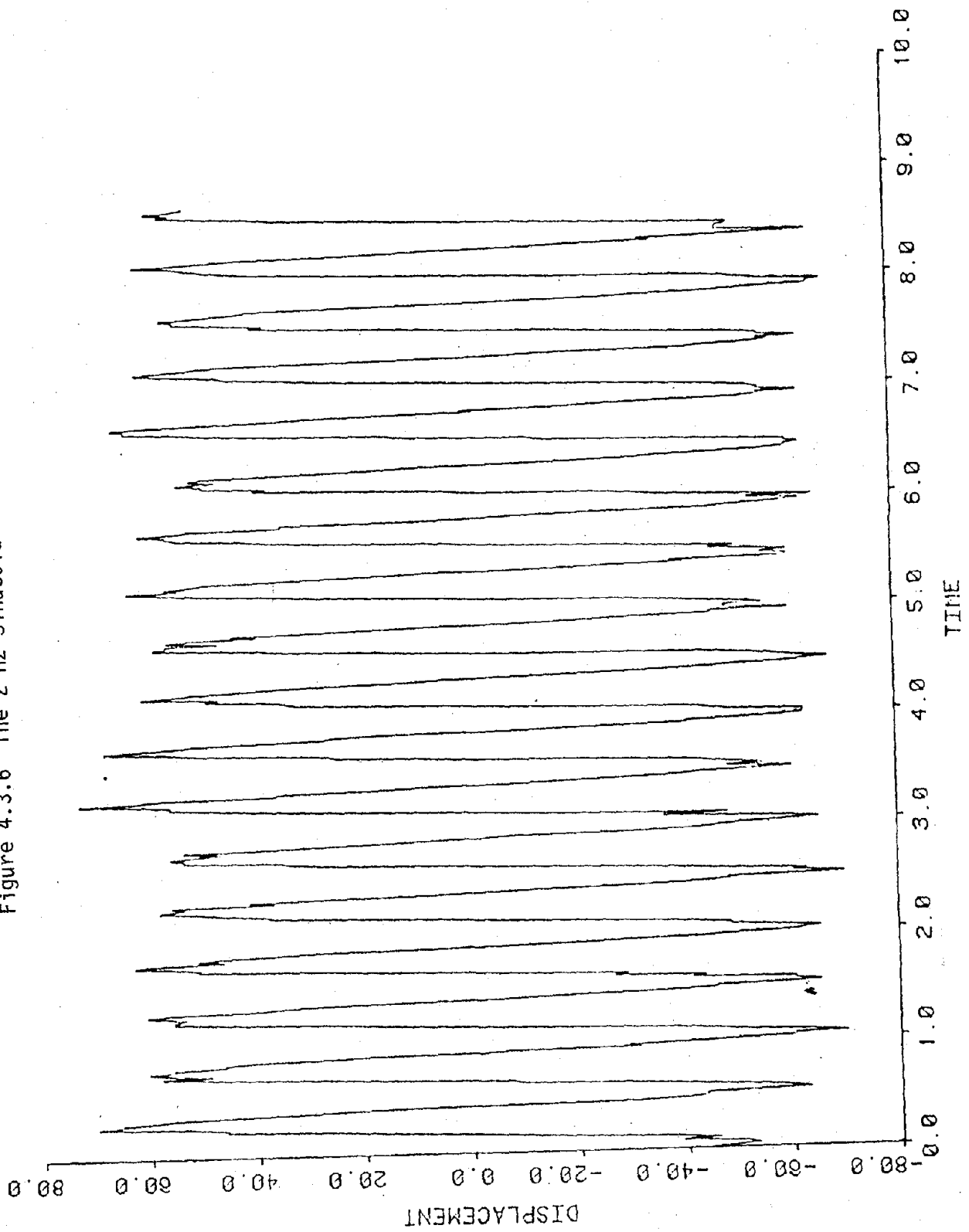
Figure 4.3.7  Absolute Acceleration Response Spectra, San Fernando
Earthquake - 9th Floor JPL (Record G111)

PERIOD (SEC)

ABSOLUTE ACC.
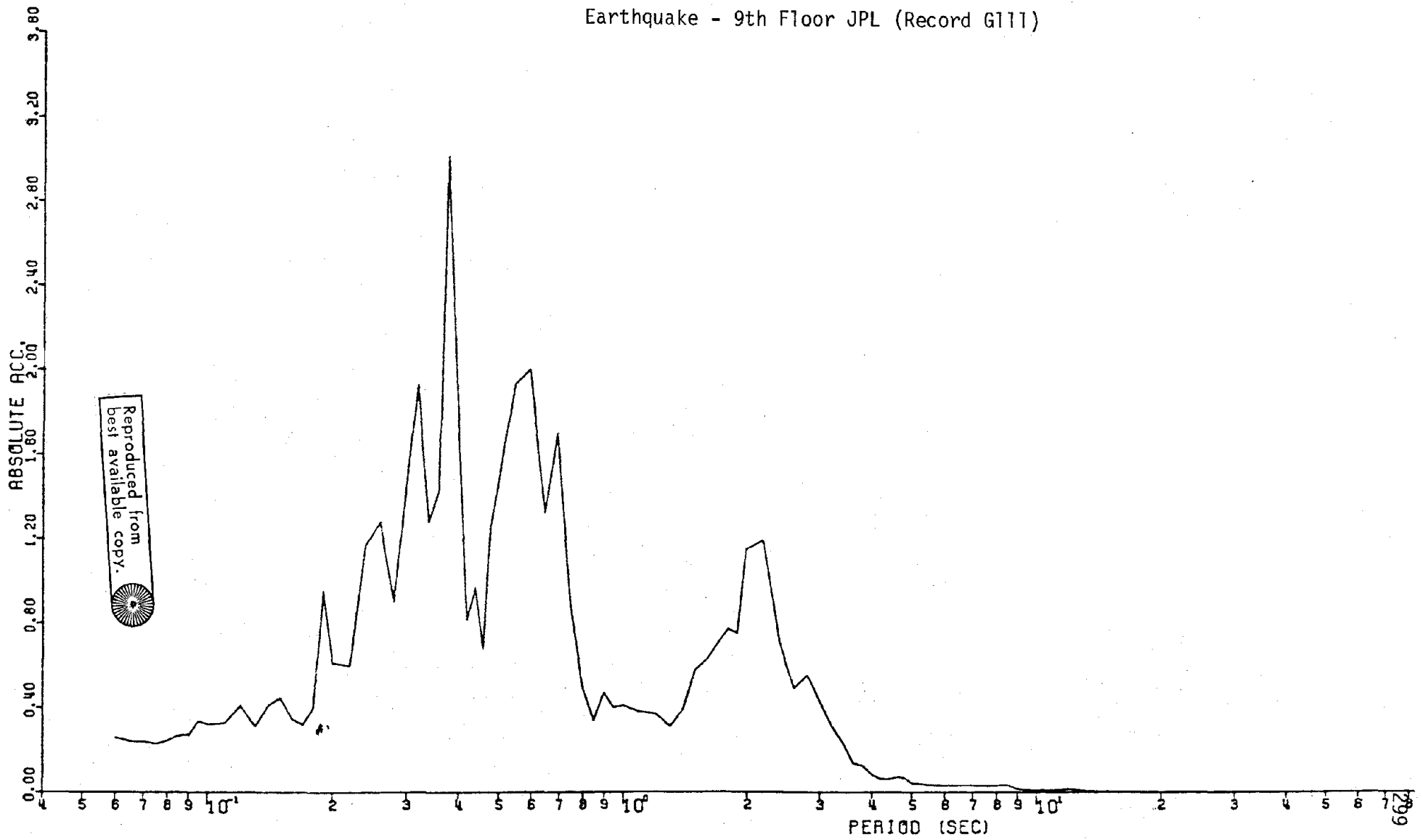
Figure 4.3.8  Experimental Hydraulic Input for Record G111

Figure 4.3.9  Time History Recorded for Record G111



DISPLACEMENT *10²

TIME
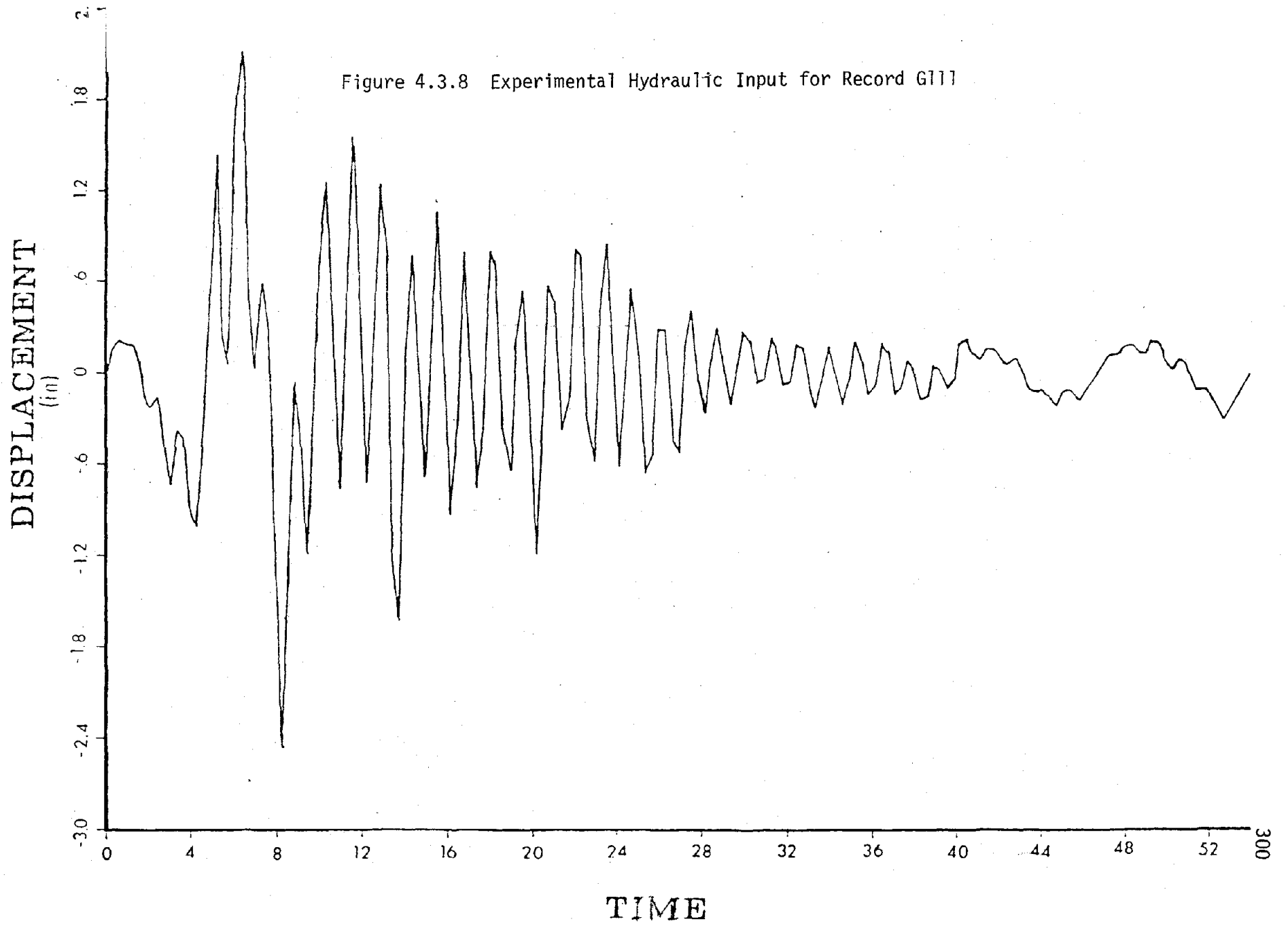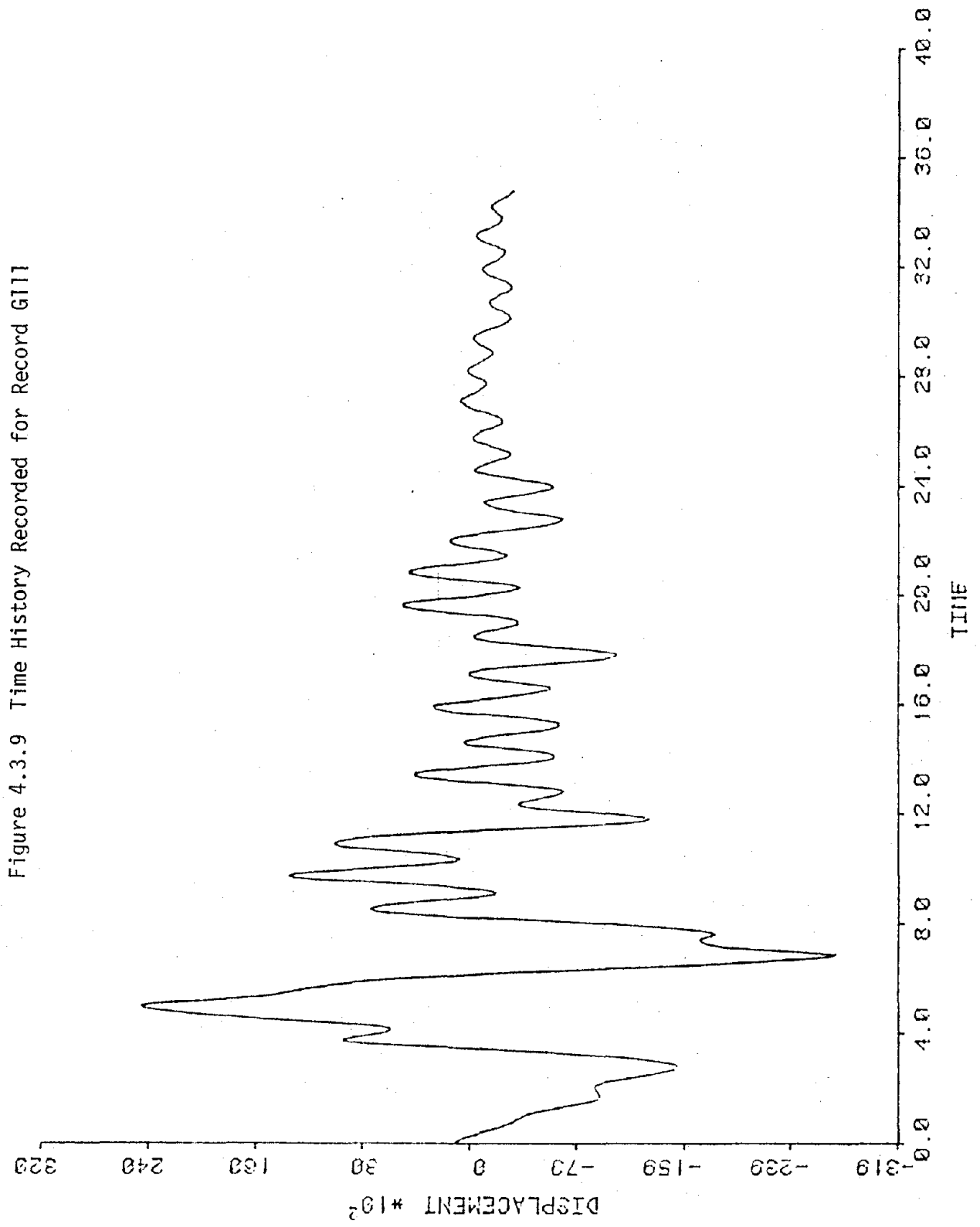
Figure 4.3.10  PSD - Left Angle - 2 Hz Input
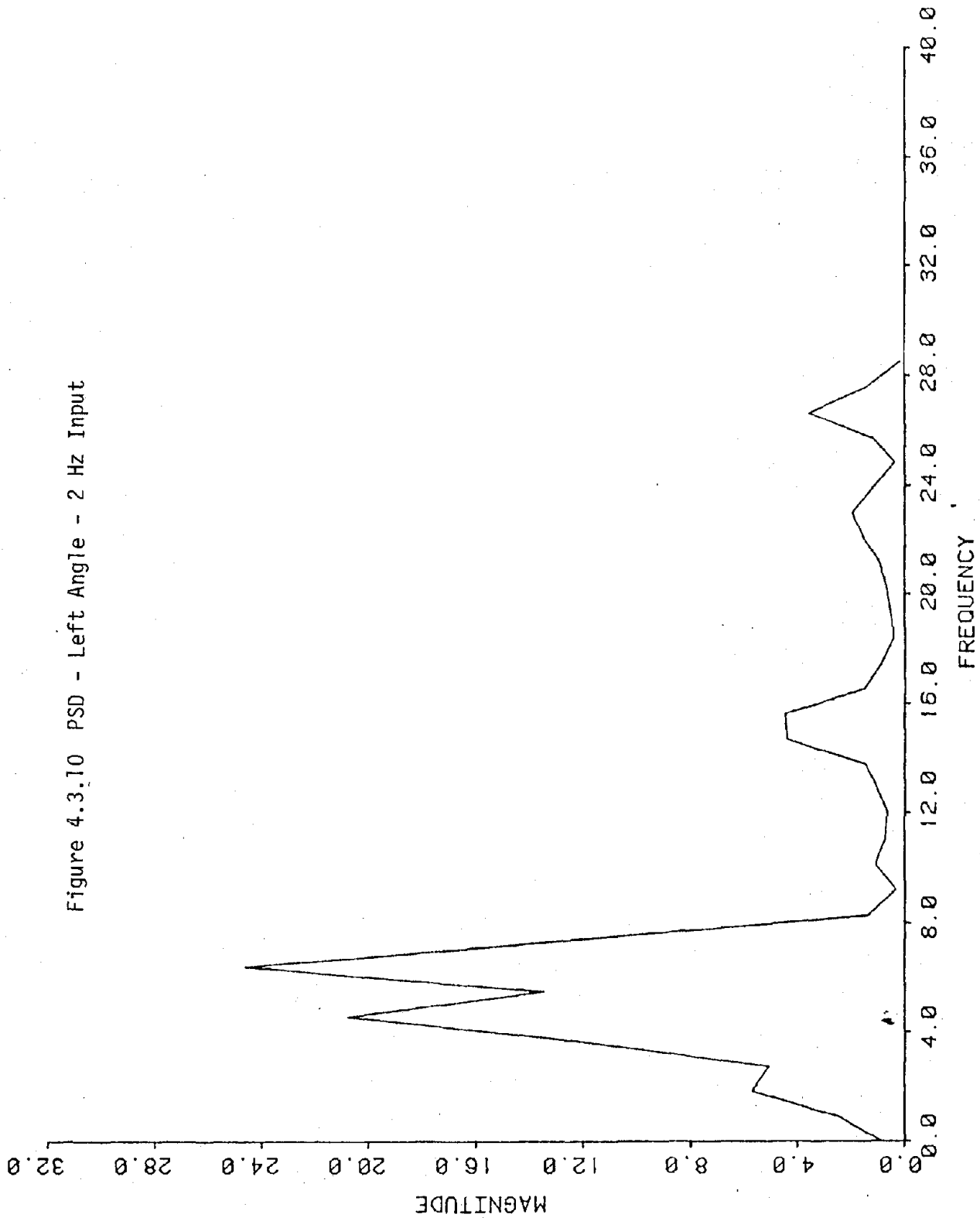
Figure 4.3.11  PSD - Right Angle - 2 Hz Input
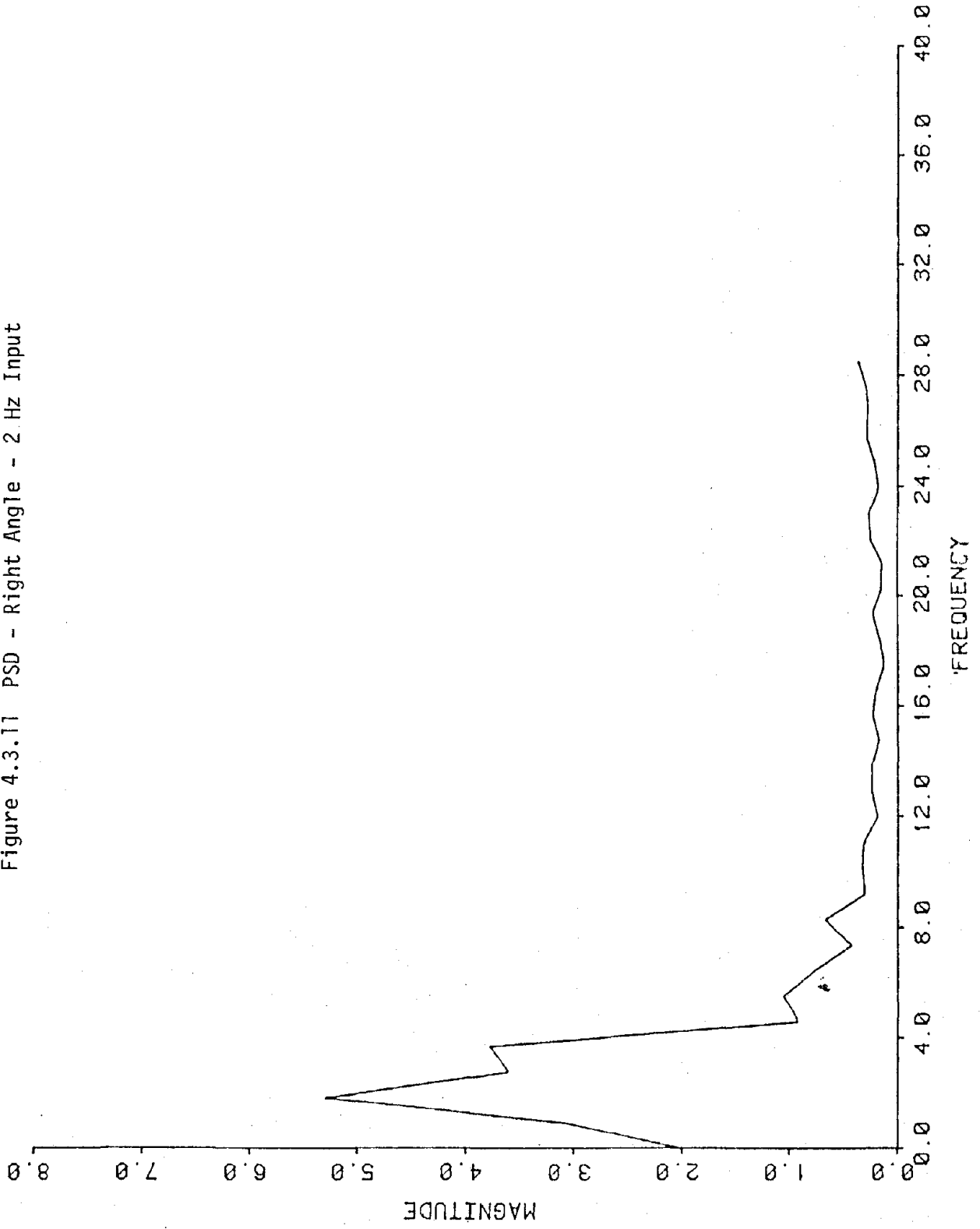
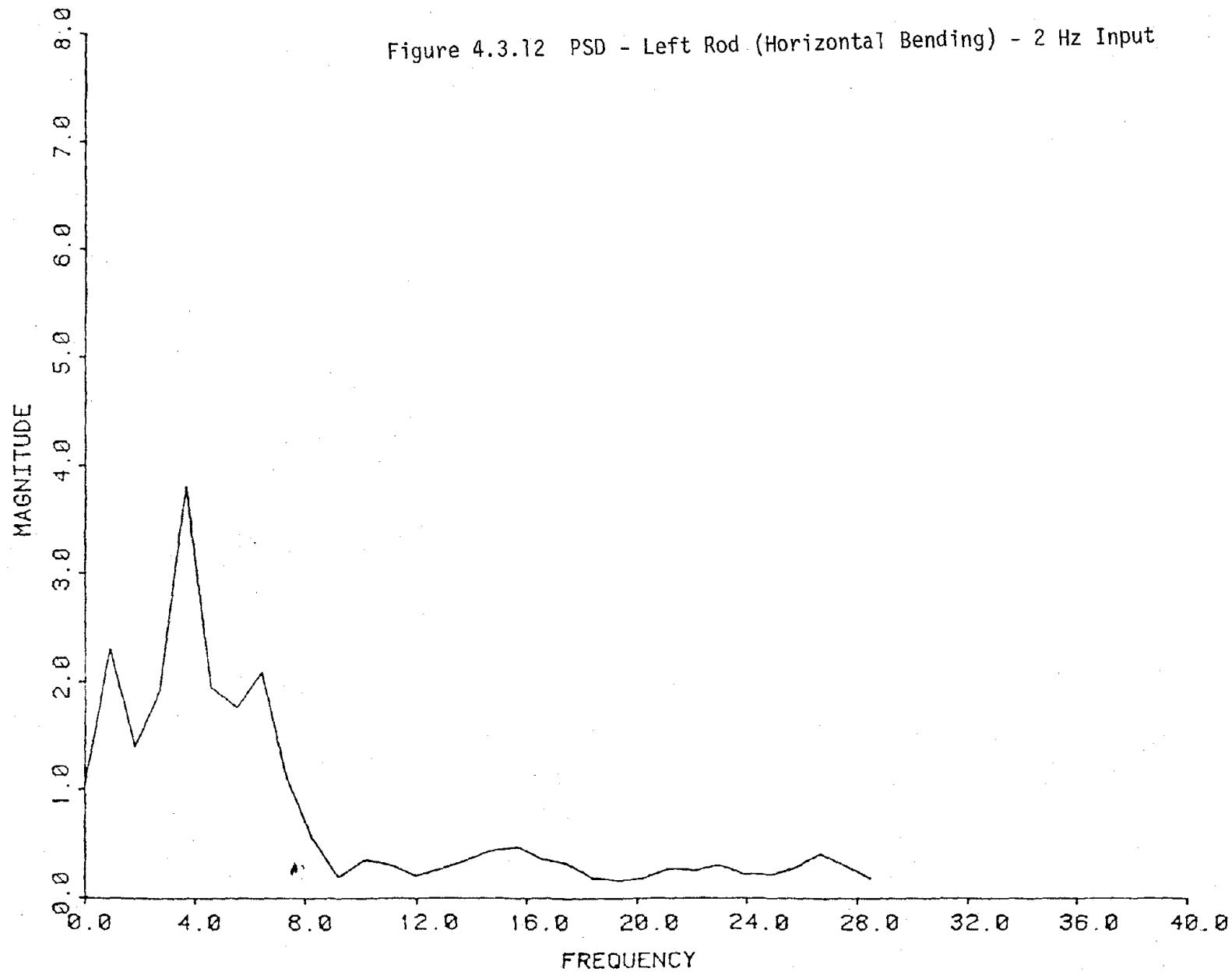Figure 4.3.12   PSD - Left Rod (Horizontal Bending) - 2 Hz Input

Figure 4.3.13  PSD – Right Rod (Horizontal Bending) – 2 Hz Input
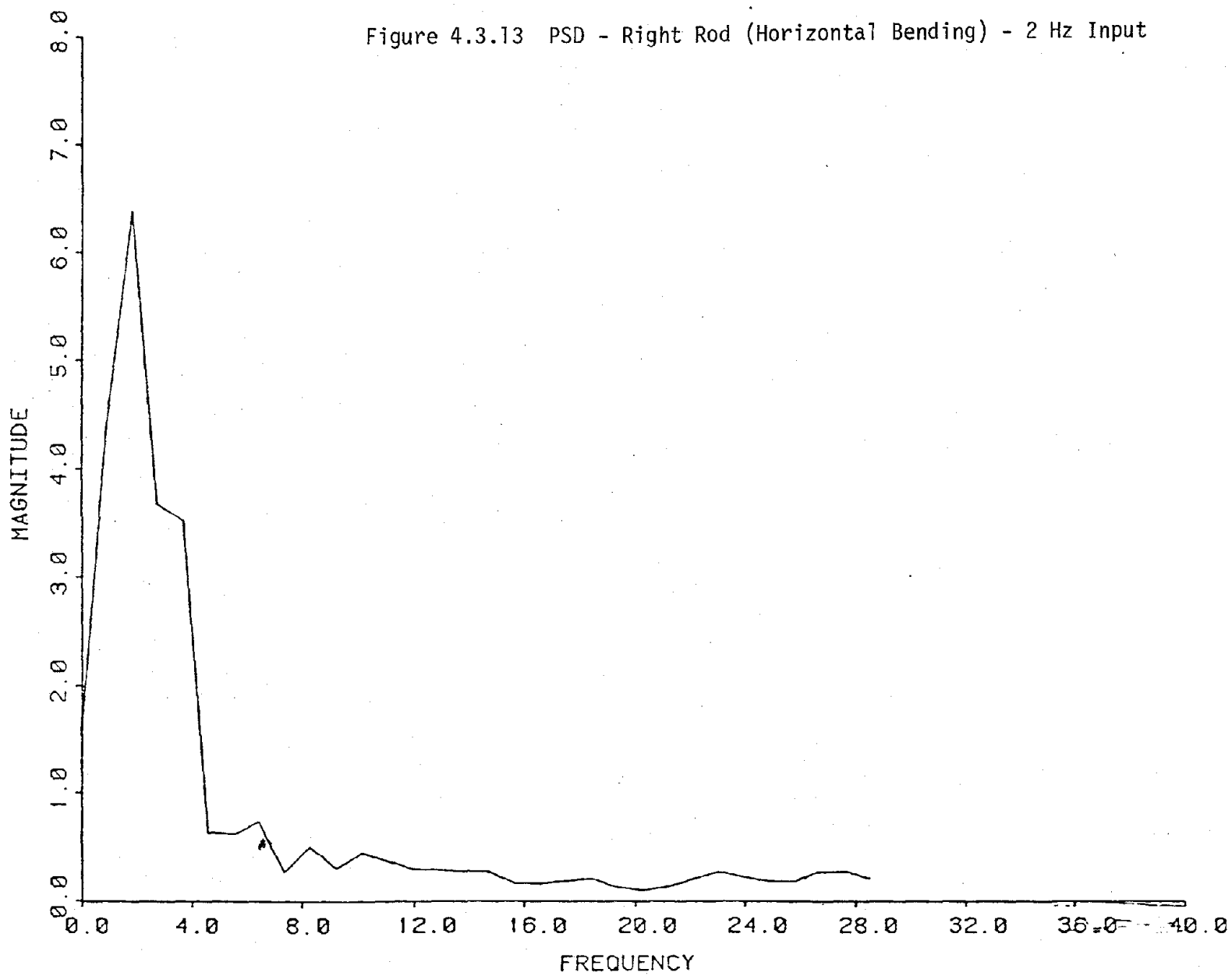
Figure 4.3.14  PSD - Left Rod (Vertical Bending) - 2 Hz Input
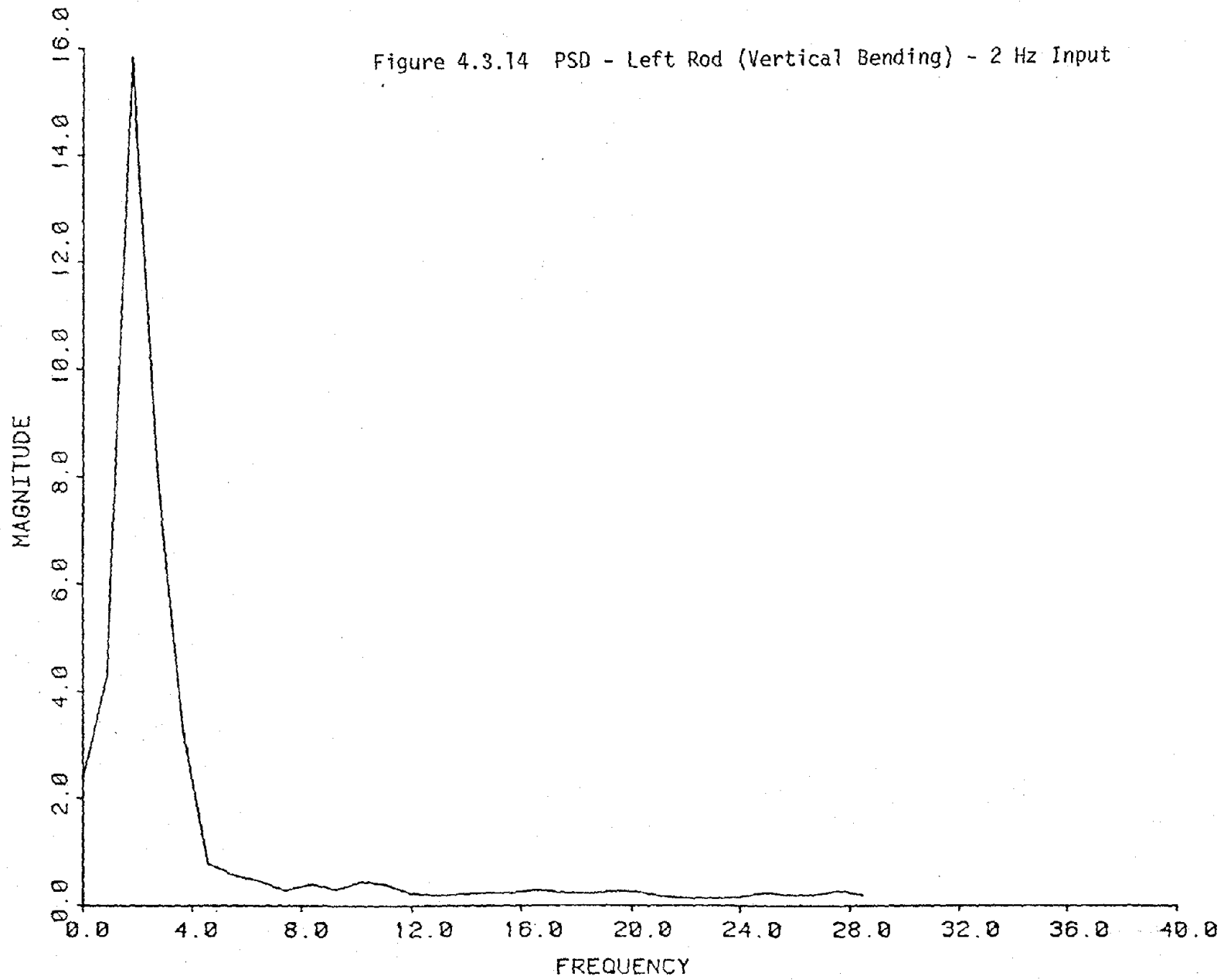
Figure 4.3.15  PSD - Right Rod (Vertical Bending) - 2 Hz Input
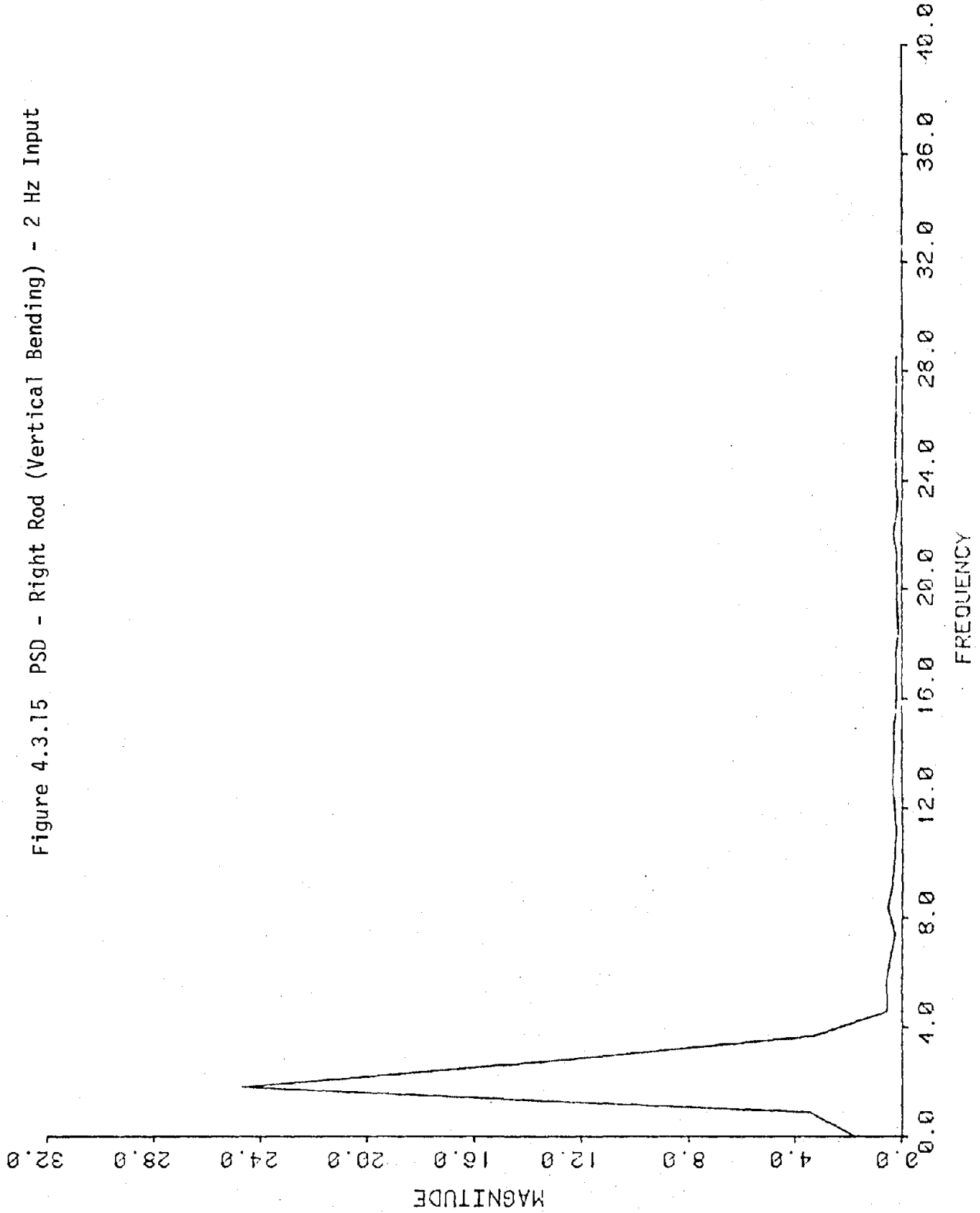
Figure 4.3.16 PSD - Backup, Bottom Center - 2 Hz Input
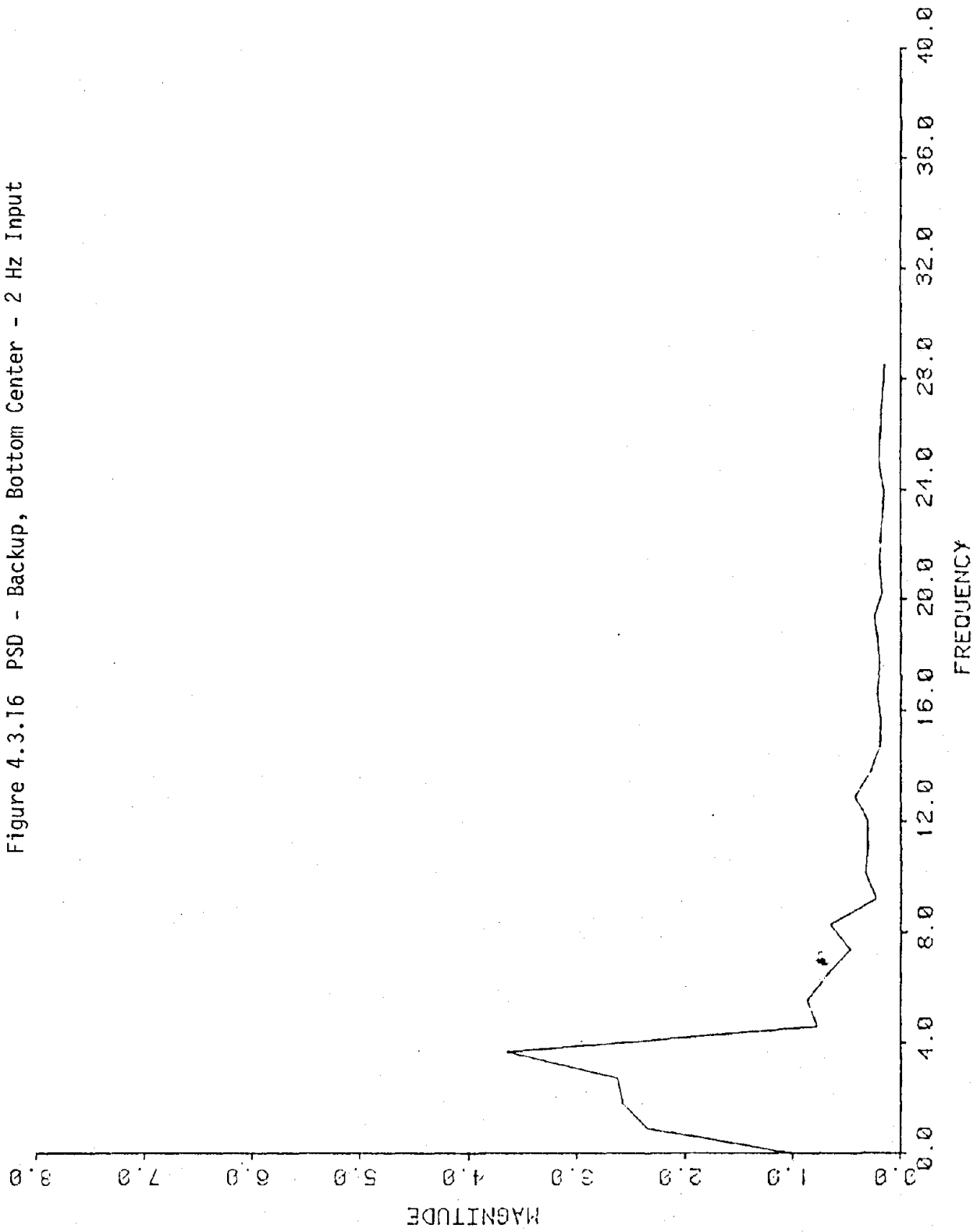
Figure 4.3.17   PSD - Backup/Bottom Left - 2 Hz Input
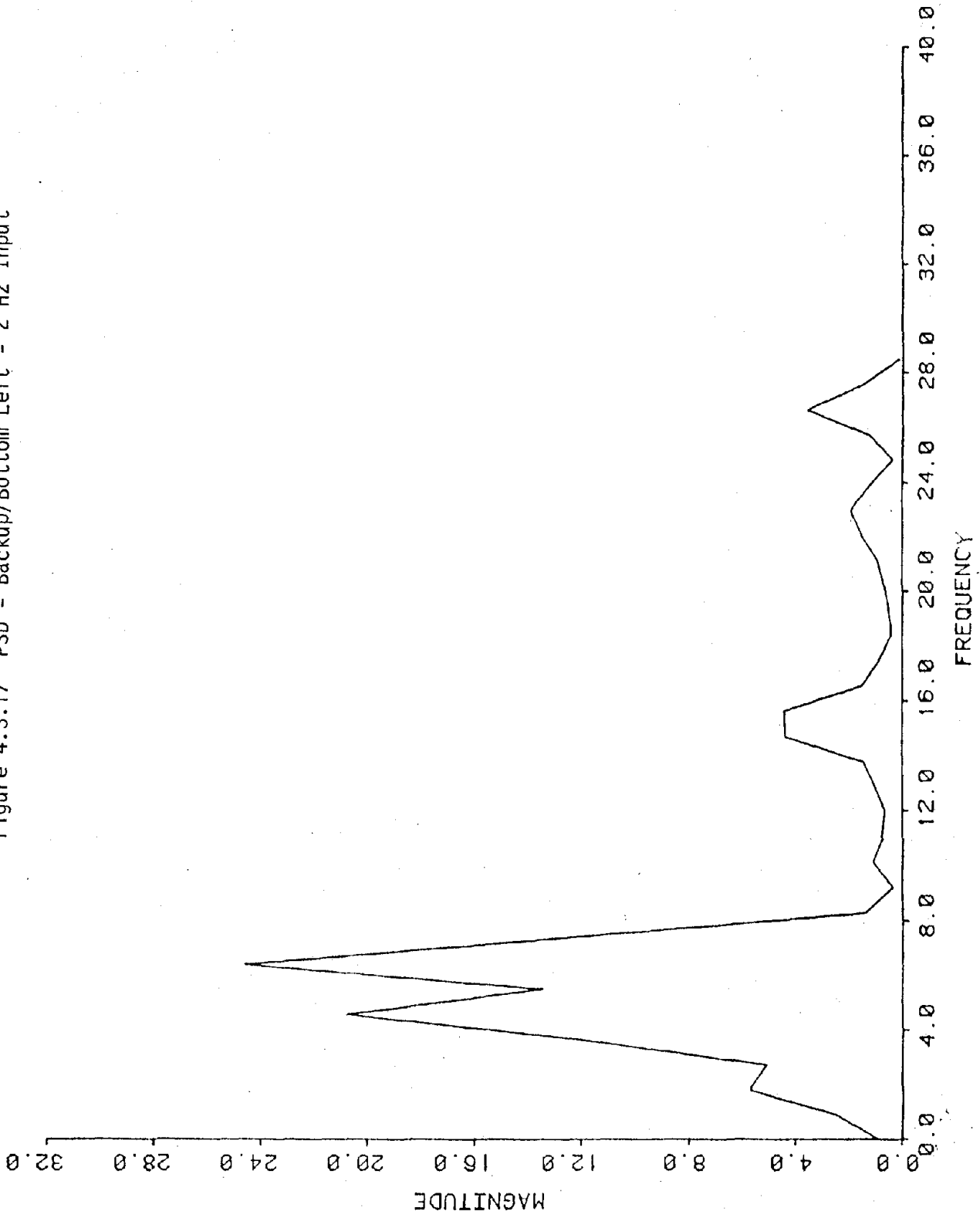
Figure 4.3.18  PSD - Right Noodle - 2 Hz Input



FREQUENCY

MAGNITUDE *10²
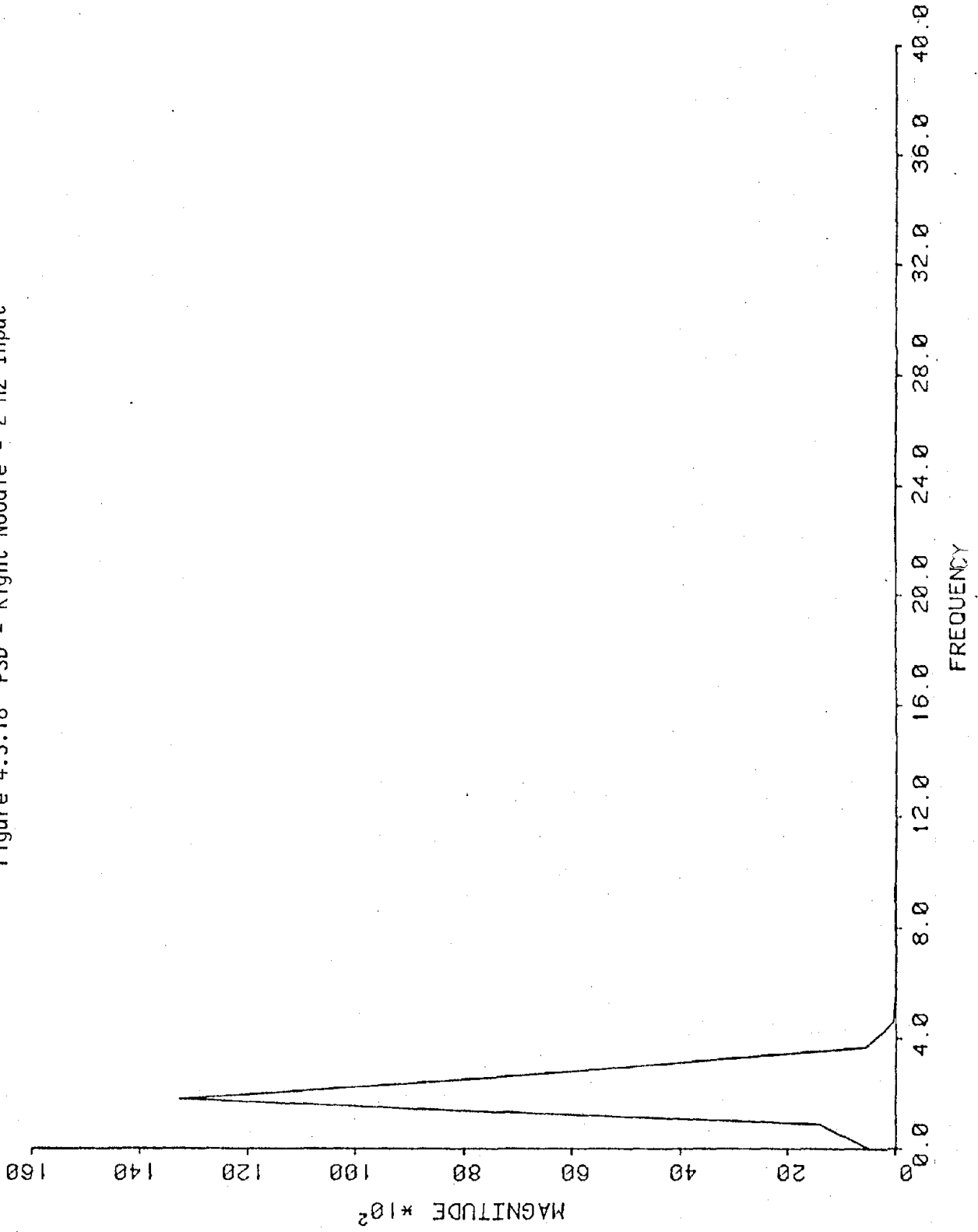
Figure 4.3.19 PSD - Middle LVDT - 2 Hz Input
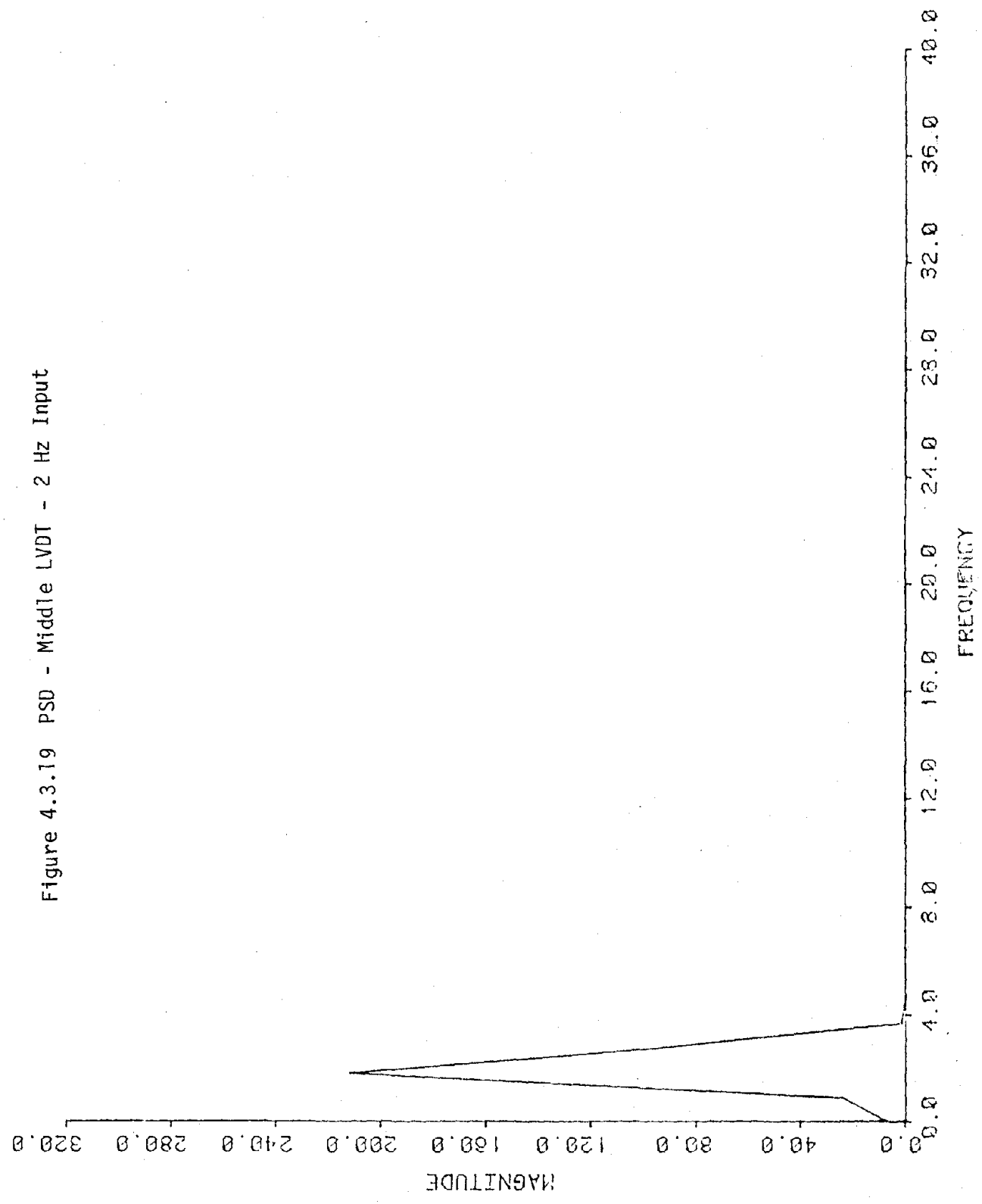
Figure 4.3.20  PSD - Top LVDT - 2 Hz Input



MAGNITUDE
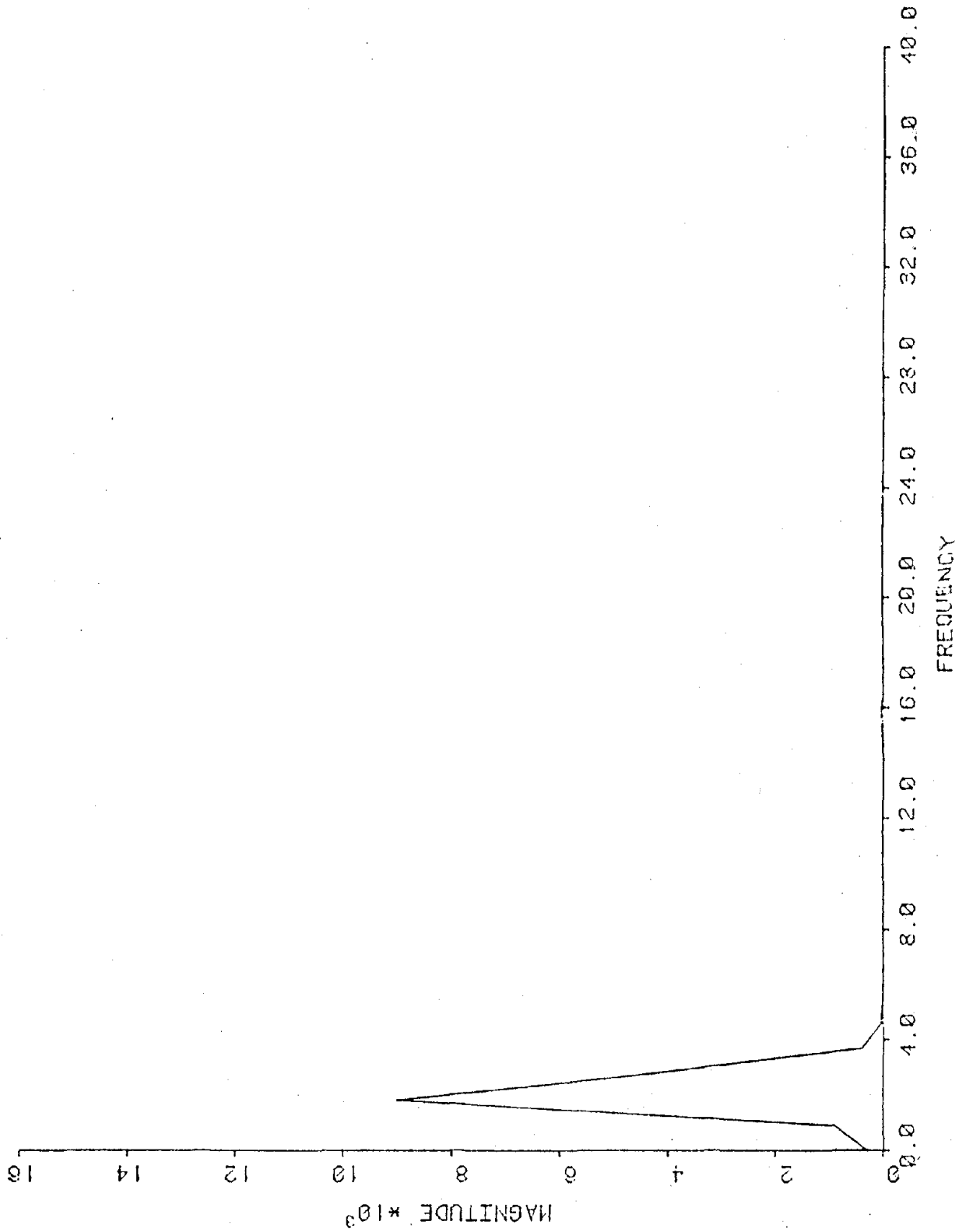
FREQUENCY
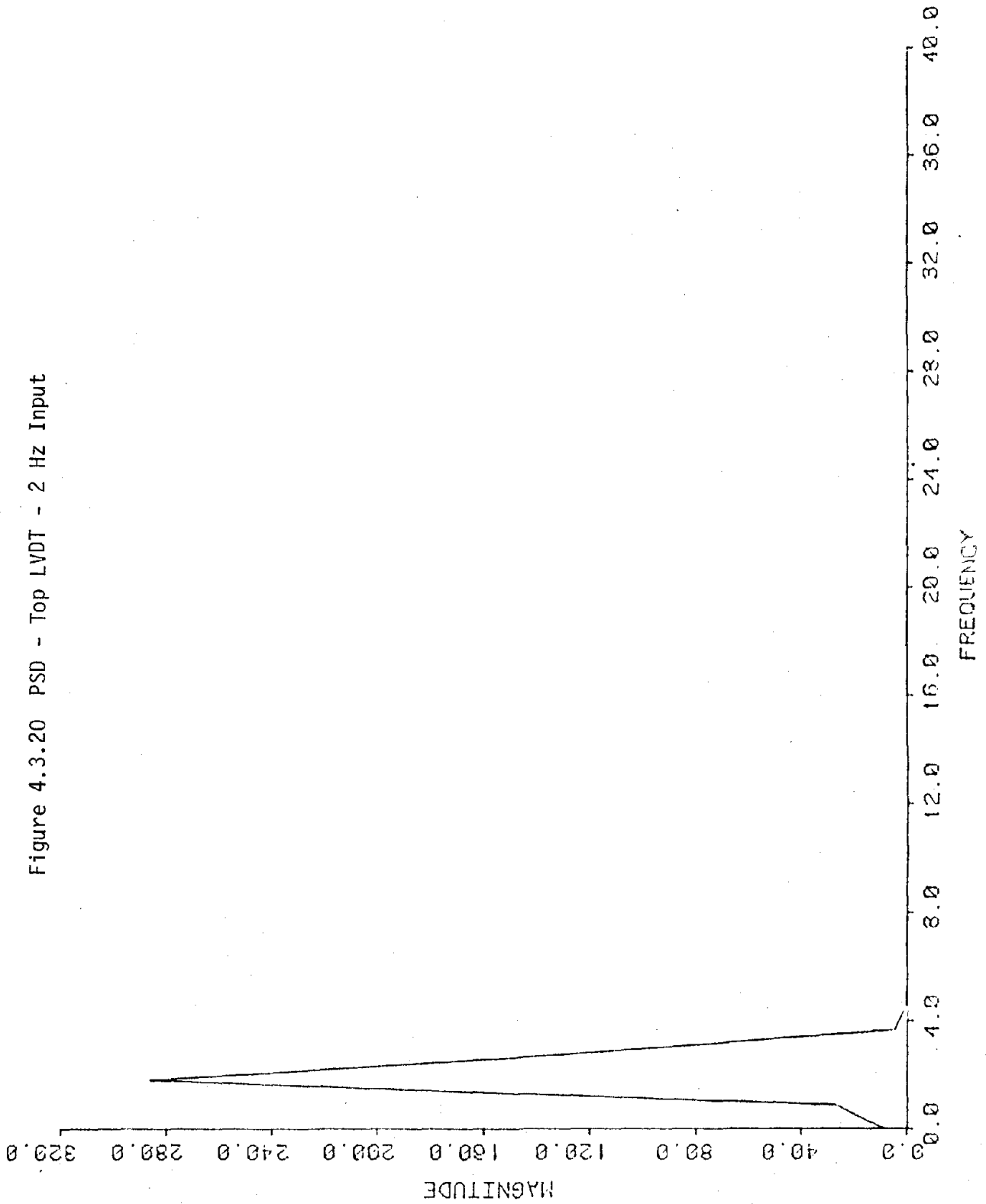
Figure 4.3.21  PSD - Accelerometer - 2 Hz Input

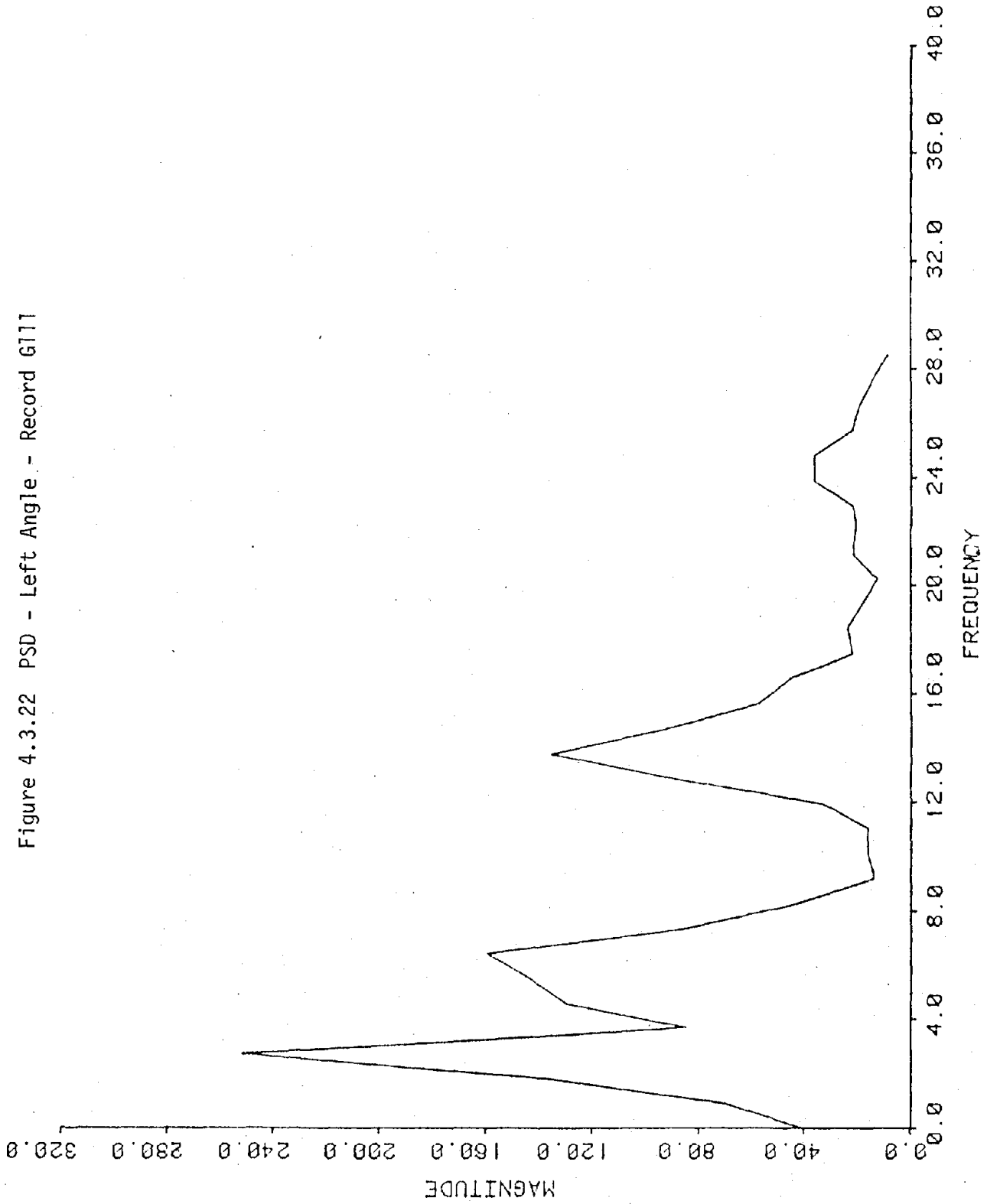Figure 4.3.22  PSD - Left Angle - Record G111

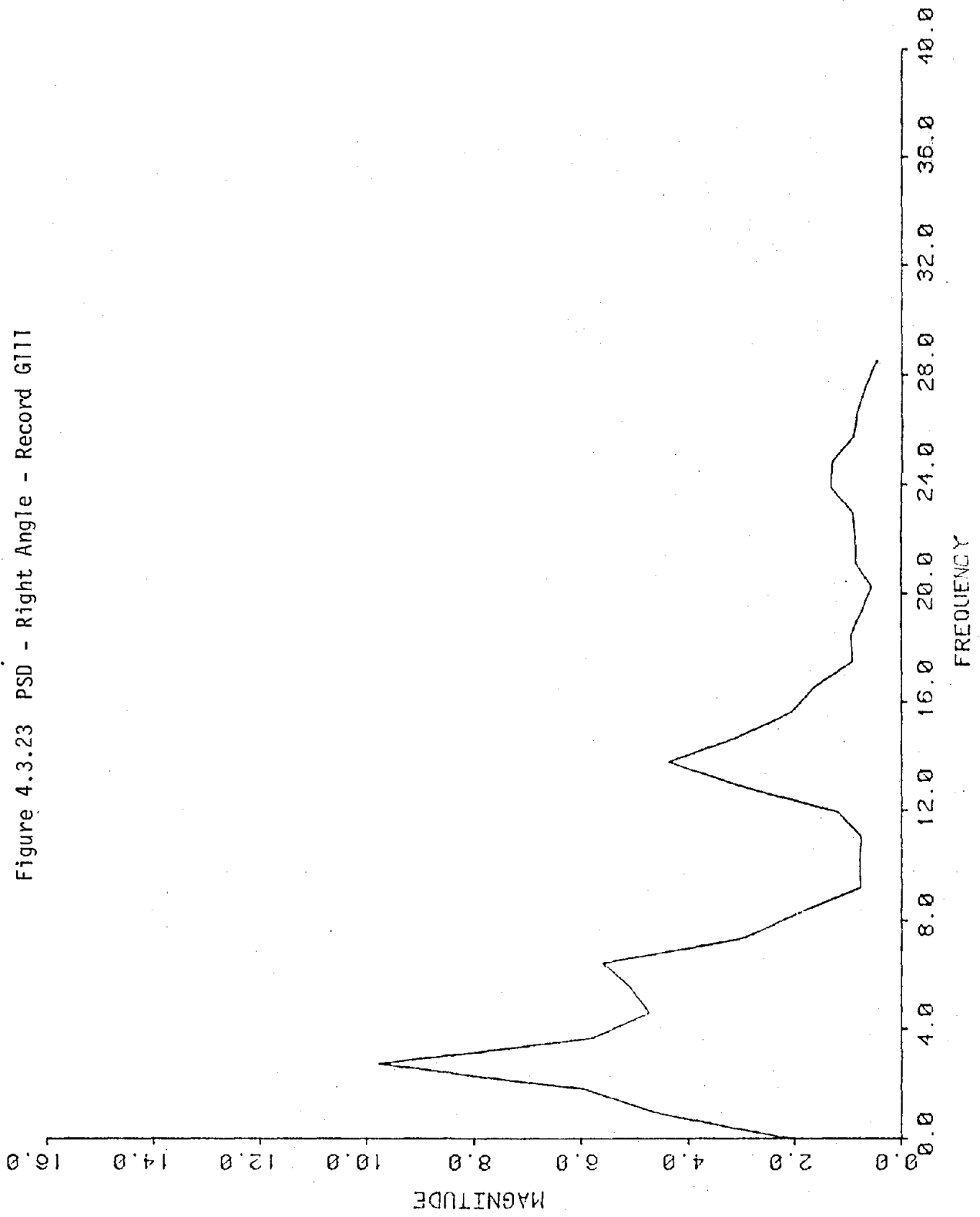Figure 4.3.23  PSD - Right Angle - Record G111

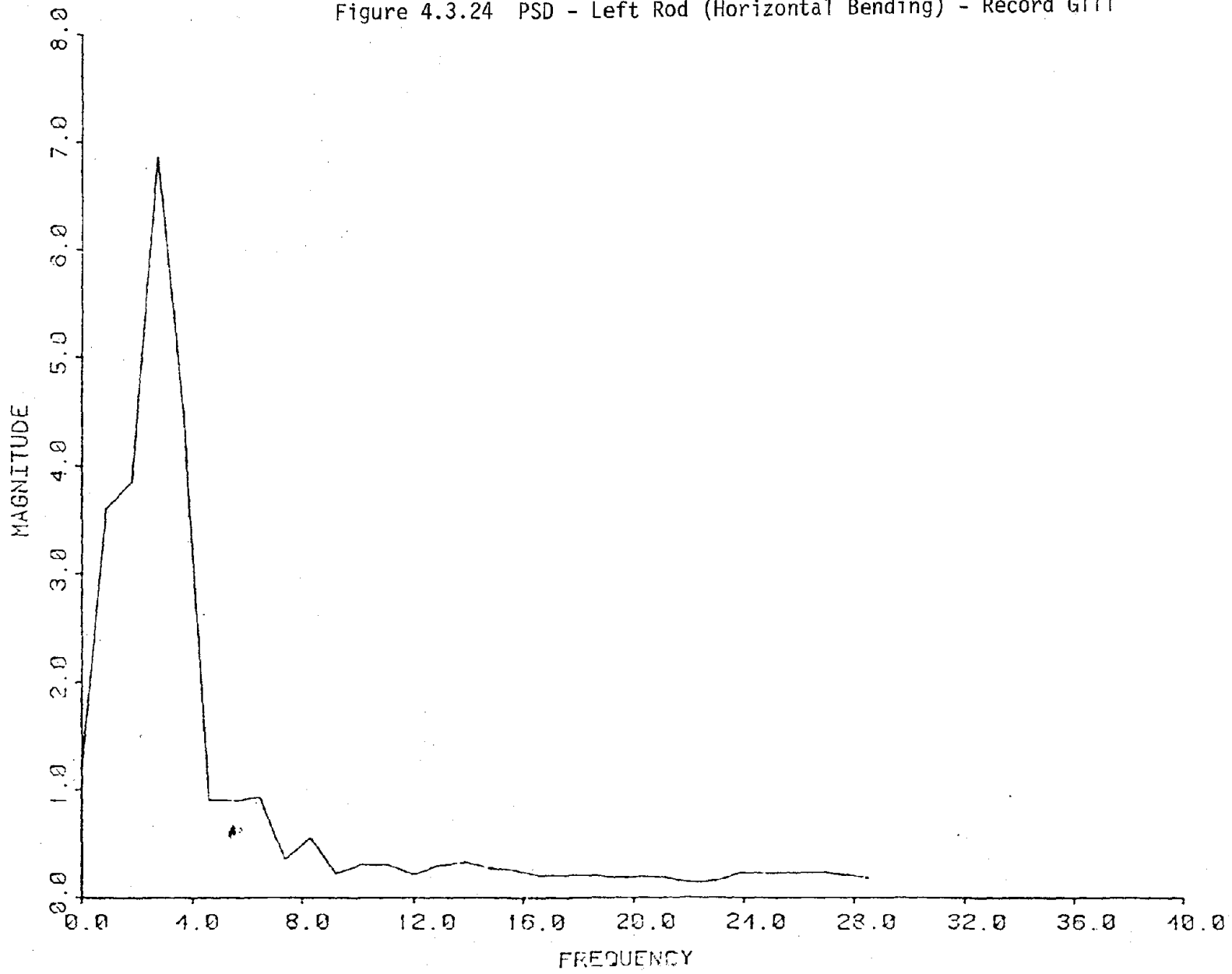Figure 4.3.24   PSD - Left Rod (Horizontal Bending) - Record G111

Figure 4.3.25  PSD - Right Rod (Horizontal Bending) - Record G111
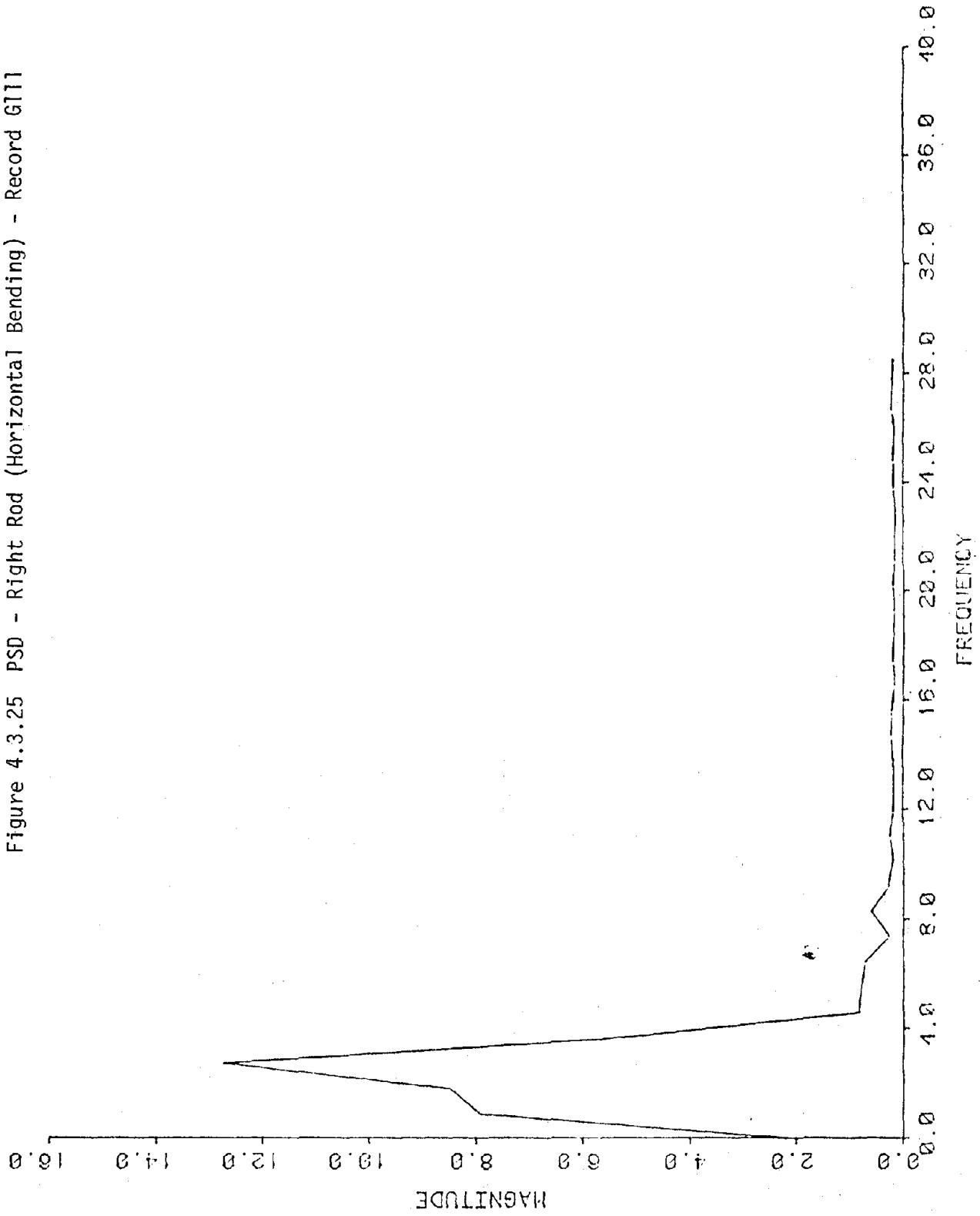
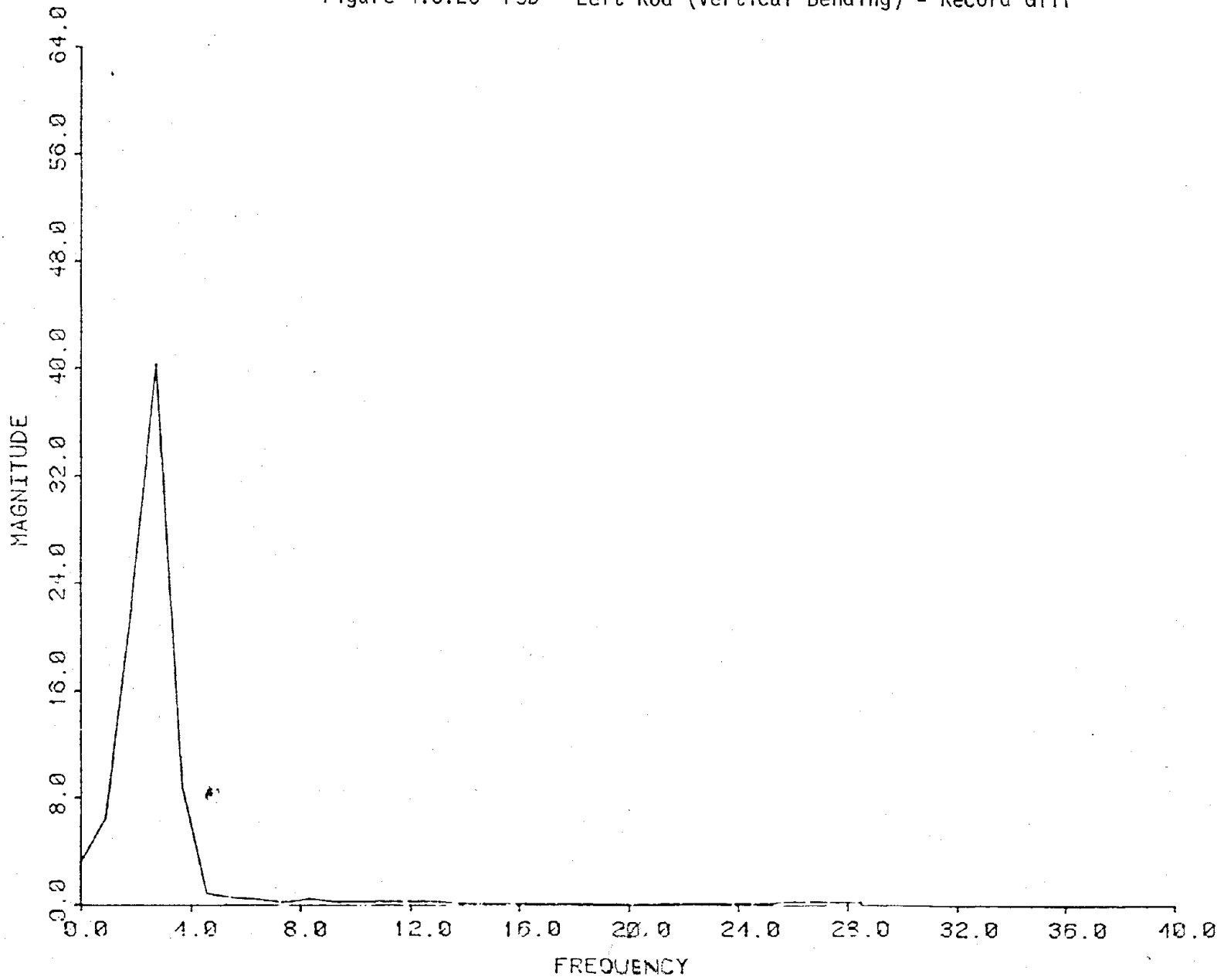Figure 4.3.26  PSD - Left Rod (Vertical Bending) - Record G111

Figure 4.3.27   PSD - Right Rod (Vertical Bending) - Record G111
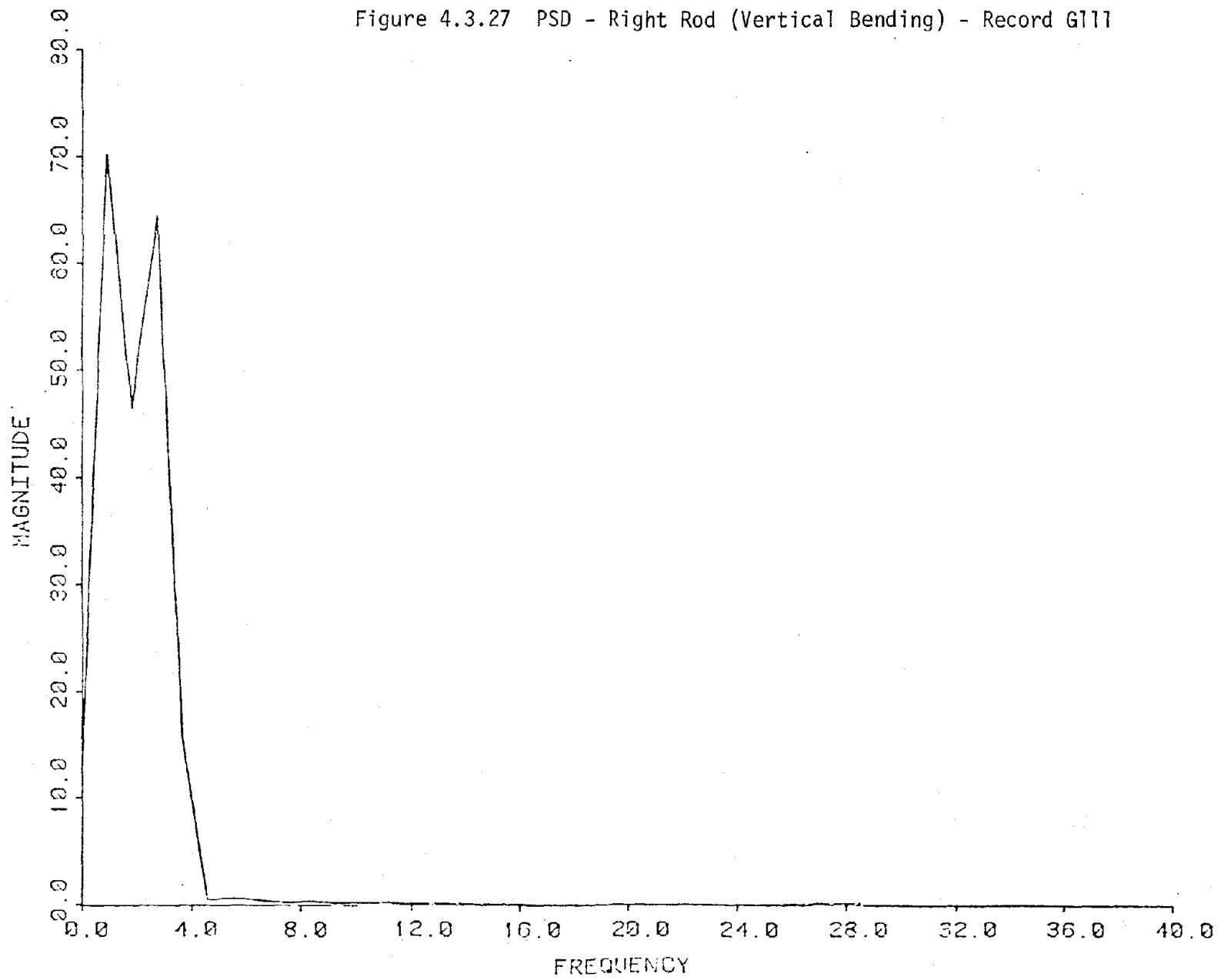
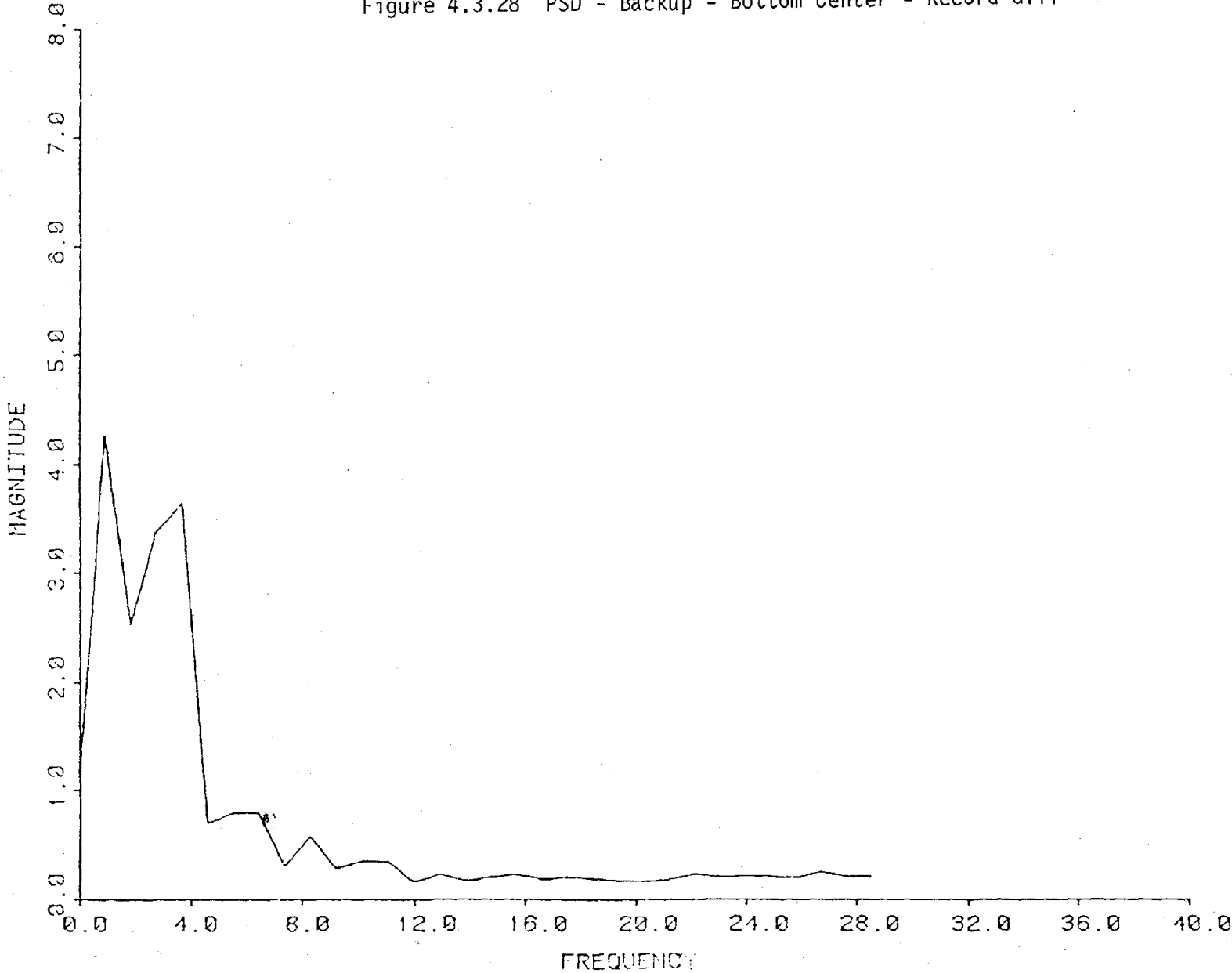Figure 4.3.28   PSD - Backup - Bottom Center - Record G111

Figure 4.3.29  PSD - Backup - Bottom Left - Record G111

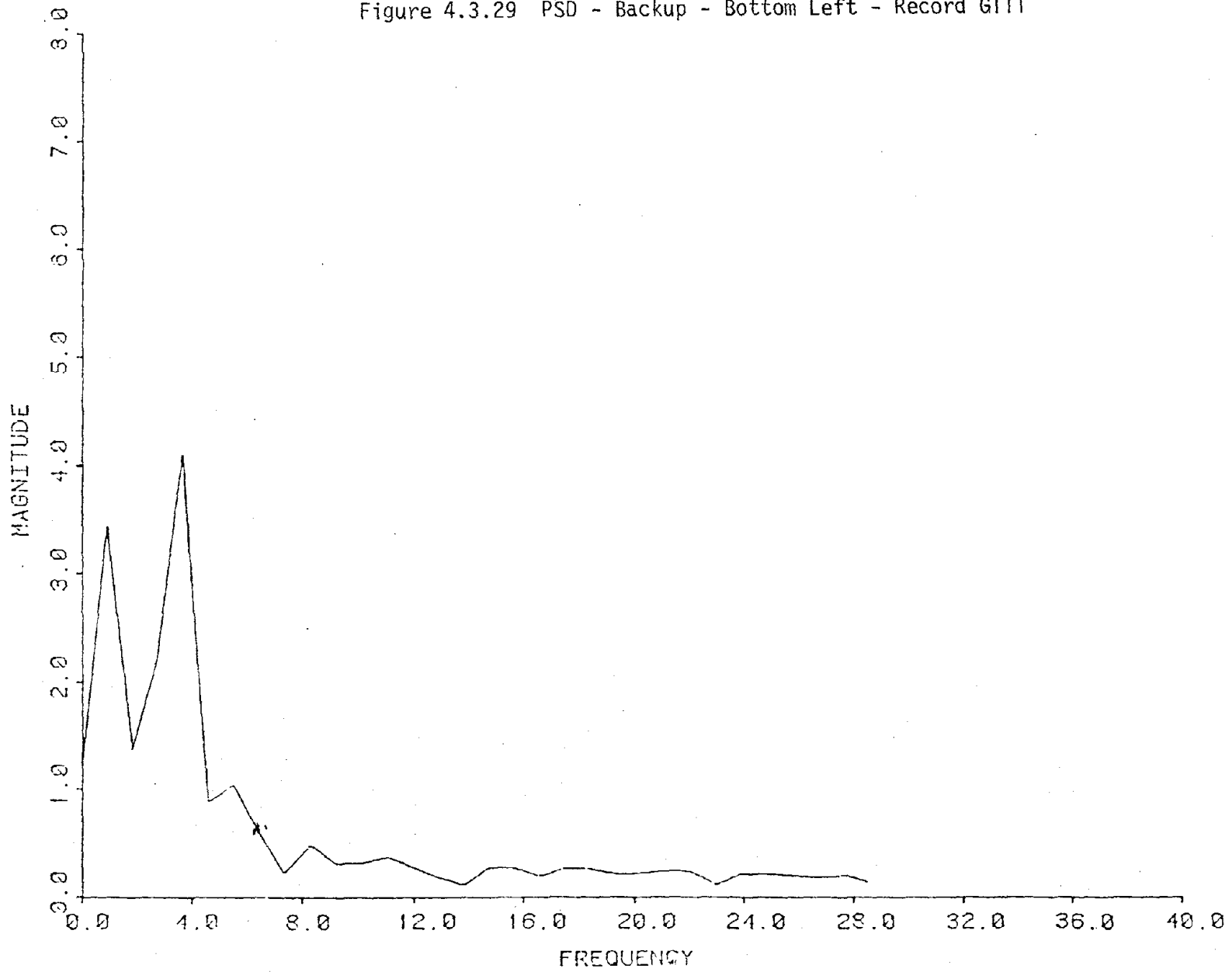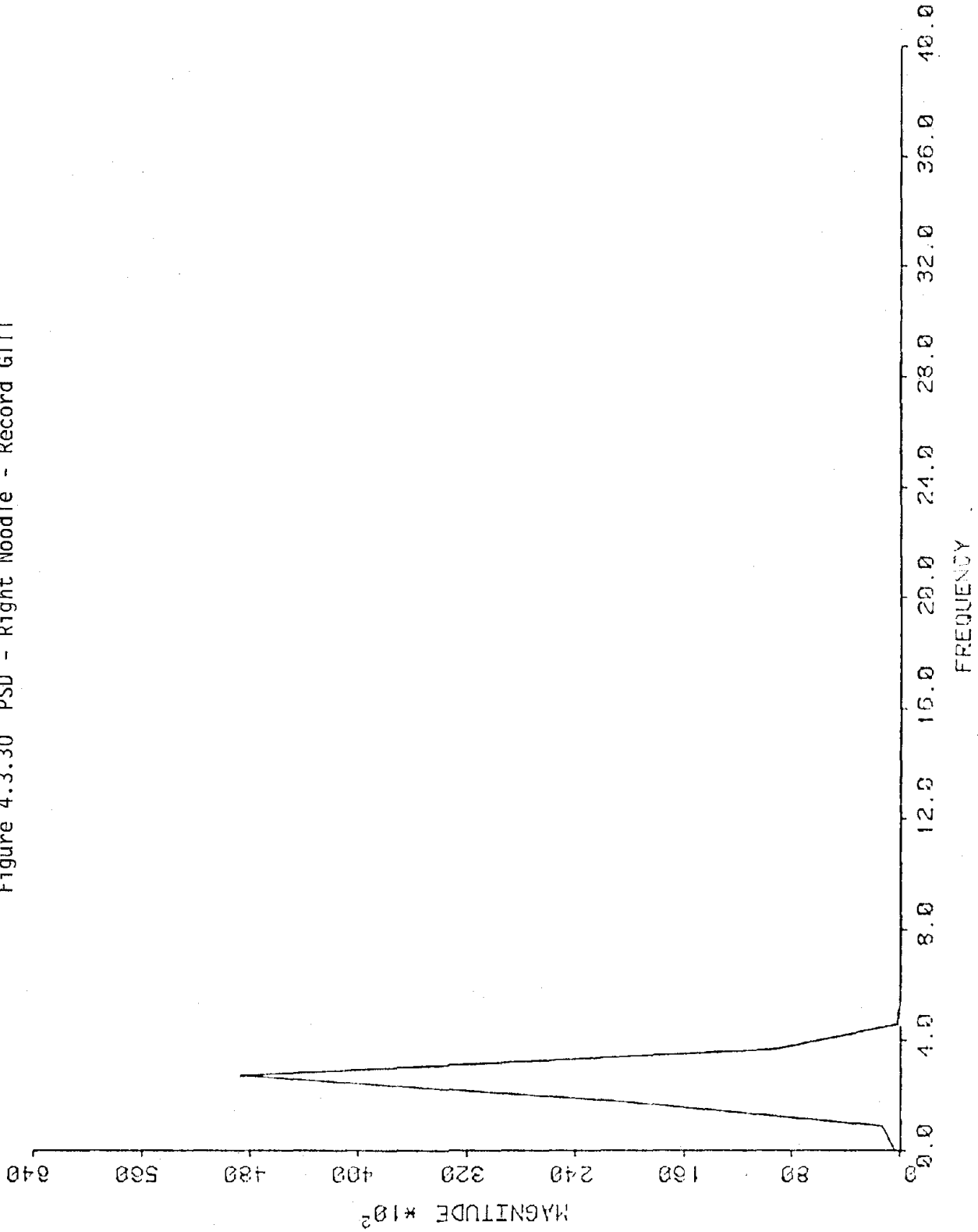Figure 4.3.30  PSD - Right Noodle - Record G111

Figure 4.3.31  PSD - Middle LVDT - Record G111
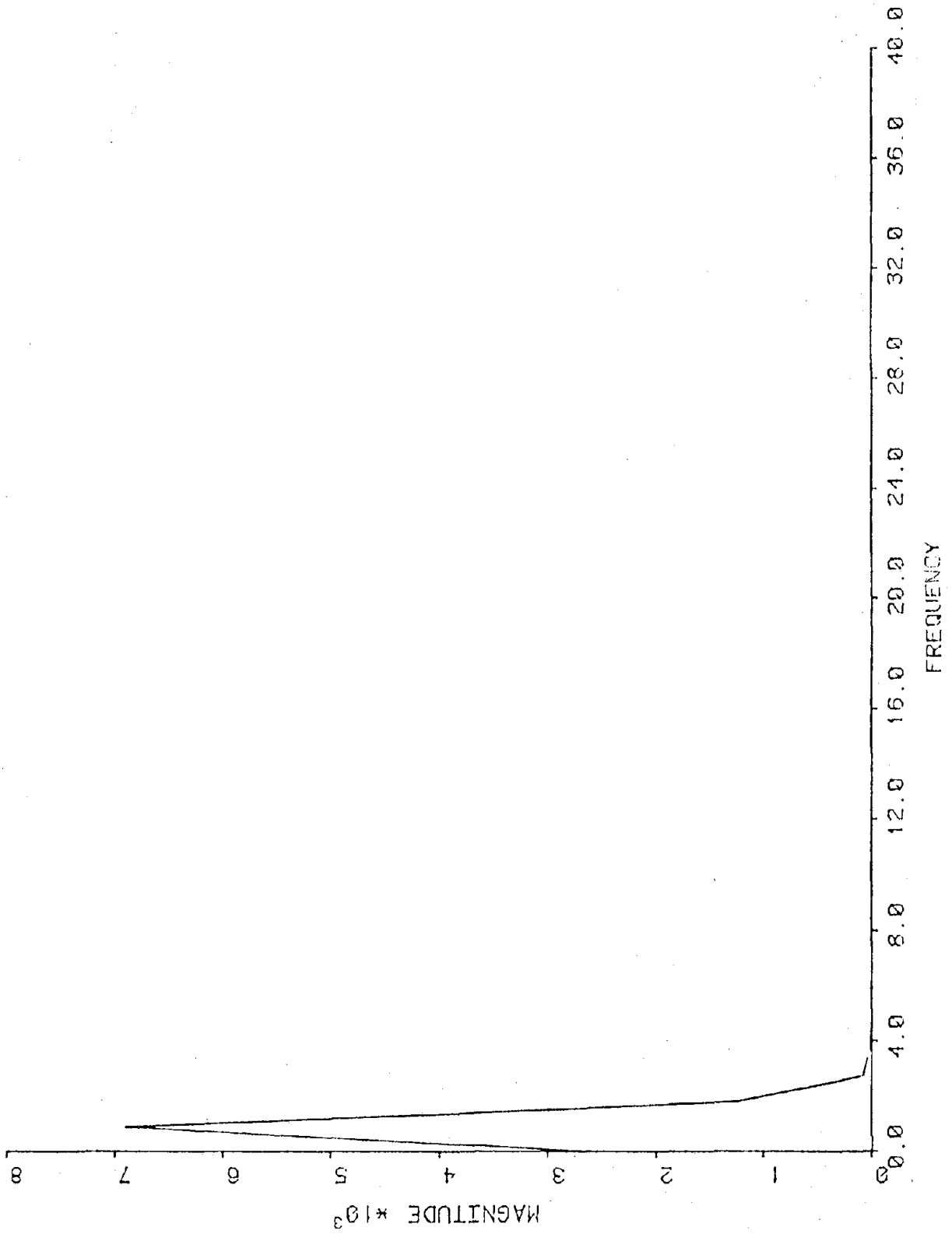


FREQUENCY

MAGNITUDE *10³

Figure 4.3.32  PSD - Top LVDT - Record G111
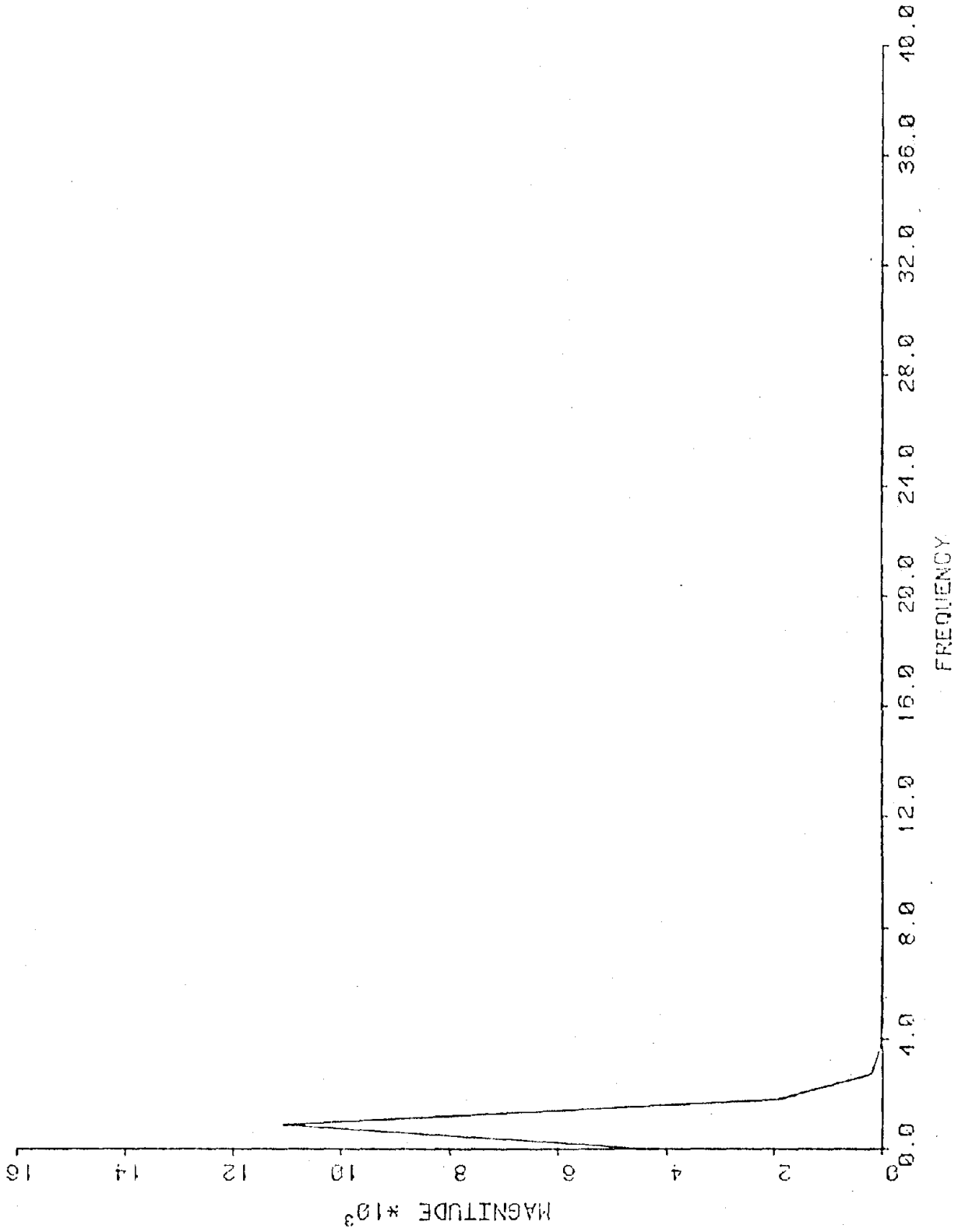
Figure 4.3.33 . PSD - Accelerometer - Record G111



FREQUENCY

MAGNITUDE *10³
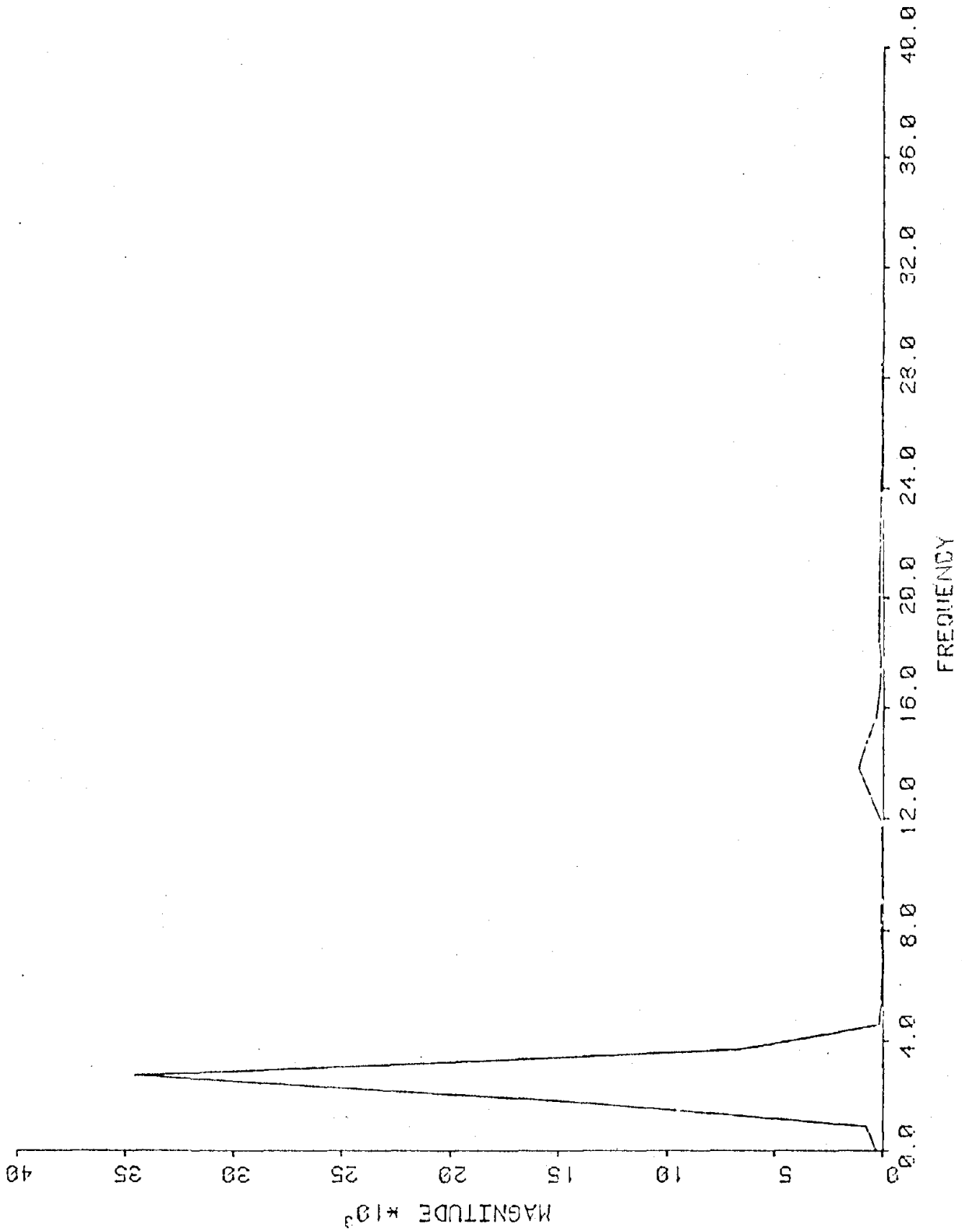
horizontal bending only reached a stress level of 20 Ksi. This result confirms the idea that the left connectors would see higher stress levels because the right connectors are next to the column and are not subject to such intense panel-frame excitation. The stress levels of the left and right rods in vertical bending were 10 ksi and 3 ksi, respectively, again the level of the left rod is greater than the right. The top LVDT shows a maximum displacement of 3.002 inches which is very close to the 3.2 maximum amplitude of the excitation. The 1G accelerometer indicated a maximum acceleration of 1.68 G which simply means that the magnitude was off scale for this sensor.

## 4.4 Summary and Conclusions

A test facility was developed in the Civil Engineering Department at the University of Idaho in order to conduct full scale dynamic tests on the behavior of certain wall assemblages. This facility consists of a braced reaction frame oriented in a vertical position with centerline dimensions of 25 ft. (horizontally) and 20 ft. (vertically). The loading is applied to the test structure through a 55 kip hydraulic actuator that is controlled by a closed-loop servo system. The data from the various transducers is collected using a PDP-11/03 micro-computer with $64^k$ bytes of core and 1 mega bytes of floppy disk storage.

The facility was used to investigate a one-story, one-bay full size rigid frame steel test structure (AISC Type 2 connections) clad with two 6 ft. by 12 ft. precast concrete panels. Each panel was fastened to the steel frame with two angles at the bottom and two rods at the top. The test structure was first subjected to loads using the swept-sine technique to obtain the natural frequencies. The test structure was also excited with the following records obtained from the 1971 San Fernando Valley earthquake (north-south component): Jet Propulsion Lab (JPL) basement and ninth floors; Caltech, Milikan Library, basement and tenth floors. The data was collected using a microcomputer, and methods of Fourier and spectral analysis were used to analyze the results. The results obtained for the ninth floor of the JPL are presented in this report. Based on the results of this experimental work, it appears that the following concluding statements can be made:

1. The seismic testing facility at the University of Idaho which is composed of the reaction frame plus the data acquisition and analysis system, is a satisfactory facility for investigating structure-cladding assemblages that are one-story high and one-bay wide.

2. The PSD plots for the connectors obtained for the San Fernando earthquake at the 9th floor of the JPL indicate that the response of the integrative lower connectors display energy contents near the lowest three natural frequencies of

the assemblage; whereas, the top dissociative connectors have energy contents near first fundamental frequency of the assemblage and also at the highest frequency content of the excitation.

3. The exceedance levels confirmed the visually observed fact that the top connectors (rods) are highly stressed in horizontal bending when the assemblage is subjected to the sample earthquake. All other strain gages indicate modest stress levels.

4. The top connectors (rods) are highly susceptible to low cycle fatigue with failure precipitated at the root of one of the threads at the location of the insert.

# REFERENCES

American Concrete Institute, Building Code Requirements for Reinforced Concrete, ACI 318-77. Detroit Michigan, August 1978.

American Institute of Steel Construction, Inc. 1977. Manual of steel construction. New York: American Institute of Steel Construction, Inc., 7th edition.

Applied Technology Council, Tentative Provisions for the Development of Seismic Regulations for Buildings ATC 3-06, U.S. Government Printing Office, Washington, D.C., 1978.

Argyris, J.H., J. St. Doltsinis, and K.J. William, "New Developments in the Inelastic Analysis of Quasistatic and Dynamic Problems," Int. J. for Numer. Meth. Engrg., Vol. 14, 1979.

Avent, R.R., L.Z. Emkin, and P.H. Sanders. June 1978. Behavior of epoxy repaired full-scale timber trusses. Journal of the Structural Division, ASCE, Vol. 104, No. ST6.

Ayres, J. Marx, Tsent-Yao Sun, and F. Brown, "Non-Structural Damage to Buildings, The Great Alaska Earthquake of 1964," Engrg., NAS, Washington, D.C., 1973.

Barkan, D.D. 1962. Dynamics of bases and foundations. Translated from the Russian by L. Drashevska, and translation edited by G.P. Tschebotarioff. New York: McGraw-Hill Book Company.

Basu, A.K., A.K. Nagpal, R.S. Bajaj, and A.K. Guliana, "Dynamic Characteristics of Coupled Shear Walls," J. Struct. Div., ASCE, Vol. 105, No. ST8, August, 1979.

Bathe, K.J., "An Assessment of Current Finite Element Analysis of Nonlinear Problems in Solid Mechanics," Proceedings SYNSPADE 1975, Academic Press, New York. 1976.

_____, "Static and Dynamic Geometric and Material Nonlinear Analysis Using ADINA," Report 82448-2, Acoustics and Vibration Laboratory, Mechanical Engineering Department, M.I.T., Cambridge, Massachusetts, May, 1976, Revised May, 1977.

_____, E.L. Wilson and F.E. Peterson, "SAP IV, A Structural Analysis Program for Static and Dynamic Response of Linear Systems," EERC 73-11 Engineering Research Center, University of California, Berkeley, California, June, 1973, Revised April, 1974.

_____, and E.L. Wilson. Numerical Methods in Finite Element Analysis, Prentice-Hall Inc., Englewood Cliffs, New Jersey, 1976.

Becker, J.M. and C. Florente, "Seismic Design of Precast Concrete Panel Buildings," Workshop on Earthquake-Resistant Reinforced Concrete Building Construction, University of California, Berkeley, California, July, 1977.

Beers, R.J., Jr., "An Analytic Study of the Interaction Between Structural Framing and Precast Curtain Walls," Masters Thesis, University of Idaho, Moscow, Idaho, 1980.

Briggs, D.W., "Development of an Element Stiffness Matrix for an Exterior Precast Concrete Curtain Wall," Masters Thesis, University of Idaho, Moscow, Idaho, 1976.

Clough, R.W., "Analysis of Structural Vibrations and Dynamic Response," Proceedings 1st U.S.-Japan Symposium on Recent Advances in Matrix Methods of Structural Analysis and Design, Tokyo, Japan, 1968.

_____ and K.J. Bathe, "Finite Element Analysis of Dynamic Response," Proceedings 2nd U.S.-Japan Symposium on Recent Advances on Computational Methods of Structural Analysis and Design, Berkeley, California, 1972.

_____, A. Niwa, and D.P. Clough. December 1979. Experimental seismic study of a cylindrical tank. Journal of the Structural Division, ASCE, Vol. 105, No. ST12.

_____ and J. Penzien, Dynamics of Structures, McGraw-Hill Inc., New York, 1975.

Cook. R.D., Concepts and Applications of Finite Element Analysis, John Wiley and Sons Inc., New York, 1974.

Desai, S.C. and J.F. Abel, Introduction to the Finite Element Method, Van Nostrand Reinhold Co., New York, 1972.

Eaton, K.J., "Cladding and the Wind," J. Struct. Div., ASCE, Vol. 102, No. ST5, May, 1976.

Fiorato, A.E., M.A. Sozen, and W.L. Gamble, "An Investigation of the Interaction of a Reinforced Concrete Frame with Masonry Filler Walls," Technical Report, University of Illinois, November, 1970.

Freeman, S.A., "Racking Tests of High-Rise Building Partitions," J. Struct. Div., ASCE, Vol. 103, No. ST8, August, 1977.

Gallager, R.H., Finite Element Analysis Fundamentals, Prentice-Hall Inc., Englewood Cliffs, New Jersey, 1975.

Gjelsvik, A., "Interaction between Frames and Precast Filler Walls," J. Struct. Div., ASCE, Vol. 100, No. ST2, February, 1974.

Goodno, B.J., "Glass Curtain Wall Elements, Properties and Behavior," J. Struct. Div., Proc. ASCE, Vol. 105, No. ST6, June 1979.

_____, K.M. Will and J.I. Craig, "Analysis of Cladding on Tall Buildings," ASCE Preprint 3744, ASCE National Convention, Atlanta, Georgia, October, 1979.

Gopu, V.K.A., and J.R. Goodman.  December 1975.  Fullscale tests on tapered and curved glulam beams.  Journal of the Structural Division, ASCE, Vol. 101. No. ST12.

Harris, C.M., and C.E. Crede.  1961.  Shock and vibration handbook.  Three volumes.  New York:  McGraw-Hill Book Company.

Huckelbridge, A.A., and R.W. Clough.  August 1978.  Seismic response of uplifting building frame.  Journal of the Structural Division, ASCE Vol. 104, No. ST8.

Hudson, D.E.  December 1977.  Dynamic tests of full-scale structures.  Journal of the Engineering Mechanics Division, ASCE, Vol. 103, No. EM6.

Hurty, W. and M.F. Rubinstein, Dynamics of Structures, Prentice-Hall Inc., Englewood Cliffs, New Jersey, 1964.

International Conference of Building Officials, Uniform Building Code, 1979 Edition.

Irwin, A.W. and A.C. Heidebrecht, "Dynamic Response of a Coupled Shear Wall Building," ASCE National Structural Engineering Meeting, Baltimore, Maryland, April, 1971.

James, M.L., G.M. Smith, J.C. Wolford, Applied Numerical Methods for Digital Computation, Thomas Y. Crowel Company Inc., 1977.

Mahin, S.A. and V.V. Bertro, "Nonlinear Seismic Response of a Coupled Wall System," J. Struct. Div., ASCE, Vol. 102, No. ST9, September, 1976.

Major, A.  1962.  Vibration analysis and design of foundations for machines and turbines.  London:  Collet's Holdings, Ltd.

Majumdar, S.N.G., and P.F. Adams.  April 1971.  Tests on steel-frame, shear-wall structures.  Journal of the Structural Division, ASCE, Vol. 97, No. ST4.

Mak, K.M., "Static and Nonlinear Analysis of the Interaction between Planar Frames and Precast Panel Walls," Masters Thesis, Washington State University, Pullman, Washington, 1977.

Manley, R.G.  1945.  Waveform analysis.  New York:  John Wiley and Sons, Inc.

Mayes, R.L., and R.W. Clough.  April 1975.  Cyclic shear tests on fixed-ended masonary piers.  Preprint 2433, ASCE Natl. Struct. Engr. Conf.

McCue, G.M., A. Vernez-Mouden, G. Kost and J.R. Benjamin, "Building Enclosures and Finish Systems:  Their Interaction with the Primary Structure during Seismic Action," Proc. U.S. Nat'l. Conf. Earthq. Engrg., June, 1975.

Mondkar, D.P. and G.H. Powell, "Evaluation of Solution Schemes for Nonlinear Structures," Int. J. for Numer. Meth. Engrg., Vol. 9, 1978.

Morris, N.F., "The Use of Modal Superposition in Nonlinear Dynamics," Computers and Structures, Vol. 7, 1977.

Murphy, L., "San Fernando, California Earthquake of February 9, 1971," NOAA, U.S. Dept. Commerce, 1973.

Nigam, N.C., and P.C. Jenings, "Calculation of Response Spectra from Strong-Motion Earthquake Records," Bulletin of the Seismological Society of America, Vol. 59, No. 2, pp. 909-922, April 1969.

Noether, G.E. 1971. Introduction to statistics--a fresh approach. Boston: Houghton Mifflin Co.

Oden, J.T., Finite Elements of Nonlinear Continua, McGraw-Hill Inc., New York, 1972.

Oppenheim, J.J., "The Effect of Cladding on Tall Buildings," Masters Thesis, Cambridge University, 1972.

Perry, C.C., and H.R. Lissner, The Strain Gage Primer, McGraw-Hill Inc., New York, 1962.

Portland Cement Institute, "Architectural Precast Concrete," First Edition, 1973. Chicago, Illinois.

Portland Cement Institute, P.C.I. Manual for Structural Design of Architectural Precast Concrete, 1977 Edition, Chicago, Illinois.

Portland Cement Institute, P.C.I. Design Handbook, Precast and Prestressed concrete, 2nd edition, 1978, Chicago, Illinois.

Prestressed Concrete Institute. 1971. PCI design handbook, precast and prestressed concrete. Chicago: Prestressed Concrete Institute.

Prestressed Concrete Institute, Structural Design of Precast Architectural Concrete, Chicago, Illinois, 1977.

Ragget, J.D., "Influence on Nonstructural Partitions on the Dynamic Response Characteristics of Structures," URS/John A. Blume & Associates, Engineers, JAB-99-94, July, 1972.

Rains, D.J., "Analytic Determination of Forces in Curtain Wall Connectors Under Seismic Loading," Masters Thesis, University of Idaho, Moscow, Idaho, 1980.

Rousseau, P.E., "Evolution of Conception of Curtain Walls in Relation with Flexibility of Structures," Proceedings ASCE-IABSE Conference, Lehigh, Pennsylvania, August, 1972.

Salmon, C.G., and J.E. Johnson. 1971. Steel structures, design and behavior. New York: Harper and Row, Publishers.

Sanders, W.W., Jr., F.W. Klaiber, H.A. Elleby, and L.W. Temin. July 1976. Ultimate load test of truss bridge floor system. Journal of the Structural Division, ASCE, Vol. 102, No. ST7.

Sessa, V., "An Experimental Study of the Mechanical Characteristics of Individual Precast Curtain Wall Connections," Masters Thesis, University of Idaho, Moscow, Idaho, 1980.

Sharpe, R.L., "Seismic Design of Nonstructural Elements," Proceedings, ASCE-IASBE Conference, Lehigh, Pennsylvania, August, 1972.

Structural Engineers Association of California (SEAOC), "Recommended Lateral Force Requirements and Commentary, Seismic Committee, 1973.

Tanner, N.S., "The Influence of a Precast Curtain Wall on the Stiffness of a High-Rise Building," Georgia Institute of Technology, August, 1974.

Thomas, D.L., "The Description and Analysis of the Reaction Frame: A Facility for Full Scale Testing of Precast Concrete Curtain Wall Behavior at the University of Idaho," Masters Thesis, University of Idaho, Moscow, Idaho, 1980.

Tso, W.K. and A. Rutenburg, "Seismic Spectral Response of Coupled Shear Walls," J. Struct. Div., ASCE, Vol. 103, No. ST1, January, 1977.

University of Idaho, Computer Services, "Calcomp Plotting System User's Guide," Moscow, Idaho.

U.S. Department of Commerce, National Oceanic and Atmospheric Administration, "San Fernando Earthquake of February 9, 1971," Volume I-Effects on Building Structures.

Weidlinger, P., "Shear Field Panel Bracing," J. Struct. Div., ASCE, Vol. 99, No. ST7, July, 1977.

Wicher, E.A., "Stochastic Analysis of Experimental Seismic Response of Architectural Precast Structural Cladding," Masters Thesis, University of Idaho, Moscow, Idaho, 1980.

Wilson, E.L. and J. Penzien, "Evaluation of Orthogonal Damping Matrices," Int. J. for Numer. Meth. in Engrg., Vol. 4, No. 1, 1972.

Kost, E. G., W. Weaver, and R. B. Barber, "Nonlinear Dynamic Analysis of Frames with Filler Panels," J. Struct. Div., ASCE, Vol. 100, No. ST4, January, 1974.

Lambe, T. W., and R. V. Whitman, Soil Mechanics. John Wiley and Sons, Inc., New York: 1969.